

https://dspace.org/

Direct methane transformation into higher hydrocarbons and oxy-products

Eskendirov, Igor

1996

http://hdl.handle.net/10539/22781

Eskendirov, Igor (1996) Direct methane transformation into higher hydrocarbons and oxy-products, University of the Witwatersrand, Johannesburg,<http://hdl.handle.net/10539/22781>

Downloaded from a DSpace repository. https://dspace.org/

DIRECT METHANE TRANSFORMATION INTO HIGHER HYDROCARBONS AND OXY-PRODUCTS

Igor Eskendirov

A thesis submitted to the Faculty of Science, University of the Witwatersrand, Johannesburg, in fulfilment of the requirements for the degree of Doctor of Philosophy.

Johannesburg , 1996

"We are perhaps not far removed from the time when we shall be able to submit the bulk of chemical phenomena to calculation".

Joseph Louie Gay-Lussac 1778-1850

DECLARATION

I declare that this thesis is my own, unaided work. It is being submitted for the Degree of Doctor of Philosophy in the University of the Witwatersrand, Johannesburg. It has not been submitted before for any degree or examination in any other University.

M. Semugopoti

(Signature of candidate)

7 day of May 1996

ABSTRACT

In present thesis the results of a study of the combined action of a solid catalyst and a gas-phase initiator, hydrogen peroxide, in the methane partial oxidation and oxidative coupling reactions are presented.

All experiments were carried out in continuous-flow installations using fixed-bed reactors. The different types of reactor systems were designed to investigate the influence of residence time, contact time and linear flow rate on the methane conversion and product selectivities.

The surface areas of the catalysts were determined by the BET method. The adsorption of methyl alcohol on the catalyst surface was characterised using FT-IR spectroscopy. X-Ray Diffraction analysis (XRD) and Scanning Electron Microscopy (SEM) coupled with Energy Dispersive X-Ray analysis (EDX) were used to determine the crystalline structure, morphology and distribution of elements on the surface of the catalysts.

The homogeneous and catalytic oxidation of methane to methanol were studied at atmospheric pressure in the temperature range 460-625°C with a feed consisting of 82% methane and 18% oxygen. The residence time was varied from 95 to 216 s.

To determine the effect of pressure on the product selectivity and methane conversion, experiments were performed at 1 and 50 bar, temperatures of 450-490°C, residence times of 5.8-102 s, and oxygen concentrations in the feed of 4.2 and 17 mol.%.

The use of 30% H_3BO_3/Al_2O_3 had a visible catalytic effect on the partial oxidation of methane performed at low pressure. In the presence of this catalyst the methanol yield was increased up to 0.18% at 550°C and the reaction temperature at which methanol was first observed was lower than that for the homogeneous reaction.

Partial oxidation of methane by oxygen in the presence of hydrogen peroxide to form formaldehyde and methanol has been studied over the series of silica supported catalysts with 3d, 4d, 4f, 5p and 6p metal oxides at 500°C under ambient pressure.

It was shown that pure precipitated SiO_2 exhibited remarkable activity toward formaldehyde formation. The presence of titanium, vanadium, chromium, iron, molybdenum, lead, bismuth and lanthanum metal oxides appeared to suppress the

activity of bare silica, as well as reduce methane conversion and therefore, formaldehyde yield, under a given set of experimental conditions. The only elements which enhanced bare silica activity were the 5p metals, tin and antimony. A maximum combined formaldehyde and methanol yield of 1.32% at a methane conversion of 3.5% was observed on the 0.1 mmol Sn/g of SiO_2 catalyst.

The positive effect of doping silica with Sn and Sb can be explained by the possible activation of hydrogen peroxide on these elements, and the formation of active radicals, presumably hydroxyl radicals.

The influence of hydrogen peroxide and its concentration in the reaction mixture on CH_4 conversion and C_{2+} hydrocarbon selectivity was examined in the gas phase as well as over a wide number of catalysts in the temperature range 400-1100°C using a reactant mixture of $CH_4/O_2/N_2$ with methane and oxygen concentrations of 35-60 and 14-30 mol.%, respectively. An aqueous solution of hydrogen peroxide with concentration varying from 2.6 to 21 wt. %, or pure water, was added to the reactant mixture via an evaporator at a rate of 0.03 ml/min.

A comparison of the apparent activation energies, obtained from the gas phase homogeneous oxidative coupling of methane in the presence and absence of hydrogen peroxide (E_a = 55.7-64.8 kJ mol^{-1} and 225.8 kJ mol^{-1}, respectively), indicate that CH_4 activation occurred via the interaction of radicals formed during the dissociation of H_2O_2.

The maximum yield of C_{2+} products, obtained on 1% Au/ 5% La_2O_3/CaO in the presence of 21 wt. % hydrogen peroxide, was 27% with a corresponding 7.3% yield of benzene; this is one of the best results obtained to date for the title reaction.

The total C_2 hydrocarbon selectivity increased from 49.6 to 62.3% at corresponding CH_4 conversions of 26.7% and 31.4% as the reactant gas was diluted by water vapour in the reaction performed on a 28% La_2O_3/ 7% SrO/CaO catalyst. An absolute yield of 20% of both C_2H_4 and C_2H_6 was obtained at a CH_4/O_2 ratio of 4.0 and a residence time of 0.11 s.

On the basis of the experimental results a reaction scheme was proposed for the homogeneous - heterogeneous activation of methane in the presence of hydrogen peroxide.

ACKNOWLEDGEMENTS

I wish to express my deep gratitude to my supervisor, Professor V.D. Sokolovskii, for his valuable insight and vast experience in catalysis. It was a great pleasure to have worked in collaboration with him.

My thanks also to my co-supervisor, Professor N.J. Coville, who made many helpful manuscript suggestions and his enthusiastic support.

I am grateful to the following people: Linda Jewell and Tracy Bromfield for their assistance in compiling this manuscript and Tracy for her wonderful help in obtaining the FT-IR spectra.

Basil Chassoulas for his much appreciated technical assistance.

I wish to thank the University, FRD and Richard Ward Endowment Fund for financial support.

PRESENTATIONS

November 1994	Methane oxidative coupling in the presence of hydrogen peroxide, Annual National Catalysis Conference, Pretoria, Republic of South Africa.
June 1995	Selective oxidative transformation of methane in the presence of hydrogen peroxide, Catalysis Conference of the Catalysis Society of South Africa, Rustenburg, Republic of South Africa.
November 1995	Direct oxidative conversion of methane into higher hydrocarbons and oxy-products in the presence of hydrogen peroxide, Fourth International Natural Gas Conversion Symposium, Kruger National Park, Republic of South Africa.

PUBLICATIONS

I. Eskendirov, V. Sokolovskii and N. Coville, Methane oxidative coupling in the presence of hydrogen peroxide, *Journal of the Chemical Society, Chemical Communication*, 1994, 2033.

I. Eskendirov, N.J. Coville and V.D. Sokolovskii, Methane oxidative coupling on the $Au/La_2O_3/CaO$ catalyst in the presence of hydrogen peroxide, *Catalysis Letters*, 1995, **35**, 33.

I. Eskendirov, B. Kabongo, L. Glasser and V.D. Sokolovskii, Kinetics by thermometry: An aldol condensation reaction, *Journal of the Chemical Society, Faraday Transactions*, 1995, **91** (6), 991.

I. Eskendirov, N.J. Coville, A. Parmaliana and V.D. Sokolovskii, Direct oxidative conversion of methane into higher hydrocarbons and oxy-products in the presence of hydrogen peroxide, Proceedings of the Fourth International Natural Gas Conversion Symposium, *Studies in Surface Science and Catalysis*, Elsevier, Amsterdam, 1996. (accepted for publication).

CONTENTS

DECLARATION ii
ABSTRACT iii
ACKNOWLEDGEMENTS v
PRESENTATIONS AND PUBLICATIONS vi
CONTENTS vii
LIST OF FIGURES x
LIST OF TABLES xvi
NOMENCLATURE xix

Chapter 1. INTRODUCTION 1
1.1. Oxidative coupling of methane 5
1.1.1. Alkali metal catalysts 9
1.1.2. Catalysts based on alkaline-earth metal oxides 13
1.1.3 Catalysts based on the oxides of rare-earth elements 19
1.1.4. Other oxide catalysts 23
1.2. Mechanism of the oxidative coupling of methane 26
1.2.1. Isotope exchange studies 26
1.2.2 Kinetics of the oxidative coupling of methane 31
1.2.3. Reaction mechanism and nature of the active sites 60
1.3. Direct oxidation of methane to oxygenates 67
1.3.1. Partial oxidation of methane to methanol 67
1.3.2. Partial oxidation of methane to formaldehyde 76
1.4. Different types of oxidants for methane oxidative coupling and selective oxidation of lower paraffins 82
1.5. Aims and scope of this study 94

Chapter 2. EXPERIMENTAL METHODS AND APPARATUS 96
2.1. Catalyst preparation 96
2.1.1. Catalysts for methane oxidative coupling 96
2.1.2. Catalysts for partial oxidation of methane to formaldehyde 97

2.1.3. Catalysts for partial oxidation of methane to methanol 97
2.2. Installation 98
2.3. The product analysis 103
2.3.1. The product analysis using gas chromatography 103
2.3.2. Quantitative determination of formaldehyde 103
2.4. Calculations and mass balance procedure 107
2.5. Experimental procedure 110
2.5.1. Oxidative coupling of methane 110
2.5.2. Partial oxidation of methane to formaldehyde 114
2.5.3. Partial oxidation of methane to methanol 115
2.6. Catalyst characterisation 117
2.6.1. Surface Area determination 117
2.6.2. X-Ray Diffraction (XRD) 117
2.6.3. Scanning Electron Microscopy (SEM) 117
2.6.4. Energy Dispersive X-Ray Analysis (EDX) 117
2.6.5. Diffuse Reflectance Fourier Transform Infra-Red Spectroscopy (DRIFTS) 118

Chapter 3. RESULTS 120
3.1. Partial oxidation of methane to formaldehyde in the presence of hydrogen peroxide 120
3.2. Partial oxidation of methane to methanol 124
3.2.1. Gas phase partial oxidation of methane to methanol 124
3.2.2. Catalytic oxidation of methane to methanol 127
3.3. Methane oxidative coupling 133
3.3.1. Catalytic oxidative coupling of methane in the absence of hydrogen peroxide 133
3.3.2. Gas phase oxidative coupling of methane in the presence of hydrogen peroxide 137
3.3.3. Catalytic oxidative coupling of methane in the presence of hydrogen peroxide 140
3.3.3.1. Pb, Fe, Mo and La promoted catalysts 141

3.3.3.2. Catalytic testing of 5% La_2O_3/CaO, 1% Au/ 5% La_2O_3/CaO and 28% La_2O_3/ 7% SrO/CaO 142
3.3.4. Catalyst characterisation 150
3.3.4.1. Surface area determination 150
3.3.4.2. XRD analysis 150
3.3.4.3. SEM and EDX analysis 156

Chapter 4. DISCUSSION 165
4.1. Partial oxidation of methane to oxy-products 165
4.1.1. Partial oxidation of methane to methanol 165
4.1.2. Partial oxidation of methane to formaldehyde over a series of silica supported catalysts 174
4.1.3. Methane oxidative coupling in the presence and absence of hydrogen peroxide 180

Chapter 5. CONCLUSION 192

REFERENCES 197

LIST OF FIGURES

Chapter 1

Figure 1.1. Thermogravimetric curves for alkali metal carbonates 8

Figure 1.2. Decomposition of alkaline earth carbonates in air 13

Figure 1.3. Decomposition temperature for the last step (leading to M_2O_3) of the lanthanide carbonates in nitrogen and carbon dioxide 16

Figure 1.4. CH_4 conversion and C_2 selectivity of Li/MgO catalyst systems at 800°C, as a function of Li salt 17

Figure 1.5. CH_4 conversion and C_2 selectivity of wt.% Li on different support 17

Figure 1.6. CH_4 conversion and C_2 selectivity of M/Li/MgO for various dopants at 800°C 17

Figure 1.7. CH_4 conversion and C_2 selectivity of fresh undoped chemical compounds 17

Figure 1.8. The temperature relationship between the electroconductivity of calcium oxide and samarium-calcium 5% Sm_2O_3/CaO systems with different samarium oxide structure (A-cubic, B-monowedge, C-cubic + monowedge) 22

Figure 1.9. The rates of methane conversion and dehydrodimerization on PbO-MgO catalysts with 5% P, 5% W, 5% Na, 5% Li, 5% K additives and without any additives 24

Figure 1.10. Concentration of acceptor sites (I_{rel}) and rate of methane dimerization on PbO-MgO catalyst 25

Figure 1.11. Conversion of methane and oxygen versus space time calculated by integration of equation (8 a) with the parameter values of Table 1.8 38

Figure 1.12. Selectivities for the main reaction products calculated by integration of equation (8 a) with the parameter values of Table 1.8 versus space time 38

Figure 1.13. Selectivities for the main reaction products calculated by integration of equation (8 a) with the parameter values of Table 1.8 versus oxygen conversion 39

Figure 1.14. Feed conversions and selectivities for the main reaction products calculated by integration of equation (8 a) with the parameter values of Table 1.8 versus the maximum reaction temperature 39

Figure 1.15. Experimental and theoretical methane converted to various products on the Li/MgO catalyst versus pseudocontact time 50

Figure 1.16. Experimental and theoretical methane converted to various products on the Li/MgO catalyst versus temperature 50

Figure 1.17. Experimental and theoretical methane converted to various products on the Li/MgO catalyst versus oxygen inlet pressure 51

Figure 1.18. Experimental and theoretical methane converted to various products on the Li/MgO catalyst versus methane inlet pressure 51

Figure 1.19. The relationship between selectivity towards ethane at low conversions and the temperature over Al_2O_3, Y_2O_3, Ta_2O_5, 20% CdO/Al_2O_3, 20% PbO/Al_2O_3, BaO, Sn-Sb-O, Fb-Sn-K-O, quartz and in the empty reactor 53

Figure 1.20. The relationship between rate of methane conversion and C_2 product formation on the degree of reduction of the catalyst 59

Figure 1.21. The relationship between methane conversion, reaction product yields and $[Li^+O^-]$ center concentration on 7% Li/MgO catalyst and dioxygen pressure in the reaction mixture 61

Figure 1.22. IR-Fourier MgO spectra of the adsorbed CH_3OH, CH_4, $(CH_3)_2SnCl_2$ and $(CH_3)_2SnCl_2$ in Kbr 64

Fugure 1.23. Typical example of the space time dependency of the conversion and the selectivity of the primary products 69

Figure 1.24. Effect of pressure on the oxidation of methane: methane conversion as a function of temperature and product selectivity as function of methane conversion 71

Figure 1.25. Effect of oxygen concentration on the oxidation of methane: methane conversion as a function of temperature and product selectivity as a function of methane conversion.....71

Figure 1.26. Arrhenius plots for CH_3 radical formation.....85

Figure 1.27. CH_4 conversion and product yields as a function of the contact time at 700°C.....87

Figure 1.28. Product selectivities as a function of the contact time at 700°C.....87

Figure 1.29. Propane conversion, selectivity towards propylene, carbon oxides and carbon balance versus time for the γ-Al_2O_3 and Fe_2O_3 catalysts.....91

Chapter 2

Figure 2.1. General scheme of experimental apparatus used for methane oxidative coupling and partial oxidation to oxygenates.....99

Figure 2.2. Diagram of the reactor system fitted with the evaporator, the heavy organic and coke trap and the trap for collecting oxy-products.....101

Figure 2.3. Different reactor systems used in the methane oxidative coupling study.....111

Figure 2.4. Different reactor systems used in the methane oxidative coupling and partial oxidation of methane to methanol.....113

Figure 2.5. Effect of reactor type on methanol selectivity at 450°C in the pressure range 1-50 bar.....115

Figure 2.6. Cross-sectional view of the variable temperature reactor cell and the sample cup of a Bruker IFS 85 FT-IR spectrometer.....119

Chapter 3

Figure 3.1. Infra-red spectra of the untreated Al_2O_3, exposed to methanol at 120°C and followed by thermal desorption at 400°C in the presence of H_2O vapour.....130

Figure 3.2. Infra-red spectra of the untreated 30% H_3BO_3/Al_2O_3, exposed to methanol at 120°C and followed by thermal desorption at 400°C in the presence of H_2O vapour 131

Figure 3.3. Arrhenius plots for C_2 hydrocarbon formation in the gas-phase homogeneous methane oxidative coupling in the presence of H_2O (CH_4/air), H_2O_2 solution of 23 wt.% (CH_4/air), H_2O_2 solution of 23 wt.% (CH_4/N_2) and H_2O_2 solution of 7.6 wt.% (CH_4/air) 139

Figure 3.4. X-ray diffraction pattern of 5% La_2O_3/CaO before and after catalytic reaction 151

Figure 3.5. X-ray diffraction pattern of 1% Au/ 5% La_2O_3/CaO before and after catalytic reaction 153

Figure 3.6. X-ray diffraction pattern of 28% La_2O_3/ 7% SrO/CaO before and after catalytic reaction 155

Figure 3.7. 5% La_2O_3/CaO after catalytic reaction: 24 hours at 650-850°C. SEM micrograph and EDX spectra of the dark area on the catalyst surface 157

Figure 3.8. 5% La_2O_3/CaO after catalytic reaction: 24 hours at 650-850°C. SEM micrograph and EDX spectra of the white particle on the catalyst surface 158

Figure 3.9. 1% Au/ 5% La_2O_3/CaO after catalytic reaction: 24 hours at 600-800°C. SEM micrograph and EDX spectra of the dark area on the catalyst surface 159

Figure 3.10. 1% Au/ 5% La_2O_3/CaO after catalytic reaction: 24 hours at 600-800°C. SEM micrograph and EDX spectra of the bright white particle 160

Figure 3.11. 28% La_2O_3/7% SrO/CaO after catalytic reaction: 72 hours at 650-950°C. SEM micrograph and EDX spectra of the dark area on the catalyst surface 161

Figure 3.12. 28% La_2O_3/7% SrO/CaO after catalytic reaction: 72 hours at 650-950°C. SEM micrograph and EDX spectra of the bright area on the catalyst surface 162

Chapter 4

Figure 4.1. Temperature dependency of the methanol, ethane and ethylene yields as well as oxygen conversion for three different residence times at 1 bar pressure..... 166

Figure 4.2. Temperature dependency of selectivity and yield of the major products at 3 bar pressure..... 168

Figur 4.3. Temperature dependency of selectivity to the major reaction products for three different residence times at 50 bar pressure..... 169

Figure 4.4. Temperature dependency of the methanol, C_2 hydrocarbons, carbon monoxide and carbon dioxide yields for three different residence times at 50 bar pressure..... 170

Figure 4.5. Temperature dependency of the methanol, ethane and ethylene yields in the catalytic partial oxidation of methane at 1 bar pressure..... 172

Figure 4.6. Comparison of methanol yields obtained by non-catalytic and catalytic partial oxidation of methane over 30% H_3BO_3/Al_2O_3, 0.6% Pt/CaO, 0.1 mmol Sn/g SiO_2 at 1 bar pressure..... 173

Figure 4.7. Product distribution yields for methane partial oxidation over supported silica catalysts..... 175

Figure 4.8. Methane conversion and selectivity to major reaction products as a function of tin loading..... 176

Figure 4.9. Effect of reaction temperature on major product yields in experiments without any liquid addition to the feed, in the presence of pure H_2O and in the presence of H_2O_2 over the 5% La_2O_3/CaO catalyst..... 181

Figure 4.10. Selectivity to C_2H_6, C_2H_4, C_{3+}, C_6H_6, CO_X as a function of CH_4 conversion in experiments without any liquid addition to the feed, in the presence of pure H_2O and in the presence of H_2O_2 over the 5% La_2O_3/CaO catalyst..... 182

Figure 4.11. Effect of reaction temperature on C_{2+} hydrocarbon yield, C_{2+} selectivity and CO_X selectivity over 1% Au/ 5% La_2O_3/ CaO in the presence of pure water, hydrogen peroxide and without the addition of any liquid 184

Figure 4.12. Effect of reaction temperature on major product yields in experiments without any liquid addition to the feed, in the presence of pure water and hydrogen peroxide over the 28% La_2O_3/ 7% SrO/CaO catalyst 186

Figure 4.13. Selectivity to C_2H_6, C_2H_4, C_{3+} and CO_X. as a function of CH_4 conversion in experiments without any liquid addition to the feed, in the presence of pure water and hydrogen peroxide over the 28% La_2O_3/ 7% SrO/CaO catalyst..... 187

LIST OF TABLES

Chapter 1

Table 1.1. Current prices (1992) of products potentially derivable from natural gas, quoted in ton equivalent (te) 3

Table 1.2. Activity data for alkali metal-containing catalysts 10

Table 1.3. Activity data of catalysts containing alkali metals and other cations showing variable oxidation states 12

Table 1.4. Activity data for alkaline earth and rare earth catalysts containing no alkali metals 14

Table 1.5. Influence of cerium oxide dopant on the C_2 hydrocarbon yield on lithium-magnesium catalyst at 750°C 21

Table 1.6. Comparison of catalytic properties of samarium-calcium catalysts of various phase contents 21

Table 1.7. Comparison of rates of oxidative dehydrodimerization (W_d) and CH_4/CD_4 isotope exchange (W_o) under catalytic conditions on alkaline earth metal oxides 28

Table 1.8. Elementary reaction steps and their respective kinetic parameters ($k = AT^n \exp(-E_a / RT)$) as used for the simulation of the gas-phase oxidative coupling of methane 33

Table 1.9. Complete methane dimerization mechanism 49

Table 1.10. Activation energies of the reactions of methane on basic catalysts 62

Table 1.11. Effect of Cu on the selectivity to methanol 74

Table 1.12. Activity and formaldehyde productivity of "fumed" M5 and "precipitated" Si 4-5 P SiO_2-supported MoO_3 and V_2O_5 catalysts in the partial oxidation of methane 77

Table 1.13. Methane partial oxidation on silica and silica-supported MoO_3 and V_2O_5 catalysts in the presence and absence gas-phase oxygen 78

Table 1.14. Influence of the nature of the oxidants on oxidative coupling reaction on MgO and Li/MgO catalysts 82

Table 1.15. Comparison of O_2 and N_2O as oxidants for the oxidative coupling of CH_4 over a Li/MgO catalyst 84

Table 1.16. Comparison of catalytic results for partial oxidation of CH_4 on $Fe_2(MoO_4)_3$ with different oxidants 86

Table 1.17. Oxidation of methane by ozone and oxygen over GaPO4 catalyst 90

Chapter 2

Table 2.1. The response factors of products and reactants obtained via calibration of the separation columns connected to a flame ionization detector (F.I.D.) or a thermal conductivity detector (T.C.D.) 108

Chapter 3

Table 3.1. Effect of the reaction temperature, contact time (τ) and the presence of H_2O_2 or H_2O on the CH_4 conversion and product selectivities over 0.1 mmol Cr/g SiO_2 120

Table 3.2. Methane partial oxidation on silica and silica-supported catalysts, including 3d, 4d, 4f, 5p and 6p metals at loadings of 0.1 mmol of M/g of SiO_2 for all samples 121

Table 3.3. Product distribution of the methane oxidation over silica catalysts impregnated with varying quantities of Sn^{4+} in the presence of H_2O_2 or H_2O 122

Table 3.4. The temperature dependency of the product yields for different residence times at 1 bar pressure 124

Table 3.5. Methane conversion, product selectivities and methanol yield obtained in the gas phase reaction at 3 bar pressure and different reaction temperature 125

Table 3.6. Methane conversion, product selectivities and methanol yield obtained in the gas phase reaction at 50 bar pressure and different reaction temperature 126

Table 3.7. Effect of reaction temperature on methanol, ethane and ethene yields for the partial oxidation of methane over various catalysts at 1 bar pressure..... 128

Table 3.8. Conversion and selectivity data for the methane oxidative coupling reaction performed in a fixed-bed continuous-flow quartz reactor with small catalytic (1.9 cm^3) and large post catalytic (26.5 cm^3) reaction zones 133

Table 3.9. Conversion and selectivity data for the methane oxidative coupling reaction performed in a fixed-bed continuous-flow quartz reactor with large catalytic (26.5 cm^3) and small post catalytic (1.9 cm^3) reaction zones 134

Table 3.10. Conversion and selectivity data for the methane oxidative coupling over 5% La_2O_3/CaO catalyst 135

Table 3.11. Influence of hydrogen peroxide on the reaction of methane oxidative coupling 137

Table 3.12. Conversion and selectivity data for the methane oxidative coupling reaction over various catalysts in the presence of 2.6 wt.% solution of hydrogen peroxide 140

Table 3.13. Influence of hydrogen peroxide on activity of 5% La_2O_3/ CaO catalyst in the methane oxidative coupling 143

Table 3.14. Influence of hydrogen peroxide on methane oxidative coupling reaction over a 1% Au/ 5% La_2O_3/CaO catalyst 144

Table 3.15. Influence of hydrogen peroxide on methane oxidative coupling reaction over a 28% La_2O_3/ 7% SrO/CaO catalyst..... 147

NOMENCLATURE

AFROX	African Oxygen LTD
BET	The method of Brunnauer, Emmett and Teller
BTU	British Thermal Unit (1055 J)
C	concentration of reagent (mol m^{-3})
CNG	compressed natural gas
E_a	activation energy (kJ mol^{-1})
EDX	Energy Dispersive X-Ray Analysis
ESR	Electron Spin Resonance
FID	Flame Ionisation Detector
FT-IR	Fourier Transform Infra-Red Spectroscopy
GC	Gas Chromatography
K	equilibrium constant
k_i	rate constant for a forward step
k_{-i}	rate constant for a backward step
LNG	liquefied natural gas
MB (C)	carbon mass balance (%)
MB (O_2)	oxygen mass balance (%)
P	pressure (bar)
R	gas constant (8.314×10^{-3} kJ mol^{-1} K^{-1})
r_i	rate of reaction i (mol m^{-3} s^{-1})
S_i	selectivity for a product i (%)
SEM	Scanning Electron Microscopy
STY	space time yield (g kg^{-1}_{cat} h^{-1})
T	temperature (°C)
t	residence time (s)
τ	contact time (s)
te	ton equivalent
TCD	Thermal Conductivity Detector
TGA	Temperature Programmed Desorption

V	reactor volume (cm^3)
W	catalyst mass (g)
W/F	pseudo-contact time (g s ml^{-1})
X_i	conversion of reagent *i* (%)
XPS	X-Ray Photoelectron Spectroscopy
XRD	X-Ray Diffraction
Y_i	yield for a product *i* (%)

Chapter 1. INTRODUCTION

Methane is the principle constituent of natural gas (either lean natural gas or associated gas from crude oil production), landfill gas, or coalbed methane. It is also a by-product from oil refining and chemicals processing. It has potential value as a source of clean fossil energy or as a raw material provided it can be brought economically to the point of use. Remote gas has no value until a means of transportation is provided and may have negative value if it is a by-product.

The first and most obvious option for methane transportation is to build a pipeline. If the market is limited and a pipeline cannot be justified then transportation as compressed natural gas (CNG) may be a viable option. Where an ocean is in the way, shipping as liquefied natural gas (LNG) has been used extensively to bring gas to the market. The other alternative, and the one which is the subject of present work, is to convert the methane to a product - either a chemical or a fuel - which can more readily be transported. If the product is a transport or heating fuel, it must then compete with comparable fuels from conventional refining of crude oil.

Recent estimates suggest that world proven reserves of natural gas are larger than those of crude oil. Natural gas is prospected and developed in conditions rather similar to those of oil and could have an important role in the energy supply of the next decades. Whereas proven crude oil reserves seems approximately constant, those of natural gas have been regularly growing and could meet demands of consumption for 300 years at the present level (Saint Just et al.[1], 1990). However, it should be stressed that the level of the oil reserves depend on the barrel price, since it could become economical to extract crude oil in more difficult conditions (deep sea fields for instance). The discovery of new fields of natural gas can also modify the situation: important gas fields were recently discovered in the Netherlands and Namibia; their capacity could reach 20 billion ton equivalent (te).

At the present time, the world price of oil has dropped to $20/barrel and very few experts are predicting much more than a modest increase in the price for the rest of this

decade. Many of the gas reserves are in regions remote from major industrial use and this is reflected in their market price. In remote regions, such as the Middle East, where gas is either co-produced with oil far in excess of any amounts that can be used locally or where the reserves are very remote from the market, as in Siberia, the gas is very cheap. Indeed, where there are restrictions on flaring natural gas from oil production wells, the cost of recompression and re-injection into the well are such as almost to give it a negative price. By contrast, in Western Europe, gas is a highly favoured fuel, and there is a much closer balance between supply and demand, with the producers currently having the edge in negotiations.

Presently, the alternatives for catalytic transformation of methane into valuable chemical commodities can be summarised as follows:

- Routes via synthesis gas
  - Fischer-Tropsch synthesis
  - Methanol and mixed alcohols
  - Methanol to gasoline and distillates
- Direct conversion
  - Partial oxidation to methanol/formaldehyde
  - Oxidative coupling
  - Reductive coupling
  - Electrophilic conversion
  - Hydrocarbon synthesis over high-silica zeolite

Table 1.1[2] gives the current price of chemicals or liquid fuels that are traded on a large scale and which could be made from natural gas, either through the synthesis route or by a new process such as oxidative coupling to ethene. A number of general observations arise from inspection of Table 1.1.

First of all, the transport market, for gasoline and diesel fuel is enormous. The chemical product market is much smaller which means that the addition or loss of a world-scale plant can have a considerable impact on price, both upwards and downwards. On the other hand, demand for these products is growing at a steady and attractive rate, compared to the relatively static transport fuel market.

Table 1.1. Current prices (1992) of products potentially derivable from natural gas, quoted in ton equivalent (te)[2].

Product	Annual world market (10^6 te^{-1})	Annual growth rate (%)	Market price ($*$te^{-1})
Methanol	20	3 - 4	110
Ammonia	110	4 - 5	100
Ethanol	2	—	350
Ethene	65	2 - 3	450
Gasoline	730	1.4	217
Diesel fuel/kerosine	900	0.7	190

The other major factor is, of course, the price that one may obtain for the product. Table 1.1 represents a snapshot of prices in the latter half of 1992. The price of ethene in particular, has been very volatile over the past few years reflecting both world events (e.g. Gulf conflict) and the loss of large scale plants. However the values quoted here do allow some qualitative remarks to be made.

1. Ethene is clearly a product which would allow highest added value to that of natural gas. The price is based on the steam cracking of ethane or naphtha and this established process is one which would be the target of any new technology based on oxidative coupling of methane.

2. Competition in the market is keeping the price of ammonia and methanol down. Even though the capital cost of steam reforming is high, the product is sold at relatively low prices. Clearly, any new plants would be sited where the feed is cheapest. Another point to be borne in mind is that for an equivalent mass, methanol has under half the enthalpy of combustion of natural gas or gasoline. Thus, as a potential transport fuel, the equivalent price for equal heat output should be rather over \$220 te^{-1}, very much the same as the price of gasoline or diesel fuel.

3. The cost of gasoline and diesel fuel, or at least the price to the consumer, is really very low. With the price of gas in Western Europe (150-190 $*$te^{-1}) there is no hope of developing a process with an end-product of gasoline at a price anywhere near that derived from the petroleum-derived equivalent. Even in the USA, the margin is insufficiently attractive to encourage development of such a process.

The main obstacle remains the cost of transportation of natural gas over large distances. Gas has a low energy density (enthalpy/volume) compared to petroleum liquids and in addition, LNG has high capital costs associated with it. The cost of transport of liquids, such as oil or methanol, does not add more than 10% to the cost of product delivered at the point of use. LNG has an important future role to play as a method of transporting natural gas to areas where it commands a high value as a premium fuel (it was imported into Western Europe in 1990 at prices estimated between \$2.7 - \$3.3 per million BTUs). It is, however, too expensive to deliver the gas at a price attractive to the chemical industry.

From the arguments presented here, it is clear why natural gas conversion is tied in with remote, and hence cheap, supplies. The one exception may possibly be the case of ethene. Assuming that a selectivity of 80% in oxidative coupling can be maintained in a large-scale plant, and taking into account the stoichiometry of the reaction, it would take only 1.4 te of methane in the form of natural gas to make 1 te of ethene. Thus, even in areas where gas is expensive, there is quite a wide margin between the current selling price of the product compared to the cost of the natural gas required to make it. The alternative would be to make ethene at locations where gas is cheap and to ship it as it is currently traded internationally in liquid form. The boiling point of ethene is 169 K, compared with 111 K for methane but the critical temperature (282 K) is much higher than that of methane (191 K). It is shipped in refrigerated, slightly pressurised tankers at a cost that is rather lower over 10 000 km than that for LNG, say \$50 te^{-1}.

The key to an economic direct conversion process is to improve selectivity without reducing conversion per pass below practical levels. There are in any case, good reasons for believing that there is an inherent limit, of the order of 30 mol%, for the yield per pass of coupled products over oxide catalysts. Attempts to force conversion lead only to increased levels of CO and CO_2.

There are many ways to activate methane: for example, Hunter and Gesser[3] have discussed photochemical and electrochemical activation, laser-induced activation, and radiolysis, as well as catalytic activation as means to achieve this aim. The right combination has yet to be discovered.

1.1. Oxidative coupling of methane

Addition of an oxidizing agent to methane alters the thermodynamics of direct methane conversion so that a favourable equilibrium can be achieved at low temperatures. It also results in large exothermic heats of reaction which control how the process is configured. Our work concentrates on two of the more promising new direct conversion technologies: (1) oxidative coupling and (2) partial oxidation to methanol/formaldehyde. In each case, the direct conversion step is followed by oligomerization of the product to liquid hydrocarbons.

Since much of the cost of the direct conversion process lies in the handling of the large heat of reaction, it is instructive to review the thermochemistry of some of the basic reactions[6]. Heats and free energies in kilojoules per mole of methane converted are as follows:

Reaction	T, (°C)	$\Delta H°$	$\Delta G°$
Oxidative coupling			
$CH_4 + 1/2O_2 \rightarrow 1/2C_2H_4 + H_2O$	800	–139	–154
$CH_4 + 1/4O_2 \rightarrow 1/2C_2H_6 + 1/2H_2O$	800	–87	–58
$CH_4 + 2O_2 \rightarrow CO_2 + 2H_2O$	800	–801	–800
Partial oxidation			
$CH_4 + 1/2O_2 \rightarrow CH_3OH$	400	–126	–92
$CH_4 + O_2 \rightarrow HCHO + H_2O$	400	–276	–291
$CH_4 + 2O_2 \rightarrow CO_2 + 2H_2O$	400	–794	–800

These large exothermic heats become even larger as the reaction selectivity decreases. For example, if 20% of the methane in the oxidative coupling reaction is converted to CO_2, the heat of the reaction per mole of methane converted is roughly doubled. It should also be noted that the ideal stoichiometric consumption of the oxidant is atom for atom with carbon converted in the case of oxygen. If these products are oligomerized to gasoline with an average carbon number of 8, then 4 moles of O_2 are required per mole of gasoline. A 20% loss in selectivity (to CO_2)

causes a 60% increase in oxygen consumption. This is the reality that any oxidative methane conversion process faces. Because of the large enthalpy, direct oxidation reactions are associated with a large adiabatic temperature rise, unless the conversion per pass is quite low, and a high activation energy (on the order of 230-250 kJ/mol) so that it may be difficult to avoid runaway in tubular reactor.

Since the first announcement of methane oxidative coupling to produce C_2 and higher hydrocarbons by Keller and Bhasin[5] in 1982, the reaction has received world-wide attention as a potentially interesting process for upgrading natural gas. A recent article by Lunsford[6] provides an overview of the process. Methyl radicals and surface hydroxyls are considered to be the primary products of the catalytic reaction, which is generally carried out over metal oxide catalysts, modified with lithium or sodium ions at about 800°C. The methyl radicals, in the gas phase, couple to form ethane. Ethylene and higher hydrocarbons are then formed from ethane by gas-phase free-radical chemistry.

There is a strong correlation between C_2 hydrocarbon selectivity and methane conversion in oxidative coupling which seems to hold for a variety of catalysts and conditions. The yield, i.e. the product of selectivity and conversion, stays relatively constant between 15% and 25%. Selectivity is a more significant economic factor than conversion but both must be considered in reactor design[7,8,9]

In general, efforts to develop oxidative coupling catalysts have taken one of two approaches, either using alternating feed conditions (redox approach), e.g. over a reducible metal oxide, or catalysts stable under co-feed conditions, i.e. containing a non-reducible metal oxide. To be effective, redox catalysts must contain a reducible metal oxide component able to supply lattice oxygen to the reaction in the absence of gaseous oxygen.

This distinction between the two types of catalysts was first made by Keller and Bhasin (1982) of Union Carbide. Using the redox approach, they noted that of the Al_2O_3 supported metal oxides tested, only those of Sn, Pb, Sb, Bi, Tl and Mn were effective in oxidative coupling. The above oxides possessed two positive oxidation states, differing by $2e^-$, and were thus capable of supplying O^{2-} to the reaction. Since this early work, and following the results obtained by Hinsen et al.[10] under co-feed conditions, Union Carbide have appeared to concentrate more on developing effective

co-feed catalysts. This has included testing various alkaline earth/metal oxide and metal/metal oxide catalysts, together with simple perovskites, metal/molecular sieves and catalysts based on Pr/Ce oxygen carriers. Judging by the recent literature, the favoured catalysts are Ba or Sr chlorides or carbonates supported on TiO_2 or Al_2O_3, with performance enhanced by various means.

It is generally observed that the maximum yield of C_{2+} (C_2H_6 and C_2H_4) is obtained at 700-900°C, so most studies have been concentrated in this temperature range. Best yields are commonly in the order of 10-20% of methane, in the feed and a limiting figure of 30% at 1 bar pressure has been predicted by Labinger and Ott[11] on the basis of a simple kinetics analysis. The main limitation to an increased yield of C_2 products was the further oxidation of products, especially of ethene, at catalytically active sites. In addition, where there is free dioxygen in the gas phase, homogeneous reactions which are essentially out of the catalyst control, will lead to CO and CO_2.

The latter view of the catalyst's primary role is to abstract hydrogen from methane in an acid-base reaction as shown in equation (1):

$$CH_4 + O^{2-}_{(S)} \rightarrow CH_3^- + OH^-_{(S)} \qquad (1)$$

where subscript (s) refers to surface species with a low coordination number.

The acid-base mechanism[12,13,14,15] suggesting that the methane activation occurs via heterolytic cleavage on low-coordination surface M^{n+}–O^{2-} ionic pairs, appears attractive. This model has an immediate consequence for a catalyst preparation strategy, because the catalytic properties can then be linked with established acid-base chemistry. The implication of equation (1) is that the effectiveness of a catalyst depends on its strength as a base. Basicity of an oxide is strongly influenced by the cation. Among the usual methods to measure solid state basicity (i.e., acid titration using Hammett indicators[16], acidic gas adsorption, viz, carbon dioxide[17,18], carbonate decomposition temperature[19,20], binding energy calculation of O_{1s} by X-ray photoelectron spectroscopy[21], determination of the concentration of base sites by the adsorption of benzoic acid from dry heptane[12] and catalytic methods[22]), the method based on the decomposition temperature of carbonate appears quite appropriate, as measurement temperatures are close to the reaction temperature, thus providing a

rationale for the poisoning effect of the reaction by-product carbon dioxide. Such a method also helps in selecting optimum reaction temperatures. In the presence of carbon dioxide, strongly basic oxides easily form weakly basic carbonates of high thermal stability. This method is based on the assumption that the higher the carbonate decomposition temperature the higher the basicity of the corresponding oxide.

It should be recognized that the basicity as determined from the carbonate decomposition temperature refers to the bulk property and that the properties of the surface sites may differ markedly. However, within a particular series of oxides the same basicity sequence is likely to be maintained for corresponding surface sites. A major variation may be encountered in the surface properties of systems that contain impurities as second or third components due to the tendency of the impurities to segregate to the surface with a concomitant change in morphology. The basicity consideration of catalysts is restricted to the bulk basicity of the pure, monophasic oxides as determined by the thermogravimetry of carbonates[19,23,24], and is illustrated in Figures 1.1-1.3 for the carbonates of alkali metals, alkaline earths and the rare earths, respectively.

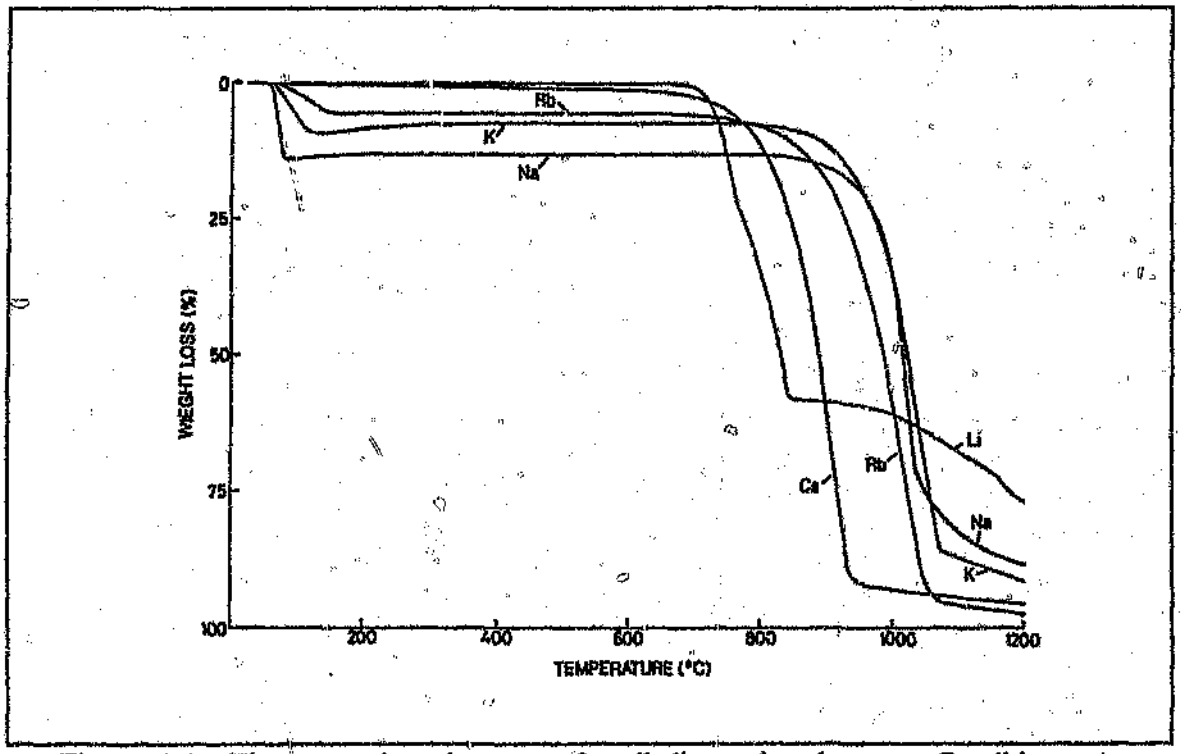


Figure 1.1. Thermogravimetric curves for alkali metal carbonates. Conditions: 4 mg samples in fused alumina cups using α-Al_2O_3 reference, 40 ml/min flow rate of air and 3°C/min heating rate[19,23].

1.1.1. Alkali metal catalysts. It is clear from Figure 1.1 that only Li_2CO_3 shows a definite decomposition around 750°C. Although the oxides of the heavier elements are expected to be more basic than Li_2O, their carbonates tend to sublime without decomposition to the oxide. This is in qualitative agreement with the catalytic activity data shown in Table 1.2 which lists a host of data, all of which are based on alkali metal catalysts in composite with various supports. Most of these catalysts are lithium-containing and, of the metals, it is only the lithium catalyst without a support which has been shown to satisfy the performance criteria. The catalytic properties have been compared on the basis of a simple assessment criterion of the sum of the methane conversion (X) and selectivity to higher hydrocarbons (S). Only those catalysts which gave a (X+S) value of at least 80, for a methane conversion of 5% or more, were selected for assessment.

The activity and selectivity of MgO modified by alkali metal cations in methane oxidative coupling was studied by Sinev et al.[25] Both the activity and selectivity decrease in the order $Li_2O/MgO < K/Cs_2O/MgO$, i.e., with increasing basicity. Cations with larger ionic radii are not able to substitute Mg^{2+}, but they presumably enter into the interstitial positions; this is evidenced by a line broadening of the X-ray diffraction patterns.

A different dependence was obtained for M_2O/Al_2O_3 by the same authors[26]. The activity and selectivity in methane oxidative coupling enhance with increasing ion radius, when going from Li to Cs. In this case, addition of an alkali cation stabilizes the cubic phase of γ-Al_2O_3 and results in aluminate formation.

A series of investigations on alkali metal oxides was performed at the Ruhr University[32,63]. The authors managed to obtain high yields of C_2 hydrocarbons at a high methane content in the reaction mixture on calcium oxide promoted with alkali metal compounds (Table 1.2). The reaction was performed at 740°C. In general, at high methane concentrations (60-70%), the samples promoted by lithium, sodium and potassium show a similar yield (12 ± 2%). But if the methane concentration is halved, a C_2 hydrocarbon yield of 17% can be obtained on a 5% NaOH/CaO catalyst at ethylene : ethane ratios close to unity. The lowest yield was obtained on catalysts promoted with transition elements, and the highest yield was found using the Na/MgO system.

Table 1.2. Activity data for alkali metal-containing catalysts[24].

Catalyst	Feed[a]	W/F[b]	T	Conversion[c]		Selectivity[d]				
	CH_4:O_2:dil	(gs/ml)	(°C)	CH_4	O_2	C_2	$C_{2=}$	C_{2+}	CO	CO_2
Li	6 : 1 : 13	0.072	850	9	30	49	29	82	5	13
$LiMg_{17}$	6 : 1 : 13	0.093	850	21	100	29	38	71	5	24
$LiMg_5$	9.6 : 1 : 4	0.22	780	13	100	42	31	73	7	20
$LiMg_{1.7}$	2 : 1 : 2	1.3	780	40	71	11	32	43	14	43
$LiMg_{4.8}$	3 : 1 : 4	5.5	770	59	85	17	36	53	2	46
$LiMgAl_{0.4}$	21 : 1 : 4	0.35	734	9	99	51	28	85	1	14
$LiMgAl_{0.8}Ni$	11 : 1 : 4	0.064	760	14	99	47	25	80	1	20
$LiMgSi_{0.3}$	11 : 1 : 4	0.24	794	15	100	33	38	81	2	17
$LiCaAl_{0.3}$	11 : 1 : 4	0.37	690	6	62	62	28	95	2	3
$LiMg_{2.7}Zn$	2 : 1 : 4.5	0.48	805	27	58	30	26	56	2	42
$LiMg_7La_{0.1}$	2 : 1 : 6.2	0.65	700	23	-	35	63	98	2	2
$LiMg_7Ce_{0.1}$	2 : 1 : 6.2	0.65	700	25	-	31	68	98	1	1
$LiMg_7Pr_{0.1}$	2 : 1 : 6.2	0.65	700	44	-	12	32	44	2	54
$LiMg_7Nd_{0.1}$	2 : 1 : 6.2	0.65	700	25	-	36	60	96	2	2
$LiMg_7Sm_{0.1}$	2 : 1 : 6.2	0.65	700	24	-	31	56	87	1	12
$LiBa_{49}$	2 : 1 : 70	2.4	800	3	-	-	-	57	3	44
$LiCa_{3.5}$	4.4 : 1 : 4	8.7	711	18	-	27	38	70	3	27
$LiLa_{1.2}$	4.4 : 1 : 4	8.8s	710	21	-	22	39	66	4	29
$LiCa_2Ti$	4.4 : 1 : 4	8.8s	707	17	-	31	40	76	2	22
Li/Sr_2TiO_4	4.4 : 1 : 4	8.8s	710	15	-	34	32	70	2	28
Li_2CO_3/Ca_{32}	9 : 1 : 3.5	0.36	740	16	91	27	41	77	-	-
K_2CO_3/Ca_{26}	9 : 1 : 3.5	0.14	740	14	91	20	42	72	-	-
Na_2CO_3/Ca_8	9 : 1 : 3.5	0.14	740	15	83	25	42	78	-	-
Na_2SO_4/Ca_{27}	9 : 1 : 3.5	0.19	740	16	92	26	45	78	-	-
K_2SO_4/Ca_{82}	9 : 1 : 3.5	0.22	740	15	85	27	42	76	-	-
Li_2SO_4/Ca_{28}	9 : 1 : 3.5	1.4	740	16	99	33	32	76	-	-
LiBe	2 : 1 : 3	0.13	760	35	80	21	44	65	-	-
$NaLaZr_2$	4 : 1 : 5	0.007	720	21	-	28	33	61	-	-
$KLaZr_2$	4 : 1 : 5	0.007	680	22	-	30	31	61	-	-

Table 1.2. (continued)

$RbLaZr_2$	4 : 1 : 5	0.007	660	23	-	31	27	58	-	-
$LiSm_4$	2.5 : 1 : 47	0.65	750	38	100	28	26	54	-	-
$NaSm_4$	2.5 : 1 : 47	0.65	750	37	100	-	-	49	-	-
KSm_4	2.5 : 1 : 47	0.65	750	38	100	-	-	50	-	-
$RbSm_4$	2.5 : 1 : 47	0.65	750	38	100	-	-	46	-	-
$CsSm_4$	2.5 : 1 : 47	0.65	750	38	100	-	-	45	-	-
$Li_{2.2}Ti$	4 : 1 : 7.5	0.16	750	10	68	46	21	73	5	22
$Na_{3.1}La$	5 : 1 : 6.5	0.65	750	26	92	32	40	77	1	21
$Na_4P_2O_7Sm_2$	2 : 1 : 3.8	0.63	828	43	-	11	35	46	-	-
$Na_2SO_4Ca_{4.8}$	5 : 1 : 3.8	0.63	800	10	26	44	33	79	7	13

Catalyst compositions have been expressed in terms of atomic ratio of the cations. Anions are not mentioned when catalyst components are likely to be essentially in an oxide form under reaction conditions, viz., salts such as hydroxide, nitrate, carbonate, acetate, etc., which decompose to oxides. Relatively more thermally stable anions such as sulphate, chloride, phosphate, etc., have been shown in the catalyst composition.

[a]CH_4:O_2:dil = volume ratio of methane : oxygen : inert diluent in the feed gas.

[b]W/F = pseudo-contact time (g s ml^{-1}) obtained by dividing catalyst mass (g) by flow rate (ml/s) under standard temperature and pressure.

[c]*Conversion* of either methane or oxygen was expressed as percent converted to products.

[d]*Selectivity* = fraction of methane converted to each particular product, viz., ethane (C_2), ethylene ($C_{2=}$), total hydrocarbons (C_{2+}), carbon monoxide and carbon dioxide, as a percentage of the total methane converted.

Other pure alkali metal carbonates are not active[27]. It is generally observed that the interaction of thermally stable carbonates with suitable supports results in destabilization of the carbonate and produces active oxide sites. For the destabilization to occur the support material should have a lower basicity. It is evident from the comparison of data that Li_2CO_3 supported on highly basic BaO ($LiBa_{49}$ in Table 1.2) gives a lower performance than the pure BaO catalyst (see Table 1.4), whereas there is a general consensus that Li/MgO being a good catalyst.

Table 1.3 gives a summary of data using alkali metal composite catalysts that also contain an element which is capable of showing variable oxidation states, viz., Fe, Co, Mn, Ti, Zr, Ce, Pr, Sn, Pb. It can be seen that with the most widely studied Li/Mg catalysts, the introduction of one of these oxides either improves the overall performance or enables the catalysts to achieve a good performance at a low temperature[28]. However, "variable valency" does not appear to be an essential criterion for effective additives. Performance enhancement of the Li/Mg catalyst in the presence of a third component consisting of the cation with the fixed valency such as B, La, Nd, etc., has also been observed by many researchers[29,30]. It is difficult to rationalize these improved selectivities in terms of the bulk basicity. Surface basicity may, however, be sufficiently different to make important contributions.

Table 1.3. Activity data of catalysts containing alkali metals and other cations showing variable oxidation states[24].

Catalyst	Feed	W/F	T	Conversion		Selectivity				
	CH_4:O_2:dil	(gs/ml)	(°C)	CH_4	O_2	C_2	$C_{2=}$	C_{2+}	CO	CO_2
$LiMg_{2.7}Mn_{0.3}$	2.1 : 1 : 4	0.48	805	39	95	22	31	53	0	47
$LiMg_{4.5}Co_{0.2}$	2.1 : 1 : 4	0.52	800	22	-	45	52	97	-	-
$LiMg_{4.5}Fe_{0.2}$	2.1 : 1 : 4	0.52	800	23	-	43	52	97	-	-
$LiMg_{4.6}Sn_{0.7}$	4.4 : 1 : 4	7.5	704	23	-	27	35	68	1	31
$LiMg_{23}Ce_{0.5}$	2 : 1 : 6	7.5	700	46	-	-	-	44	-	-
Li_2TiO	2 : 1 : 0	0.65	760	22	98	42	13	58	0	42
Li_2CeO_2	2 : 1 : 0	0.65	788	38	100	14	34	52	0	48
Li_2ZrO_2	2 : 1 : 0	0.65	794	38	100	13	32	49	0	51
$Li_{1.1}Pr_6O_{11}$	2 : 1 : 0	0.65	784	40	100	16	28	52	0	48
$LiThO_2$	2 : 1 : 0	0.65	805	31	100	13	33	53	0	47
$NaPbO/SiO_2$	31 : 1 : 4	2.4	840	6	100	47	33	87	3	10

1.1.2. Catalysts based on alkaline-earth metal oxides. Although the pure alkali metal oxide catalysts usually perform poorly (due to excessive stability and high volatility of their carbonates), the alkaline earths, especially the strongly basic ones - SrO or BaO - are capable of giving high selectivities [31,32,33]. Definite trends of increase in the performance including C_{2+} selectivities, were observed with an increase of basicity in the alkaline earth oxides in the sequence - MgO, CaO, SrO and BaO[13,19,34]. The data in Table 1.4 indicate that SrO or BaO require, for maximum performance, higher reaction temperatures (800°C or above). This can be understood in the light of the high decomposition temperatures of $SrCO_3$ or $BaCO_3$ as shown in Figure 1.2. This trend continues even in composite catalysts. Thus, the data in Table 1.4 show that, in composites with MgO-ZrO_2, CaO required 620°C for a good performance; SrO, 700°C; and BaO, 800°C[35]. These data also indicate that, with suitable additives, the strontium or barium catalysts require lower optimum temperatures than when no additive is present. This clearly demonstrates the effective role played by the additive in lowering the carbonate decomposition temperatures. Significant lowering of the decomposition temperature of $SrCO_3$ or $BaCO_3$ have been observed in the presence of suitable additives[36]. Decomposition maxima for the pure alkaline earth carbonates in flowing air are: $MgCO_3$, 420°C; $CaCO_3$, 670°C; $SrCO_3$, 860°C; and $BaCO_3$, 990°C.

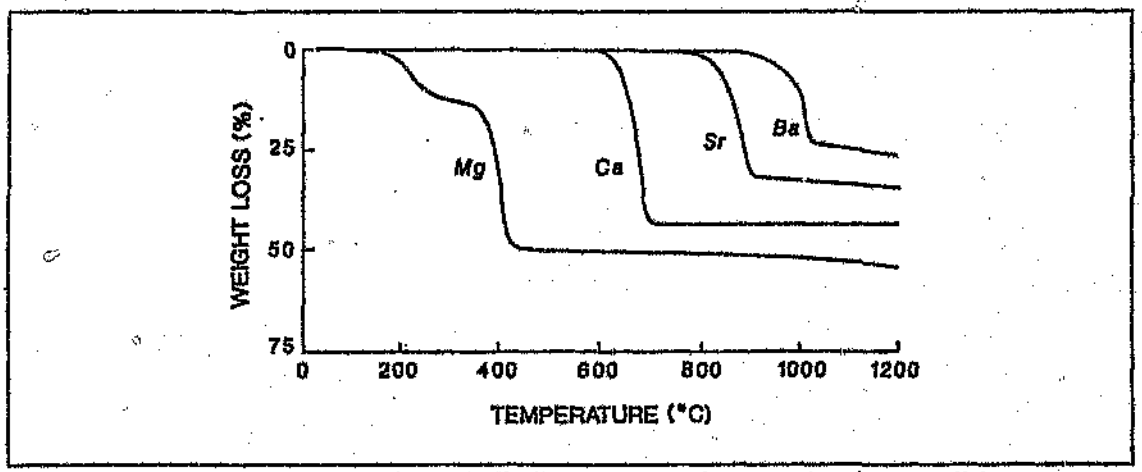


Figure 1.2. Decomposition of alkaline earth carbonates in air. Conditions: 4 mg sample in fused alumina cup using α–Al_2O_3 reference, 3°C/min heating rate and 40 ml/min air flow rate[19,23].

Table 1.4. Activity data for alkaline earth and rare earth catalysts containing no alkali metals[24].

Catalyst	Feed	W/F	T	Conversion		Selectivity				
	CH_4:O_2:dil	(gs/ml)	(°C)	CH_4	O_2	C_2	$C_{2=}$	C_{2+}	CO	CO_2
CaO	19 : 1 : 0	0.052	850	8	87	-	-	75	-	-
MgO	19 : 1 : 0	0.052	850	5	71	-	-	70	-	-
SrO	19 : 1 : 0	0.052	850	9	92	-	-	79	-	-
BaO	19 : 1 : 0	0.052	850	7	76	-	-	84	-	-
SrO	8 : 1 : 3	25	740	12	88	28	36	72	3	25
BaO	8 : 1 : 3	16	740	14	98	32	31	70	0	30
ZrO_2	4 : 1 : 5	0.065	820	18	-	20	23	53	-	-
$CaZrO_3$	4 : 1 : 5	0.065	700	20	-	32	30	63	-	-
$SrZrO_3$	4 : 1 : 5	0.065	740	21	-	34	34	68	-	-
$BaZrO_3$	4 : 1 : 5	0.065	820	20	-	33	33	66	-	-
$CaZr_{0.9}Mg_{0.1}$	4 : 1 : 5	0.065	620	19	-	33	29	62	-	-
$SrZr_{0.9}Mg_{0.1}$	4 : 1 : 5	0.065	700	23	-	35	33	68	-	-
$BaZr_{0.9}Mg_{0.1}$	4 : 1 : 5	0.065	800	22	-	32	33	65	-	-
Ca_4Ba	10 : 1 : 4	0.11	800	15	96	38	31	69	8	21
Sm	6 : 1 : 0	0.039	750	20	95	-	-	62	-	-
La	9 : 1 : 0	0.002	850	13	82	-	-	70	-	-
Sm	9 : 1 : 0	0.002	850	12	83	-	-	71	-	-
Eu	9 : 1 : 0	0.002	850	11	72	-	-	71	-	-
Ho	9 : 1 : 0	0.002	850	11	63	-	-	71	-	-
Gd	6 : 1 : 13	0.23	800	19	100	27	31	61	10	29
La	6 : 1 : 13	0.18	750	20	100	31	26	59	8	33
$MgLa_{15}$	6 : 1 : 13	0.18	750	21	100	32	28	65	9	26
$CaLa_{24}$	6 : 1 : 13	0.18	750	19	100	31	29	64	9	26
$SrLa_{53}$	6 : 1 : 13	0.18	750	21	100	35	29	69	5	26
$BaLa_{83}$	6 : 1 : 13	0.18	800	20	100	34	31	68	3	29
$Ca_{11}Ba$	5 : 1 : 6.6	0.53	800	23	100	27	34	61	-	-
La	4 : 1 : 45	0.007	750	12	27	17	47	67	18	15
$MgLa_{0.1}$	4 : 1 : 0	0.019	800	24	-	24	39	63	-	-

Table 1.4. (continued)

$CaLa_{0.06}$	4 : 1 : 0	0.025	800	24	-	35	33	68	-	-
CaY_2	10 : 1 : 0	0.018	826	11	75	27	42	69	18	13
SrY_2	10 : 1 : 0	0.018	778	15	92	36	41	77	7	16
BaY_2	10 : 1 : 0	0.018	772	15	94	38	39	77	6	18
$SrTh_2$	10 : 1 : 0	0.06	807	12	74	38	37	75	9	16
$SrLa_2$	10 : 1 : 0	0.018	759	15	100	44	34	78	4	18
PbO/22MgO	9 : 1 : 53	0.16	800	13	97	54	16	71	1	28
$PbMg_{15}$	2 : 1 : 19	0.99	800	39	100	21	26	47	1	52
$AgLa_{66}$	6 : 1 : 13	0.18	800	20	100	32	28	63	5	32
$BiMg_5$	5 : 1 : 19	1.2	800	20	90	37	25	63	0	37
$BiLa_{12}$	6 : 1 : 13	0.18	750	18	100	35	27	65	2	33

These temperatures are sensitive to the presence of carbon dioxide, increasing sharply as the partial pressure of carbon dioxide increases[19]. This explains why these catalysts are so easily poisoned by carbon dioxide.

Methane oxidative coupling on 3-7% Li_2O/MgO was described by Lunsford et al.[37] and Larkins et al.[38] For pure MgO the yield of C_2 hydrocarbon was only 7%, while for 7% Li/MgO catalyst at 720°C a 19.4% yield of C_2 hydrocarbon was attained at 50% selectivity and an ethylene : ethane ratio of 1:5. During the reaction CH_3OH and HCHO were also formed in trace quantities. However, the catalyst lost its activity with time. According to the authors, the active centres are generated through the substitution of Mg^{2+} cations by monovalent lithium, resulting in the formation of Li^+O^- defects. The catalyst was activated by a Li loading of 0.1 wt.%. At higher than 7 wt% Li loading the overall activity decreased due to the loss of surface area from Li_2CO_3 sintering, but the selectivity to C_2 remained stable at around 80%.

As illustrated in Figure 1.4 doping with Li_2CO_3 or LiOH salts resulted in a catalyst with similar activity (~20% methane conversion and ~70% C_2 selectivity). Catalysts derived from LiCl salts on MgO also had high methane conversion but the selectivity to C_2 was lower. A Li_2SO_4 derived catalyst system had low activity, while LiF derived catalyst system was found to be inactive.

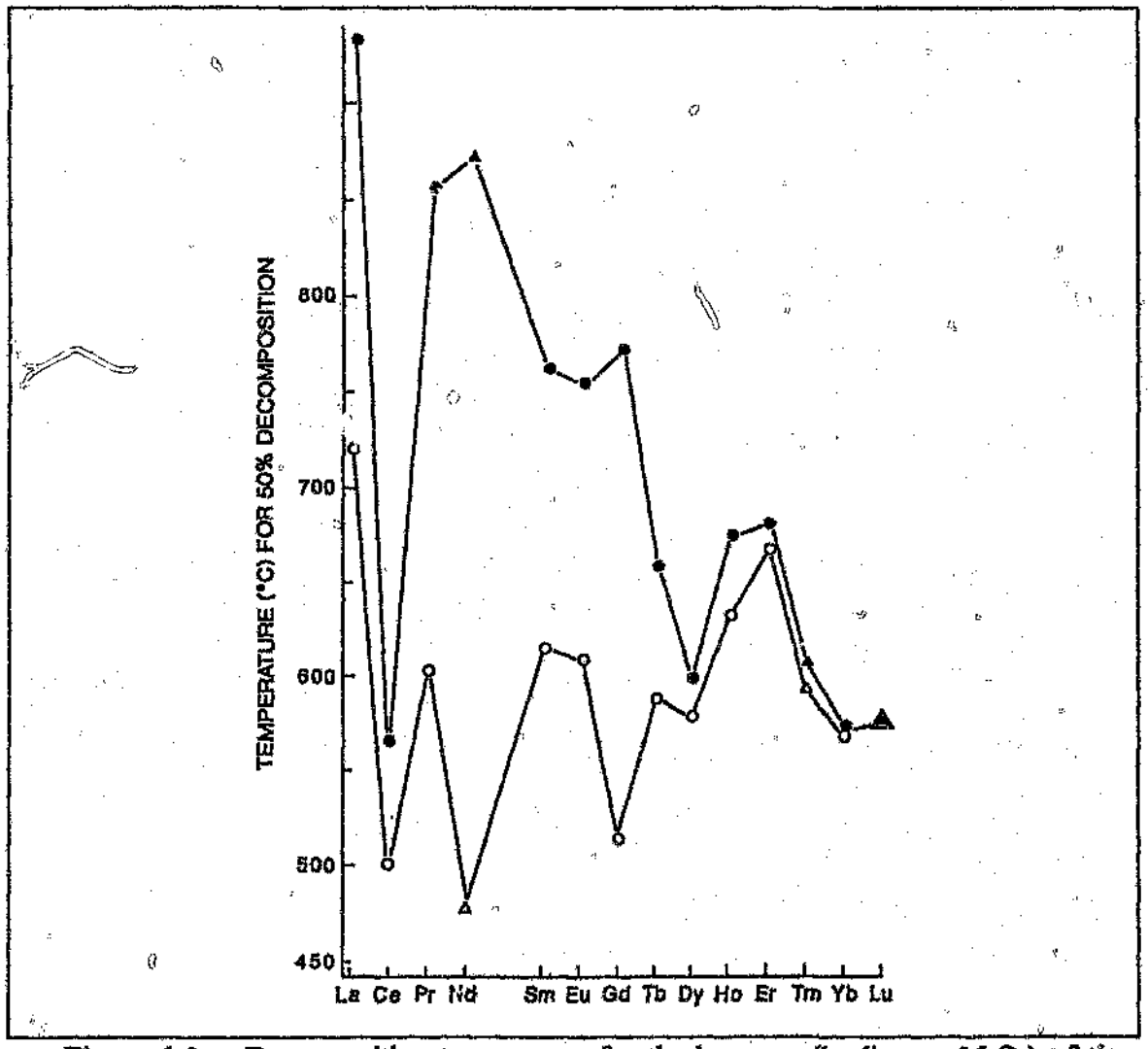


Figure 1.3. Decomposition temperature for the last step (leading to M_2O_3) of the lanthanide carbonates: (o) in nitrogen, (●) in carbon dioxide. Data for Nd, Tm and Lu[39] are shown by (Δ) in vacuum and (▲) in 500 Torr CO_2, respectively.

The activity of $Mg(OH)_2$ and of MgO based catalysts is similar, as shown in Figure 1.5, with 20-25% conversion and 70% C_2 selectivity. $Ca(OH)_2$ had a slightly lower activity (~15%), while the SiO_2 and TiO_2 based catalysts have low activity (≤ 5%) at 800°C. Although the γ-Al_2O_3 based catalyst has high activity (21%) the selectivity to C_2 is only half that of the MgO based catalyst.

The effects of doping the Li/MgO catalyst with 2 mol % transition metal relative to lithium is shown in Figure 1.6. The presence of the transition metal generally, with chromium being the exception, increased the CH_4 conversion at 800°C. In terms of C_2 selectivity manganese, iron and cobalt were most effective. A temperature dependence

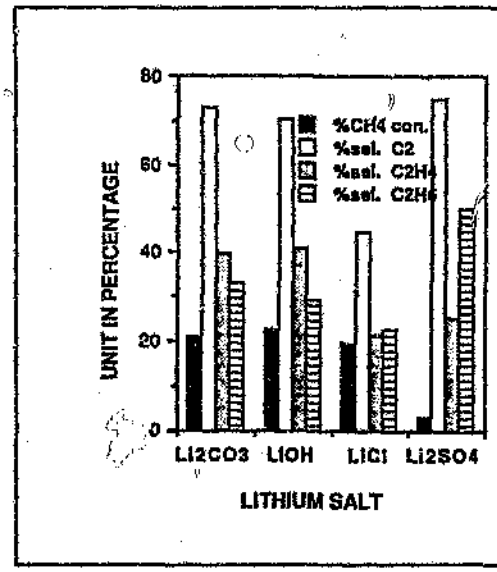


Figure 1.4. CH_4 conversion and C_2 selectivity of 6% Li/MgO catalyst systems at 800°C, as a function of Li salt[28].

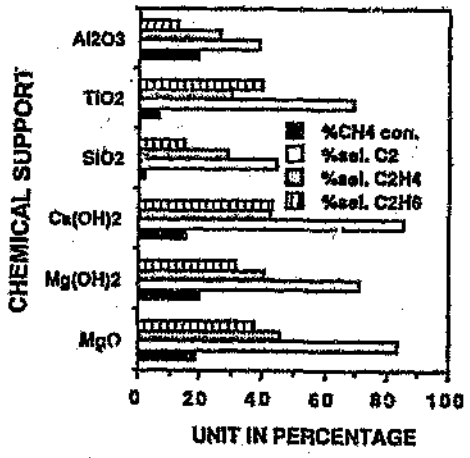


Figure 1.5. CH_4 conversion and C_2 selectivity of 6 wt. % Li (derived from Li_2CO_3) on different support[28].

study showed that the Mn doped catalyst had comparable activity to an undoped Li/MgO catalyst at 50°C lower temperature. The effect of CO on the activity of Mn/LiMgO catalyst was also determined. As the partial pressure of CO in the reactant mixture was increased the conversion of methane decreased and the selectivity to C_2

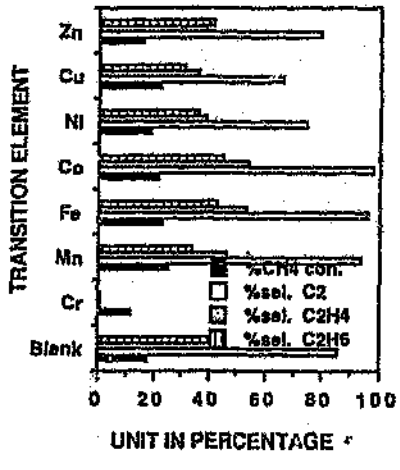


Figure 1.6. CH_4 conversion and C_2 selectivity of 6% Li/MgO doped with 2 mol. % of various dopants at 800°C[28].

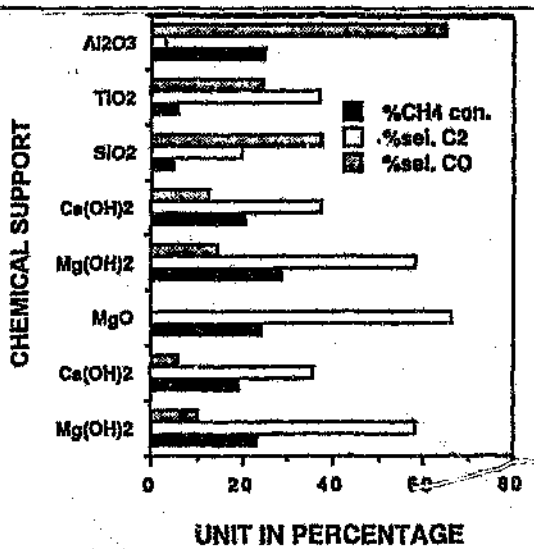


Figure 1.7. CH_4 conversion and C_2 selectivity of fresh undoped chemical compounds[28].

increased but no significant difference in product distribution was observed. When CO was present in the reactant gas it was preferentially oxidized to CO_2. This result indicates that [illegible]dation of CO only competes for surface oxygen sites with the oxidative dehydrogenation of methane. Less oxygen is available for the full oxidation of product and hence the selectivity to C_2 increased.

The selectivity to CO over a fresh catalyst was found to increase with the acidity of the surface (Figure 1.7). These surfaces are likely to generate intermediate species which preferentially oxidize to carbon oxide. The data in Figures 1.4 and 1.7 also support the view that acidic sites are not primarily responsible for the cleavage of the $H\text{-}CH_3$ bond in methane to form methyl radicals since the CH_4 conversion is higher in general for the more basic oxides.

The presence of transition metal oxides on the surface increases the concentration of surface oxygen and hence the oxidative reaction is facilitated. Since chromium oxide is a very good oxidation catalyst it results in the full oxidation of the hydrocarbons to carbon dioxide (Figure 1.6) although conversion is low.

Total oxidation to CO_2 and to CO_2 bonded in the form of stable Li_2CO_3 occurs on the active and selective Li/MgO catalyst. The excess of Li_2CO_3 in Li/MgO has practically no effect on the rate of catalyst interaction with CH_4[40]. Presumably, only that part of Li which is incorporated into the MgO structure forming the substitution type of a solid solution and, correspondingly, Li^+O^- centers, is of essential importance for the activation of the CH_4 molecule. Li^+ and Mg^{2+} ions have almost the same ion radii: 0.068 and 0.066 nm, respectively. Under catalytic conditions, the carbonate can be partially converted to LiOH according to the reaction:

$$[CO_3]_{(S)} + H_2 \leftrightarrow 2[OH]_{(S)} + CO$$

and swept away in the form of CO by the gas flow (hydrogen is always present in appreciable amounts among the reaction products).

A considerable yield of C_2 hydrocarbons was obtained by Aika et al.[31] on simple oxides of alkaline-earth metals. The C_2 hydrocarbon yield and the selectivity rose in proportion to the atomic number of the metal. Thus, when moving from MgO to BaO

the selectivity to C_2 increased from 4.4 and 11.7% for MgO to 15.2 and 45.4% for BaO, respectively.

The positive effect of water vapour on C_2 hydrocarbon yield was reported by Matsukata et al.[41] At the same time water vapour as well as CO_2 were found to provide almost no effect on the oxidative dehydrodimerization of methane on pure MgO[42].

One may consider that CO_2 and water vapour suppress the deep oxidation of methane and reaction products on one hand and block the active surface centers, producing surface carbonates and hydroxides on the other hand. The nature of the influence of carbon dioxide and water vapour will be determined by the stability of the corresponding carbonates and hydroxides on the catalyst surface, which is why it should depend on either the catalyst's nature or the reaction conditions (temperature) and the concentration of dopants introduced.

1.1.3. Catalysts based on the oxides of rare-earth elements Sensitivity of decomposition temperatures to the presence of carbon dioxide (and hence the extent of poisoning by carbon dioxide) is greatly reduced when the lanthanide carbonates, especially, the heavier carbonates are used as shown in Figure 1.3. The thermogravimetry (TGA) data in this figure was collected using a heating rate of 10°C/min. This is expected to give rise to higher apparent decomposition temperatures (by say 30-50°C) than when applying a heating rate of 3°C/min as used for the data in Figures 1.1 and 1.2. Note that Figure 1.3 refers to the decomposition of the last decomposition step which is thought to reflect the maximum basicity of the oxide. Complete decomposition of the lanthanide carbonates usually takes place in two or three regions of temperature indicating the presence of oxides with different basicity[20].

As summarized in Table 1.4 the lighter lanthanides, with the exception of those showing variable oxidation states (Ce, Pr and Tb), give good performance.

Otsuka et al.[43,44] discovered that the oxides of rare-earth elements possessed high catalytic activity. These authors investigated the catalytic properties of the whole range of rare-earth elements and reported more than 90% selectivity towards C_2 hydrocarbon formation for all but the three oxides mentioned above. These oxides, Ce, Pr and Tb,

fall outside of the general correlation. Low activity of the Ce-containing samples might be associated with the formation of a $MgCeO_2$ phase. The rate of C_2 hydrocarbon formation on Pr_2O_3 and Tb_2O_3 at T < 700°C is 1 to 2 orders of magnitude smaller than that on other oxides, but at higher temperatures and conversions they are reduced and lose their activity. As the data in Table 1.4 shows, lanthanum, samarium, europium, gadolinium, holmium and yttrium are the most suitable lanthanide catalysts. The basicity reflected in Figure 1.3 suggests La_2O_3 to be the best catalyst which may indeed be the case. However, with other oxides the performance-basicity relationship was found to be less straightforward than for the alkaline earths. Irregularities were thought to arise from the presence of other less basic sites[45,46] probably involving peroxide and superoxide species which are also present[47,48,49,50] and which promote sequental oxidation of C_{2+} hydrocarbon to CO_X. Thus, the differences in the catalytic performance of various polymorphic phases of $La_2O_2CO_3$[51], Sm_2O_3[52], etc., may be attributable to differences in basicity and/or electrical properties (e.g., oxygen-ion conductivity). When the weakly basic oxides are contacted with a layer of alkali metal carbonate, especially Li_2CO_3, strongly basic sites are generated through destabilization of Li_2CO_3 and suppression of acidic sites. Table 1.2 lists a host of examples of improved performance for alkali metal doped lanthanide catalysts. Thus, an (X+S) of about 80, commonly observed for La_2O_3, increases to 98 when it is doped with lithium[53]. Even the weakly basic cerium oxide which was shown to be a strong methyl radical absorber, once coated with alkali metal, becomes a methane coupling catalyst[54].

Interesting results were obtained by Hoffman et al.[55], who studied the catalytic properties of a CeO_2-MgO-Li_2CO_3 system in the oxidative dehydrodimerization of methane. The addition of cerium oxide to the lithium-magnesium system considerably improved the C_2 hydrocarbon yield and increased the catalyst stability under comparable conditions (Table 1.5). The cerium oxide dopant is assumed to accelerate the regeneration of active centers of lithium-magnesium catalysts.

A dopant of lithium in lanthanum oxide did not provide any noticeable effect on its catalytic properties. A slight decrease in the C_2 product yield was observed by the these authors. At the same time the composition with calcium oxide provided a high activity and selectivity towards C_2 hydrocarbons, the analogy with samarium oxide was noted. The C_2 hydrocarbons yield of 16.3% was attained at 800°C.

Table 1.5. Influence of cerium oxide dopant on the C_2 hydrocarbon yield on lithium-magnesium catalyst at 750°C [55].

Component content (wt. %)		Yield of C_2,
Li_2CO_3	CeO_2	max. (%)
4	0	9
6	0	6
5	10	10
5	50	12
5	90	10

The influence of samarium oxide promotion with alkali and alkaline earth metals studied by Roos et al.[56] showed that a calcium oxide dopant increased both yield and selectivity of C_2 products on Sm_2O_3. However, a lithium dopant worsened the catalytic properties of samarium oxide prepared in this work. The authors considered the inhibiting effect of lithium to be caused by its influence on the structural transformation of the cubic form of samarium oxide to a monowedge one, which, according to the reported data, is less active.

A detailed study of the Sm_2O_3-CaO system was also reported by Sokolovskii et al.[57] These authors considered a catalyst containing a mixture of two phases of samarium

Table 1.6. Comparison of catalytic properties of samarium-calcium catalysts of various phase contents (5% Sm_2O_3/CaO, 90% CH_4, 10% O_2, $\tau = 0.1$s)[57].

Structure of Sm_2O_3	$BET_{S.A.}$ (m^2/g)	T (°C)	CH_4 conversion(%)	Yield(%) C_2H_4	Yield(%) C_2-C_4	C_2-C_4 selectivity	O_2 conversion(%)
Cubic	4.1	700	4.3	0.1	1.5	36.9	49
		750	5.5	0.5	2.5	46.2	53
Monowedge	4.2	700	4.3	0.1	1.6	38.1	56
		750	7.8	1.0	3.8	48.9	72
Monowedge +	4.3	700	8.9	0.8	4.8	54.6	78
cubic		750	13.0	2.7	8.8	66.0	93

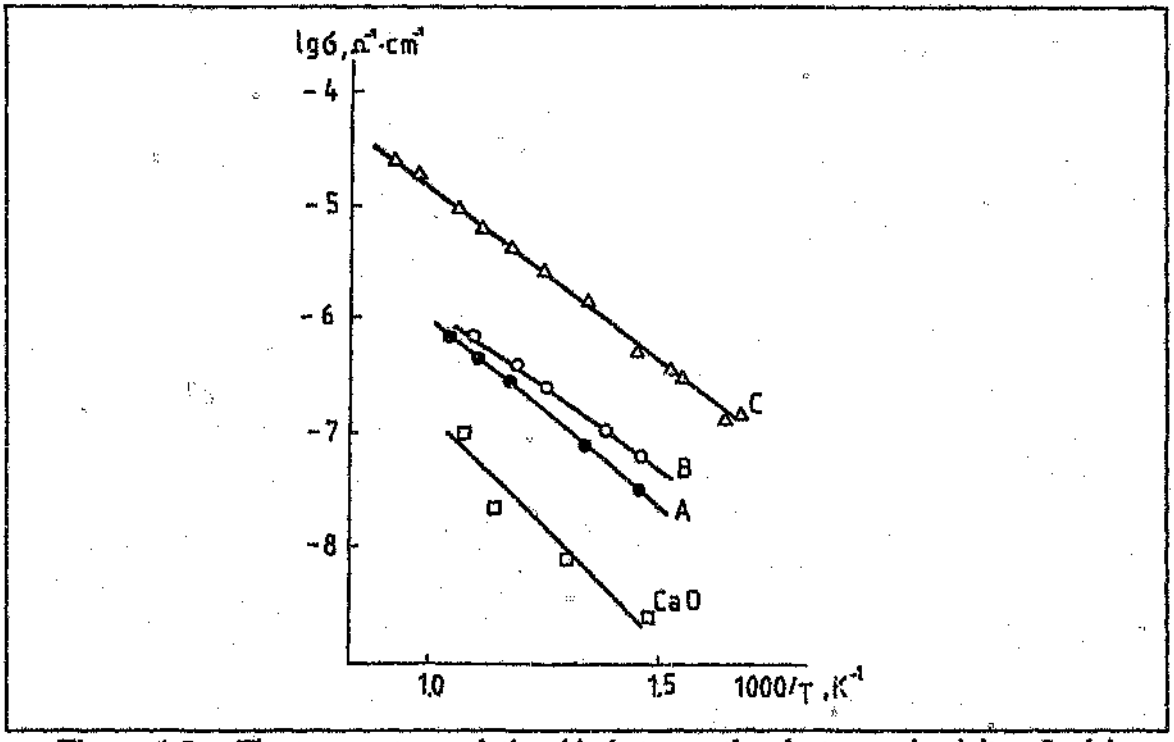


Figure 1.8. The temperature relationship between the electroconductivity of calcium oxide and samarium-calcium 5% Sm_2O_3/CaO systems with different samarium oxide structure (A-cubic, B-monowedge, C-cubic + monowedge)[57].

oxide – cubic and monowedge – to be the most active and selective (Table 1.6).The higher selectivity of this catalyst is likely to be provided by the high mobility of its oxygen, which was characterized by the ionic electroconductivity of the catalyst (Figure 1.8).

The highest reaction rate for Sm_2O_3 (828 μmol $s^{-1}g^{-1}$) at 750°C has been found by Otsuka et al.[43] The selectivity increased as the temperature increased in the 600-800°C interval. Some side reactions occured at higher temperatures. Many catalysts are not stable under the reaction conditions because of both a loss of active component and overheating in the course of this highly exothermic process. Often the most efficient catalysts can function only if mixtures with low CH_4 and O_2 concentrations are employed. As a result, the C_2 product concentrations in the reaction mixture turn out to be low and this prevents their isolation by using conventional methods.

1.1.4. Other oxide catalysts. Total oxidation proceeds via redox processes on the vast majority of transition element oxides with lattice oxygen of the catalyst being involved. Among those catalysts which are not represented by the oxides of alkali and alkaline earth elements manganese containing systems appear to be the most efficient.

Pure oxides are catalysts used for the total oxidation of methane, but when supported or entering into the composition of compounds, they can become active and selective catalysts for the oxidative coupling reaction. For the Mn/SiO_2 catalyst the S-value was found to be 27%[58]. A modification of the catalyst by sodium essentially increases both the activity and selectivity. This is associated with a specific interaction between sodium and manganese and give rise to a non-stoichiometric β-$Na_{0.7}MnO_2$ phase. The formation of the α-$NaMnO_2$ phase is also likely[59]. The 13% Na/ 17% MnO/SiO_2 composition was the most efficient, and when present, CH_4 conversion was found to be 45% at S = 60-65% (850°C, contact time = 0.5 s, $CH_4/O_2 = 2$). For a $NaMnO_4/MgO$ catalyst an 18.8% yield was obtained at 900°C under the same reaction conditions.

Thomas et al.[60] investigated the $Pb_2Mn_2Si_2O_9$ catalytic system (centhrollite). The authors obtained a 20.5% yield of C_2 products at 68% selectivity at 800°C and using a reaction mixture containing methane and oxygen at a 1:1.13 ratio diluted with dinitrogen.

Rather low C_2 hydrocarbon yields were recorded for lead and bismuth oxides, if the latter were not combined with a basic support. The yields were approximately 5%[61,62] for either individual oxides or a mixture of the oxides supported on Al_2O_3. At the same time, as was mentioned above, the yields of C_2 hydrocarbons on alkaline earth oxides promoted with these elements exceeded 20%, confirming the important role of the basic component in these catalysts.

Rather low yields (less than 1%) were obtained either on lead compounds like salts of oxygen-containing acids (molybdenium, tungsten, chromium, phosphorus, sulfuric acids)[63]. Thus, the most efficient catalysts for the oxidative dehydrodimerization of methane under continuous conditions are systems based on the oxides of alkaline earth and rare earth elements.

Oxides of lead are not more basic than MgO, and the support materials, e.g., silica or alumina, have little activity themselves. Thus, simple acid-base properties seem unable to account for these catalytic properties, unless perhaps synergy with the support leads to an unusual surface morphology that produces a high density of oxide sites with low coordination number. The bulk basicity is then inadequate to describe the basic property of the surface. This possibility is supported by the data of Jezl et al.[64] where the performance of a PbO/SiO_2 catalyst remained virtually unchanged after introduction of sodium in the formulation. The work of Sokolovskii et al.[12,34] with composite PbO-MgO catalysts showed a direct relationship between the density of surface basic sites and the rate of hydrocarbon formation. The dependence of catalytic properties on the concentration of base sites, found from adsorption of benzoic acid, was examined using a lead-magnesium system with acidic (P, W) and alkaline (Li, Na, K) additives. These additives were introduced into Pb-Mg catalysts via impregnation of the binary system with solutions of nitrates of alkaline elements or of $(NH_4)_{10}W_{12}O_{41} \cdot nH_2O$ and $(NH_4)_3PO_4 \cdot 3H_2O$. The results obtained are shown in Figure 1.9 which shows that an increase in the concentration of basic sites leads to an increase in the overall rate of methane conversion as well as in the rate of C_{2+} products formation.

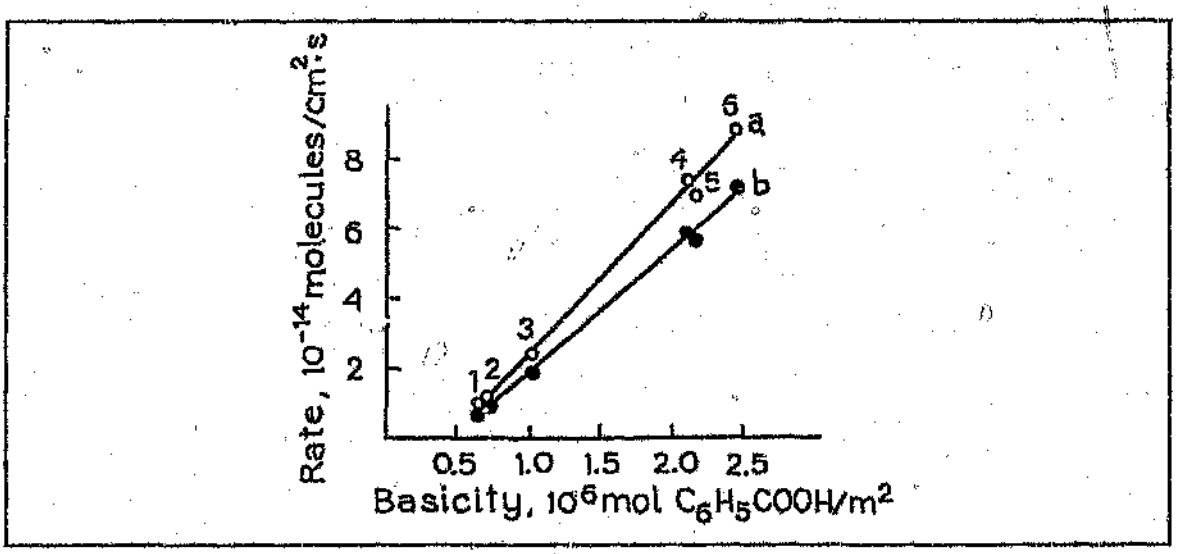


Figure 1.9. Rates of methane conversion (a) and dehydrodimerization (b) on PbO-MgO catalysts with additives: (1) 5% P, (2) 5% W, (4) 5% Na, (5) 5% Li, (6) 5% K and (3) without additives[12].

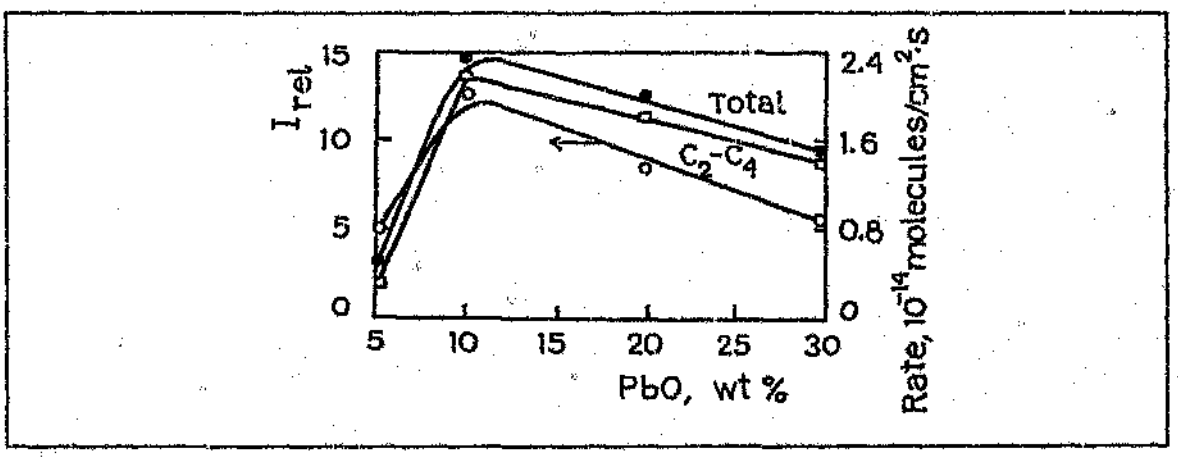


Figure 1.10. Concentration of acceptor sites (I_{rel}) and rate of methane dimerization on PbO-MgO catalyst [12].

As found by ESR, addition of lead oxide results in the appearance of one-electron acceptor sites in the catalyst which may be attributed to a compressed tetrahedron, $(PbO_4)^{5-}$. A clear correlation was found between the rate of methane conversion to C_{2+} hydrocarbons and the concentration of acceptor sites which depended upon the content of lead oxide in the catalyst (Figure 1.10).

Again, the performance of optimum PbO-MgO catalysts was shown to be further improved as its basicity were boosted by alkali metal promotion. A similar relationship between basicity and performance has also been reported for alkali metal promoted Bi-Mn catalysts[65].

These results are probably close to the limit for the high temperature oxidative coupling of methane. Labinger[66] estimated the limiting yield of C_2 hydrocarbons in this reaction accounted for the ratio of the rate constants of methane, ethane and ethylene conversion and for the possibility of improvement in the activity of the catalysts, which has an influence on the rate ratio of methane activation and the oxidation of the intermediate and final products. For a reaction mixture pressure of 1 bar the estimate of the limit yield value is ca. 30%.

1.2 Mechanism of the oxidative coupling of methane

The successful achievements in the development of the process of methane oxidative coupling stimulated a great number of studies on the mechanism and kinetic regularities of this reaction. Most attention was paid to the mechanism of methane activation and the states of oxygen participating in the reaction. The general scheme for the product formation in dimerization and deep oxidation, and the description of the process and its kinetics for some specific catalysts have also been considered. A survey of the current literature in this area is given below.

1.2.1. Isotope exchange studies. A number of investigations have utilized isotopically labeled gases to study the reaction and the reaction mechanism[67,68,69,70,71]. These investigations have used labeled oxygen, ^{13}C labeled methane and CH_4/CD_4 mixtures in the feed gas. The reaction has been examined under steady-state conditions using unlabeled and labeled reactants. One of the benefits of using isotopically labeled reactants under steady-state reaction conditions is that component concentrations remain unchanged, so the isotopic yields can be determined by monitoring the molecular ion fragments for the labeled and unlabeled species of each reactant or product. The transients provide information about the relative lifetimes of surface species, or in the case of oxygen, the importance of lattice oxygen versus adsorbed or gas-phase oxygen.

Two different routes have been proposed for the formation of the methyl radicals required for dimerization to ethane (equation (1)). The first involves the removal of a proton from a methane molecule on the basic site, leading to the formation of a methyl anion[34,46,72] on the surface of the catalyst - a carbanionic fragment $M\text{-}CH_3$. Subsequent transfer of the electron from the methyl anion and the proton to acceptor sites on the catalyst and the oxygen results in the formation of a methyl radical and water via an OH intermediate.

In this scenario, the activation of methane in both the oxidative coupling reaction and the deuterium exchange reaction involves the same initial step, i.e., heterolytic splitting of the C-H bond. The rate of methane conversion in the coupling reaction can

therefore be expected to correlate with the catalyst's ability to effect such splitting as measured by the rates of deuterium exchange.

The second proposed mechanism for the methyl radical formation involves the formation of a transition complex consisting of the adsorbed methane molecule and the surface oxygen[73,74,75], which subsequently dissociates yielding a methyl radical and water (or its precursor, e.g., OH). In this case the rate of methane conversion under the oxidative coupling conditions can be expected to correlate with the ability of the catalyst to activate oxygen as measured by the rates of the O-O bond splitting reaction. Such a correlation could be expected to be more pronounced under the conditions of high oxygen conversion, i.e., where the methane conversion rate may be limited by the availability of oxygen[27].

The dependence of the rate of methane oxidative dehydrodimerization on oxides of alkaline earth metal based catalysts on the concentration of base sites was studied by Sokolovskii et al.[12,76] The dehydrodimerization rates were compared with the concentration of one-electron sites and the rate of the CH_4/CD_4 isotope exchange.

The authors observed heterolytic activation of methane on magnesium oxide containing low-coordination sites experimentally and suggested a possible role of this process in oxidative dehydrodimerization of methane.

After a high temperature treatment of magnesium oxide under vacuum, which results in the appearance of low-coordination sites, the catalyst revealed activity towards H/D isotope exchange of methane. However, oxygen adsorption led to complete deactivation of the sample, most probably, by destroying low-coordination sites. However, as has already been mentioned, heterolytic activation of methane occurs only on low-coordination sites. To verify whether low-coordination sites which can activate methane are retained during the course of oxidative dehydrodimerization in a methane-oxygen mixture, they studied the CH_4/CD_4 isotope exchange directly in the process.

The results obtained are listed in Table 1.7. As can be seen in the table, on magnesium oxide a rather fast isotope exchange occurs, which may provide evidence for a high concentration of low-coordination sites on its surface.

Table 1.7. Comparison of rates of oxidative dehydrodimerization (W_d) and CH_4/CD_4 isotope exchange (W_o) under catalytic conditions on alkaline earth metal oxides. Conditions: T = 800°C, the reaction mixture composition: 45% CH_4, 45% CD_4 and 10% O_2 [76].

Catalyst	Rate, 10^{-14}molec./cm^{2}s			Basicity	$\frac{W_d}{W_o + W_d}$
	W_o	W_d	Overall	10^6mol C_6H_5COOH/m^2	
MgO	1.9	0.09	1.99	2.14	0.045
CaO	12.0	6.50	18.5	7.94	0.350
10% PbO/MgO	1.1	0.50	0.8	1.11	0.625

As has been mentioned, the isotope exchange in methane on magnesium oxide begins at fairly low temperatures[77]. From this fact it follows that the primary heterolytic activation of methane is relatively fast. The total rate of methane activation (defined as a sum of observed rates of exchange and dimerization) increases with increasing basicity of the oxide, which is in agreement with the conclusion about heterolytic activation of methane at catalyst base sites. At the same time, the rate ratio exchange and dimerization is different for different oxides (Table 1.7).

A simultaneous occurrence of exchange and dimerization indicates that the rate of the primary activation of methane is high enough to provide a pathway for both reactions.

It seems likely that the step of the heterolytic dissociation of methane on MgO is fast and reversible and that the rate-determining step is the splitting of a M-CH_3 bond. The binding energy in this case can reach 200-300 kJ/mol. Note that the presence of an inorganic anion at the metal ion makes the M-CH_3 bond stronger[78]. The dependence of the dimerization rate on the concentration of acceptor sites (Figure 1.10) allows one to suppose that the rupture of this bond is accompanied by an electron transfer from the anionic fragment into the catalyst acceptor site. Due to an increase in the proportion of acceptor sites when passing from pure magnesium oxide to the lead-magnesium system, the difference between the rates of isotope exchange and oxidative dimerization has a tendency to decrease (Table 1.7). However, the rate of the exchange is still much higher than that of dimerization.

The methane oxidative coupling reaction over $MnMoO_4$ and alkali (Li, Na, K) promoted $MnMoO_4$ at 700°C using $^{12}CH_4/^{13}CH_4$ transient isotopic labeling experiments under steady-state reaction conditions was investigated by Ozkan et al.[79]

The highest activity was observed over the Na-promoted catalyst, but the most selective catalyst for C_2 hydrocarbon formation was the K-promoted catalyst. When the conversion level was kept at 10% for all catalysts, a selectivity of 41% to C_2 hydrocarbon was obtained for the K-promoted catalyst as compared to 1, 3 and 10% for the unpromoted $MnMoO_4$, and the $MnMoO_4$ catalysts promoted with Li and Na, respectively.

Methane was found to quickly decay in ^{12}C content during the gas-phase holdup time and no ^{12}C labeled methane molecules were later detected. The short residence time of methane on the surface could indicate weak interaction, or irreversible adsorption leading to further reaction.

The unlabeled carbon monoxide rapidly disappeared for the Li- and Na-promoted $MnMoO_4$ catalyst, but did remain longer on the catalyst surface for unpromoted and K-promoted $MnMoO_4$ catalyst. The longer residence time of carbon monoxide for these catalysts may indicate a multi-step reaction, strong adsorption, or readsorption of the product or a longer residence time for a species which is a precursor for carbon monoxide. To determine which one of these possibilities would explain the observed data better, the authors ran a series of experiments where pulses of CO and CO_2 were passed over the catalyst under the. reaction conditions. The results showed no difference in the length of time that it took for these species to go through the system. These experiments indicated that it is not the interaction of the final products, i.e., CO and CO_2 with the surface that leads to a slower decay behavior for CO, but the surface residence of another species which could be a precursor to CO.

This observation, combined with the observation that the ^{12}CO signal did not decline to zero within the gas-phase hold-up time over $K/MnMoO_4$, leads to the suggestion that methyl radicals have a longer "surface life" over $K/MnMoO_4$ and that CO, in part, is formed from the methyl radicals. The longer surface residency of methyl radicals, on the other hand, could allow for the desorption and subsequent coupling of these species into C_2 hydrocarbons leading to higher C_2 selectivity.

The persisting non-zero signal observed for unlabeled ethane and ethylene suggests that the sites which provide a longer "surface life" for methyl radicals are the controlling factors for increased C_2 selectivity. This observation combined with the increased selectivity of the K-promoted catalyst for C_2 species implies that these sites, which appear to be associated with the formation/retention of methyl radicals, could be attributed to the presence of K-promoter ions on the surface of the catalyst.

It is interesting to analyze the data reported by Cant et al.[80] In this work the kinetic isotope effect was studied in the methane oxidative coupling reaction on Li/MgO, Sm_2O_3 and $SrCO_3$ and simultaneously the rate of CH_4/CD_4 exchange was measured. An evident inverse correlation between the isotope effect and the ratio of isotope exchange and dimerization rates is observed. The lowest kinetic isotope effect is found for $SrCO_3$, and the greatest ratio of exchange and dimerization rates is observed for the same catalyst. Since it is a considerably strong base, strontium carbonate is assumed to heterolytically dissociate the C-H bond in methane rather easily. At the same time it is likely to contain rather a small amount of accepting centers. Consequently the partial reversibility of the first stage:

$$CH_4 + M^{2+}O^{2-} \leftrightarrow CH_3^- M^{2+} + H^+O^{2-}$$

is provided and, thus, the observed value of the isotope effect is decreased and the ratio of exchange and dimerization rates increased. This is also supported by the recorded decrease of the isotope effect when the dioxygen conversion is raised. Under the conditions of raised dioxygen conversion the catalyst is more reduced. This slows down the relative rate of second stage:

$$CH_3^- M^{2+} \rightarrow CH_3^{\cdot} + M^{2+}$$

and increases the reversibility of the first stage and diminishes the value of the observed kinetic isotope effect.

In summary, the mechanism of the heterolytic activation of methane in the process of oxidative coupling seems to be more likely for several reasons: (1) The catalysts for oxidative coupling are either solid bases or contain basic elements as a rule. In these

systems the isotope exchange in methane proceeds rather easily at low temperatures. (2) The presence of radical centers on the catalyst at high temperatures, assisted by molecular oxygen, may provide the chain processes and gives rise to decreased selectivity, which can be avoided by heterolytic activation. (3) The low activation energies are typical of radical detachment and thus it is difficult to explain the observed high activation energies for the oxidation coupling reaction. The activation energy for a heterolytic mechanism may be rather high.

1.2.2 Kinetics of the oxidative coupling of methane. The oxidative coupling of methane is usually carried out in the presence of catalysts and requires temperatures up to 900°C. At these temperatures, non-catalytic reactions in the gas phase, however, play an essential role in the formation of higher hydrocarbons. It is generally accepted that the most widely studied alkali metal/alkaline earth metal oxide and the rare earth metal oxide catalysts can act as a methane activator and in particular as a producer of methyl radicals, with the subsequent reactions taking place in the gas phase.

The reaction between methane and oxygen is certainly initiated on the catalytic surface, but there is still some debate as to whether the methyl species produced by dissociative adsorption of methane continue to react on the surface or whether they are completely desorbed as radicals into the gas phase before a further reaction goes on.

In a recent review, Lunsford[6] has pointed out the importance of branched chain reactions in the gas phase with respect to the generation of methyl radicals. Consequently, he proposed that catalysts might be an important initiator of the chain reaction, but not a major source of methyl radicals. Kinetic models based on the free-radical mechanism have been set up in order to understand the role played by the gas-phase reactions and the interaction between the gas-phase reactions and the reactions on the catalyst surface.

Kimble and Kolts[81] have set up a model consisting of a methane activation through a hydrogen abstraction by the catalyst surface and a number of subsequent free-radical reactions among the hydrocarbons without involving any oxygen-containing species. With this model, the methane conversion as well as C_{2+} selectivities were calculated. Good agreement between the model prediction and experiments was obtained for the

dependence of conversion and selectivities with time. Naturally, the dioxygen conversion and the CO_x selectivities could not be calculated.

A kinetic model for the gas phase reaction. The studies of Baerns et al.[82] and Marin et al.[83] have attempted to establish a detailed kinetic model for the oxidative coupling of methane at atmospheric pressure in the gas phase. In their studies they attempted to determine a set of reliable Arrhenius parameters for the elementary radical reactions involved under these conditions by the careful selection from data bases and by means of a regression analysis of experimental data. The important chains, branched or non-branched, which lead to the formation of the major products, were identified.

From the literature, it is known that, in principle, several hundred elementary reaction steps entailing approximately 40 species may occur in the oxidative conversion of methane. To reduce these numbers to values that can be simulated by available computer programs, it was required to select the important steps and species by taking into account the existing experimental evidence. A detailed analysis of previously reported reaction models, in particular those presented by Baerns (1990), leads to a network consisting of 66 reactions among the 20 retained species, as shown in Table 1.8.

The reaction network includes 20 species, out of which 11 are molecules: dihydrogen, water, hydrogen peroxide, dioxygen, methane, methanal, carbon monoxide, carbon dioxide, ethyne, ethene and ethane; and 9 are radicals: hydrogen and oxygen atoms, OH, HO_2, CHO, and CH_3O radicals, and methyl, vinyl, and ethyl radicals.

The elementary reactions considered can be grouped as follows:

(a) primary initiation, reactions 1 and 2

(b) methyl radical generation, reactions 3-6, in which a radical abstracts a hydrogen atom from methane forming a methyl radical

(c) methyl radical oxidation to CH_3O and CH_2O, reactions 7-10

(d) methyl radical coupling to C_2 components, reactions 11-13

(e) oxidation of CH_3O and CH_2O to carbon monoxide and dioxide, reactions 14-28

(h) hydrogen-oxygen reactions, reactions 50-66

Table 1.8. Elementary reaction steps and their respective kinetic parameters ($k = AT^n \exp(-E_a / RT)$) as used for the simulation of the gas-phase oxidative coupling of methane [82,83].

no.	Reaction	A ($m^3 mol^{-1} s^{-1}$)	n	E_a (kJ mol^{-1})
1	$CH_4 \rightarrow CH_3 + H$	0.370E+16	0.0	434.00
2	$CH_4 + O_2 \rightarrow CH_3 + HO_2$	0.746E+07	0.0	192.78
3	$CH_4 + H \rightarrow CH_3 + H_2$	0.220E–01	3.030	43.62
4	$CH_4 + O \rightarrow CH_3 + OH$	0.120E+02	2.168	62.65
5	$CH_4 + OH \rightarrow CH_3 + H_2O$	0.132E+09	2.400	33.71
6	$CH_4 + HO_2 \rightarrow CH_3 + H_2O_2$	0.598E+08	0.0	95.98
7	$CH_3 + O_2 \rightarrow CH_3O + O$	0.781E+09	0.0	124.80
8	$CH_3 + O_2 \rightarrow CH_2O + OH$	0.536E+08	0.0	101.00
9	$CH_3 + OH \rightarrow CH_3O + H$	0.864E+09	0.0	75.21
10	$CH_3 + HO_2 \rightarrow CH_3O + OH$	0.804E+08	0.0	0.00
11	$CH_3 + CH_3 \rightarrow C_2H_6$	0.125E+08	0.0	0.00
12	$CH_3 + CH_3 \rightarrow C_2H_5 + H$	0.940E+08	0.0	108.24
13	$CH_3 + CH_3 \rightarrow C_2H_4 + H_2$	0.100E+11	0.0	134.00
14	$CH_3O \rightarrow CH_2O + H$	0.158E+15	0.0	115.00
15	$CH_3O + O_2 \rightarrow CH_2O + HO_2$	0.660E+05	0.0	10.90
16	$CH_2O + O_2 \rightarrow CHO + HO_2$	0.200E+08	0.0	163.00
17	$CH_2O + H \rightarrow CHO + H_2$	0.250E+08	0.0	16.70
18	$CH_2O + O \rightarrow CHO + OH$	0.350E+08	0.0	14.70
19	$CH_2O + OH \rightarrow CHO + H_2O$	0.580E+08	0.0	5.00
20	$CH_2O + HO_2 \rightarrow CHO + H_2O_2$	0.100E+07	0.0	33.50
21	$CH_2O + CH_3 \rightarrow CHO + CH_4$	0.241E–01	2.810	22.65
22	$CHO + M \rightarrow CO + H + M$	0.500E+16	–2.140	85.50
23	$CHO + O_2 \rightarrow CO + HO_2$	0.410E+07	0.0	0.00
24	$CHO + CH_3 \rightarrow CO + CH_4$	0.120E+09	0.0	0.00

Table 1.8. (continued)

25	$CO + O_2 \rightarrow CO_2 + O$	0.250E+07	0.0	200.00
26	$CO + O + M \rightarrow CO_2 + M$	0.620E+03	0.0	12.60
27	$CO + OH \rightarrow CO_2 + H$	0.440E+01	1.500	−3.10
28	$CO + HO_2 \rightarrow CO_2 + OH$	0.390E+09	0.0	103.88
29	$C_2H_6 \rightarrow C_2H_5 + H$	0.500E+17	0.0	372.00
30	$C_2H_6 + O_2 \rightarrow C_2H_5 + HO_2$	0.400E+08	0.0	213.00
31	$C_2H_6 + H \rightarrow C_2H_5 + H_2$	0.118E−02	3.500	20.33
32	$C_2H_6 + OH \rightarrow C_2H_5 + H_2O$	0.142E+05	1.040	7.60
33	$C_2H_6 + HO_2 \rightarrow C_2H_5 + H_2O_2$	0.290E+06	0.0	62.50
34	$C_2H_6 + CH_3 \rightarrow C_2H_5 + CH_4$	0.550E−06	4.018	34.87
35	$C_2H_5 + HO_2 \rightarrow CH_3 + CH_2O + OH$	0.240E+08	0.0	0.00
36	$C_2H_5 + OH \rightarrow C_2H_6 + O$	0.300E+06	0.0	25.00
37	$C_2H_5 \rightarrow C_2H_4 + H$	0.596E+14	0.0	167.66
38	$C_2H_5 + O_2 \rightarrow C_2H_4 + HO_2$	0.588E+07	0.0	26.14
39	$C_2H_4 + O_2 \rightarrow C_2H_3 + HO_2$	0.281E+07	0.0	144.55
40	$C_2H_4 + H \rightarrow C_2H_3 + H_2$	0.150E+09	0.0	42.70
41	$C_2H_4 + O \rightarrow C_2H_3 + OH$	0.130E+06	0.630	5.70
42	$C_2H_4 + OH \rightarrow C_2H_3 + H_2O$	0.612E+08	0.0	24.70
43	$C_2H_4 + CH_3 \rightarrow C_2H_3 + CH_4$	0.199E+07	0.0	51.46
44	$C_2H_4 + O \rightarrow CH_3 + CHO$	0.127E+03	1.489	1.80
45	$C_2H_4 + OH \rightarrow CH_3 + CH_2O$	0.830E+07	0.0	0.00
46	$C_2H_3 + C_2H_6 \rightarrow C_2H_4 + C_2H_5$	0.600E−03	3.300	43.90
47	$C_2H_3 \rightarrow C_2H_2 + H$	0.121E+16	0.0	176.44
48	$C_2H_3 + O_2 \rightarrow C_2H_2 + HO_2$	0.198E+06	0.0	0.00
49	$C_2H_2 + O_2 \rightarrow CHO + CHO$	0.341E+07	0.0	143.36
50	$O_2 + H \rightarrow O + OH$	0.156E+12	0.910	140.85
51	$O_2 + H + M \rightarrow HO_2 + M$	0.200E+07	0.800	0.00
52	$O + HO_2 \rightarrow O_2 + OH$	0.200E+08	0.0	0.00
53	$O + H_2 \rightarrow OH + H$	0.150E+02	2.0	31.60
54	$O + H_2O \rightarrow OH + OH$	0.460E+04	1.300	71.50

Table 1.8. (continued)

55	$O + H_2O_2 \rightarrow OH + HO_2$	0.631E+07	0.0	20.75
56	$OH + H_2 \rightarrow H_2O + H$	0.100E+03	1.600	13.80
57	$OH + H + M \rightarrow H_2O + M$	0.220E+11	2.000	0.00
58	$OH + HO_2 \rightarrow H_2O + O_2$	0 200E+08	0.0	0.00
59	$OH + H_2O_2 \rightarrow H_2O + HO_2$	0.175E+07	0.0	1.33
60	$HO_2 + H \rightarrow O_2 + H_2$	0.250E+08	0.0	2.90
61	$HO_2 + HO_2 \rightarrow O_2 + OH + OH$	0.200E+07	0.0	0.00
62	$HO_2 + H_2 \rightarrow H_2O_2 + H$	0.300E+08	0.0	109.00
63	$OH + OH + M \rightarrow H_2O_2 + M$	0.320E+11	-2.000	0.00
64	$HO_2 + H \rightarrow OH + OH$	0.150E+09	0.0	4.20
65	$H_2O_2 + H \rightarrow OH + H_2O$	0.100E+08	0.0	16.60
66	$H + H + M \rightarrow H_2 + M$	0.180E+07	1.000	0.00

A common practice in combustion studies is to use the modified Arrhenius equation for the rate coefficient of the elementary steps, i.e.,

$$k = AT^n \exp(-E_a/RT) \qquad (1\text{ a})$$

with three temperature-independent parameters: the activation energy E_a, the pre-exponential factor A, and the exponent n which accounts for the variations with temperature of the E'_a and A' terms in the simple Arrhenius equation with two parameters:

$$k = A' \exp(-E'_a/RT) \qquad (2\text{ a})$$

If a linear relation is assumed for the variation of E'_a with temperature:

$$E'_a = E_a + CT \qquad (3\text{ a})$$

Integration of

$$E'_a = RT^2(\partial \ln k/\partial T) \qquad (4\ a)$$

gives

$$\ln k = -\frac{E_a}{RT} + \frac{C}{R}\ln T + \ln C' \qquad (5\ a)$$

therefore $A = C'$ and $n = C/R$. Combining this effect with the variation of A' yields the values reported in the literature for n, ranging from –2 to 4.

The rate coefficient for the reverse step was calculated by means of the equilibrium constant and the rate coefficient for the forward step k_i, according to

$$k_{-i} = k_i / K_i \qquad (6\ a)$$

The equilibrium constant, K_i, is calculated at a measured temperature by using the CHEMKIN thermodynamic data base of the Sandia National Laboratory.

The affinity for a reaction A + B → P + Q is given by the Gibbs free energy difference with the minus sign:

$$A = RT\ \ln K_i + RT\ \ln \frac{C_A C_B}{C_P C_Q} = RT\ \ln \frac{\vec{r}_i}{\overleftarrow{r}_i} \qquad (7\ a)$$

The value of the affinity of a reaction provides direct information on the direction in which it proceeds and its approach to equilibrium.

The reactor model was reduced to a set of continuity equations for the species involved. The flow pattern in the reactor was assumed to be of the plug flow type. With these assumptions, the continuity equation for component j at the steady state is given by

$$\frac{dF_j}{dz} = \frac{\pi d_t^2}{4} \sum_i \nu_{ij} r_i \qquad (8\ a)$$

with F_j, the molar flow rate of the jth component (mol/s); z, the length along the reactor (m); ν_{ij}, the stoichiometric coefficient of the jth component in the ith reaction, negative for a reactant and positive for a product; and initial conditions, $F_j = F_{j,0}$ at $z = 0$.

Every reaction consists of both a forward and a backward step. The rate of reaction i, r_i, is given by

$$r_i = \vec{r}_i - \overleftarrow{r}_i = k_i \prod_j C_j^{\alpha_{ij}} - k_{-i} \prod_j C_j^{\alpha_{-ij}} \qquad (9\ a)$$

in $mol^{-3}s^{-1}$, with $\vec{r}_i$ and $\overleftarrow{r}_i$ being the rate of the forward and backward steps respectively, k_i and k_{-i} the corresponding rate coefficients, and C_j the concentration of component j in mol m^{-3}. As only elementary steps are considered, the reaction orders, α_{ij} and α_{-ij}, are equal to the molecularities of the involved reactants. Integration of the continuity equations (8 a) leads to the concentrations of all the involved components.

The feed conversions and product selectivities calculated with the parameter estimates in Table 1.8 are in good agreement with the experimental observations. Figure 1.11 shows that, at 100% oxygen conversion, the conversion of methane is still far from 15%. Figure 1.12 shows the selectivities of some important products versus space time at the set of conditions corresponding to Figure 1.11. Obviously, the highest C_2 hydrocarbon selectivity is attained at the shortest space time, corresponding to low conversion levels. Extrapolation to zero space time indicates, however, a significant direct oxidation of methane to CO. Figure 1.13 depicts the selectivity versus oxygen conversion. The calculated and experimental product distribution are shown to be in good agreement. In Figure 1.14, the calculated effect of temperature on feed conversions and selectivities is compared with the observed effect. The temperature here refers to the maximum in the axial temperature profile, denoted as T_{max} in Figures 1.11-1.13. At higher temperatures, the calculated C_2 hydrocarbon selectivities are a

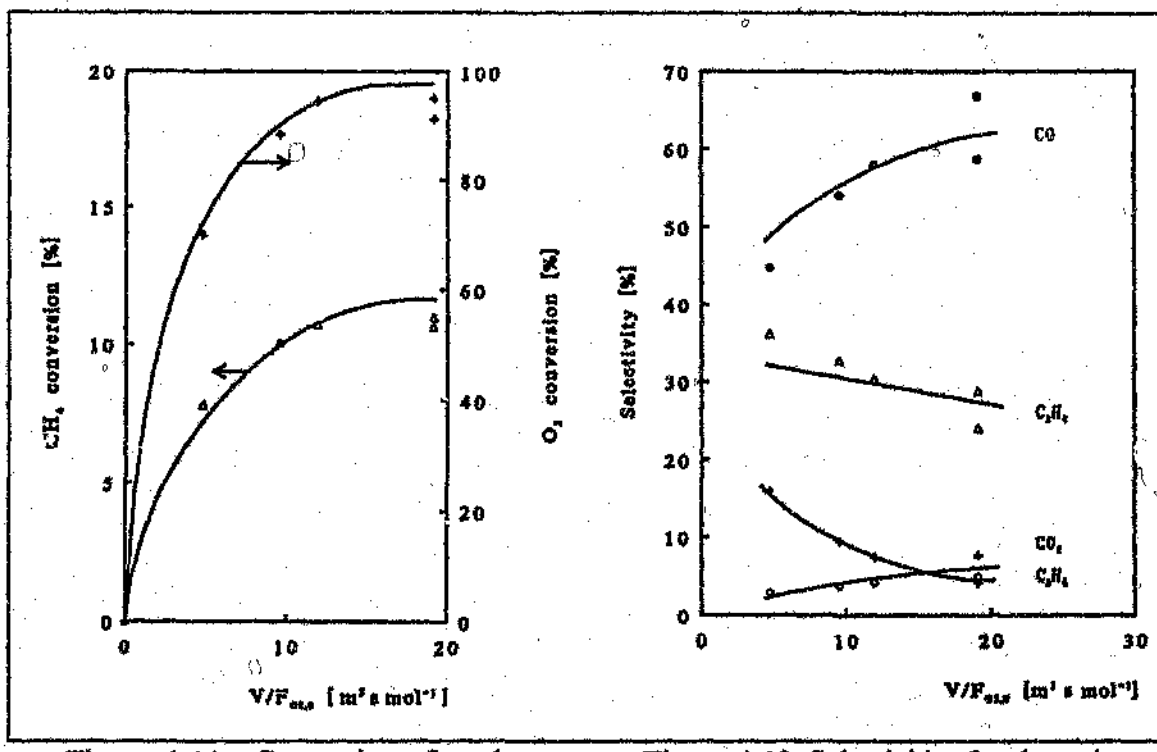


Figure 1.11. Conversion of methane and oxygen versus space time. Full lines: calculated by integration of equation (8 a) with the parameter values of Table 1.8. Points, experimental: (Δ) CH_4; (+) O_2; T_{max}=790°C, CH_4/O_2=10 [83].

Figure 1.12. Selectivities for the main reaction products versus space time. Full lines: calculated by integration of equation (8 a) with the parameter values of Table 1.8. Points, experimental: (Δ) C_2H_4, (+) C_2H_6,(●) CO and (o) CO_2 [83].

little higher than observed and the opposite is true for CO_X. The effect of temperature is most pronounced on the conversion of oxygen, less on the selectivities to C_2 and CO_X, and least on the conversion of methane because of stoichiometric limitations. The selectivity to C_2 hydrocarbons decreases with increasing temperature. This indicates that ethane formation via a non-activated recombination of two methyl radicals is important.

The important chains in the network were assessed by a contribution analysis. The integral contribution factors used in the following sections were calculated with the parameters in Table 1.8. The conclusions deduced from the following discussion can be considered as typical for the chains determining the selectivity of the oxidative coupling of methane beyond the primary initiation period.

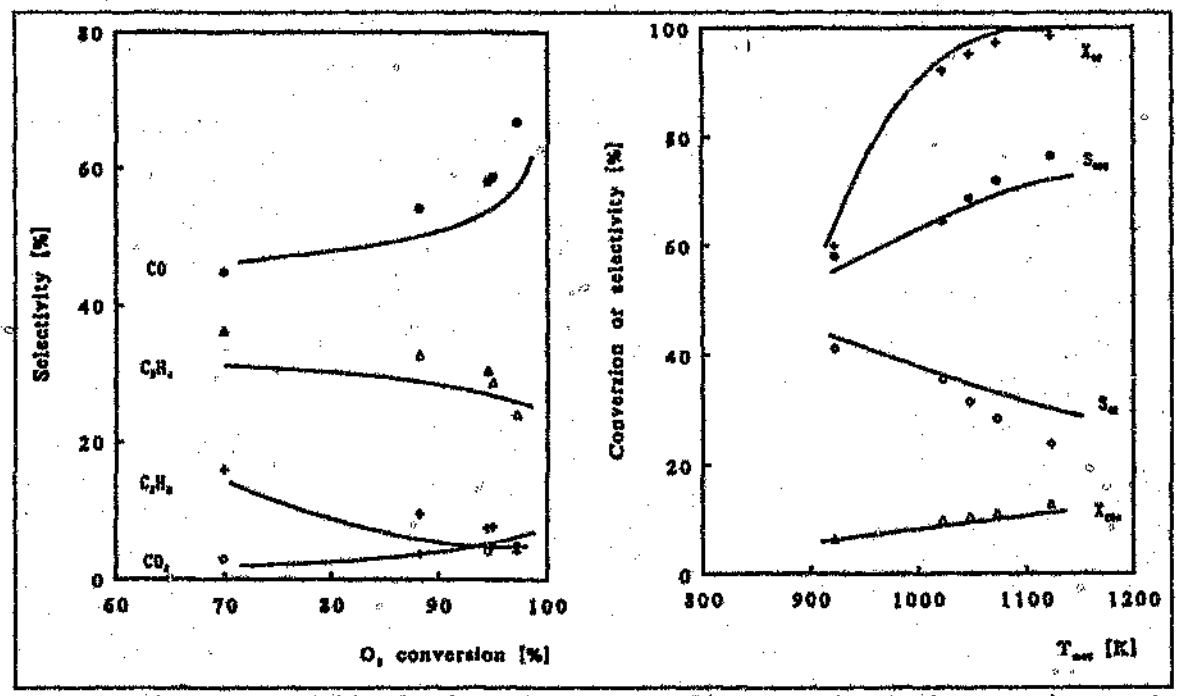


Figure 1.13. Selectivities for the main reaction products versus oxygen conversion. Full lines: calculated by integration of equation (8 a) with the parameter values of Table 1.8. Points, experimental: (Δ) C_2H_4, (+) C_2H_6, (●) CO and (○) CO_2. T_{max} = 790°C, CH_4/O_2 = 10 [83].

Figure 1.14. Feed conversions and selectivities for the main reaction products versus the maximum temperature along the reactor. Full lines: calculated by integration of equation (8 a) with the parameter values of Table 1.8. Points, experimental: (Δ) CH_4 conversion; (+) O_2 conversion; (●) C_2 selectivity; (○) CO_X selectivity [83].

Activation of methane and chains to methyl radicals. The methyl radicals are involed in 23 reactions (Table 1.8). More than 90% of the radical is formed in merely three steps. All three reactions in which methyl radicals are formed are hydrogen abstractions from a methane molecule by a radical:

$$CH_4 + H \rightarrow CH_3 + H_2 \qquad (3\ b)$$

$$CH_4 + OH \rightarrow CH_3 + H_2O \qquad (5\ b)$$

$$CH_4 + HO_2 \rightarrow CH_3 + H_2O_2 \qquad (6\ b)$$

while the primary initiation of gas-phase methane oxidative coupling occurs by hydrogen atom abstraction with molecular oxygen

$$CH_4 + O_2 \rightarrow CH_3 + HO_2 \qquad (2\ b)$$

and contributes less than 0.1%, and the unimolecular dissociation of methane, (step (1 b), Table 1.8), even less.

Part of the generated methyl radicals is oxidized towards methoxy species

$$CH_3 + O_2 \rightarrow CH_3O + O \qquad (7\ b)$$

which subsequently decompose into hydrogen atoms and formaldehyde. The hydrogen atoms combine with oxygen in the presence of third bodies to form hydroperoxy radicals,

$$O_2 + H + M \rightarrow HO_2 + M \qquad (51\ b)$$

while formaldehyde yields formyl radicals which are rapidly oxidized to carbon monoxide

$$CHO + O_2 \rightarrow CO + HO_2 \qquad (23\ b)$$

These are the most significant oxygen reactions during the initiation period.

At space times in the range of 3.0-3.4 s molecular oxygen is consumed by reaction with formyl radicals (23 b), hydrogen atoms (51 b), ethyl and vinyl radicals

$$C_2H_5 + O_2 \rightarrow C_2H_4 + HO_2 \qquad (38\ b)$$

$$C_2H_3 + O_2 \rightarrow C_2H_2 + HO_2 \qquad (48\ b)$$

The average contributions of those species to the oxygen specific destruction rate are 39% formyl, 16% hydrogen atom, 17% ethyl and 25% vinyl in the main oxidation region.

In contrast to high-temperature combustion, only small amounts of molecular oxygen participate in the chain branching process

$$H + O_2 \rightarrow OH + O \qquad (50\ b)$$

under the selected operating conditions. The oxygen atoms generated from steps (7 b) and (50 b) react with methane towards methyl and hydroxyl species

$$CH_4 + O \rightarrow CH_3 + OH \qquad (4\ b)$$

This reaction is important only in the initiation period and its relative significance diminishes at space times higher that 2 s.

Hydroxyl, hydroperoxy radicals and hydrogen peroxide. More than half of the OH radical is formed in a secondary initiation step

$$H_2O_2 + M \rightarrow 2OH + M \qquad (63\ b)$$

which is fast compared to other initiations. This is a branching step in which a relatively unstable molecule of hydrogen peroxide gives rise to two OH radicals. Another one-fifth of the OH radicals result from

$$CH_3 + HO_2 \rightarrow CH_3O + OH \qquad (10\ b)$$

and less than one-tenth from

$$CH_3 + O_2 \rightarrow CH_2O + OH \qquad (8\ b)$$

H_2O_2 originates almost exclusively from step (6 b). Thus the HO_2 radical is obviously the primary source for OH radicals, taking step (10 b) also into consideration. The HO_2 radical, in turn, is formed directly from dioxygen, either via step (23 b) and/or via step (38 b):

$$CHO + O_2 \rightarrow CO + HO_2 \quad (23\ b)$$

$$C_2H_5 + O_2 \rightarrow C_2H_4 + HO_2 \quad (38\ b)$$

The consumption of the OH radicals is greater than 90% in step (5 b) and produces methyl radicals. Therefore, it may be concluded that, under typical methane coupling conditions, the OH radical generated by a branching step plays a substantial role in generating methyl radicals.

The dominant chains that lead to the formation of the methyl radical; i.e., steps (5 b) and (6 b) account for over three-fourths of the methyl radical production.The global reactions (i) and (ii) can both be considered as branched chains, the common branching step being the decomposition of the hydrogen peroxide:

$$2CH_4 + O_2 + CH_2O \rightarrow 2CH_3 + CO + 2H_2O \quad (i)$$

$$2CH_4 + O_2 + C_2H_5 \rightarrow 2CH_3 + C_2H_4 + 2H_2O \quad (ii)$$

The hydrogen abstraction reactions in (5 b) and (6 b) and, hence, OH and HO_2 as chain carrier are also common to both chains. In a study of the oxidation of methane by oxygen in the temperature range of 500-550°C, Vardanyan and Nalbandyan[84] came to similar conclusions concerning the chain branching. They pointed to the decomposition of methyl hydroperoxide and hydrogen peroxide as branching steps. Moreover, they anticipated that the role played by hydrogen peroxide as a chain-branching agent would increase sharply with increasing temperature.

The hydrogen atom is formed mainly in unimolecular radical decompositions, such as

$$CHO + M \rightarrow H + CO + M \quad (22\ b)$$

$$C_2H_3 \rightarrow H + C_2H_2 \quad (47\ b)$$

$$C_2H_5 \rightarrow H + C_2H_4 \quad (37\ b)$$

$$CH_3O \rightarrow H + CH_2O \quad (14\ b)$$

while the rest, less than one-fifth, originates from step (3 b), i.e., from molecular hydrogen.

Selective path to hydrocarbons. The major routes to methyl radical generation are hydrogen abstractions from methane molecules by hydroxyl radicals, hydroperoxy radicals, and hydrogen atoms

$$CH_4 + OH \rightarrow CH_3 + H_2O \qquad (5\ b)$$

$$CH_4 + HO_2 \rightarrow CH_3 + H_2O_2 \qquad (6\ b)$$

$$CH_4 + H \rightarrow CH_3 + H_2 \qquad (3\ b)$$

At an oxygen conversion of 50% (τ = 3.2 s) the contribution of those reactions to the specific methane consumption and CH_3 formation rates read 45% hydroxyl, 16% hydroperoxy and 39% hydrogen atom. At higher conversions the pyrolytic hydrogen abstraction (3 b) becomes the dominant CH_3 formation process with a 90% contribution at complete oxygen consumption.

Some of the methyl radicals generated by the above reactions are converted to ethane molecules via the chain termination step

$$CH_3 + CH_3 \rightarrow C_2H_6 \qquad (11\ b)$$

The contribution of (11 b) to the specific CH_3 consumption rate declines from 82% at τ = 0.2 s to 45% at τ = 3 s, and then decreases rapidly to less than 2% within the main oxidation region. More than 90% of the total ethane production is due to step (11 b) which slows down the methane oxidation chain because of net consumption of two methyl radicals.

Ethane undergoes a series of dehydrogenation steps resulting in the formation of ethyl radicals

$$C_2H_6 + CH_3 \rightarrow C_2H_5 + CH_4 \qquad (34\ b)$$

$$C_2H_6 + H \rightarrow C_2H_5 + H_2 \qquad (31\ b)$$

The methyl reaction is the dominant ethane consumption channel exhibiting minimum and maximum specific destruction rates of 43% and 80%, respectively. Step (31 b)

becomes important late in the reaction (37% contribution at τ = 3.8 s). Attack by hydroxyl radicals

$$C_2H_6 + OH \rightarrow C_2H_5 + H_2O \qquad (32\ b)$$

is another significant route with a 35% maximum specific ethane consumption rate at τ = 3.2 s, while becomes ineffective due to OH depletion at high temperatures.

Ethylene originates from ethyl radicals through a thermal decomposition and direct oxidation with molecular oxygen

$$C_2H_5 \rightarrow C_2H_4 + H \qquad (37\ b)$$

$$C_2H_5 + O_2 \rightarrow C_2H_4 + HO_2 \qquad (38\ b)$$

The oxidative step has a 42% average contribution to the ethane formation rate up to a reaction time of 3 s and then declines rapidly to less than 2% at 3.6 s because of the low oxygen concentration levels. By contrast, the significance of the thermal decomposition route increases from an average 49% at 3 s to about 80% at the reactor exit.

Part of the ethylene is converted back to ethyl radicals via

$$C_2H_4 + H \rightarrow C_2H_5 \qquad (40\ b)$$

whereas another fraction undergoes hydrogen abstraction to vinyl radicals

$$C_2H_4 + CH_3 \rightarrow C_2H_3 + CH_4 \qquad (43\ b)$$

These reactions account for 60% and 24%, respectively of the average specific ethylene consumption rate at space times higher than 3 s. Other reactions of less importance are the hydroxyl attack on vinyl radical and formaldehyde

$$C_2H_4 + OH \rightarrow C_2H_3 + H_2O \qquad (42\ b)$$

$$C_2H_4 + OH \rightarrow CH_2O + CH_3 \qquad (45\ b)$$

with a combined 4% average specific ethylene consumption rate in the main oxidation region. A small fraction of the vinyl radicals is converted to acetylene through reaction (48 b) and also by direct thermal decomposition.

Non-selective path to oxygenates and carbon oxides. The non-selective path of the mechanism consists of two branches: (1) Oxidation of methyl radicals to methoxy species by HO_2 (step (10 b)), and (2) Oxidation of vinyl radicals to formaldehyde and formyl radicals by molecular oxygen

$$CH_3 + HO_2 \rightarrow CH_3O + OH \qquad (10\ b)$$

$$C_2H_3 + O_2 \rightarrow CH_2O + CHO \qquad (48'\ b)$$

Almost all methoxy species formed within the main oxidation section originate from step (10 b) which is also responsible for producing 12% of the CH_3 destruction rate at $\tau = 3.2$ s. Reaction (7 b) is important only in the initiation period. The CH_3O radicals decompose rapidly

$$CH_3O \rightarrow CH_2O + H \qquad (14\ b)$$

contributing an average 48% to the formaldehyde formation rate. The vinyl radical route is equally significant with average contributions of 49% and 33% to the specific CH_2O and CHO formation rates. Nearly 95% of the vinyl radical destruction in the main oxidation region is due to reaction (48' b). Step (45 b) also converts small amounts of ethylene to formaldehyde.

Formaldehyde undergoes dehydrogenation to formyl radicals by reaction with methyl radicals, hydrogen atoms and hydroxyl species,

$$CH_2O + CH_3 \rightarrow CHO + CH_4 \qquad (21\ b)$$

$$CH_2O + H \rightarrow CHO + H_2 \qquad (17\ b)$$

$$CH_2O + OH \rightarrow CHO + H_2O \qquad (19\ b)$$

and to a lesser extent with hydroperoxy radicals and molecular oxygen

$$CH_2O + HO_2 \rightarrow CHO + H_2O_2 \quad (20\ b)$$

$$CH_2O + O_2 \rightarrow CHO + HO_2 \quad (16\ b)$$

Note that about 10% of the methyl radical consumption in the main oxidation region is caused by reaction (21 b).

Formyl radicals are rapidly converted to carbon monoxide by reaction with oxygen and by thermal decomposition

$$CHO + O_2 \rightarrow CO + HO_2 \quad (23\ b)$$

$$M + CHO \rightarrow M + CO + H \quad (22\ b)$$

The oxidative step is four times more significant than thermal decomposition up to a space time of 3 s.

The non-selective path ends with the production of small amounts of carbon dioxide through carbon monoxide oxidation with HO_2 and OH species

$$CO + HO_2 \rightarrow CO_2 + OH \quad (28\ b)$$

$$CO + OH \rightarrow CO_2 + H \quad (27\ b)$$

The hydroperoxy route appears to be five times more important than the hydroxyl route in the main oxidation region. The direct oxidation of carbon monoxide with molecular oxygen

$$CO + O_2 \rightarrow CO_2 + O \quad (25\ b)$$

is of minor significance under the conditions used in the present simulation.

Based on the reaction-path analysis results certain conclusions can be drawn on the feasibility of an optimum cofeed catalyst design that might enhance the overall coupling performance[85].

In order to minimize the gas-phase oxidation of methyl radicals to oxygenates the catalyst surface should have the potential for reducing the concentration of

hydroperoxy species to the lowest possible level. This will diminish the extent of step (10 b), presumably without affecting the selective chain propagation branch to a significant extent since in catalytic oxidative coupling the latter is mainly supplied by the surface network. To minimize the gas-phase hydroperoxy radical pool the catalyst should promote the following processes: (a) surface deactivation of HO_2 radicals, (b) surface oxidation of oxygenated species directly to carbon oxides and water so as to lessen the effect of step (23 b), (c) surface dehydrogenation of ethane and ethyl species directly to ethylene and water in order to minimize the extent of step (38 b), and (d) coupling of hydrogen atoms with oxygen containing surface species towards water in order to diminish reaction (51 b).

To minimize the rate of homogeneous ethylene combustion (step (48' b)), the catalyst surface should also have the highest possible capacity for reducing the gas-phase oxygen concentration in the main oxidation region by strongly catalyzing selective and secondary non-selective reactions requiring direct participation of adsorbed oxygen molecules.

Surface deep oxidation of carbon monoxide to carbon dioxide (secondary non-selective reaction) appears to be one of the reasons for the larger hydrocarbon yields obtained with co-feed catalysts as compared to the homogeneous case. This was verified by simulating the effect of a hypothetical surface which drives the coupling reaction in the gas phase and catalyzes the direct oxidation of carbon monoxide to carbon dioxide. For example, reducing the activation energy of step (25 b) from 200 to 80 kJ/mol increased the yield by almost 50% since smaller amounts of oxygen were available in the main oxidation region to oxidize alkyl radicals. Higher rates of carbon monoxide to dioxide oxidation, however, will tend to reduce the coupling activity of alkali metal supported catalysts due to excessive surface carbonate formation.

A higher rate of oxygen adsorption on the surface will increase the concentration of active oxygen centres, which in turn will induce a larger flux of methyl radicals generation through methane activation and, consequently, a higher rate of hydrocarbon formation since the coupling reaction is second order in methyl concentration. This is the principal reason for the larger yields obtained in the presence of co-feed coupling catalysts. The rates of surface dehydrogenation of ethane and hydrogen oxidation towards ethylene and water will likewise increase. These selective processes are also

beneficial for diminishing the hydroperoxy radical pool as discussed above. However, high concentration of ethylene and methyl species also promote vinyl radical generation via the hydrogen abstraction reaction (43 b), which in turn increases the rate of partial oxidation of vinyl (and methyl) radicals towards oxygenates. These considerations are reflected on the space time dependence of the major product selectivities. Methane oxidative coupling catalysts with high affinity towards oxygen adsorption are expected to improve the product yields only if the secondary ethylene combustion reaction does not offset the gains from the enhanced hydrocarbon formation.

A microkinetic model. A microkinetic model was constructed by Dumesic et al.[86] in an attempt to explain quantitatively the behavior of a Li/MgO catalyst for oxidative methane dimerization. Microkinetic analysis permits the construction of a simple kinetic model that describes in a satisfactory manner the overall experimental methane consumption observed for an alkali metal promoted alkaline earth metal oxide catalyst. The model was obtained through microkinetic analysis of the experimental evidence accumulated for the methane and oxygen surface interaction steps.

This model consisted of the 12 steps listed in Table 1.9. Seven of these steps are meant to be elementary steps. In contrast, steps 6, 7, 9, 11 and 12 (Table 1.9) represent parts of the process consisting of more than one elementary step but whose elementary breakdown is not significant under the reaction conditions.

If it is assumed that step (1) in Table1.9 is in equilibrium, step (2) is reversible, step (3) is irreversible, and the coverage of M–O–M is essentially 1.0, then it can be shown that the rate of overall methane consumption is given by

$$r_{OV} = (a / 4)\,[(a^2 + 16b)^{1/2} - a] \qquad (1\,c)$$

where r_{OV} = overall methane consumption rate, $a = k_3 P_{CH4} / (k_2')^{1/2}$, $b = k_2 (K_1 P_{O2})^{1/2}$, K_1 = equilibrium constant for step (1), k_2 = forward rate constant for step (2), k_2' = reverse rate constant for step (2), k_3 = rate constant for step (3), P_{CH4} = methane pressure and P_{O2} = oxygen pressure.

Table 1.9. Complete methane dimerization mechanism[86].

Step	Reaction
	Methyl radical production
1	$O_2 + 2M–O–M \leftrightarrow 2M–O–O–M$
2	$M–O–O–M \leftrightarrow 2M–O\cdot$
3	$CH_4 + M–O\cdot \leftrightarrow CH_3\cdot + M–OH$
4	$2M–OH \leftrightarrow H_2O + M–O–M$
	Coupling
5	$2CH_3\cdot \leftrightarrow C_2H_6$
	C_1 oxidation
6	$CH_3\cdot + O_2 \rightarrow CH_2O + OH\cdot$
7	$CH_2O + OH\cdot + 3/4O_2 \rightarrow CO_2 + 3/2H_2O$
8	$CH_3\cdot + M–O\cdot \leftrightarrow M–OCH_3$
9	$M–OCH_3 + 3/2O_2 \rightarrow CO_2 + H_2O + M–OH$
	Ethane dehydrogenation
10	$C_2H_6 + M–O\cdot \leftrightarrow C_2H_5\cdot + M–OH$
11	$C_2H_5\cdot + 1/4O_2 \rightarrow C_2H_4 + 1/2H_2O$
	C_2 oxidation
12	$C_2H_4 + 2O_2 \rightarrow 2CO + H_2O$

In general, step (5) in Table 1.9 represents the coupling process, in which the C_1 species capable of undergoing coupling is denoted CH_X. This species may be either a gaseous $CH_3\cdot$ radical or a surface methoxy species at this point. The authors defined r_5 as the forward rate of this elementary step, k_5 as the forward rate constant, and P_{CH3} as the pressure of gaseous $CH_3\cdot$ species. The rate of step (5) can then be expressed as follows:

$$r_5 = k_5 (P_{CH3})^2 \qquad (2\,c)$$

Step (5) in Table 1.9 is assumed to be irreversible. Thus, when the rate of C_2 hydrocarbon combustion is negligible, r_5 should equal the experimentally determined rate of C_2 production. Therefore, equation (2 c) can be rewritten as follows:

$$R_{C2} = k_5 (P_{CH3})^2 \qquad (3\ c)$$

where R_{C2} is defined as the net rate of C_2 hydrocarbon production. The authors also defined r_{COx} as the net rate of production of CO_X species, Assuming gas-phase oxygen and the surface species M–O· and M–O–O–M are responsible for oxidation of C_1 species, it can be written as follows:

$$r_{COx} = k_8 P_{CH} \theta_{MO} + k_2 K_1^{1/2} P_{CH3} P_{O2}^{1/2} + k_6 P_{CH3} P_{O2} \qquad (4\ c)$$

where k_8, k_2 and k_6 are rate constants, θ_{MO} is the fractional coverage of M–O· species, K_1 is equilibrium constant for step (1), P_{CH3} and P_{O2} are pressures of gaseous species.

Figures 1.15-1.18 show comparisons between experimental and model activities and

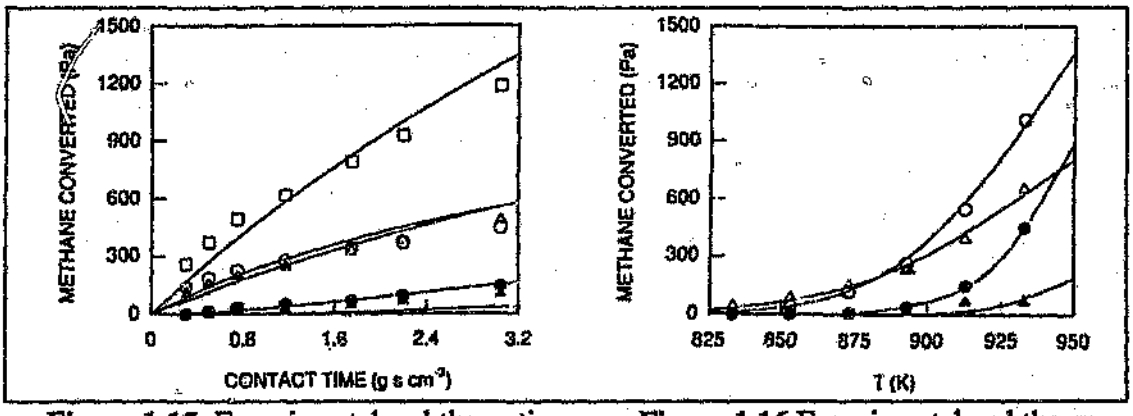


Figure 1.15. Experimental and theoretical methane converted to various products versus pseudocontact time, W/F. Catalyst: Li/MgO (W = 1g), T = 620°C, P_{CH4} = 40 kPa, P_{O2} = 8 kPa Solid lines: model summarized in Table 1.9. (□) overall, (o) to C_2H_6, (●) to C_2H_4, (Δ) to CO_2, (▲) to CO [86].

Figure 1.16. Experimental and theoretical metane converted to various products versus temperature. Catalyst: Li/MgO (W = 1g). Total flow rate: 0.83 ml/s. Total reactor pressure: 101.3 kPa Solid lines: model summarized in Table 1.9. (□) overall, (o) to C_2H_6, (●) to C_2H_4, (Δ) to CO_2, (▲) to CO [86].

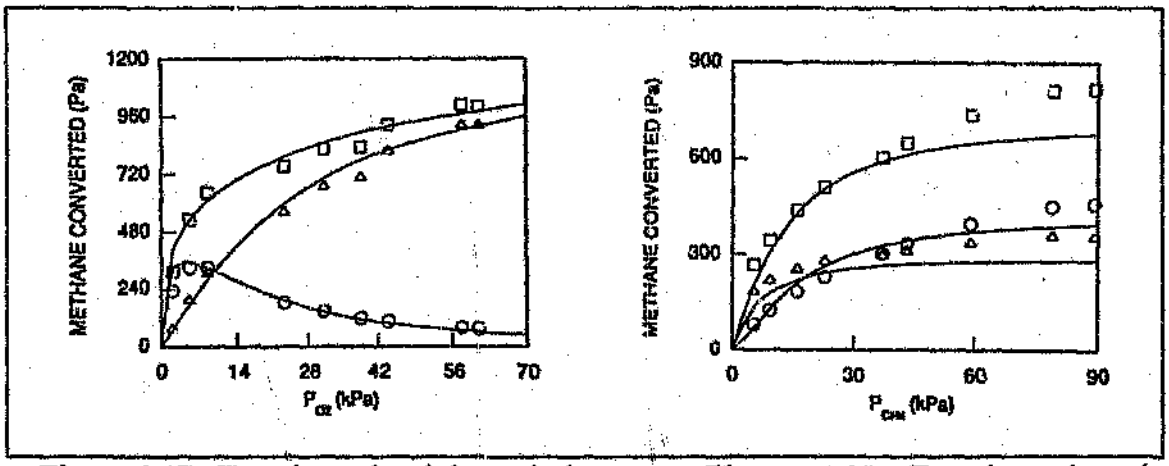


Figure 1.17. Experimental and theoretical methane converted to various products versus oxygen inlet pressure. Catalyst: Li/MgO (W = 1g), T = 620°C, P_{CH4} = 40 kPa. Solid lines: model summarized in Table 1.9. (□) overall, (o) to C_2H_6, (o) to C_2H_4, (Δ) to CO_2, (Δ) to CO [86].

Figure 1.18. Experimental and theoretical methane converted to various products versus methane inlet pressure. Catalyst: Li/MgO (W = 1g), P_{O2} = 8 kPa, total reactor pressure: 101.3 kPa. Solid lines: model summarized in Table 1.9. (□) overall, (o) to C_2H_6, (o) to C_2H_4, (Δ) to CO_2, (Δ) to CO [86].

selectivities at low conversions. The figures demonstrate that the agreement between the model and experiments in this range of reaction conditions is satisfactory both qualitatively and quantitatively. It is possible that the small disagreement between model and experiments regarding the catalytic behavior versus contact time is due to carbonate formation at high contact times.

The microkinetic analysis outlined above provides insight into the processes responsible for catalytic activity and selectivity. With the 12 steps listed in Table 1.9, the model was unable to predict a limit to C_2 hydrocarbon yield close to that observed experimentally.

According to the authors, active sites appear to be produced via two elementary steps. In the first step, surface peroxide species form as gaseous dioxygen adsorbs on the catalyst. In the second step, methane-activating sites are produced as the surface peroxide species undergo O–O bond cleavage. The second step is a key process in determining overall activity. It also leads to the conclusion that the main route through which C_1 species undergo combustion probably involves gaseous O_2. In this case, the

rate of coupling is determined by the square of the $CH_3\cdot$ radical concentration while the rate of C_1 oxidation is determined by the $CH_3\cdot$ radical concentration to the first power times the oxygen pressure. This result suggests that an effective catalyst must be able to produce high $CH_3\cdot$ radical concentrations at low oxygen pressure. The production of $CH_3\cdot$ radicals is not an equilibrium process, and its rate of production is determined mainly by the generation of active sites. Accordingly, the most effective catalysts are those that can form high concentrations of surface peroxide species at the low oxygen pressure. Alkali metals are known to form stable bulk peroxides, which explains why in general oxides containing these materials have been found to be effective dimerization catalysts.

A detailed study of the kinetics of methane oxidative coupling on 20% PbO/Al_2O_3 catalyst was reported by Krylov et al.[87] The measurements were carried out in a flow reactor, the fractional conversions of the reagents did not exceed 10%. The reactor was considered to be a non-gradient one, and the rate was calculated as for a differential reactor.

The heterogeneous-homogeneous model is directly used to develop the kinetic equations:

$$(1)\ O_{(S)} + CH_4 \xrightarrow{k_1} OH_{(S)} + CH_3$$

$$(2)\ 2CH_3\cdot \xrightarrow{k_2} C_2H_6$$

$$(3)\ CH_3\cdot + O_2 \overset{K_3}{\leftrightarrow} CH_3O_2\cdot$$

$$(4)\ 2CH_3O_2\cdot \xrightarrow{k_4} CO + CO_2 + H_2O$$

$$(5)\ CH_3\cdot + CH_3O_2\cdot \xrightarrow{k_5} CO + CO_2 + H_2O$$

where $O_{(S)}$ represents active oxygen, which is the center for methyl radical formation. Reaction (3) is assumed to be an equilibrium reaction. At temperatures higher than 650°C the equilibrium is shifted to the left, towards methylperoxide decay. In this temperature region one can obtain the best selectivity to C_2 products.

At temperatures lower than 650°C the equilibrium is shifted to methylperoxide formation. The isomerization and decay of this species may provide the chain reactions which result in the formation of deep oxidation products.

For the quasi-steady-state approximation the following analytical ex[illegible]on for the limiting selectivity relative to ethane formation was obtained:

$$S_{lim} = \frac{k_2}{k_2 + K_3 P_{O2} (k_4 K_3 P_{O2} + k_5)} \qquad (1\,d)$$

where, k_i are the rate constants of the corresponding stages of the scheme; K_3 is the equilibrium constant of methylperoxide formation.

The comparison of the theoretical and experimental values obtained on various catalysts (including the empty reactor) have shown that the latter do not exceed the theoretical curve, calculated in accordance with the known constants of gas phase chain reactions (Figure 1.19). The selectivity values, which are low in comparison to the calculated ones, may be accounted for by the additional contribution of heterogeneous reactions assisted by active forms of surface oxygen to the reaction of deep oxidation.

Most often, the kinetics of oxidative coupling is described by a formal power equation:

$$r = kP^m_{CH4} P^n_{O2} \qquad (2\,d)$$

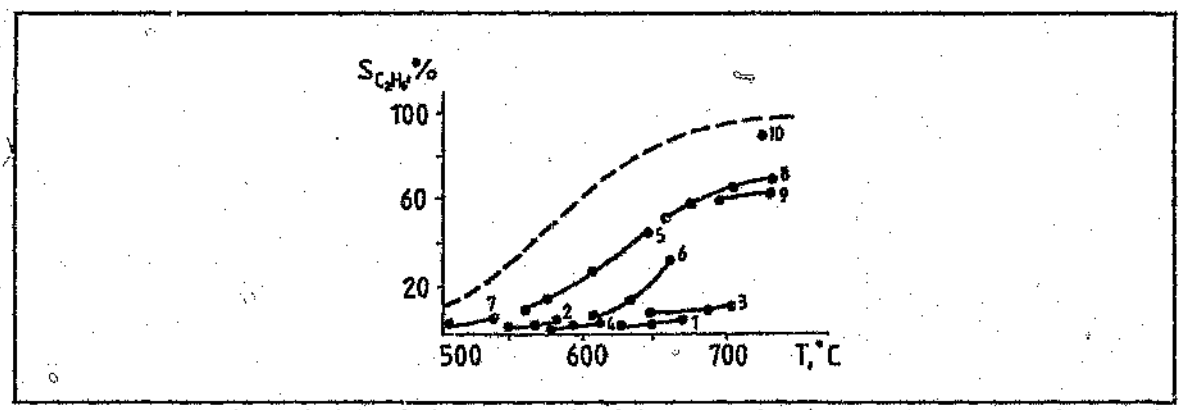


Figure 1.19. The relationship between selectivity towards ethane at low conversions and the temperature. (1) θ - Al_2O_3; (2) Y_2O_3; (3) Ta_2O_5, (4) 20% CdO/Al_2O_3; (5) 20% PbO/Al_2O_3; (6) BaO; (7) Sn-Sb-O; (8) Pb-Sn-K-O; (9) quartz; (10) empty reactor; dotted line-S_{lim} calculated from equation (1 d) [87].

In most cases, m is higher than n, and the reaction order with respect to methane is close to unity, whereas the reaction order with respect to oxygen is near zero.

A Mars-van Krevelen type equation, characteristics of the processes which proceed via a redox mechanism, was obtained for the kinetics of methane oxidative coupling for 20% PbO/Al_2O_3:

$$r = \frac{k_{red} P_{CH4} k_{ox} P_{O2}}{k_{red} P_{CH4} + k_{ox} P_{O2}} \qquad (3\ d)$$

where k_{red} and k_{ox} stand for the rate constants for reduction of active centers by methane and their reoxidation by oxygen, respectively. A Langmuir type equation was applied for the kinetics of oxidative coupling on Sm_2O_3, Li/MgO, $BaCeO_3$, and LaCe/NiO[88,89]:

$$r_1 = \frac{k_1 P_{CH4}}{k_2 + k_3 P_{CH4}} \times \frac{k_2' P_{O2}}{k_2' + k_3' P_{O2}} \qquad (4\ d)$$

The authors believe that agreement of this equation with the experimental data supports the mechanism of surface interaction between CH_4 and O_2. It is easy to verify that equation (4 d) can be readily reduced to equation (3 d).

It was noted that the E_a-values for oxidative coupling on a number of catalysts lie within the interval of 200-220 kJ/mol. An analysis of equation (3 d) showed that the following relation for the efficient activation energy E_{eff} is valid:

$$E_{eff} = \frac{\chi E_{red} + E_{ox}}{1 + \chi} \qquad (5\ d)$$

where E_{red} and E_{ox} are the activation energies for catalyst reduction and oxidation, respectively, and $\chi = k_{ox} P_{O2} / k_{red} P_{CH4}$. At $\chi \sim 1$, E_{eff} is close to1/2 ($E_{red} + E_{ox}$). If E_{ox}

increases linearly with decreasing E_{red}, the E_{eff} value will be approximately constant for a series of catalysts, but if the rates of reduction or reoxidation are substantially different, the process rate will be controlled by the kinetic parameters of the slow step.

Most often, the kinetics of complete methane oxidation on the same catalysts is described by power- or Langmuir type equations. If, for oxidative coupling, $m > n$ is more typical, then $n > m$ is characteristics of complete oxidation to CO_2. This appears to support the idea that complete oxidation is controlled by the catalyst oxidation stage. In most cases, the E_a values for total oxidation are substantially below those for oxidative coupling and amount to 130-170 kJ/mol. This means that the mechanism of total oxidation and oxidative coupling are quite different. These reactions proceed in parallel routes on different active sites.

Ethane undergoes further oxidative dehydrogenation according to the following mechanism:

(6) $C_2H_6 + O_S \rightarrow C_2H_5^{\cdot} + (OH)_S^{\cdot}$

(7) $C_2H_5^{\cdot} + O_S \rightarrow C_2H_4 + (OH)_S^{\cdot}$

(8) $2(OH)_S^{\cdot} \rightarrow O_S + H_2O$

The C–H bond energy in methane is 434 kJ/mol, and the bond energy in ethane is 400 kJ/mol. Provided the Polanyi-Semenov equation:

$$E = E_0 + 0.75\Delta H \qquad (6\,d)$$

is valid, such a difference in the C–H bond energy ($E_{C\text{-}H}$) should lead to a difference of 25.5 kJ/mol in the activation energies for methane and ethane. For a given pre-exponential factor, at the oxidative coupling temperature of ~750°C, the rate of ethane interaction with the surface centers forming $C_2H_5^{\cdot}$ would be greater by one order of magnitude. Correspondingly, ethane must react with the surface at temperatures 100-150°C lower. The rate of ethane interaction with the 20% PbO/Al_2O_3 catalyst for methane oxidative coupling is higher than that of methane interaction by a factor of 10-20[90]. The rate of oxidative dehydrogenation of C_2H_6 to C_2H_4 is higher than that of methane oxidative coupling by a factor of 4-5.

In the gas phase, $C_2H_5\cdot$ radicals can be transformed into ethyl peroxide radicals, which react further:

(9) $C_2H_5\cdot + O_2 \leftrightarrow C_2H_5O_2\cdot$

(10) $C_2H_5O_2\cdot \rightarrow C_2H_4 + HO_2$

(11) $C_2H_6 + HO_2\cdot \rightarrow C_2H_5\cdot + H_2O_2$

(12) $H_2O_2 + M \rightarrow 2OH\cdot + M$

(13) $OH\cdot + C_2H_6 \rightarrow C_2H_5\cdot + H_2O$

$C_2H_5O_2\cdot$ also forms some products of complete oxidation when interacting with the surface. The reaction rates for $C_2H_5O_2\cdot$ in the gas phase are considerably higher than those for $CH_3O_2\cdot$. Therefore, the probability for the interaction of $C_2H_5O_2\cdot$ with the surface is substantially smaller than that of $CH_3O_2\cdot$. Correspondingly, the selectivity of oxidative dehydrogenation of C_2H_6 is higher as compared to methane oxidative coupling. For 3% Li/MgO catalyst at 600°C, the selectivity of C_2H_6 transformation into C_2H_4 was 75% at 40% conversion.

The kinetics of ethane oxidative dehydrogenation on the 20% PbO/Al_2O_3 catalyst is described by an equation similar to equation (3 d), which can be obtained by assuming the involvement of two oxidized sites in the process:

$$r_2 = \frac{4k_{red} P_{C2H6} k^2_{ox} P^2_{O2}}{[k_{ox} P_{O2} + (k^2_{ox} P^2_{O2} + 8\, k_{red} P_{C2H6} k_{ox} P_{O2})^{1/2}]^2} \qquad (7\,d)$$

where k_{red} is the rate constant for reduction of the active centers by ethane. The rate constants for reoxidation, k_{ox}, measured in the experiments with methane and ethane, turned out to be very close; from this fact the conclusion was drawn concerning the participation of active sites common to both processes.

Though Langmuir equations are in good agreement with the kinetics, as was mentioned above, this cannot serve as any proof in favour of the adsorption mechanism in which the adsorbed forms of molecular oxygen and methane are key reactants in the reaction. The kinetic constants obtained are rather formal.

Analogous equations were obtained by Sokolovskii et al.[91] without recourse to a Langmuir-Hinshelwood mechanism. They considered the scheme for the separate interaction, in which the stages of reductant and oxidant interaction with the catalyst surface included two steps:

$$(1)\ CH_4 + z_1 \leftrightarrow CH_3^- z_1H^+$$

$$(2)\ CH_3^- z_1H^+ \xrightarrow{-e} CH_3 + z_1H^+$$

$$(3)\ 2z_1H^+ \leftrightarrow H_2O + z_1 + \square$$

$$(4)\ O_2 \overset{+e}{\leftrightarrow} O_2^-$$

$$(5)\ O_2^- + \square \rightarrow O^{2-} + O \rightarrow O^{2-}$$

where $z_1 = M^{n+}O^{2-}$, $\square$ is the oxygen vacancy.

The reduction stage includes the step of heterolytic methane activation with subsequent electron transfer to the accepting center, radical formation and the reduction of the surface. The stage of reoxidation includes the formation of an adsorbed oxygen form (e.g., as is shown in the scheme above, it can be an ion-radical O_2^-), which is reduced to the lattice oxygen ion if an oxygen vacancy is present.

Assuming:

$$z_1 + CH_3^- z_1H^+ >> z_1H^+ + \square$$

under steady-state conditions, this scheme is transformed to provide the following expression for the rate of methane consumption and methyl radical formation:

$$r = \frac{(a_1'P_1 + K'a_2'P_2 + a_1'a_2'P_1P_2)K_2}{(1 + a_1'P_1)(1 + a_2'P_2)} \qquad (1\,e)$$

where $a_1' = \frac{K_1}{K_{-1} + K_2}$; $a_2' = \frac{K_4}{K_{-4} + K_5\square}$; $K' = \frac{K_5\square}{K_{-1} + K_2}$ and

K_i are the direct and reversal constants of the corresponding stage, P_1,P_2 are the partial methane and dioxygen pressures. Under the condition when $(a_1'P_1 - K'a_2'P_2) \ll a_1'a_2'P_1P_2$, the equation transforms to an expression :

$$r = \frac{K_2\, a_1'a_2'P_1P_2}{(1 + a_1'P_1)\,(1 + a_2'P_2)} \qquad (2\,e)$$

Evidently, in the general case, coefficient a_i'may either decrease or increase with a temperature rise. For the adsorption process due to the positive adsorption heat $E_{-4} > E_4$. At low temperatures and high activation energy E_{-4} the inequality $E_{-4} \ll K_5$ □ may be true, because the activation energy of stage (5) may be low. If at the same time $E_5 < E_4$, then a_2' will rise with the temperature. Along with the temperature rise due to inequality $E_5 < E_{-4}$ the ratio of the items in the denominator for a_2' will change. The situation may arise, when $E_{-4} \gg K_5$ □. In this case a_2' will be the true adsorption coefficient which should decrease with rising temperature.

In the case when the first stage is the limiting ($E_{-1} \ll K_2$) equation (2 e) is transformed to:

$$r = \frac{K_1\, a_2'P_1P_2}{(1 + a_1'P_1)\,(1 + a_2'P_2)} \qquad (3\,e)$$

A kinetic isotope effect should be present and thus was observed[80]. By contrast, when stage (2) is limiting ($E_{-1} \gg K_2$) one can obtain the expression:

$$r = \frac{K_2K_{p1}\, a_2'P_1P_2}{(1 + K_{p1}P_1)\,(1 + a_2'P_2)} \qquad (4\,e)$$

where a_1' transforms the equilibrium constant of stage (1) (K_{p1}) and the isotope effect should be very small. According to equation (2 e) in the general case the reaction rate

should decrease with the rise of vacancy concentration or the level of catalyst reduction (excluding the conditions when $a_2'P_2 >> 1$).

The data of Sokolovskii et al.[91], presented in Figure 1.20, which relate to a study of the rate dependencies for the oxidative coupling of methane on 2% PbO/MgO upon the level of the catalysts reduction. The catalyst was reduced by CO pulses, then a pulse of methane-dioxygen mixture was supplied (CH_4 : O_2 = 9:1) and the rate was measured. A hyperbolic fall of the dimerization rate with the surface reduction level is observed, which corresponds to equation (2 e) under the condition that $a_2'P_2 << 1$.

A detailed kinetic model based on a free-radical mechanism has been developed, which allows the adequate calculation of the feed conversions and product selectivities under process conditions typical for the oxidative coupling of methane. For that matter the available kinetic data bases are not reliable enough, and an estimation of the most important parameters in the model by regression of the experimental data was necessary. A contribution analysis revealed the essential features of the complex reaction network by identifying the important chains. Large amounts of methyl radicals

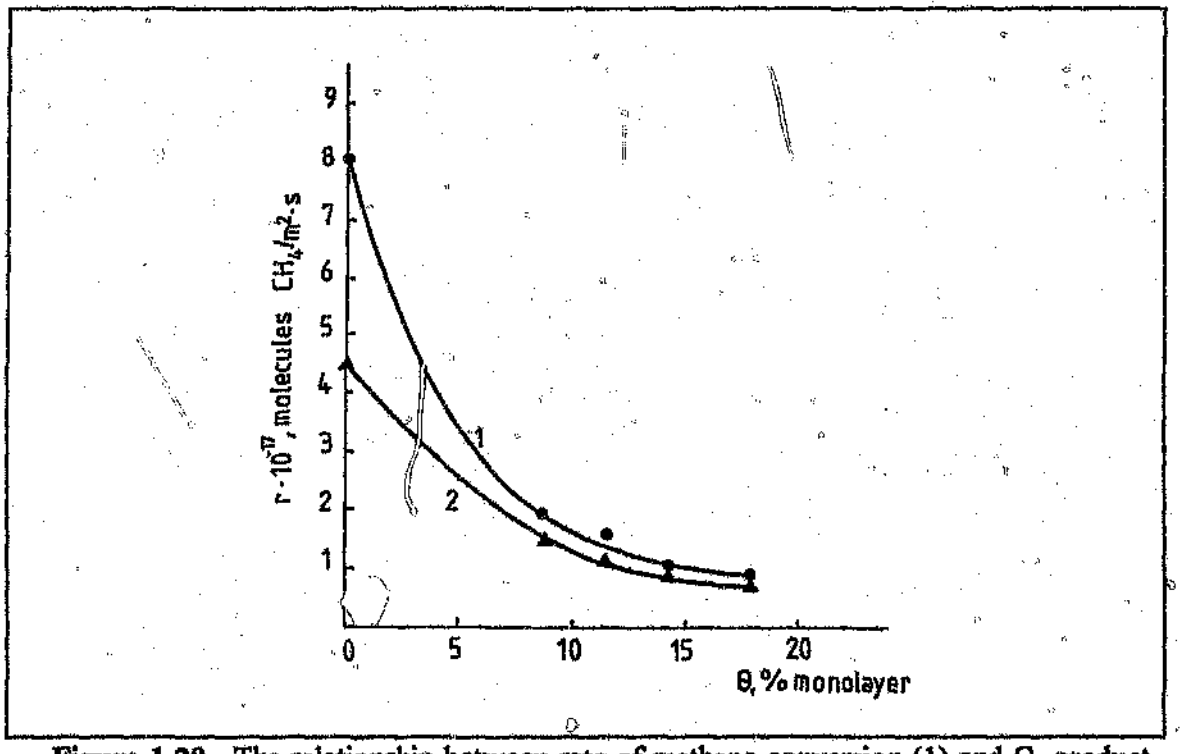


Figure 1.20. The relationship between rate of methane conversion (1) and C_2 product formation (2) on the degree of reduction of the catalyst (θ). Reaction conditions: T = 800°C, 10% PbO/MgO, CH_4 : O_2 = 9:1 [91].

are formed through branched chains, which degenerate via a termination step to produce the desired product ethane. The decomposition of hydrogen peroxide is the main branching step. Dehydrogenation of ethane leads to ethene. The dehydrogenation via the thermal decomposition chain dominates the oxydehydrogenation via the oxidative chain. Carbon monoxide formation is mainly due to the oxidation of the methyl radical at the conversion levels investigated.

1.2.3. Reaction mechanism and nature of the active sites. At present there are two main mechanisms; one is based on O^- as the active site, whilst the other is based on O^{2-} having a low coordination number.

The original Lunsford[6,92,93,94] mechanism is described in terms of equations (1 f-4 f):

$$O^-_{(s)} + CH_4 \rightarrow OH^-_{(s)} + CH_3\cdot \qquad (1\ f)$$

$$CH_3\cdot + CH_3\cdot + M \rightarrow C_2H_6 \qquad (2\ f)$$

$$2OH^-_{(s)} \rightarrow O^{2-}_{(s)} + [\ ] + H_2O \qquad (3\ f)$$

$$O^{2-}_{(s)} + [\ ] + 1/2O_2 \rightarrow 2O^-_{(s)} \qquad (4\ f)$$

where [ ] represents an anion vacancy and the subscript (s) a surface species.

The original assignment of activity in Li/MgO catalysts (containing various Li : Mg ratios) to specific Li^+O^- centers was based on the observation of a parallelism between the density of Li^+O^- centers and the number of methyl radicals formed, and also the rate of ethane formation. Indeed, up to P_{O2} = 50 Torr a correlation between Li^+O^- concentration and C_2 product yield is observed. However, this correlation becomes reversed for higher pressures. The best correlation was recorded between Li^+O^- concentration and deep oxidation product yields (Figure 1.21)[73].

The appearance of a radical center in a binary oxide system is provided by the substitution of bivalent magnesium ion by univalent lithium ion. The addition of larger ions (Na^+, for example) should not produce these centers, which is confirmed by the authors in their experiments on the doping of MgO with sodium carbonate.

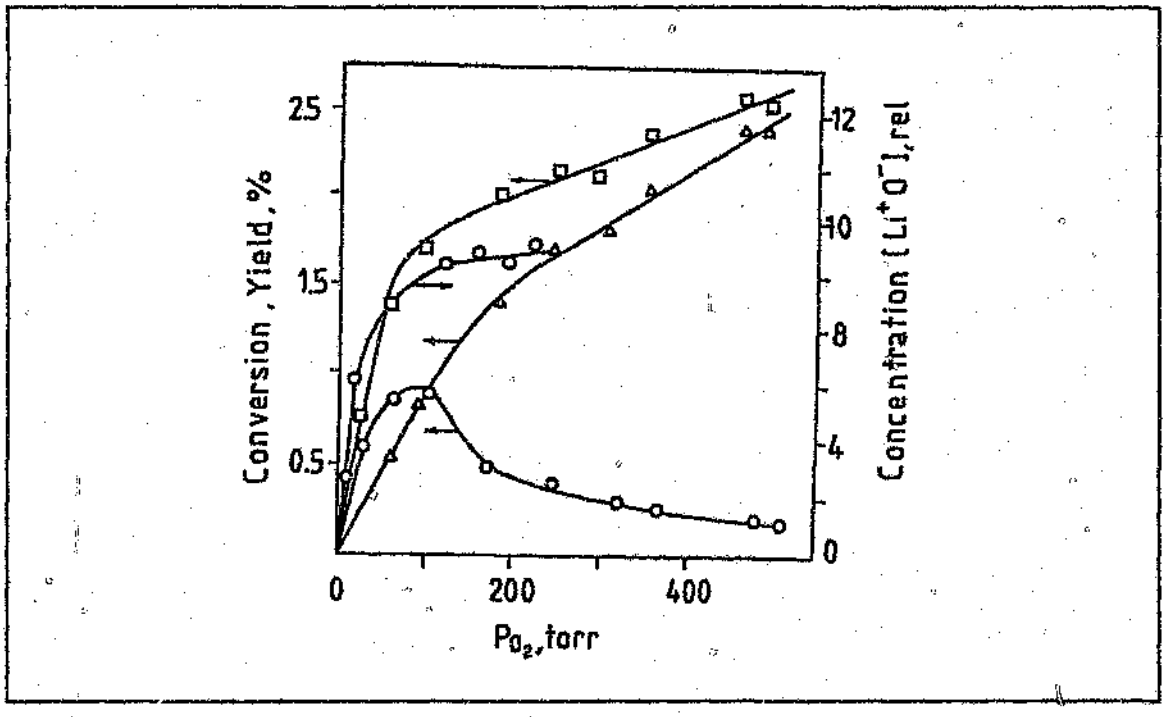


Figure 1.21. The relationship between methane conversion, reaction product yields and [Li^+O^-] center concentration on 7% Li/MgO catalyst and dioxygen pressure in the reaction mixture (□) CH_4, (o) $C_2H_4 + C_2H_6$, (Δ) $CO + CO_2$. Reaction conditions: T = 620°C, pseudo-contact time = 0.83 g s/ml, P_{CH4} = 300 Torr)[73].

At the same time, the introduction of sodium ions into calcium oxide allows an increase in the yield of dimerization products according to the same hypothesis.

Later, however, it was demonstrated that magnesium oxide promotion with sodium ions more efficient than a lithium-magnesium catalyst for methane dimerization[95]. These results cast doubt on Lunsford's concept of methane activation.

The reactions of radical detachment usually have low activation energies. The activation energy for the reaction of O^- with hydrogen was determined by Kazanskii et al.[96] to be ~15 kJ/mol. At the same time, the reaction of oxidative methane dehydrodimerization is known to have a very high activation energy (Table 1.10). The value of 230 kJ/mol was obtained by Lunsford et al.[73] for the lithium-magnesium system. In order to resolve this contradiction, it was considered that the stage of active center regeneration is the limiting one:

Table 1.10. Activation energies of the reactions of methane on basic catalysts [12].

Catalyst	Reaction	E_a (kJ/mol)
MgO	Oxidative dimerization	260
Sb$_2$O$_3$-MgO	Oxidative dimerization	250
Li/MgO	Oxidative dimerization	230
MgO	Non-oxygen dimerization	250
BaO_2	Non-oxygen dimerization	60

$$2[Li^+OH^-] \rightarrow Li^+O^{2-} \cdot Li^+[\ ] + H_2O \qquad (5\,f)$$

$$Li^+O^{2-} + Li^+[\ ] + 1/2O_2 \rightarrow 2Li^+O^- \qquad (6\,f)$$

These stages may be characterized by a high activation energy which may also characterize the total activation energy. But the reaction also proceeds with a high E_a value in the non-oxidative mode (without O_2 in the reaction mixture) when the regeneration of active centers is not included (Table 1.10).

Thus, the assumption that the regeneration of active centers is the limiting stage of the process does not resolve the contradiction in the present hypothesis about the participation of O^- in methane activation and the observed high activation energy.

Among other oxygen ion-radical forms, anion-radicals O_2^- are observed most frequently on the surface of oxide catalysts[97,98,99]:

$$CH_3^- + O_2 \rightarrow CH_3\cdot + O_2^- \qquad (7\,f)$$

The O_2^- superoxide species is known to be very reactive and capable of promoting deep oxidation of the hydrocarbons to CO_x[100]. Obviously, for the reaction to be carried out in the catalytic mode, the surface O_2^- needs to be rapidly dissipated via a complex series of equilibria. Similary the surface OH^- (equations (1) and 1 (f)) must also be thermally decomposed by such mechanisms as shown by equation (3 f). The implication of equation (7 f) is that the higher hydrocarbons can only be generated in the presence of oxygen. This also implies that the generation of higher hydrocarbons in the absence of oxygen in the feed, will only be possible if the catalyst possesses the

capacity to store oxygen, i.e., variable oxidation states. However O_2^- are unstable at the temperature of oxidative coupling.

Another plausible active center for oxidative coupling is a peroxide-ion O_2^{2-}, whose stabilization is possible in those systems that contain alkali and alkali-earth cations. Krylov et al.[101] mentioned the possibility of obtaining selectivity towards C_2 hydrocarbon close to 100% for BaO_2. However, with Ba/La_2O_3 catalysts the population of O_2^{2-} species as determined by X-ray photoelectron spectroscopy (XPS)[48] showed no relationship with the catalytic performance.

The correlation between the activation energy and the heat of hydrogen detachment by a variety of fragments is in good accordance with Semenov's rule for radical moieties (equation (6 d)). The experimentally determined activation energy of the reaction of methane with peroxide ion also fits the general picture. This data provides the conclusion that methane activation occurs on peroxide ion via the detachment of a hydrogen atom and methyl radical formation. This conclusion is further substantiated if the interaction of methane with barium peroxide is considered, for which the applied activation energy was measured. However, this activation energy (60 kJ/mol) is considerably lower than energies measured over the oxides of alkaline earth metals. This contradiction is not removed when the change of concentration of the surface forms with temperature is considered, because the reaction of peroxide formation from oxide and oxygen is an exothermic one. Thus, the concentration of peroxide ions should decrease with rising temperature and the observed activation energy will be still lower.

Against this background, the alternative acid-base mechanism of Sokolovskii et al.[102,103,104] suggesting that the methane activation occurs via heterolytic cleavage on low coordination surface M^{n+}–O^{2-} ionic pairs, appears attractive. The efficient catalysts for the oxidative coupling of methane are generally strong bases. The methane activation in these systems may occur via its interaction with an acid-base pair with subsequent proton detachment and metal-methyl compound formation, in which the methyl group is negatively charged. The rate of oxidative dehydrodimerization on the set of catalysts was shown to rise with an increase in the concentration of the basic centers (Figure 1.9, and Table 1.7).

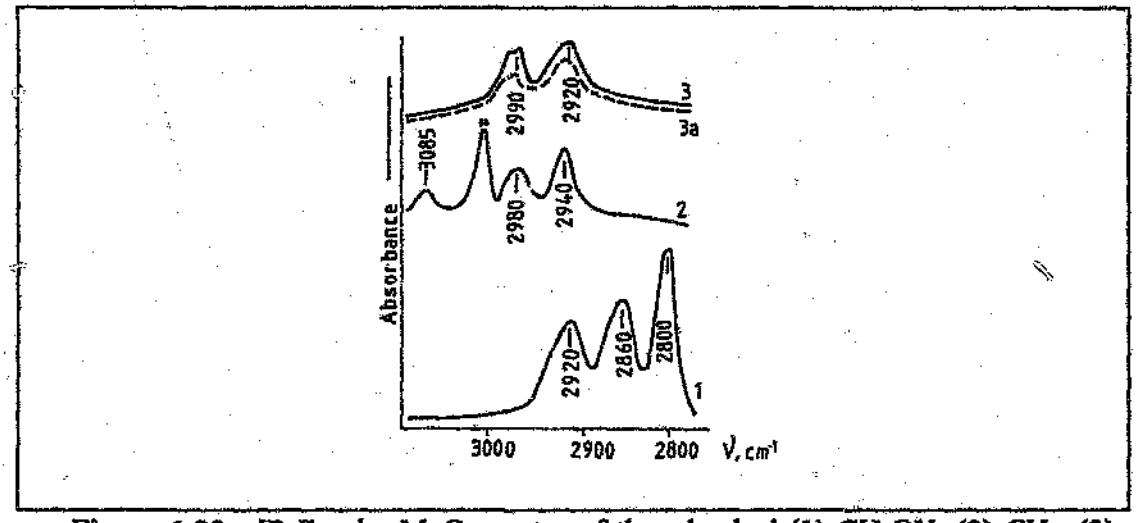


Figure 1.22. IR-Fourier MgO spectra of the adsorbed (1) CH_3OH, (2) CH_4, (3) $(CH_3)_2SnCl_2$, (3 a) $(CH_3)_2SnCl_2$ in Kbr. (*) – the absorbence line corresponding to gaseous CH_4 [12].

To characterize methane activation on basic catalysts, methane adsorption on magnesium oxide was studied by IR-Fourier transform spectroscopy [12]. The interaction of methane with the surface of magnesium oxide at 300°C gives rise to the appearance of bands at 3650 cm^{-1} ascribed to hydroxyl groups and of new bands in the region 2940 and 2980 cm^{-1} associated with C–H stretching vibrations (Figure 1.22). As the temperature was increased up to 500°C, a concerted decrease in band intensities was observed. This is evidence that a dissociatively adsorbed state of methane is present on the surface of magnesium oxide. A comparison of the bands observed in the spectra of materials containing metal-methyl and methoxy groups suggests that adsorbed CH_3 groups are bound to magnesium ions. Support for this conclusion comes from experiments in which CH_3OH and $(CH_3)_2SnCl_2$ was adsorbed onto MgO (Figure 1.22). Note also that a band at 3085 cm^{-1} was observed after exposure of a sample with methane adsorbed at 300°C. This is suggestive of C–H stretching vibration associated with a double bond and can be attributed to the molecule of ethylene.

According to the heterolytic mechanism of methane activation the scheme for interaction of methane with the surface of basic catalysts is as follows:

$$CH_4 + M^{2+}O^{2-} \leftrightarrow CH_3^- M^{2+} + H^+O^{2-} \qquad (1\,g)$$

$$CH_3^- M^{2+} \xrightarrow{-e} CH_3\cdot + M^{2+} \qquad (2\,g)$$

The first stage is the heterolytic dissociation of methane to produce a surface metal-methyl compound. The coordinatively unsaturated metal ion, paired to a strong nucleophile (O^{2-} ion), may act as an active center. The results of quantum-mechanical calculations for the interaction of a methane molecule with MgO show that the interaction energy is positive only for the coordinatively unsaturated Mg^{2+} ions. For Mg^{2+} with coordination number three the energy of the $Mg–CH_3$ bond is close to the activation energy of the oxydehydrodimerization of methane observed on this catalyst. In a recently published investigation on the oxidative coupling of methane on ultrafine crystalline magnesium oxide doped with lithium[14], a considerable amounts of coordinatively unsaturated centers were observed. According to the luminescence spectra, the assumed coordination number of magnesium was three. The lithium dopant is assumed to be responsible for the generation of coordinatively unsaturated centers. These centers are considered to be the centers of methane activation, which is confirmed by the correlation between the luminescence intensity of these centers (λ_{max} = 1450 nm) and the catalyst activity.

Earlier work by Garrone and Stone[105] on basic oxides indicated that surface sites with different coordination numbers, e.g., 5, 4 or 3, showed different acid-base properties and different reactivities towards adsorbed molecules. Basicity increases with increased coordinative unsaturation. Thus, molecules with relatively low pK_a values, e.g., CH_3OH or water (pK_a = 16) dissociate extensively on MgO even at the least reactive $Mg_{5C}^{2+}–O_{5C}^{2-}$ pairs whereas the dissociation of ammonia or C_2H_4 (pK_a = 36) or methane (pK_a = 40) requires the sites of greatest coordinative unsaturation ($Mg_{3C}^{2+}–O_{3C}^{2-}$). The authors gave an estimate of the relative proportions of surface ion pairs $Mg_{5C}^{2+}–O_{5C}^{2-}$, $Mg_{4C}^{2+}–O_{4C}^{2-}$ and $Mg_{3C}^{2+}–O_{3C}^{2-}$ in polycrystalline MgO, there were 90%, 10% and 1%, respectively.

The anion methyl form may donate its electron to an accepting center and transform to a methyl radical, which then dimerizes. This stage can proceed with intermediate transformation of metal-methyl groups to methoxy groups. If there is an insufficient supply of these centers on the surface this step may become the limiting one. Metal ions with transient valence in the oxidized state as well as electrophilic forms of oxygen and defects of the crystalline lattice, including hole centers of the catalyst such as V-centers (the analogs of O^- in solid oxide) may act as accepting centers. However,

these latter defects are not located on the catalyst surface, so cannot act as centers of radical detachment. In this case a correlation between the dimerization rate and the concentration of hole centers in the catalyst may be observed.

Studies on the mechanism of methane oxidative coupling are continuing. At present, one may mention several more or less well-established facts.

1. Methane oxidative coupling proceeds via a heterogeneous-homogeneous mechanism that implies the interaction of CH_4 molecule with the surface $O_{(S)}$ oxygen centers and the formation of OH groups on the surface and $CH_3^{\cdot}$ radicals in the gas phase.

2. The strongly basic oxides of alkali metals, alkaline earths and the rare earths constitute the best catalytic material. These trends can be explaned by an acid-base mechanism which is based on the assumption that methane activation proceeds via heterolytic cleavage on a basic O^{2-} site with a low coordination number.

3. Ethane is formed by recombination of $CH_3^{\cdot}$ radicals in the gas phase. The probability of this reaction on the catalyst surface is low.

4. Ethane can be converted into ethylene by oxidative dehydrogenation of C_2H_6 by an interaction with the surface oxygen, $O_{(S)}$, or in the gas phase.

5. Complete oxidation to CO occurs either in the gas phase through oxidation of formyl radicals, CHO (or by thermal decomposition) or on the surface via interaction between $CH_3^{\cdot}$, $C_2H_5^{\cdot}$, C_2H_6, or C_2H_4 and mobile oxygen (O^{2-}). Further oxidation of CO yields CO_2.

1.3 Direct oxidation of methane to oxygenates

1.3.1. Partial oxidation of methane to methanol The world consumption of methanol today is in excess of 25 million tons per year and growing steadily. This indicates that methanol is still gaining importance in the bulk chemical market. More than one-third of the produced methanol is used to make formaldehyde, the rest is mainly used for the production of acetic acid and gasoline octane improvers such as methyl-tert-butyl ether. Promising new areas for methanol are the direct use in fuels or in fuel cells as well as feedstock for Mobil's MTG (methanol-to-gasoline) process.

The existing commercial process for methanol production involves two steps. In the first step hydrocarbons are reformed to synthesis gas at high temperatures. This step is highly endothermic, so that some of the hydrocarbons have to be burned in order to run the process. The second step is the low-pressure methanol synthesis, where the syngas is catalytically converted to methanol at around 250°C and 50 bar. The hydrocarbon sources for the first step include natural gas, petroleum residues, naphtha, and coal, the first being by far the most important.

The direct partial oxidation of methane has been investigated by several authors. The published results for the homogeneous gas phase reaction seem to be very promising in respect to methanol selectivity, but in most of the studies the yield is still far too low to be of economic interest.

There seems to be little dispute about the mechanism, which has a first step:

$$CH_4 + O_2 \rightarrow CH_3 + HO_2$$

The equilibrium

$$CH_3 + O_2 \leftrightarrow CH_3O_2$$

plays a key role in the way products vary with temperature. The source of methanol is the methoxy radical, CH_3O, formed from the methylperoxy radical, CH_3O_2, reacting with hydrogen atoms from the various species present. As methane is present in excess, it is the most probable source of the hydrogen atoms, as in:

$$CH_3O + CH_4 \rightarrow CH_3OH + CH_3$$

Parkyns et al.[2] also drew attention to the possible influence of the OH radical on events, as it reacts with any source of hydrogen atoms to form water. This is essentially a stable product under condition of these experiments (400-500°C) and considerations of hydrogen balance show that for each molecule of water formed, the selectivity of methane conversion to methanol must fall below 100%. The modelling studies of these authors gave an upper limit of 67%.

One explanation for the lower selectivities is the possible further oxidation of methanol to other products such as formaldehyde and especially, CO_x and water. Burch et al.[106] showed, however, that methanol was a surprisingly stable molecule in a glass-lined reactor even in the presence of oxygen. In the presence of copper, however, over-oxidation was quite rapid.

Many researchers have looked at the possibility of enhancing the methanol yield by by packing the reactor with different materials to check both adverse and useful catalytic activity. The results confirm that glass is a reasonably inert surface for these reactions (i.e., the oxidation of methane to methanol and further oxidation to carbon oxides). For pressures above 40 bar stainless steel was only a little more reactive than glass, in agreement with the experience of Burch et al. Copper, on the other hand promotes complete oxidation to carbon dioxide. This finding casts considerable doubt on the validity of work of previous authors, who suggested that copper aided the formation and overall yield of methanol.

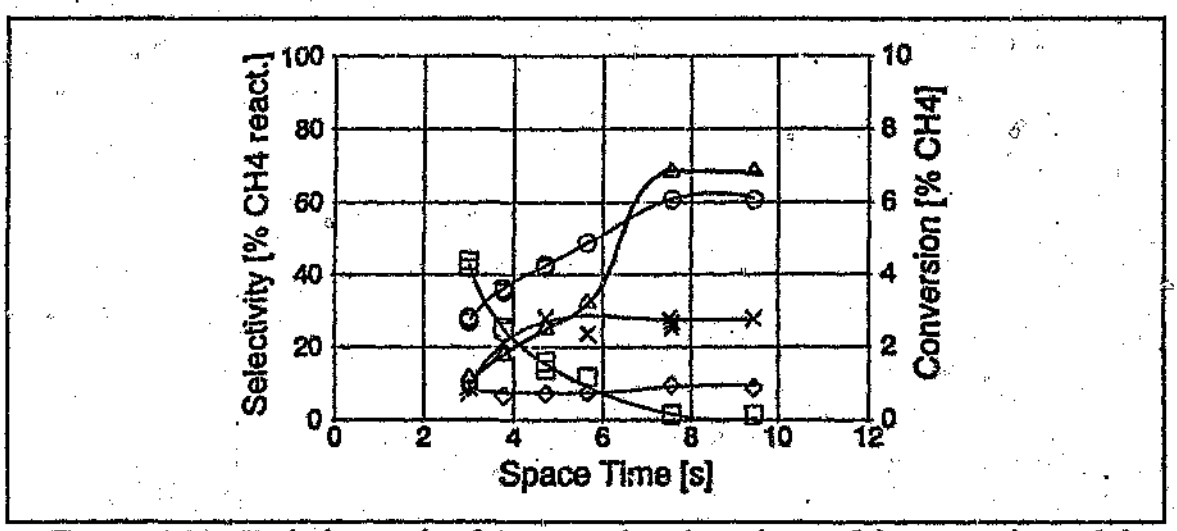
Morton et al.[107] also pointed out that the treatment of alonising a steel tube to protect it from oxidative attack, a not uncommon practice, had to be used with care. They found that the coating of alumina produced with this treatment was highly active in the methanol dehydration with dimethyl ether as a major product. This activity could be partially suppressed by washing the alonised coating with a KOH solution to neutralise acid sites on the alumina.

Rytz and Baiker[108] have also examined the effect of packing a glass-lined tubular flow reactor with quartz chips with a diameter in the range of 1-2 mm. Experiments were performed at pressures of 20-50 bar, temperatures of 425-500°C, space times of 3-12 s, and oxygen concentrations in the feed of 3, 5, and 10 mol%.

The major products found were carbon monoxide, water, and methanol with smaller amounts of formaldehyde, carbon dioxide, and ethylene. Ethane and formic acid were sometimes detected in trace quantities.

For the following observations the reaction temperature, the pressure, and the oxygen partial pressure were kept constant and only the space time was varied by changing the total flow through the reaction system. A typical example of the dependency of the selectivity and the methane conversion on the space time is shown in Figure 1.23. Obviously a higher space time increases the conversion.

At low conversion, the selectivity to methanol is very small, almost zero, but it increases with increasing space time. This may be indicative of methanol being a secondary product. The selectivity increase, however, continues only to the point where the O_2 conversion reaches 100%, and then it remains at approximately the same level before starting to drop slightly. In Figure 1.23 oxygen reaches a total conversion at the point where the CH_4 conversion starts to level off. Note that, at very low conversion, the selectivity to ethylene is high, but it drops sharply when the conversion exceeds 2% as other products start to appear. This would suggest that ethylene is a primary product. Interestingly, the ethylene yield is found to be almost independent of the space time.



Fugure 1.23. Typical example of the space time dependency of the conversion and the selectivity of the primary products. Reaction conditions: P = 50 bar, T = 450°C and 5% O_2. (o), carbon monoxide; (◊), carbon dioxide; (□), ethylene; (×), methanol (all left y axis); (Δ), conversion (right y axis) [108].

The selectivity to formaldehyde increases with decreasing space time, but it never surpasses 10%. When the oxygen conversion reached 100%, formaldehyde could no longer be detected as a product. The selectivity to carbon monoxide is almost zero at low space times and low conversion, but as the residence time increases, the selectivity to carbon monoxide also goes up. When the oxygen conversion reaches 100%, the selectivity increases very little before leveling off and remaining at the level even at longer space times. The fact that carbon monoxide appears as a product only if the conversion exceeds 1% indicates that it is a secondary product like methanol.

The selectivity to carbon dioxide does not change very much over the range of the reaction parameters, and carbon dioxide is present even when the conversion is very low; this may indicate that carbon dioxide like ethylene is a primary product.

To determine the effect of the pressure on the selectivity and the conversion, experiments were carried out in a pressure range between 20 and 50 bar. The other reaction parameters (i.e., temperature and oxygen partial pressure) were kept constant. As is to be expected, at higher pressures, the conversion of methane increases. It reaches a maximum when all the oxygen is consumed.

Carbon monoxide selectivity increases monotonically with rising pressure. The selectivity to methanol also goes up with increasing pressure, until the oxygen conversion reaches 100%. The selectivity to formaldehyde is always below 10% and it drops to practically zero with rising pressure. The pressure dependency of the ethylene selectivity shows behavior similar to the corresponding space time dependency.

As expected, the conversions of methane and oxygen increase with increasing temperature. The selectivity to methanol seems to increase at low conversion levels and decline at higher conversion levels, when the temperature is increased. The selectivity to carbon monoxide, however, is almost unaffected by an increasing temperature. This is also true for carbon dioxide, the selectivity of which, as has been mentioned earlier, stays at approximately the same level for all the reaction conditions. At low conversions the ethylene selectivity is high, but with increasing conversion it drops sharply to insignificance at high conversion levels.

Rather similar results have been reported by Haruta et al.,[109] this time using an empty quartz tube (diameter = 10 mm, heating volume = 24 ml). Even under normal pressures (1.5-3.0 bar), they observed the formation of methanol by gas phase reaction

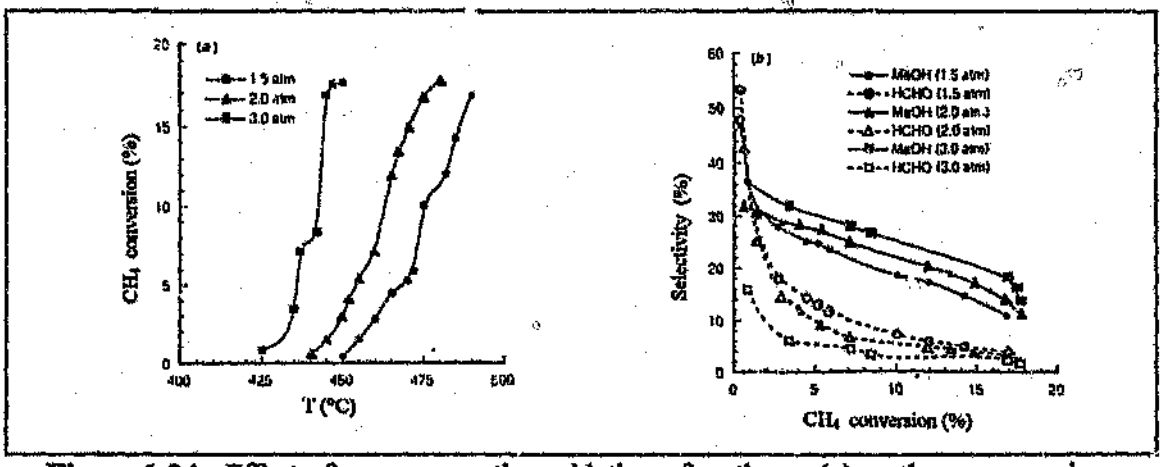


Figure 1.24. Effect of pressure on the oxidation of methane: (a) methane conversion as a function of temperature; (b) product selectivity as function of methane conversion. Reaction conditions: $CH_4 : O_2 = 4:1$, flow rate = 15 ml/min, residence time = 96 s [109].

of methane with oxygen in the 425-490°C range with methanol selectivities exceeding 30% at a methane conversion of 5%.

Figure 1.24 (a) shows the conversion of methane under different pressures as a function of reaction temperature. An increase in pressure shifts the reaction curves toward lower temperatures, in agreement with the previously reported results for the high pressure reactions, and also makes the slopes of the curves greater.

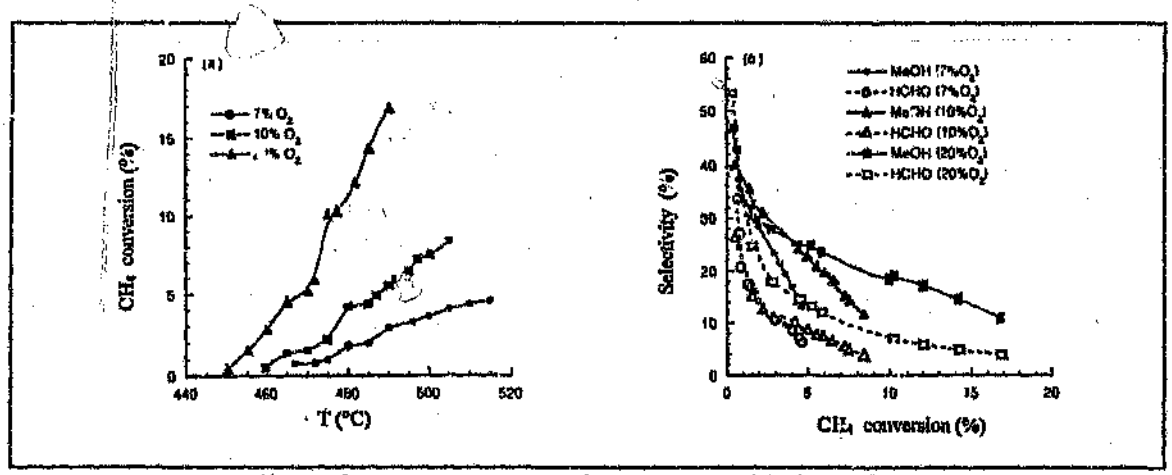


Figure 1.25. Effect of oxygen concentration on the oxidation of methane: (a) methane conversion as a function of temperature; (b) product selectivity as a function of methane conversion. Reaction conditions: $CH_4 : O_2 = 4:1$, flow rate = 15 ml/min, residence time = 96 s, pressure = 1.5 bar [109].

Thus, to increase methane conversion from 6.7 to 14%, a temperature increase of only ~5°C was sufficient at 3.0 bar, while an increase of more than 15°C was needed at 1.5 bar.

The selectivities to methanol and formaldehyde plotted against CH_4 conversion (Figure 1.24 (b)) show that at the very beginning of the reaction, the selectivities to HCHO were larger than to CH_3OH. As the reaction progressed with an increase in reaction temperature, selectivities to HCHO markedly decreased and became smaller than those for CH_3OH. Since methanol and formaldehyde are easily attacked by radical species resulting in the formation of carbon oxides, an increase in methane conversion always causes a decrease in the selectivities to these partial oxidation products.

Since oxygen is the limiting reactant in these reactions, as shown in Figure 1.25 (a), increasing O_2 concentration appreciably decreases the reaction temperature. Figure 1.25 (b) shows that at low methane conversions (below 2%), the methanol selectivities are little affected by O_2 concentration; however, at higher methane conversions, higher O_2 concentrations become advantageous for methanol formation. Consequently, the formation of the partially oxidized products is more favoured when a higher oxygen concentration is used.

As generally expected, in order to obtain the same methane conversion, higher temperatures are needed for shorter residence times. It was observed that for obtaining a methane conversion of about 7% by the reaction of methane with oxygen at a concentration of 20% under 3 bar, the reaction temperatures required were 435, 455 and 468°C at residence times of 96, 32 and 24 s, respectively. Within the range of the residence times investigated, however, methanol selectivities were found to be little affected.

Attempts have been made to influence the initiation reaction, i.e., by addition of small amounts of other initiating species. Thus, Omata et al.[110] placed a Pt wire at the entrance to a conventional flow quartz tube at 42.5 bar with a methane/air mixture at CH_4/O_2 ratio of 30. Heating the platinum wire to about 250°C lowered the temperature at which the reaction started from 420°C to 380°C. Lowering of the temperature by 40°C was observed throughout the range studied but there was almost no effect on the selectivity to methanol which was low throughout the experiments (18.8% selectivity for a methane conversion of 2.4% in the presence of Pt).

They rationalised their results by assuming that the Pt wire produced methyl radicals:

$$CH_4 + R^{\bullet} \rightarrow CH_3 + RH$$

which then enhanced the conventional activation step by forming methyl-peroxy species:

$$CH_3 + O_2 \rightarrow CH_3O_2$$

Addition of H_2 to the extent of 4 mol% of the methane both in the presence and absence of Pt did not affect the extent of conversion of methane but did increase the selectivity to methanol, from 6.7% to 34.2% but at a very low conversion level of methane (0.2%) at 380°C. This was accounted for by the increased tendency of CH_3O radicals to react to give methanol rather than decompose to formaldehyde and hence to oxides of carbon:

$$CH_3O + H_2 \rightarrow CH_3OH + H$$

Catalytic oxidation of methane to methanol. Most workers generally found that passing methane/oxygen mixtures over a catalyst yielded results inferior to those obtained in its absence. They have also reported that metals such as Ni, Cu, Ag, steel and certain alloys appear to have a catalytic effect. The results show that at relatively low pressures the use of metallic reactors and/or catalysts leads to the formation of complete oxidation products. However, at higher pressures none of the experimental parameters studied had a significant influence on the selectivity to methanol.

Investigations on the stability of methanol at high temperatures and pressures in the presence of oxygen performed by Burch et al.[111] showed that loss of methanol through further oxidation is unimportant except in the presence of metals such as Cu. In the presence of methane and oxygen some methanol is destroyed, and this is attributed to reactions involving methyl radicals produced during the activation of methane by oxygen. However, this loss of methanol is insufficient to account for the low overall selectivity observed. It is concluded that the detailed design of the reactor may be of critical importance in obtaining high methanol yields.

Table 1.11. Effect of Cu on the selectivity to methanol. The reaction mixture comprised $CH_4 : O_2 : N_2 = 20 : 1 : 19$ [111].

P (bar)	Flow rate (ml/min)	T (°C)	X_{CH4} (%)	S_{CH3OH} (%)	
				Cu	Non
10	30	450	1.3	< 10	41
32	30	450	3.5	20 - 25	35
30	240	475	2.2	< 20	29

The purpose of the work of Burch et al. was to examine the relative importance of homogeneous gas-phase and surface-catalysed processes in the direct synthesis of methanol from methane at high pressures and temperatures.

The results obtained in their work showed clearly that the choice of reactor is important, especially when operating at low pressures. Thus, when using a steel reactor no methanol is produced until the pressure exceeds 20 bar, whereas with a glass-lined reactor methanol is observed at all pressures ≥ 5 bar. Furthermore, although the selectivity to methanol in a steel reactor increases with pressure it is still less than that observed with a glass-lined reactor at 50 bar.

They have also investigated the effect of using a Cu insert in the steel reactor. No methanol was detected at 10 bar. When 500 mg of Cu turnings were placed in the Pyrex-lined reactor the results shown in Table 1.11 were obtained. Comparison with the results obtained in the absence of Cu show clearly that Cu catalyses the complete oxidation of methane and/or methanol. Numerous other metallic and non-metallic catalysts were tested, but in all cases the selectivity to methanol was much lower than that obtained from the purely homogeneous reaction.

The stainless steel is a less reactive surface, but even at temperatures around 450°C more than 50% of the methanol produced was destroyed by further oxidation. In a Pyrex-lined reactor the methanol is remarkably stable, and there is virtually no further oxidation, even at 500°C. This would tend to suggest that the low overall selectivities which they observed are not due to loss of methanol once formed.

Very recently, Chun and Anthony[112] have also published results which gave the same conclusion. At pressures of 50 bar and short residence times (2-5 seconds). They

obtained better methanol yields for the homogeneous gas phase reaction then for the reactions carried out in the presence of numerous catalysts in a temperature range of 370-480°C.

To investigate if homogeneous reactions occur in the void volume of the catalyst bed and if mixed oxide catalysts inhibit homogeneous reactions, the temperature profile, conversions, and product selectivities were compared using Pyrex beads and potential catalysts. For this investigation, 0.125/0.149 mm Pyrex beads, 0.125/0.149 mm vanadium pentoxide pellets, and 0.074/0.149 mm 25% Ag/α-alumina were used.

The methanol selectivities for the empty Pyrex tube at low oxygen conversions were significantly higher than the methanol selectivities at the higher oxygen conversions. The methanol selectivity with an empty tube at a methane conversion of 4.0% was 39.7%, but the methanol selectivity with 0.125/0.149 mm Pyrex beads at a methane conversion of 0.7% was 42.4%. These results indicate that the surface of Pyrex glass inhibits the free-radical reactions. The conversions of methane with the 0.125/0.149 mm vanadium pentoxide (residence time 4.5 s) and with 0.074/0.149 mm 25% Ag/α-alumina loading were less than 1.5% at 450°C. For CuMo/Si-S, 25% CuO/α-alumina, FeMo/Si-S or V_2O_5/Ti-I the reaction did not occur at temperatures less than 520°C and 50 bar. These results suggest that homogeneous reactions are occurring in the void volume of the catalyst bed, and the catalysts are not very active.

The inhibiting effect of oxide catalysts can be explained by free-radical chemistry. The gas-phase homogeneous oxidation of methane is a free-radical chain reaction with initiation, propagation and termination. The initiation step is hydrogen abstraction from methane by molecular oxygen:

$$CH_4 + O_2 \rightarrow CH_3 + HO_2$$

The HO_2 radicals produced from this reaction propagate the primary chain reaction. It is common knowledge that the chain reactions terminate at the surface of mixed oxide catalysts probably by removal of species such as HO_2 or H_2O_2. Therefore, the reaction temperature with mixed oxide catalysts is higher than the reaction temperature in an empty tube.

1.3.2. Partial oxidation of methane to formaldehyde. Catalytic partial oxidation reactions of methane to C_1 oxygenates have been intensively studied worldwide during the last decade by many research groups. Most studies have focussed on increasing the overall formaldehyde yields and selectivities, while very few efforts have been placed on a mechanistic understanding of the reaction. Silica has been widely used as a support for metal oxide catalysts for methane partial oxidation to oxygenates. A number of papers have shown that silica itself has some catalytic activities for methane oxidation to formaldehyde. Kasztelan and Moffat[113] have shown that up to 4.5% of the methane co-fed with O_2 can be converted at 593°C at relatively high contact times, but selectivity to formaldehyde was poor (8%) and no formaldehyde was detected with N_2O as oxidant.

There has been a suggestion in previous literature that dioxygen may be over-active and may oxidise any formaldehyde produced to carbon oxides. Nitrous oxide has been proposed as an alternative, although the evidence for improvement has never been convincing. The catalyst group at Limerick[114] has investigated the use of both oxidants in a series of metal oxide catalysts supported on silica. They confirm that only molybdenum or vanadia show any activity towards formaldehyde formation. Over a range of 500 to 800°C, the conversion of methane was low (< 1% for both Mo and V) using N_2O and the selectivity to formaldehyde modest (21% at 0.9% conversion). An interesting point was made in that the conversion depended quite markedly on the CH_4/oxidant ratio, being much greater when methane was present in excess. The authors comment that this effect tended to obscure the effect of the choice of the oxidant, so that it was not easy to say which was the more selective reagent. None the less, nitrous oxide did not have a decisive advantage over oxygen, in line with earlier results.

They also have reported the inability of Fe, Ag, Cr, Na and Co ions to improve the activity of silica-supported MoO_3 and V_2O_5 catalysts. For unpromoted V_2O_5/SiO_2 catalysts, they found that a V_2O_5 loading in the range 1.8-7.2 wt.% gave the best performance. Such a high activity of the medium loaded V_2O_5 catalysts has been attributed to their capability to readily undergo a reduction-reoxidation process in the reaction conditions.

Table 1.12. Activity and formaldehyde productivity of "fumed" M5 and "precipitated" Si 4-5 P SiO_2-supported MoO_3 and V_2O_5 catalysts in the partial oxidation of methane [115].

Sample	BET S.A. ($m^2 \cdot g^{-1}$)	T (°C)	Reaction rate (10^{-7} $mol_{CH4} \cdot g^{-1}_{cat} \cdot s^{-1}$)	Selectivity (%)			STY_{HCHO} ($g \cdot kg^{-1}_{cat} \cdot h^{-1}$)
				HCHO	CO	CO_2	
4.5% MoO_3/SiO_2 M5	165	550	0.57	95	–	5	6.16
		600	2.93	91	5	4	29.51
		650	13.65	86	9	5	126.78
2.2% V_2O_5/SiO_2 M5	191	550	9.98	82	15	3	88.31
		600	58.34	50	23	27	318.05
		650	216.98	30	35	35	687.46
4% MoO_3/SiO_2 Si 4-5P	187	550	1.00	70	–	30	7.60
		600	3.13	70	–	30	22.70
		650	10.50	70	2	28	76.10
5% V_2O_5/SiO_2 Si 4-5P	231	550	15.27	61	2	37	100.55
		600	60.87	48	14	38	318.05
		650	210.61	35	51	14	793.48

Parmaliana et al.[115] have presented a comparative study of the catalytic properties of various bare SiO_2 samples and differently loaded MoO_3/SiO_2 and V_2O_5/SiO_2 catalysts in the partial oxidation of methane to formaldehyde. The experiments were performed using a specifically designed batch reactor, provided with an external recycle pump and a liquid product condenser placed downstream of the reactor and maintained at –15°C, which traps the oxygenated products and prevents their further oxidation. The reaction mixture consisted of 18.2 mmol of methane, 9.1 mmol of oxygen ($CH_4/O_2 = 2$) and 54.6 mmol of helium as diluent.

Amongst the different SiO_2 samples, the highest HCHO productivity expressed as space time yield (STY_{HCHO}, $g \cdot kg^{-1}_{cat} \cdot h^{-1}$) is found with "precipitated" silica, while "fumed" SiO_2 results in the least reactive silica.

Table 1.13. Methane partial oxidation on silica and silica-supported MoO_3 and V_2O_5 catalysts in the presence and absence gas-phase oxygen [115].

Catalyst	T (°C)	Reagents	Rate of product formation (10^{17} molec · g^{-1}_{cat} · s^{-1})		
			HCHO	CO	CO_2
SiO_2 Si 4-5P	550	$CH_4 + O_2$	0.63	2.61	12.30
		CH_4	–	–	–
	600	$CH_4 + O_2$	1.68	6.90	2.61
		CH_4	–	–	–
	650	$CH_4 + O_2$	3.54	16.80	6.33
		CH_4	–	0.75	–
4% MoO_3/SiO_2 Si 4-5P	550	$CH_4 + O_2$	0.30	0.48	1.08
		CH_4	–	–	–
	600	$CH_4 + O_2$	0.90	1.05	1.95
		CH_4	–	–	–
	650	$CH_4 + O_2$	2.55	3.60	2.25
		CH_4	–	–	–
5% V_2O_5/SiO_2 Si 4-5P	550	$CH_4 + O_2$	1.68	2.46	1.38
		CH_4	–	–	–
	600	$CH_4 + O_2$	3.60	20.04	8.28
		CH_4	–	1.35	–
	650	$CH_4 + O_2$	5.76	76.50	16.80
		CH_4	0.30	7.20	3.30

The activity data of the oxide catalysts supported on "fumed" M5 silica and "precipitated" Si 4-5 P SiO_2 are presented in Table1.12 in terms of reaction rate, product selectivity, and STY_{HCHO}. These results indicate that MoO_3 and V_2O_5 do improve the catalytic properties of "fumed" SiO_2. The promoting effect of V_2O_5 is more pronounced than that of MoO_3 even if the loading of V_2O_5 is lower than that of MoO_3. In fact, V_2O_5 exerts a promoting effect on the activity of "precipitated" SiO_2 similar to that observed for the addition of V_2O_5 to the "fumed" SiO_2. This is in

agreement with the literature data, while MoO_3 decreased the original activity of the bare "precipitated" SiO_2 sample. The different promoting effect of MoO_3 and V_2O_5 on the reactivity of the silica surface can be explained by invoking a different capability of such supported oxides in stabilising reduced states of metal ions. According to the literature data, Mo ion on the SiO_2 surface exists in octahedral coordination which assists the stabilisation of the highest oxidation state (Mo^{VI}). On the contrary, for V_2O_5/SiO_2 catalysts it has been claimed that V ions form surface compounds with lower coordination number which assist the stabilisation of lower oxidation states.

The partial oxidation of organic compounds usually proceeds via a stepwise mechanism, while the data presented in Table 1.13 suggest that the partial oxidation of methane to HCHO on silica-based oxide catalysts in the temperature range 550-650°C occurs mainly through a concerted mechanism without participation of lattice oxygen. It can then be proposed that O_2 species, more active than lattice O_2 ions ($O^{2-}_{(l)}$), are involved in the title reaction. These active species can be created in the process of gas-phase O_2 ($O_{2(g)}$) interaction with the reduced sites (*RS*) on the catalyst surface. If such an interaction proceeds with rather a low rate some intermediate species $(O)^*_s$ (between initial state ($O_{2(g)}$) and final state ($O^{2-}_{(l)}$)) can have a long lifetime. This condition likely occurs on the catalyst surface having rather a low density of electrons which avoids a rapid deep reduction of molecular oxygen to lattice ions ($O^{2-}_{(l)}$):

$$O_{2(g)} \xrightarrow{RS} (O)^*_s \rightarrow O^{2-}_{(l)}$$

Taking into account that the catalysts possess a very low concentration of reduced sites (~ 0.01% of O_2 monolayer) for O_2 activation, the above condition related to the long lifetime of active intermediate O_2 species $(O)^*_s$, which should be realised on the catalysts. Then, it can be proposed that the amount of specific reduced sites having the capability to activate gas-phase O_2 and stabilise surface active oxygen species $(O)^*_s$ governs the catalytic behaviour of silica-supported oxide catalysts in the partial oxidation of methane. This statement is strictly supported by the straight correlation between density of reduced sites and STY_{HCHO} for different silica-supported oxide catalysts.

The next important point for the partial oxidation relates to the activation of the hydrocarbon molecule. This activation can occur on acidic sites on the oxide surface. The data clearly shows that the CH_4 activation process is not the rate-determining step for the partial oxidation of methane. Indeed, a different order for the acidity and activity properties of the unpromoted and MoO_3 and V_2O_5 doped SiO_2 catalysts has been found. As shown above the reason for the different catalytic activities observed in such oxide catalysts lies in their different abilities to activate gas-phase oxygen. This means that redox properties play a prominent role in controlling the activity of the oxide catalysts in the partial oxidation of CH_4 to HCHO. Then, taking into account the above experimental findings as well as the literature data dealing with the suitability of the SiO_2 surface in activating CH_4 molecules, the following reaction pathway seems adequate for describing the partial oxidation of methane with O_2 on silica-based oxide catalysts:

$$CH_4 + L \leftrightarrow (CH_4)^*_S + (O)^*_S \rightarrow P$$

$$\uparrow$$

$$RS$$

$$+$$

$$O_{2(g)} \text{ or } O_{2(S)}$$

where $(CH_4)^*_S$ and $(O)^*_S$ indicate CH_4 and O_2 surface activated species respectively, P refers to HCHO and CO_2, and L and RS represent specific surface centers for CH_4 activation and the reduced surface site, providing molecular oxygen activation from gas-phase ($O_{2(g)}$) or adsorbed form ($O_{2(S)}$), respectively.

To summarise work to date in this field, there now seems to be a consensus that the use of nitrous oxide offers no advantage in respect of selectivity to formaldehyde over the use of dioxygen. Formaldehyde seems to be a primary product and methanol which is sometimes observed in very small amounts, is probably formed in a parallel reaction. All pathways can be accounted for in terms of homolytic reactions, even those on the surface, with CH_3 as a primary reactant. At temperatures of 650°C or lower, CH_3O_2 is formed in the gas phase and is the most likely source of oxygenates.

The partial oxidation of methane to formaldehyde with molecular O_2 over bare SiO_2 and silica-supported MoO_3 and V_2O_5 catalysts proceeds mainly via a concerted mechanism without participation of lattice oxygen.

The acidic properties of silica-based oxide catalysts seems to exert no direct influence on the reaction pathway of the methane partial oxidation.

A direct relationship exists between the density of reduced sites and the reactivities of oxide catalysts in the partial oxidation of methane to formaldehyde. The catalytic activity of these catalysts is controlled by the capability to provide activation of gas-phase oxygen into active species by reduced sites on the catalyst surface.

1.4 Different types of oxidants for methane oxidative coupling and selective oxidation of lower paraffins

In most studies on the oxidative coupling of CH_4 to C_2H_6 and C_2H_4, molecular oxygen has been used as the oxidant. Because the coupling reaction is a complex network of heterogeneous and homogeneous reactions, it is instructive to employ other oxidants, such as nitrous oxide. Otsuka and Nakajima[116] obtained kinetic data for the oxidative coupling reaction over Sm_2O_3, using N_2O as the oxidant. They observed that for the oxidative coupling reaction at a relatively low temperature (550°C) using N_2O as oxidant resulted in the formation of C_2H_6 with high selectivity, while complete oxidation occurred with O_2 as the oxidant. Moreover, N_2O decomposition was believed to be the rate-limiting step in the catalytic cycle.

Hutchings et al.[117,118] have also compared N_2O and O_2 as oxidants. The results of their experiments presented in Table 1.14 show that the exchange of O_2 for N_2O at 530°C has no effect upon the yield and selectivity of C_{2+} hydrocarbons on magnesium oxide, while on Li/MgO the selectivity increases markedly, but the conversion is diminished by an order of magnitude (this could be the reason for the rise in selectivity)

Table 1.14. Influence of the nature of the oxidants on oxidative coupling reaction on MgO and Li/MgO catalysts (CH_4/oxidant = 3.3-3.5)[117].

Catalyst	Oxidant	T (°C)	X_{CH4} (%)	Selectivity (%)		
				C_2H_4	C_2H_6	C_{2+}
MgO	O_2	550	3.0	0.4	1.6	2.0
Li/MgO	O_2	550	1.6	5.0	17.5	22.5
MgO	N_2O	550	1.8	0.3	1.6	1.9
Li/MgO	N_2O	550	0.2	7.0	75.8	82.8
MgO	O_2	720	5.2	28.4	18.4	46.8
Li/MgO	O_2	720	2.7	26.5	38.9	65.4
MgO	N_2O	720	3.0	2.7	1.6	4.3
Li/MgO	N_2O	720	0.3	9.3	38.9	48.2

Increasing the temperature to 720°C resulted in a decrease in both conversion and tivity for the two catalysts when O_2 was replaced by N_2O. For MgO it was an order of magnitude.

The origin of CO_2 during the oxidative coupling of CH_4 is still a matter of conjecture; however, it is clear that certain important gas phase reactions occur with O_2, but not with N_2O. For example, the reaction:

$$CH_3 + O_2 \rightarrow CH_2O + OH$$

supplies hydroxyl radicals which are known to be chain carriers in the combustion of hydrocarbons. By contrast, the analogous reaction with N_2O:

$$CH_3 + N_2O \rightarrow CH_3O + N_2$$

does not form OH radicals. The previous attempts to model the heterogeneous-homogeneous coupling reaction over Li/MgO with O_2 as the oxidant suggested that gas phase reactions did not account for more than 10% of the CO_x at short residence times, at 700°C, and with low partial pressures of reagents. If this is indeed the case, then one must look for other explanations for the differences in the product selectivities between O_2 and N_2O as oxidants. Molecular oxygen may form a different type of active site on the surface that is responsible for the complete oxidation of the hydrocarbons in the system. Such a site might be O_{3s}^- ions, which are known to be formed at low temperatures by the reaction:

$$O_s^- + O_2 \rightarrow O_{3s}^-$$

were the subscript "s" refers to a surface species. In stoichiometric reactions ozonide ions were found to be much less selective than O_s^- ions in the dehydrogenation of alkanes over MgO.

As an oxidant for a kinetic study N_2O has a distinct advantage over O_2 with respect to the range of CH_4/O_2 ratios that can be explored. At CH_4/O_2 ratios ≤ 1, complete combustion begins to dominate, whereas, with N_2O as the oxidant large C_2 selectivities

Table 1.15. Comparison of O_2 and N_2O as oxidants for the oxidative coupling of CH_4 over a Li/MgO catalyst. ($P(CH_4)$ = 30 kPa, $P(O_2)$ = 5.6 kPa and $P(N_2O)$ = 68 kPa)[119].

Oxidant	T (°C)	X_{CH4} (%)	Selectivity (%)				
			C_{2+}	C_{2-}	C_3	CO_2	CO
O_2	635	3.0	7	22	1	46	25
O_2	646	3.9	10	24	1	44	21
O_2	665	7.1	16	37	2	34	11
O_2	680	10.7	22	36	4	32	6
N_2O	635	2.2	16	63	12	9	0
N_2O	650	3.1	23	59	10	9	0
N_2O	665	4.8	29	50	11	9	0
N_2O		6.8	35	44	11	10	0

are observable under differential conditions, even at CH_4/O_2 ratios of 0.1. As a consequence the entire range of rate-limiting steps may be examined, from oxygen incorporation in the catalyst at one extreme to C-H bond breaking at the other extreme. Since nonselective secondary reactions involving the oxidant are less likely to occur, it is also possible to study the rate of methyl radical formation over a much broader range of oxidant partial pressures with N_2O than with O_2.

The recent investigation of Lunsford et al.[119] was carried out in an effort to explore further the mechanism of the oxidative coupling reaction over Li/MgO catalysts using N_2O as the oxidant. In this study an attempt was made to compare N_2O and O_2 as oxidants at a near equal level of CH_4 conversion. This was achieved by measuring the CH_4 conversion level at an arbitrary set of N_2O and CH_4 pressures, and then substituting O_2 for N_2O. The O_2 pressure was adjusted such that the CH_4 conversions were similar at 646-650°C. The results, as shown in Table 1.15, may be summarized as follows: (1) comparable CH_4 conversions were achieved at a much lower partial pressure of O_2, (2) the C_{2+} selectivity was greater with N_2O as the oxidant, (3) a considerable amount of C_3 product was found with N_2O, and (4) CO was detected only in the presence of O_2.

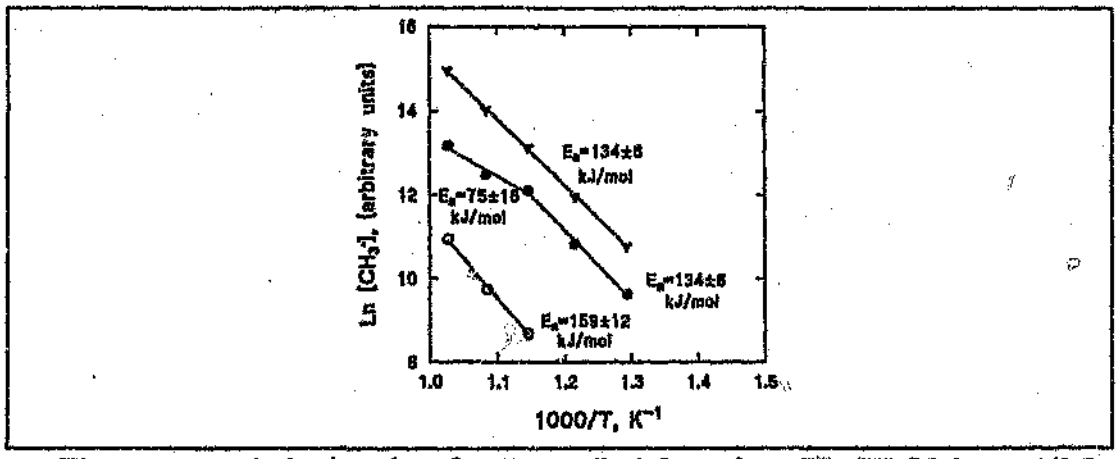


Figure 1.26. Arrhenius plots for CH_3 radical formation: (▼) CH_4/N_2O = 1.1/3.8 ml/min, (●) $Ar/CH_4/N_2O$ = 3.8/1.1/0.025 ml/min and (o) $CO_2/CH_4/N_2O$ = 3.8/1.1/0.025 ml/min [119].

Methyl radical formation was observed over the Li/MgO catalyst both at small and large CH_4/N_2O ratios. The Arrhenius plots, shown in Figure 1.26, reveal that the rate of production of CH_3 radicals increases with N_2O partial pressure. Previously it was reported that the CH_3 radical production rate increased almost linearly with respect to N_2O pressure up to a CH_4/N_2O ratio of unity, and at larger N_2O pressures the rate did not increase substantially. The change in E_a at 700°C from 75 ± 16 to 134 ± 8 kJ/mol as the CH_4/N_2O ratio increased is also consistent with a change in the rate-limiting step. Apparently, when the temperature becomes < 600°C, the rate-limiting step changes at the large CH_4/N_2O ratios, and it becomes the same as at the small CH_4/N_2O ratios; namely, C-H bond breaking. The E_a associated with this rate-limiting step is 134 ± 8 kJ/mol. It is important to note that these E_a values were obtained under catalytic conditions, but at very low CO_2 partial pressures. As pointed out previously, the rate-limiting step may be a function of the total pressure, as well as the CH_4/N_2O ratio and the temperature.

When CO_2 was substituted for Ar as the matrix-forming gas, there was a dramatic decrease in the production of CH_3 radicals, and the E_a increased by about 84 kJ/mol. A similar phenomenon was observed with O_2 as the oxidant.

The oxidant may drastically change the reaction sequence in the partial oxidation of methane to oxygenates. Otsuka and Wang[120] have reported that the product distributions for partial oxidation of methane on $Fe_2(MoO_4)_3$ catalyst were changed

Table 1.16. Comparison of catalytic results for partial oxidation of CH_4 on $Fe_2(MoO_4)_3$ with different oxidants. Reaction conditions: T = 725°C, W = 0.5 g, F_{total} = 3.6 dm^3/h, P (CH_4) = P (oxidant) = 25.3 kPa [120].

Oxidant	X_{CH4} (%)	Selectivity (%)				
		HCHO	C_2H_6	C_2H_4	CO	CO_2
O_2	2.6	49.2	0	0	47.7	3.1
N_2O	1.6	23.0	39.8	6.2	27.3	3.7

remarkably when the oxidant was switched from oxygen to nitrous oxide. When oxygen was used as the oxidant, the main products were HCHO and CO. However, when nitrous oxide was used, the formation of HCHO was greatly suppressed and C_2 hydrocarbons (C_2H_6 and C_2H_4) were produced.

Table 1.16 shows typical examples of the results for the oxidation of methane with N_2O and O_2 on a $Fe_2(MoO_4)_3$ catalyst under the same reaction conditions. When oxygen was used as the oxidant, HCHO and CO were the main products. A small amount of CO_2 and a trace of CH_3OH (selectivity < 0.1%) were also detected. However, C_2 hydrocarbons were not produced at all. In contrast to this, C_2 hydrocarbons became the predominant products when N_2O was used instead of O_2. This observation is quite unexpected, because N_2O has been believed to be a better oxidant than O_2 for the partial oxidation of CH_4 to oxygenates over molybdenum based oxides.

In order to obtain information about the reaction pathways, the changes in the product distributions with contact time have been observed for the oxidation of methane using N_2O at 700 and 725°C. As shown in Figure 1.27, the CH_4 conversion increased linearly with the contact time (expressed as W/F) at 700°C. The HCHO yield also increased linearly with the contact time, but the increase in the yield of C_2 products (C_2H_6 and C_2H_4) obviously slowed down at longer contact time. In contrast to this deceleration of the increase in C_2 yield, the CO yield increased more steeply at longer contact time. The change of the product selectivities at 700°C is shown in Figure 1.28.

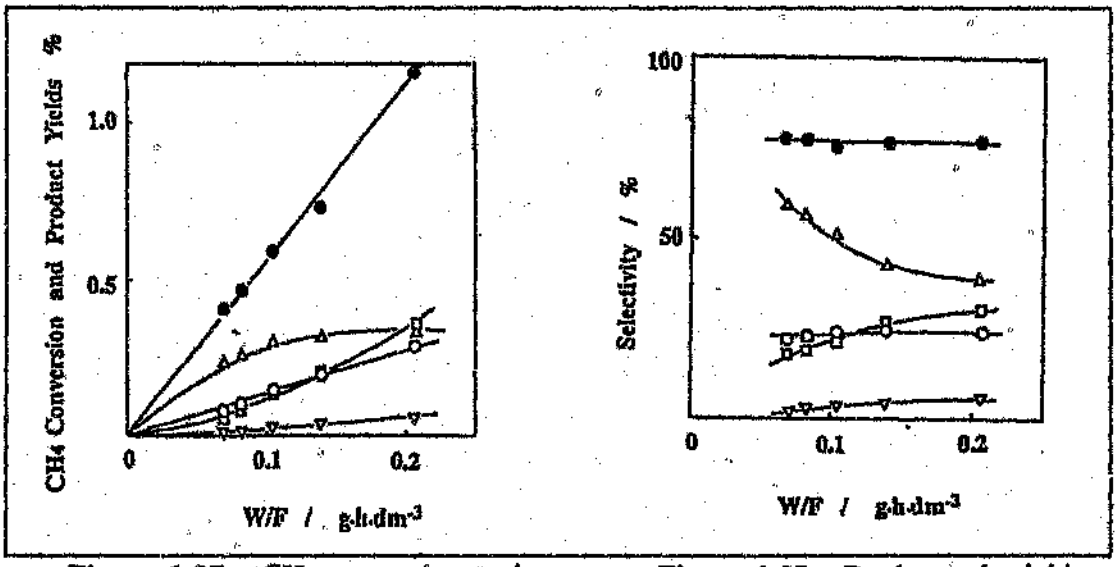
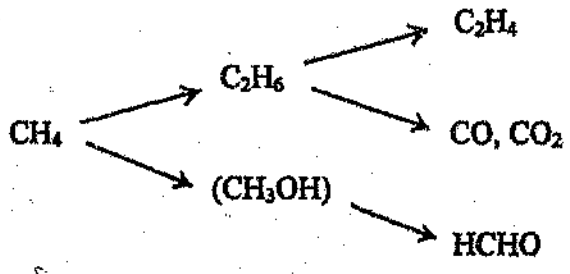


Figure 1.27. CH_4 conversion and product yields as a function of the contact time at 700°C. (●) CH_4 conversion, (○) HCHO yield, (Δ) C_2 yield, (□) CO yield, (▽) CO_2 yield [120].

Figure 1.28. Product selectivities as a function of the contact time at 700°C. (○) HCHO, (Δ) C_2, (□) CO, (▽) CO_2, (●) $C_2 + CO + CO_2$ [120].

The HCHO selectivity and the sum of the selectivities of C_2, CO and CO_2 are almost constant with the change in contact time. These results suggest that HCHO is formed in parallel with other products, namely, C_2H_6, C_2H_4 and carbon oxides (CO and CO_2). The observation that the selectivities of carbon oxides increase with a decrease in the selectivity of C_2 hydrocarbons (mainly C_2H_6) suggests that carbon oxides are the consecutive products from C_2H_6.

As a summary, the pathways for partial oxidation of CH_4 by N_2O over $Fe_2(MoO_4)_3$ can be written as



Though methanol was formed only in a trace amount, the possibility that CH_3OH is the precursor to HCHO cannot be excluded. In fact, the results of the oxidation of methanol by N_2O over $Fe_2(MoO_4)_3$ under similar reaction conditions showed that methanol was very easily transformed to HCHO.

This reaction pathways relates specifically to N_2O as an oxidant. The authors have also proposed that the reaction using O_2 over the same catalyst proceeds as follows:

$$CH_4 \rightarrow CH_3OH \rightarrow HCHO \rightarrow CO \rightarrow CO_2$$

It is to be noted that, when N_2O is used as the oxidant, C_2H_6 is formed as one of the primary products, and thus the product distributions in the two cases are notably different (Table 1.16).

Oxygen has been the oxidant of choice of most workers, although investigations have also been carried out by several groups of workers on other oxidants such as N_2O, CO_2, O_3, and even NO, NO_2, SO_2 or SO_3. With O_3, NO, NO_2, SO_2 or SO_3, carbon oxides tend to dominate the product spectrum[121,122]. Due to its high cost, nitrous oxide as oxidant is unattractive for viable industrial processes, although some interesting catalytic data have been reported. One such example is the work by Shepelev and Ione[121] who reported 9.6% CH_4 conversion with up to 90% selectivity to higher hydrocarbons, mostly aromatics and naphthalenes using nitrous oxide over a pentasil zeolite at only 400°C. This catalyst gave only 5% selectivity to hydrocarbons using oxygen and gave no hydrocarbons at all when other oxidants such as NO, NO_2 or SO_3 were used.

Gesser and Hunter[123] have investigated the possible activating effect of ozone on the methane - and ethane - oxygen reaction. They have demonstrated that it is possible to sensitize the oxidation of alkanes by converting a portion of the oxygen in an homogeneous oxidative system to ozone. In the reactor itself the ozone decomposes thermally to produce molecular oxygen and oxygen atoms which then initiate the chain reaction. The ozone was produced by a conventional electrical "silent discharge" in oxygen. At 400°C with a ratio of CH_4/O_2 of 12-13, about 2% of the methane was converted to methanol following ozanisation. With ethane, a complex mix of

oxygenates, methanol, formaldehyde, acetaldehyde and ethanol with a total selectivity of up to 95.7% was observed but at hydrocarbon conversions of < 1%.

The proposed mechanism is:

for ozone: $O_3 \rightarrow O_2 + O$

for methane: $O + CH_4 \rightarrow CH_3 + OH$

$OH + CH_4 \rightarrow CH_3 + H_2O$

$CH_3 + O_2 \rightarrow CH_3O_2$

for ethane: $O + C_2H_6 \rightarrow C_2H_5 + OH$

$OH + C_2H_6 \rightarrow C_2H_5 + H_2O$

$C_2H_5 + O_2 \rightarrow C_2H_5O_2$

When the O_3/O_2 reaction with methane or ethane was allowed to proceed at room temperature, no products were observed. This result indicates that the direct reaction of O_3 with the hydrocarbon does not occur.

A study of the oxidative dimerization and selective oxidation of methane over magnesium oxide and gallium phosphate catalysts with O_2 and O_3 as the oxidants was reported by Sokolovskii et al.[124]

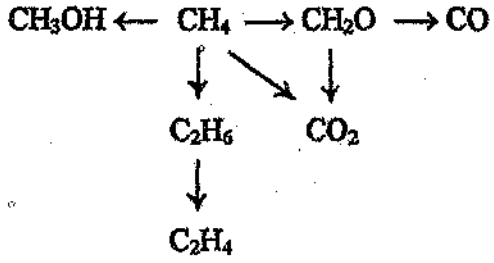
The comparison of the methane conversion and ozone decomposition rates (Table 1.17) indicates the radical character of the methane activation in ozonized oxygen. It is also confirmed by the methane conversion rate independence on the reaction temperatures ranging from 500 to 600°C in ozonized oxygen.

Methane oxidation by oxygen over gallium phosphate starts at 560-570°C. The selectivity to formaldehyde at the constant methane conversion increases with temperature. Considering the selectivity to the reaction products as a function of methane conversion one can conclude that the formation of the oxidation products (methanol and formaldehyde) and dimerization products (ethane and ethylene) proceeds via a parallel mechanism. Carbon oxides form by the further oxidation of formaldehyde.

Table 1.17. Oxidation of methane by ozone and oxygen over $GaPO_4$ catalyst. Reaction conditions: $CH_4 : O_2 = 2:1$, concentration of ozone = 0.02 vol.%, contact time = 0.7-0.8 s. (O_2^* - ozonized oxygen) [124].

T (°C)	Oxidant	Rate, 10^{10}mol/m^{2}s		Selectivity (% mol)					
		CH_4	O_3	CH_2O	C_2	C_2H_4	CO	CO_2	CH_3OH
500	O_2^*	118.1	10.4	45.8	–	–	–	54.2	–
500	O_2	–	–	–	–	–	–	–	–
550	O_2^*	232.4	9.9	42.1	3.7	–	37.5	16.3	0.4
550	O_2	–	–	–	–	–	–	–	–
575	O_2^*	193.8	11.0	73.7	2.5	0.1	6.2	15.4	0.9
575	O_2	78.0	–	78.1	0.3	0.3	11.2	10.0	0.4
600	O_2^*	227.2	11.5	71.8	6.5	0.3	13.7	7.0	0.9
600	O_2	167.0	–	70.1	0.4	0.3	16.1	12.8	0.6

The authors suggested the following general scheme for methane conversion over gallium phosphate:



On the basis of the experiments on methane oxidation by ozonized oxygen, it is possible to conclude, that methane activation by the radical oxygen species (O, O^-) under the action of gas phase oxygen at lower temperatures promotes the formation of the selective oxidation products.

Although these results are interesting, it has to be said that they were all obtained at about 1 bar pressure because the silent discharge is inherently a low pressure process. It is improbable, therefore, that the benefits of the activation by ozone could be applied to the high pressure selective oxidation of methane.

The catalytic properties of Al, Ga, Si, Bi, Pb and Fe oxides and graphitized carbon towards propane oxidation by SO_2 were studied by Sokolovskii et al.[125] in a continuous flow reactor at 600-640°C. Oxidative condensation products (OCP) containing C, H, O and S which form during the reaction over Ga, Al, Si oxides and carbon, were shown to be active towards propylene formation.

Propylene, ethylene, methane, carbon oxides and sulphur were the main products formed during propane oxidation over the studied catalysts. In the initial period of reaction CS_2 and H_2S were formed on a number of catalysts. For Ga, Al and Si oxides, propane conversion and selectivity towards propylene increased with time of stream (Figure 1.29 (a)), while for Fe, Bi, Pb oxides propane conversion decreased (Figure 1.29 (b)).

As shown by the chemical analysis data, Ga, Al and Si oxides do not change their phase composition during the reaction, but the oxidative condensation products, containing C, H, O and S, were deposited on the surface. Depending on the reaction time, Fe, Bi and Pb oxides undergo phase changes, i.e., become sulphidized. No formation of OCP was observed on these catalysts.

For identical reaction mixture compositions, the composition of the OCP formed was also similar. As the surface of catalysts was packed with OCP, the activities became

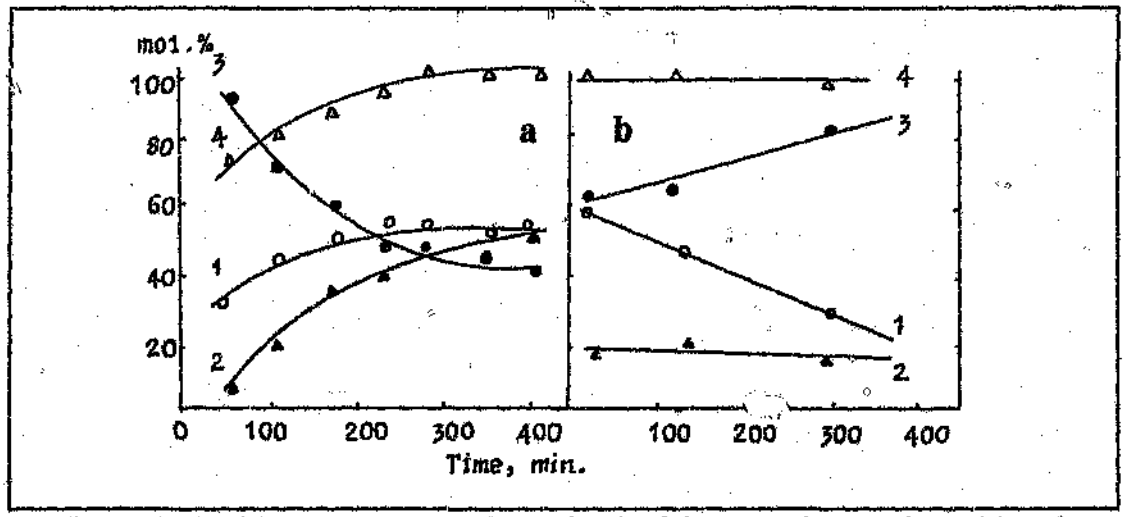


Figure 1.29. (1) Propane conversion, (2) selectivity towards propylene, (3) carbon oxides and (4) carbon balance vs. time for (a) γ-Al_2O_3 and (b) Fe_2O_3 catalysts. Contact times: for γ-Al_2O_3 = 1 s, for Fe_2O_3 = 25 s [125].

similar. Sulphidization of the catalysts did not lead to an increase in propylene formation rate. Thus, the active catalyst for selective propane oxidation with SO_2 is an oxidative condensation product occuring on the mineral substrate.

The authors have suggested that in selective propane oxidation with SO_2, the products of oxidative condensation containing C, H, O and elementary sulphur are the active species. Taking into account the observed composition of the reaction products and the rate dependence, the scheme for propylene formation can be presented as follows:

$$SO_2 + 3\,Z \rightarrow ZS + 2\,ZO$$

$$ZS + RH_2 \rightarrow R + SH_2Z$$

$$SH_2Z + ZO \rightarrow ZS + H_2O + Z$$

$$ZS \leftrightarrow Z + S$$

where Z are the active sites on the condensation product.

It is known that elementary sulphur can selectively dehydrogenate hydrocarbons and for this reason the effect of sulphur vapour treatment of the catalyst on activity towards propylene formation has been tested. The rate of propylene formation over the catalyst treated with sulphur vapours increased considerably. In all cases, treatment of the catalyst with the reaction mixture, sulphur vapours or sulphur dioxide resulted in an increase in the yield of propylene with increasing sulphur content on the catalyst surface.

The free sulphur can interact with unsaturated hydrocarbons (e.g., oxidehydrodimerization of toluene to dibenzyl or the dehydrocoupling of isobutene to 2,5-dimethylhexene reactions) forming high boiling sulphur compounds, which may deactivate the catalyst by accumulation on its surface. One may decrease such contact deactivation by introducing sufficient amounts of dioxygen into the reaction mixture to prevent the deposition of such sulphur compounds but insufficient for deep oxidation to occur. The positive effect achieved by the addition of optimum amounts of dioxygen results from the formation of hydrogen sulphide and its subsequent oxidation to sulphur dioxide. This provides a more efficient utilization of the process in the catalyst bed.

Sulphur dioxide is in general a milder oxidant than dioxygen. However, technological complications may arise due to the corrosive nature of sulphur compounds and the separation of sulphur from the reaction products.

Many researchers have attempted to increase the productivity and selectivity of direct oxidation and oxidative coupling of methane to avoid "the limiting yields", e.g., by increasing pressure; by using different oxidants such as N_2O, O_3, SO_2, SO_3, carbon oxides, and even NO or NO_2; or by introduction chlorine-containing substances into the reaction mixture.

As was mentioned above, many oxidants are unattractive for viable industrial processes, due to their high cost, corrosive nature or a lack of activity under the appropriate reaction conditions. Chlorine-containing catalysts in oxidative coupling of methane may be able to transcend the C_{2+} hydrocarbon yield limitation but there are other problems, notably lack of stability and, as in case of SO_2, the introduction of species that lead to severe corrosion problems.

The ultimate goal might well be a single-step process from methane to higher hydrocarbons or oxy-products. There are many alternative ways to activate the CH_4 molecule and the right combination of catalyst, reaction condition, oxidant and suitable reactor has yet to be discovered.

1.5 Aims and scope of this study

As the products of methane selective oxidation (CH_3OH, HCHO) are much less stable than CH_4 and could readily be oxidized into carbon oxides, a catalyst which facilitates the formation of oxygenates without catalyzing their further oxidation is required. Many attempts have been made to find a catalyst for direct methane oxidation to methanol, but no catalytic effect has been demonstrated. The published results on the homogeneous gas phase reaction by contrast seem promising with respect to methanol selectivity, but in most of the studies reported to date the yield is still far too low to be of economic interest.

Remarkable progress along this direction has been achieved in the last decade with the development of metal oxide catalysts for the oxidative coupling of methane towards more valuable hydrocarbon products (C_{2+}). Despite variations in the experimental conditions employed by different workers, certain trends emerge from the global performance data. Thus, the strongly basic oxides of alkali metals, alkaline earth and rare earth metal oxides constitute the best catalytic material. Unfortunately, all catalysts developed to date are characterized by a strong inverse relationship between methane conversion and hydrocarbon selectivity, imposing a barrier to the maximum attainable hydrocarbon yield and greatly reducing the economic prospects of a commercial methane oxidative coupling process.

The best yields of C_2 products are commonly of the order of 10-20% and a limiting figure of 30% at 1 bar pressure has been predicted by Labinger and Ott[126] on the basis of a simple analysis of kinetic data. The main limitation to the increased yield of C_2 products is the further oxidation of products, especially of ethene, on the catalytically active sites. In addition, when free dioxygen present in the gas phase, homogeneous reactions which are essentially beyond control of the catalyst, will lead to CO and CO_2.

The possibility of methane oxidative coupling via a heterogeneous-homogeneous mechanism, i.e., a reaction initiation on the catalyst surface and continuation of oxidation in the gas phase, suggests a route to increasing the C_2 product yield by improving the gas phase reaction. One such approach could be via the introduction of a gas phase initiator into the reaction mixture.

Hydrogen peroxide could be such an initiator as well as an oxidant either for the homogeneous non-catalytic methane oxidative coupling or for oxidative conversion of methane in the presence of a catalyst. The possibility of the formation of hydrogen peroxide *in situ* in the process of oxidative coupling on solid catalysts[127] suggests that it may also be used for the subsequent activation of methane in the gas phase, resulting in the formation of additional amounts of C_2 products. Hydrogen peroxide could also serve as a source of active species, e.g., peroxide or superoxide surface species or HO_2 and OH radicals. These species could interact with methane to form reactive surface intermediates or gas-phase methyl radicals, which could recombine to form ethane, an ethyl radical, or ethylene.

It has been shown, that the oxidation of methane to formaldehyde is governed by the formation of active oxygen species on the catalyst surface, which interact with methane. Based upon knowledge of these radical reactions, active oxygen species are predicted to be produced from hydrogen peroxide, which contains active partially reduced oxygen. Hence, the active species could be formed more readily from hydrogen peroxide than from molecular oxygen and the reaction could proceed under "milder" conditions.

The above study constitutes the basis of this thesis work.

Chapter 2. EXPERIMENTAL METHODS AND APPARATUS

2.1. Catalyst preparation

2.1.1. Catalysts for methane oxidative coupling. A range of different catalysts were used in the methane oxidative coupling study. Two metal oxides, CaO and MgO, were chosen as the supports for most of the catalysts. The reason for this is that these alkaline-earth metal oxides are well known and have been extensively characterized.

The 0.6% Pt/CaO and 0.25% Fe/CaO catalysts were prepared by incipient wetness impregnation of calcium oxide (CP grade, BDH) with aqueous solutions of $Pt(HCl)_6 \cdot 6H_2O$ and $Fe(NO_3)_3 \cdot 9H_2O$ followed by drying for 10 hours at 120°C and calcination at 800°C for 6 hours. Prior to use, the catalysts were compressed, crushed and screened to a particle size of 0.50-0.85 mm.

The lead (IV) oxide supported on magnesium and calcium oxides (both used in their chemically pure grade, BDH) were prepared using an impregnation method by adding aqueous solutions of lead nitrate of the correct concentrations to CaO and MgO. The impregnated samples were dried at 120°C until all the water had evaporated, pelletized (0.50-0.85 mm) and calcined at 800°C for 6 hours.

The 5.5% MoO_3/ 21% La_2O_3/CaO and 5.5% MoO_3/ 21 %La_2O_3/MgO catalysts were prepared by impregnation of lanthanum-calcium oxide and lanthanum-magnesium oxide with an aqueous solution of $(NH_4)_6Mo_7O_{24} \cdot 4H_2O$. The lanthanum-calcium (21% La_2O_3/ CaO) and lanthanum-magnesium oxides (21% La_2O_3/MgO) were prepared by wet mixing of appropriate quantities of lanthanum oxide and CaO, MgO (all CP grade, BDH) followed by drying overnight at 120°C and calcination at 800°C for 6 hours.

The 7% SrO/ 28% La_2O_3/CaO catalyst was prepared by heating an aqueous slurry of $Sr(NO_3)_2$, $La(NO_3)_3 \cdot 6H_2O$ and $Ca(NO_3)_2 \cdot 4H_2O$ (CP grade, Aldrich) to 100°C for several hours while stirring vigorously and then evaporating the water. The dry sample

was calcined in air at 800°C for 6 hours, compresse and sieved to 0.50-0.85 mm particle size.

The 1% Au/ 5% La_2O_3/CaO catalyst was prepared by impregnation of lanthanum-calcium oxide with a solution of $AuCl_3$ in absolute ethyl alcohol. The lanthanum-calcium oxide (5% La_2O_3/CaO) was prepared by wet mixing of appropriate quantities of lanthanum oxide and calcium oxide (CP grade, BDH). The impregnated sample was dried overnight at 120°C and then calcined at 800°C for 6 hours. The catalyst was compressed and subsequently crushed to obtain the used particle size fraction of 0.50-0.85 mm.

2.1.2. Catalysts for partial oxidation of methane to formaldehyde. The series of silica supported catalysts with 3d, 4d, 4f, 5p and 6p - metal oxides was prepared by the impregnation of precipitated silica (Si 4-5P, Akzo product) with aqueous solutions of Cr, Fe, Pb, La nitrates and titanium chloride; basic solutions (pH = 11) of ammonium heptamolybdate and ammonium metavanadate; a solution of Bi nitrate in 10 wt.% HNO_3; and a solution of Sn bromide in absolute ethyl alcohol (all CP grade). After impregnation, the catalysts were dried overnight at 120°C and calcined at 600°C for 8 hours. The metal loading was 0.1 mmol/g of SiO_2 for all samples. In addition, Sn/SiO_2 catalysts were prepared with the loading of Sn^{4+} varied between 0.03 and 1.0 mmol/g of SiO_2. All the catalysts were compressed and subsequently crushed to a particle size of 0.50-0.85 mm.

2.1.3. Catalysts for partial oxidation of methane to methanol. Only three catalysts have shown activity in catalysing this reaction: 0.6% Pt/CaO, 0.1 mmol Sn/g SiO_2 (the methods of preparation are described above) and 30% H_3BO_3/Al_2O_3 which was prepared by incipient wetness impregnation of Al_2O_3 (Al - 3982T, Engelhard) with an aqueous solution of boric acid whose concentration was selected to give 30% H_3BO_3 on the surface of alumina. The resulting slurry was stirred on a water bath at 80°C until dry and then subsequently calcined in air in two steps: 10 hours at 120°C and 5 hours at 300°C. After calcination the catalyst was compressed and crushed to obtain the particle size fraction of 0.50-0.85 mm.

2.2 Installation

All experiments were carried out in a continuous-flow installation using a fixed-bed reactor. A proc ss flow diagram of the apparatus and reactor system is shown in Figure 2.1.

The pre-reactor zone. As the schematic diagram in Figure 2.1 illustrates the reactant gases (CH_4, 99.9% BT Grade, AFROX and $N_2 + O_2$, Special Gases, AFROX, 25% N_2 and 75% O_2) were supplied from cylinders, and the flow was controlled using mass flow regulators (*MFR*) and flow meters (*FM*). The two reactant gases were then combined through a "X" shaped union (Union Cross, Swagelok) before the mixed reactant gases were passed to a liquid Pyrex evaporator (*E*) with an internal diameter of about 20 mm. The pressure in the system was controlled using a pressure gauge (Ashcroft) - (*M*). A thermocouple-well was located on the top of the evaporator and the thermocouple passed down the centre of the evaporator which was heated by an electric heating cord. The thermocouple, which controlled the temperature of the evaporator fitted into the well and was of the J-type. A liquid inflow tube was located at the bottom of the evaporator and led to a peristaltic pump (*P*) through the relief valve (*RVI*). This pump was conected to a flask which contained the liquid of concern. The reaction mixture then left the evaporator at an exit tube near the bottom of the evaporator which led into the reactor. The exit tube was also heated along its whole length. It was usually held at a temperature of 150°C to prevent condensation of the liquid of concern.

The reactor zone. A diagram of the reactor system with the evaporator, the heavy organic and coke trap (*Trap1*), and the trap for collecting oxy-products (*Trap2*) is shown in Figure 2.2. The *Trap2* was cooled with dry ice , whereas the *Trap1* was held at room temperature during experiments.

The type of apparatus and reactor used in the reactor zone of the installation was dependent on the type of experiment that was being performed. The appropriate reactor was mounted vertically inside electrically heated furnaces (*EF1 and EF2*) which are shown in Figure 2.1. The length of the heating jacket for reaction was 32 cm

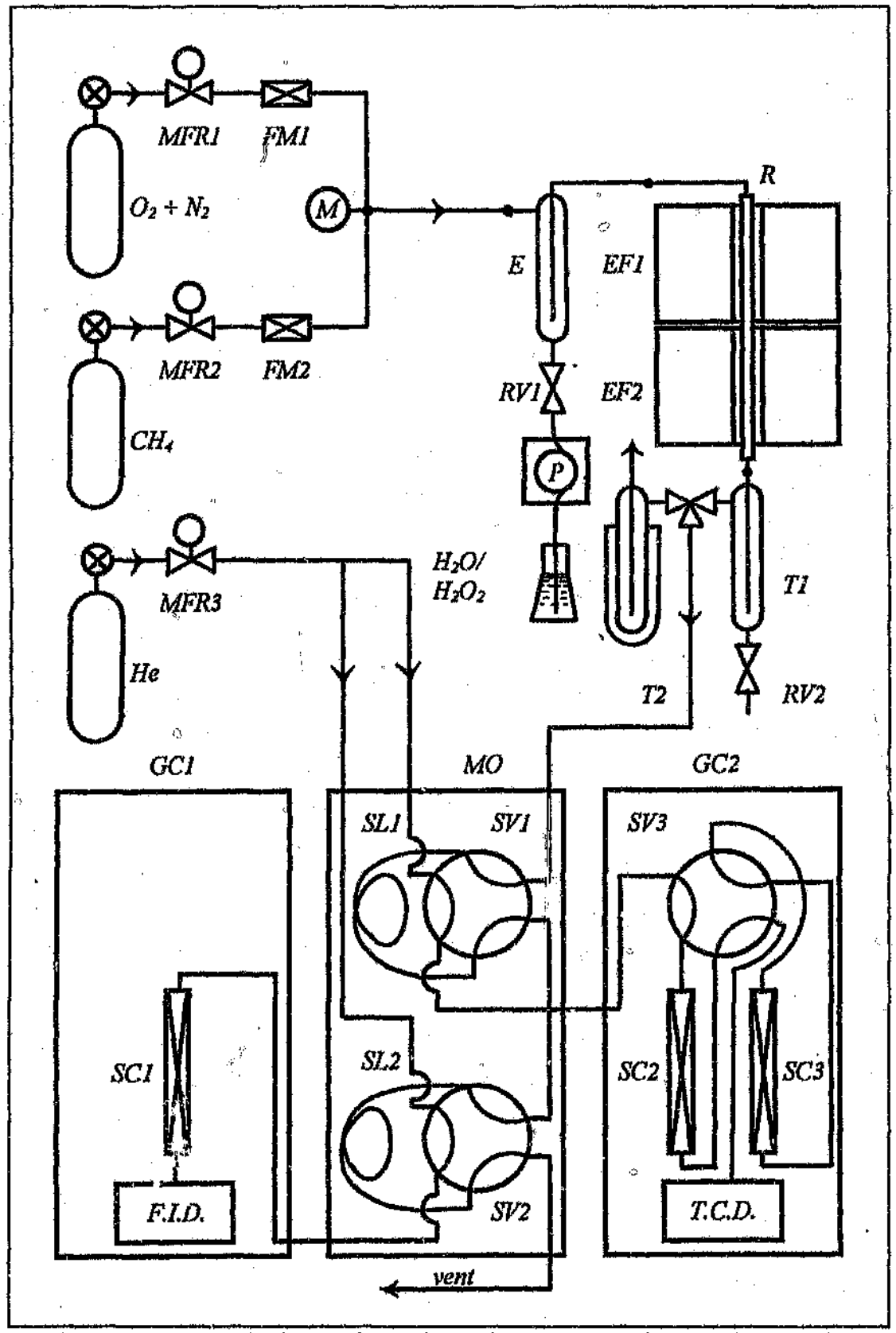


Figure 2.1. General scheme of experimental apparatus used for methane oxidative coupling and partial oxidation to oxygenates.

which was divided into two equal heating zones: the main reaction zone (contained the catalyst) and the post-catalytic reaction zone (specifically designed for study of purely homogeneous reactions). Temperatures in these reaction zones were controlled using two K-type thermocouples mounted externally between the reactor and the electric furnaces to avoid problems due to the reactivity of the thermocouple material.

There is some concern regarding the influence of aspects of the experimental procedure adopted by researchers on a catalyst's apparent performance. For example, due to the highly exothermic nature of the reaction, temperature in various zones of the catalyst bed may be quite different. The use of hot spot temperatures has often been recommended. From the temperature profile, which was measured for methane oxidative coupling condition by moving the thermocouples up and down inside the electric furnaces, the constant temperature zone appears to be about 30 cm long. Outside this zone, the temperature falls rather steeply from the maximum to the temperature of the electric furnace. A temperature controller (REX-C100) allowed the reactor to be operated isothermally. This means that the conversion outside the reaction zone would be limited and considered negligible as compared to the conversion in the reaction zone. Therefore, we have correlated the conversion, yield and selectivity data with the maximum reactor temperature.

The post-reactor and analysis zone. The reactor effluent flowed through *Trap1*, then *Trap2*, cooled in a dry ice bath (–78°C) and heat-traced lines to the middle oven (*MO*), which was held at a temperature of 170°C. The gas lines connecting the traps with the middle oven and the gas chromatographs were heated to 170°C to prevent condensation of the products. Inside the middle oven the reactor effluent entered the six-port T.C.D. gas-sampling valve (Valco) - (*SV1*), configured so as to allow the product gases to flush a sample-loop (*SL1*) of 0.95 ml in volume before passing through to the six-port F.I.D. gas-sampling valve (*SV2*). This valve was also present in the middle oven and was configured to flush a 0.49 ml sample-loop (*SL2*). The exit tube out of the second valve was then passed to the exterior of the middle oven where the reactor effluent flowed through a bubble-flow meter, which allowed an accurate measure of the gas flow rate, before being vented. The product gas sample collected in the T.C.D. sample-loop could be injected into the gas chromatograph (Hewlett-Packard 5710A) - (*GC2*), equipped with a thermal conductivity detector (*T.C.D.*).

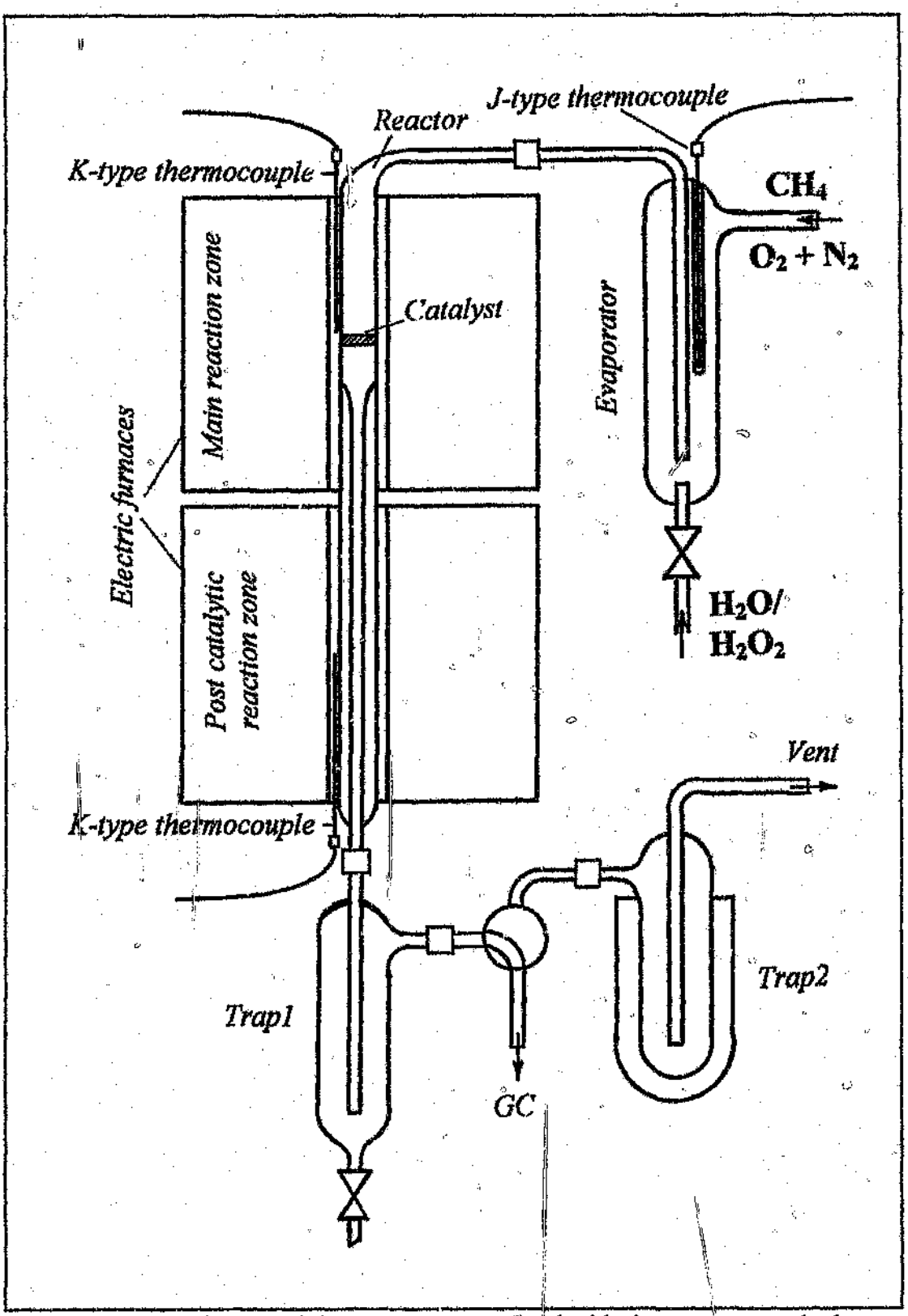


Figure 2.2. Diagram of the reactor system fitted with the evaporator, the heavy organic and coke trap (*Trap1*), and the trap for collecting oxy-products (*Trap2*).

A third valve was located in the oven of *GC2*. This was also the six-port gas-sampling valve (*SV3*) configured so as to allow for selection between one of two separation columns (*SC2* and *SC3*); namely molecular sieve 13X (1.5m length × 1/8"o.d.) and Carbosieve SII (2m length × 1/8"o.d.). Both of these columns were connected to the *T.C.D.* detector. Likewise the sample of the product gases collected in the F.I.D. sample-loop could also be injected into the gas chromatograph (Hewlett-Packard 5790A) - (*GC1*), equipped with a flame ionization detector (*F.I.D.*), which was connected to the Porapak QS column (2m length × 1/8"o.d.) - (*SC1*). Heavy hydrocarbons (C_{6+}) and oxy-products were collected in *Trap1* and *Trap2* and then analyzed by an off-line GC, equipped with a F.I.D. detector and a DB5 capillary column (30m × 0.25 mm I.D.). Helium was used as a carrier gas for all gas chromatographs at a pressure of 300 kPa and a flow rate of 30 ml/min. The resulting integrator report was read and saved into the computer for later data evaluation. The integrator (Varian 4290) also controlled the ovens, all the valves and the chromatographs, through a control-box.

2.3 The product analysis

2.3.1. The product analysis using gas chromatography. The reaction products were analyzed by on-line sampling using gas chromatography. A Porapak QS column was used for the separation of CH_4, C_2 (C_2H_4, C_2H_2 and C_2H_6), C_3 (C_3H_6 and C_3H_8), C_4, C_5, C_6H_6, CH_3OH and HCHO. A Carbosieve SII column was used for CO and CO_2 analysis and a molecular sieve 13X column for O_2 and N_2 analysis. Nitrogen was used as a marker to determine changes in the reaction mixture volume during the reaction. Benzene, toluene, naphthalene and other heavy hydrocarbons (C_{6+}) were analyzed by an off-line GC with DB5 capillary column. The response factors for the reactants and products were determined using certified calibration gases. Calibration of methanol and formaldehyde was achieved with a 10% HCHO aqueous solution stabilized with 2% CH_3OH. Having obtained the mole percentages of the products via calibration, the CH_4 conversion, the product selectivities with respect to CH_4, and the product yields also with respect to CH_4 were then calculated.

2.3.2. Quantitative determination of formaldehyde. Formaldehyde was condensed from the exit reactor stream in *Trap2* and quantitatively determined by iodometric titration or by a spectrophotometric method with chromotropic acid[128,129]. The last procedure has been well-established as a reliable method for determining small amounts of formaldehyde in aqueous solutions.

Determination of aldehydes in water-soluble samples by iodometric titration (sodium bisulfite method).

Reagents: Iodine solution (standard 0.1 *N*). 12.69 g of CP (BDH) iodine was dissolved in a solution of 24 g of CP potassium iodide in 200 ml of distilled water and diluted to 1 liter. The solution was stored in a clean, brown, glass-stoppered bottle.

Iodine solution (standard 0.01 *N*). This solution was prepared by accurate dilution of the standard 0.1 *N* solution. It was stored in a clean, brown, glass-stoppered bottle and a fresh solution was made at least every three days.

Sodium bicarbonate (CP 99.5%, LABCHEM).

Sodium bisulfite solution (0.1%). 0.50 g of CP (BDH) sodium bisulfite was dissolved in distilled water, made up to 500 ml and well mixed. A fresh solution was made every day.

Starch indicator solution.

Procedure: With the aid of a measuring cylinder, 100 ml of the sodium bisulfite solution was poured into a 250-ml conical flask and allowed to stand in an ice bath for 15 min. 25 ml of the sample was added and mixed with the reagent. 1 ml of starch indicator was added to the conical flask and the solution titrated quickly with 0.1 *N* iodine solution to within an estimated 0.5 ml of the end point. The titration with 0.01 *N* iodine solution was complet as determined by the first permanent blue end point. 1 g of sodium bicarbonate was added, mixed well, and titrated with the 0.01 *N* iodine solution until the blue color at the end point persisted for 5 min.

Calculation: The formaldehyde content of the sample was calculated using the following equation:

$$\text{Formaldehyde, mol} = (N)\,(T)\,0.05/2\,(V) \qquad (1\text{ h})$$

where N = normality of the standard iodine solution,

T = volume of iodine solution used in the titration after addition of sodium bicarbonate, ml,

V = volume of sample taken, ml.

Determination of formaldehyde by colorimetric chromotropic acid method.

Apparatus: Micropipets, Kirk-type,covering the range from 10 to 1000 μliters.

Spectrophotometer, Sequoia-Turner 340, equipped with 1-cm cell.

Steam bath designed so that 50-ml volumetric flasks, except for the upper portion of the neck, are entirely enclosed by the bath and protected from light.

Reagents: Sulfuric acid, CP, 98% concentrated (SAARCHEM).

Benzene, AR, 99.0% (SMM).

Sodium bisulfite solution (0.02 *N*). 2 g of powdered CP (BDH) sodium metabisulfite was dissolved in 1 liter of distilled water. This solution was prepared fresh daily.

Chromotropic acid reagent: 4.0 g of chromotropic acid (1,8-dihydroxynaphthalene- 3,6-disulfonic acid), practical grade (Eastman Kodak) was dissolved in 100 ml of distilled water and the solution was filtered into a 2-liter flask. 300 ml of water was placed in another 2-liter flask and 700 ml of cold concentrated sulfuric acid was slowly added with continuous chilling and gentle swirling. The chilled acid solution was added to the filtered chromotropic acid solution in small increments with stirring and cooling. The reagent was stored in a dark, glass-stoppered bottle and usually prepared every week.

Standard formaldehyde solution (approximately 0.06 mg/ml). A solution of formaldehyde (approximately 6 mg/ml) was prepared by weighing 8.5 g of formaldehyde solution (AR, 37-40%, SMM) into a 500-ml volumetric flask, diluting to the mark with water, and mixing. The solution was then transfered to a 500-ml brown glass, screw-cap bottle. 1.00 ml of the standardized formaldehyde solution by means of a micropipet was pipeted into a 100-ml volumetric flask, diluted to the mark with 0.02 *N* sodium bisulfite solution, and mixed. This solution had a formaldehyde concentration of approximately 0.06 mg/ml; the actual concentration was calculated using the sodium bisulfite method described above. This solution was used for several months.

Calibration of apparatus. By means of micropipets, exactly 0, 0.100, 0.200, 0.400, 0.600, 0.800, and 1.00 ml of the standard formaldehyde solution (~ 0.060 mg/ml) was introduced into separate dry 50-ml volumetric flasks. Sufficient sodium bisulfite solution was added to make a total volume of 5 ml. From a buret 40 ml of chromotropic acid was added while swirling the contents of the flask. The unstoppered flasks were heated inside a steam bath, protected from light, for 30 min. The flasks were then removed from the steam bath and cooled down almost to room temperature. The absorbance (at 570 nm) of the solutions containing 0, 0.100, 0.200, 0.400, 0.600, 0.800, and 1.00 ml of the standard formaldehyde solution was placed in a 1-cm cell and a calibration curve (graph of absorbance vs concentration of formaldehyde) was plotted.

Procedure. By means of a micropipet, 0.100 ml of sample was transfered into a clean, dry 50-ml volumetric flask. For samples expected to contain less than 0.006 mg/ml of formaldehyde 1.00 ml of sample was used. Sufficient sodium bisulfite solution was added to make a volume of 5 ml. If less than 1.00 ml of the sample

solution was taken, sodium bisulfite solution was added to bring the total volume to 5 ml.

From a buret 40 ml of chromotropic acid reagent was added while swirling the contents of the flask. The unstoppered flask, protected from light, was heated by means of a steam bath for 30 min. When the concentration of formaldehyde was less than 0.006 mg/ml, the sample was heated for only 15 min. The flask was then removed from the steam bath, allowed to come almost to room temperature and flask content mixed thoroughly. The absorbance of the sample solution was measured relative to distilled water at 570 nm in a 1-cm absorption cell. A blank determination using 5 ml of sodium bisulfite solution in place of the sample was usually made.

Calculation. The absorbance found for the blank determination was subtracted from that found for the sample. Using a calibration curve, the concentration of formaldehyde in the sample was determined. The formaldehyde content of the sample (mol %) was calculated using the following equation:

$$\text{Formaldehyde, mol} = (c_F)\,(V)\,(D)/(M) \qquad (2\text{ h})$$

where: c_F = the concentration of formaldehyde in the sample,

V = volume of sample obtained during the experiment,

M = molar mass of formaldehyde (30 g mol^{-1}),

D = the sample dilution factor (100,250 or 500).

2.4 Calculations and mass balance procedure

The nitrogen present was used as an inert marker to determine changes in the volume of the gas mixture during the reaction for purposes of mass balance. The amount of nitrogen was measured on the molecular sieve column in a blank experiment at 200°C and subsequently during the reaction. This was done since the conversion of methane was found to be extremely low at temperatures below 300°C and at atmospheric pressure, with traces of carbon oxides and C_2H_6 being the only detectable carbon-containing compounds. A dilution factor (α) was calculated for every individual run by taking the final quantity of nitrogen leaving the reactor during the reaction (N_{N2}^{EXP}) and dividing by the initial quantity of nitrogen measured during the blank experiment (N_{N2}^{O}). The dilution effect was then accounted for by dividing the amount of each substance (products or reactants) obtained during experiment by this dultion factor.

The final amount (μmol) of each substance leaving the reactor (n_i) was calculated by dividing the area counts (N_i) obtained from the resulting integrator report by the response factor (f_i) determined via calibration. The list of the response factors is given in Table 2.1.

The ratio of the volumes of the F.I.D. and T.C.D. sample-loops ($V_{SL2}/V_{SL1} = 0.52$) was used as a correction factor in calculations of the final amounts of products and reactants which were analyzed by the gas chromatograph, equipped with a T.C.D. detector. This was done to eliminate the effect of the different sample-loops volumes.

The relationships used to calculate the methane conversion (X_{CH4}), the selectivity (S_i) and the yield (Y_i) for a product i , as well as carbon and oxygen mass balances (MB) are as follows:

$$X_{CH4}(\%) = \frac{100 \sum c n_i^{EXP}}{n_{CH4}^{O}} \qquad (1\,i)$$

$$S_{C2}(\%) = \frac{200 \sum n_{C2}^{EXP}}{\sum c n_i^{EXP}} \qquad (2\,i)$$

Table 2.1. The response factors of products and reactants obtained via calibration of the separation columns connected to a flame ionization detector (F.I.D.) or a thermal conductivity detector (T.C.D.).

Product/reactant	Response factor f_i (N_i · counts/μmol)
F.I.D. detector	
CH_4	53869
C_2H_4	99118
C_2H_2	96425
C_2H_6	101004
C_3H_6	150833
C_3H_8	151371
C_{4+}	202008
C_6H_6	303282
T.C.D. detector	
CH_4	780
O_2	971
N_2	1036
CO	930
CO_2	1029

$$S_{C3+C4}(\%) = \frac{300\sum n_{C3}^{EXP} + 400\sum n_{C4}^{EXP}}{\sum c_i n_i^{EXP}} \quad (3\text{ i})$$

$$S_{C6H6}(\%) = \frac{600\, n_{C6H6}^{EXP}}{\sum c_i n_i^{EXP}} \quad (4\text{ i})$$

$$S_{COx}(\%) = \frac{100\, n_{COx}^{EXP}}{\sum c_i n_i^{EXP}} \quad (5\text{ i})$$

$$Y_i(\%) = \frac{[S_i(\%)]\,[X_{CH4}(\%)]}{100} \qquad (6\,i)$$

$$MB(C)(\%) = \frac{100\sum c_i n_i^{EXP} + n_{C4}^{EXP}}{n_{CH4}^{O}} \qquad (7\,i)$$

$$MB(O_2) = \frac{100(2(n_{O2}+n_{C2H4}+n_{C3H8})+3(n_{CO}+n_{C2H2}+n_{C3H6}+n_{CH4})+4n_{CO2}+9n_{C3H6}+n_{C2H6})^{EXP}}{2n_{O2}^{O}} \qquad (8\,i)$$

where: c_i stands for the number of carbon atoms in one molecule of a product i,

n_i^{EXP} - the amount of product or reactant obtained during the reaction, (μmol),

n_i^{O} - the initial amount of the reactant measured during the blank experiment, (μmol).

In the present research, the carbon and oxygen mass balances were generally better than 98-99% for all the runs.

Definition of residence time (t) and contact time (τ). The residence time of the reactant mixture in experiments performed at pressures of 3 and 20 bar was defined as

$$t = \frac{V}{v}\,\frac{P}{P^{O}}\,\frac{T^{O}}{T} \qquad (9\,i)$$

where: V = volume of the reaction zone, (ml),

v = volumetric flow rate of feed at ambient temperature (T^{O}) and atmospheric pressure (P^{O}), (ml/s),

T = hot spot temperature of the reaction zone, (°C),

P = pressure in the reactor, (bar).

The contact time was defined as the ratio of the catalyst volume, expressed in ml, and the volumetric flow rate of feed at ambient temperature and atmospheric pressure.

2.5 Experimental procedure

The parameters used in the experiments (i.e., pressure, temperature, residence time and O_2 concentration) were varied over a wide range, but care was taken to always remain outside of the explosion limits with the CH_4/O_2 gas mixtures.

Cooper and Wiezevich[130] investigated the upper explosive limit of methane-oxygen mixtures by varying the temperature and pressure. They reported that explosion did not occur with 14% oxygen at temperatures less than 410 °C and pressures less than 14 bar. Melvin[131] investigated the occurrence of explosions with 10% air (90% methane) in a sodium silicate vessel at 12 bar and 350°C, and found that explosions could occur in this region. However, he reported that the occurrence of explosions were not reproducible. He also found that packing the vessel with stainless steel strips to raise the surface to volume ratio to 12:1 suppressed explosion at pressures of 102 bar for mixtures containing less than 40% air. All of the above mentioned authors postulated that the packing of the vessel increased the rate of surface destruction of radicals rather than accelerating oxidation catalyzed by the surface. Even though oxidation of methane has been studied by many researchers, no explosions have been reported with less than 10% oxygen (90% methane) in the feed at a pressure of 50 bar.

2.5.1. Oxidative coupling of methane. The reaction mixture, consisting of methane, oxygen and nitrogen with a concentration of O_2 of 14, 22.5, 28, or 30 mol% ($CH_4/O_2/N_2$ = 35/14/51, 70/22.5/7.5, 62.5/28/9.5 or 60/30/10) depending on the experiment, was fed to the appropriate reactor at a flow rate which ensured the attainment of contact times equal to 0.52-0.11 s.

The gas phase oxidative coupling of methane in the presence of hydrogen peroxide was performed in the temperature range of 400 to 800°C with the reaction mixtures CH_4-N_2 and CH_4-air, and a total flow rate of 40 to 100 ml/min. An aqueous solution of hydrogen peroxide with concentrations of either 7.6 or 23 wt.% with a flow rate of 0.03-0.09 ml/min was added to the reaction stream. In the blank experiments pure water was used instead of the hydrogen peroxide solution.

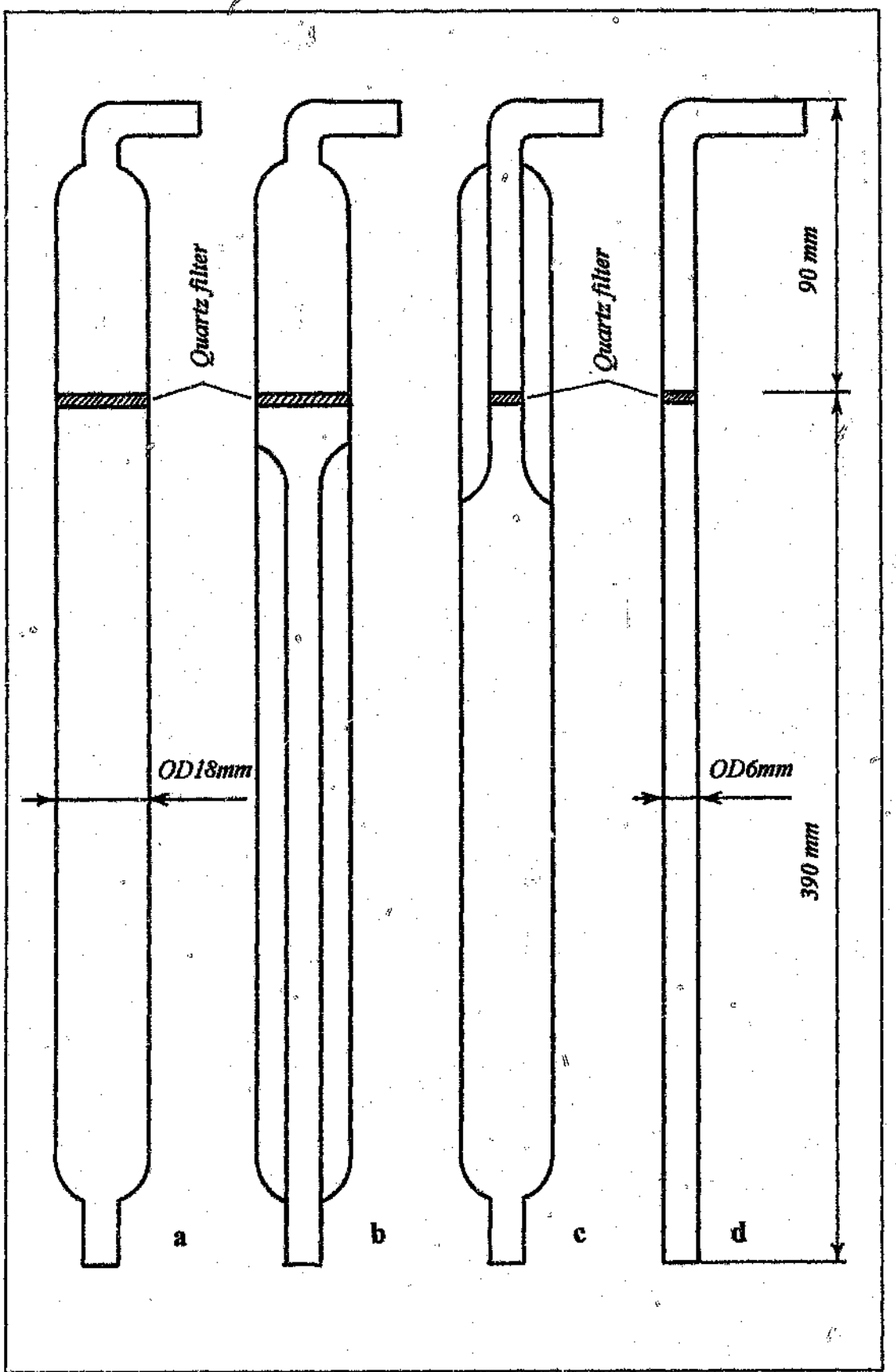


Figure 2.3. Different reactor systems used in the methane oxidative coupling study.

Catalytic testing was carried out in the temperature range of 600 to 1100°C under atmospheric pressure in a fixed-bed continuous-flow quartz reactor using 0.10-1.00 g of catalyst. The depth of the catalyst bed was 0.4-7.5 cm, depending on the i.d. of the reactor system. Five different types of reactor systems (a, b, c, d and e) were designed to investigate the influence of residence time, contact time and linear flow rate on the methane conversion and product selectivities (Figures 2.3 and 2.4). The upper section, which contained the catalyst, was 18 mm o.d. for reactors "a" and "b", and only 6 mm o.d. for reactors "c" and "d". The lower section was constructed of 18 mm o.d. quartz tubing for reactors "a" and "c", and 6 mm o.d. tubing for reactors "b" and "d". So that all combinations of large and small main reaction and post catalytic zones were investigated. It was suggested by Baldwin et al.[132] and Thomas et al.[133] that the large volume of empty space after the catalyst bed contributes significantly to homogeneous gas phase reaction. Whereas, the use of a small catalytic reaction zone (~ 1.89 cm^3 for the reactors "c" and "d") followed by a space where the temperature is much lower (200-300°C) ensures that the reaction is mostly heterogeneous. The smaller diameter of the post catalytic reaction zone ("b" and "d") allowed the products to pass rapidly out of the hot main reaction zone without subsequent oxidation of C_2 - C_6 hydrocarbons to carbon oxides.

Reactor "e" was designed for investigation of the highly exothermic methane oxidative coupling reaction in the adiabatic mode. The outer wall of the reactor was insulated by a double layer of quartz filled with air. This reactor device (Figure 2.4) permitted experimental data to be obtained which were unaffected by heat-transfer from the catalyst to the reactor wall and from the wall to the internal surface of the heating jacket. The thermocouples centered in the main reaction and the post catalytic zones were also covered by a quartz tube. The hot-spot temperature was measured in the middle of the catalyst bed.

Blank experiments were carried out at 200°C at the beginning of every run. Approximately 2 hours were required to reach steady-state conditions. This was determined by sampling the reactant stream repeatedly until the analytical results were reproducible. The temperature was subsequently increased to the reaction temperature and the experiment was performed under stabilized conditions (i.e., pressure, temperature, product selectivity, and CH_4 conversion). The analysis was done using a

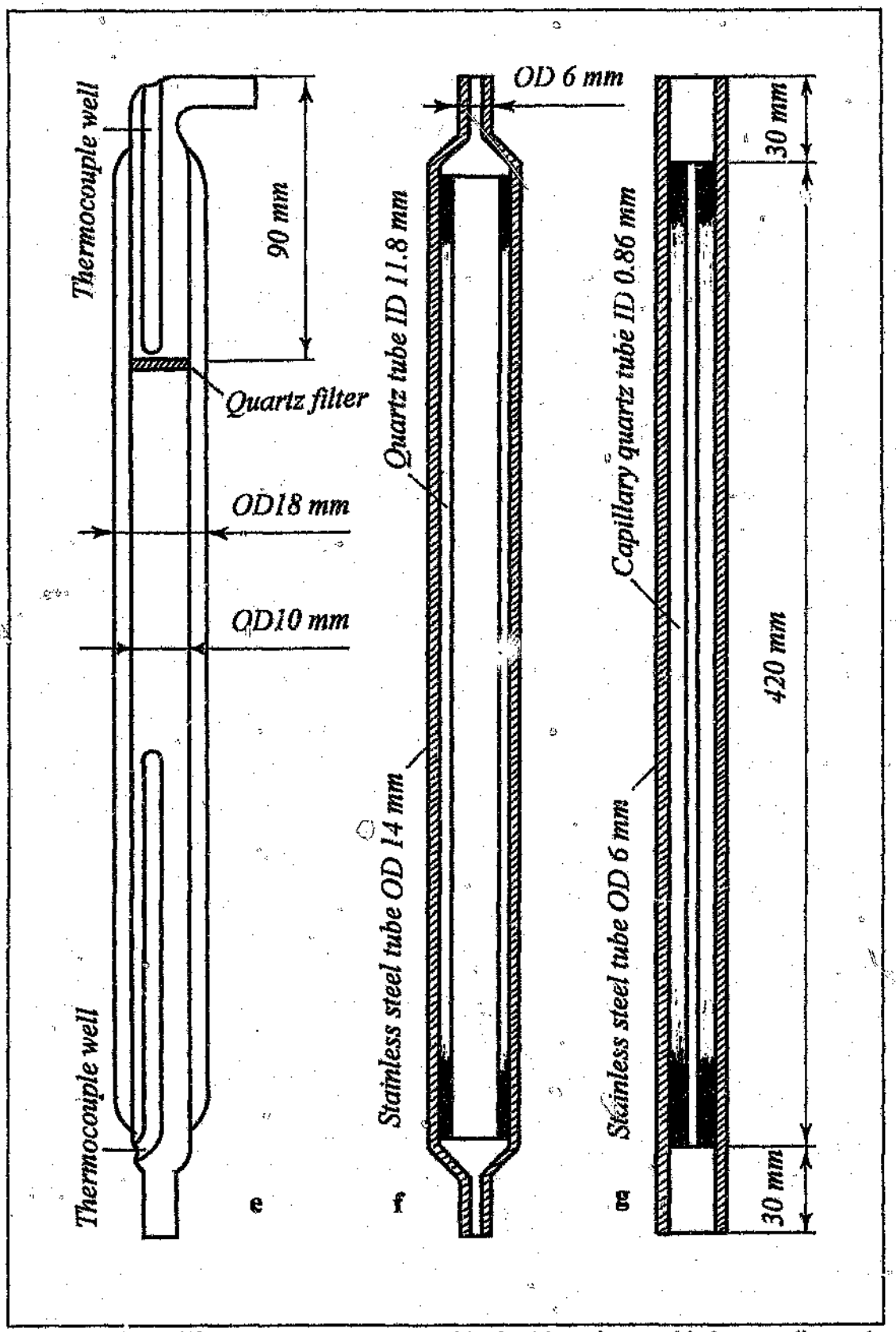


Figure 2.4. Different reactor systems used in the (e) methane oxidative coupling and (f, g) partial oxidation of methane to methanol.

temperature ramp which lasted 35 min, so that it was possible to analyze on-line gas samples every 60 min. After a run the reactor was first cooled and then the reagent gases switched off. All acquired data and calculations were then processed using LOTUS-123 software.

Visual inspection of the internal wall and the surface of the catalyst after the experimental runs did not indicate the formation of any carbon residues during reaction. All results reported were obtained under conditions where no carbon deposition occurred.

2.5.2. Partial oxidation of methane to formaldehyde. The reaction was carried out at atmospheric pressure in a quartz reactor (Figure 2.3 (b)) with an internal diameter of 15 mm, narrowing down to 4 mm behind the catalyst layer; this shape increased the rate of removal of post catalytic reaction gas from the main reaction zone and restricted the possibility of secondary transformations of reaction products beyond the catalyst. Except where otherwise indicated 0.25 g of the catalyst was employed. A mixture of methane, oxygen and nitrogen was passed through the reactor with flow rates of 180, 45 and 15 ml/min respectively, which corresponded to a contact time of 0.12 s. An aqueous solution of hydrogen peroxide (21 wt.%) was added to the reaction mixture through the evaporator at a rate of 0.12 ml/min. During catalyst testing the main reaction zone was held at 500°C (at which the hydrogen peroxide decomposition was negligible) and the post reaction zone at 250°C. Formaldehyde was condensed from the exit reaction stream in a dry ice trap at −78°C and quantitatively determined by the aforementioned methods.

Blank tests with the empty reactor have shown that contributions from reactor wall and gas phase reactions were negligible. In order to elucidate the role of oxygen and hydrogen peroxide in the formation of oxy-products, experiments with the reaction mixture without hydrogen peroxide or oxygen were performed. Also in the blank experiments pure water was used instead of the hydrogen peroxide solution.

The results obtained for a given set of reaction parameters were reproducible, in the sense that the selectivity and the conversion were practically the same when the experiment was repeated with identical reaction parameters.

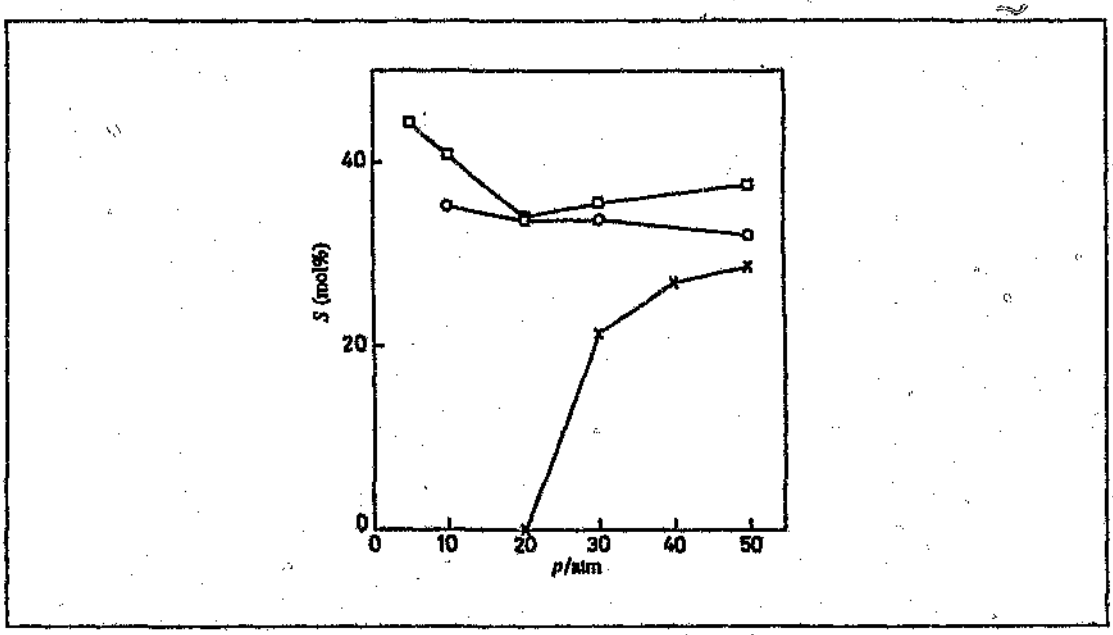


Figure 2.5. Effect of reactor type on methanol selectivity at 450°C in the pressure range 1-50 bar: (x), 316 stainless steel; (o), quartz; (□), Pyrex [106].

2.5.3. Partial oxidation of methane to methanol. Much of the early work on the partial oxidation of methane was performed in metal reactors. The results obtained by Burch et al.[106] (Figure 2.5) show clearly that the choice of reactor is important, especially when operating at lower pressures. Thus, when using a steel reactor no methanol is produced until the pressure exceeds 20 bar, whereas with a glass-lined reactor methanol is observed at all pressures greater than or equal to 5 bar. Furthermore, although the selectivity to methanol in a steel reactor increases with pressure it is still less than that observed with a glass-lined reactor at 50 bar. In the light of these results all our subsequent work was performed using the quartz and quartz-lined reactors.

The homogeneous and catalytic oxidation of methane to methanol were studied at atmospheric pressure in the temperature range 460-625°C with a feed consisting of 82% methane and 18% oxygen in the quartz reactor (Figure 2.3 (a)) with an internal diameter of 15 mm. The residence time was varied from 95 to 216 seconds by changing the total flow from 11.4 ml/min to 5 ml/min through the reaction system.

To determine the effect of pressure on the product selectivity and the methane conversion, experiments were carried out at 3 and 50 bar respectively in the temperature range 430-490°C. The direct oxidation of methane to methanol was

performed at 3 bar pressure in the reactor (Figure 2.4 (f)) which consisted of an Inconel stainless steel tube with an inner diameter of 13 mm and length of 420 mm, of which 300 mm were heated by the electric furnaces. A close-fitting quartz tube was inserted into this tube making the actual internal diameter 11.8 mm; this gave a heated reactor volume of 32 cm^3. The well-mixed reactant gases ($CH_4 : O_2 : N_2 = 80 : 17 : 3$) were passed at 21 ml/min (residence time = 102 s) through the reactor and a Whitey microfine needle valve was used to control the flow rate as well as maintain a backpressure. The products were analyzed by on-line gas chromatography. The gas line connecting the reactor with the GC was heated to 170°C to prevent condensation of methanol and water.

The experiments were also performed using the high-pressure flow microreactor shown in Figure 2.4 (g), which was constructed of a 420 mm quartz capillary tube (0.86 mm i.d.) inserted into a 316 stainless steel tube; this corresponded to a heated reactor volume of 0.17 cm^3. A standard reactant mixture of methane and oxygen (95.8% CH_4 and 4.2% O_2) was used under 50 bar pressure with 29, 31 and 33 ml/min flow rates, which gave residence times of 6.6, 6.2 and 5.8 *s* respectively. The temperature dependency of the methane conversion and the product selectivities was determined by varying the temperature and keeping the other reaction parameters (i.e., pressure, residence time and oxygen feed concentration) constant. The major products found were carbon monoxide, water, and methanol with smaller amounts of carbon dioxide and ethane. Ethylene and formaldehyde were sometimes detected in trace quantities. The selectivity, conversion and yield of all major products were calculated from the GC analysis data with respect both to CH_4 and O_2. The carbon mass balance was 98 ± 0.5% and the oxygen mass balance was 99 ± 0.5%

2.6 Catalyst characterisation

2.6.1 Surface Area determination. The method of Brunnauer, Emmett and Teller (BET) based on the low temperature consecutive adsorption and desorption of nitrogen gas was used to determine the total surface area of the catalysts. Liquid nitrogen was used as the coolant to affect the adsorption. The equipment was constructed in our laboratory[134]. This equipment was calibrated using samples of known surface area. Results are quoted as m^2/g.

2.6.2. X-Ray Diffraction (XRD). XRD has been used in some cases for bulk characterisation of the support and catalysts. After reaction samples were removed from the reactor, crushed to < 45 μm, pressed into a disk and analyzed by X-ray diffraction using a Phillips PW1830 powder diffractometer and Cu Kα radiation under the following conditions: tube voltage, 40 kV; current, 20 mA; angular diffraction from 2θ = 10-140; step scan width, 0.02°/s; counting time, 0.5 s/step. Samples were also analyzed before reaction, but after thermal treatment.

2.6.3. Scanning Electron Microscopy (SEM). Scanning electron microscopy was used to analyze the morphology of the catalysts employed in the methane oxidative coupling reaction. For conventional work a Jeol JSM-840 analytical scanning electron microscope operating at 20 keV was used, which was capable of a point-to-point resolution of 0.28 μm. An improved tungsten filament was used at 2400°C.

SEM specimens were prepared by placing a droplet of ethanol solution, containing the ground catalyst powder in suspension, on a carbon-film-coated copper grid followed by blotting on filter paper and air drying. The coating material primarily conducts charge and heat from the specimen to the stub, in addition it does not readily react with the specimen surface or oxidize over a long period of time. Gold and gold-palladium system are particularly useful in this respect.

2.6.4. Energy Dispersive X-Ray Analysis (EDX). Compositional data on individual crystals as well as the distribution of elements on the surface of the catalyst were obtained using energy dispersive X-ray analysis facilities coupled to the scanning

electron microscope. EDX spectra were obtained using a [illegible]000-QX system equipped with a AN10000 detector (with a beryllium window). The energy resolution of the EDX system was 149 eV at 5.9 keV. The EDX was capable of fixed spot, line scans, and mapping plots. Samples were mounted on graphite stubs and approximately 300 Å of gold was sputtered onto the catalysts to ensure adequate conductivity. A beam, 10 nm in diameter, which covered a particle, was used to generate an EDX spectrum. The collection time was usually 100 s. During the collection, the beam was sometimes spread (underfocussed or overfocussed) for a while to obtain an image of the particle and the beam relocated on the particle to compensate for any specimen shift.

The detector efficiency factors for aluminum and platinum were unity. The γ-Al_2O_3 was used as a standard for calibration. Generally, $C_\alpha/C_\beta = (K_\alpha/K_\beta)\,(I_\alpha/I_\beta)$, where C_α is the weight of the α element, K_α is the elemental sensitivity factor of α, and I_α is the EDX intensity of α. When the detector efficiency of the (K, L, M) line of element α is ε instead of unity, the real intensity will be $I_\alpha^{(real)}$, where $I_\alpha^{(real)} = \varepsilon \cdot I_\alpha$. The elemental sensitivity factors K_α were taken from the Operator's Manual of the LINK system. They were $K_{OK} = 1.0$, $K_{AlK} = 1.17$, $K_{ReM} = 1.56$.

2.6.5. Diffuse Reflectance Fourier Transform Infra-Red Spectroscopy (DRIFTS).
Infra-red studies of the interaction of methyl alcohol with catalysts used in the direct oxidation of methane to methanol were carried out on a Bruker IFS 85 FT-IR spectrometer. A DRA-2CI, (Harric Scientific Corp.) DR optical attachment had been installed in the sampling compartment of the spectrometer. A water cooled silicon carbide IR source was used with a DTGS detector. The IR spectra were recorded in the range 4000-1250 cm^{-1} using Bruker OPUS software.

Infra-red studies of successive additions of the methanol indicate the build-up of various alcohol species on the catalyst surface which can be characterized mainly by their CO stretching bands and also by the presence of OH and CH bands. Infra-red desorption studies at room and at elevated temperatures were used to investigate the stability of the adsorbed species. All IR spectra of adsorbed species were corrected against the background spectrum and the band intensity was calculated in integrated absorbance.

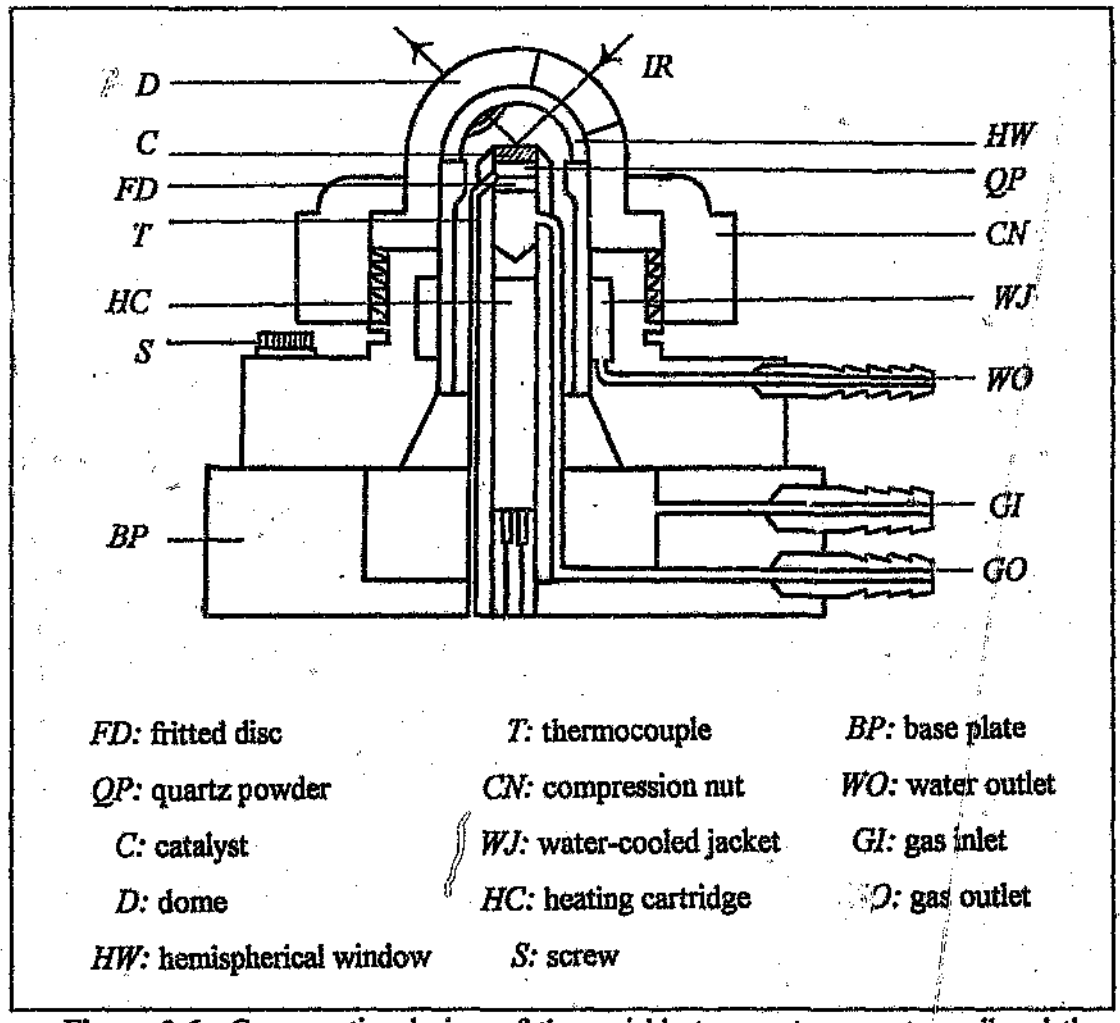


Figure 2.6. Cross-sectional view of the variable temperature reactor cell and the sample cup of a Bruker IFS 85 FT-IR spectrometer.

An *in situ* reaction cell shown in Figure 2.6 was employed for all the IR spectroscopy performed. The cell consisted of three main components: the base plate onto which the cylindrical heating post containing the sample cup was attached; a water-cooled enclosing jacket and a dome containing the IR transparent windows. When the cell was used to record DR-IR spectra of catalysts under reaction conditions, a dome containing , a single hemispherical crystal of ZnS was employed. When carrier gas (N_2, 99.8% BT Grade, AFROX) containing methanol was introduced into the cell at 120°C, the contributions due to IR absorptions of reagent molecules in the internal volume between the hemispherical window and the top of the sample cup were undetectable (confirmed using a nonadsorbing sample). Details of the design of the reaction cell and IR instrument were obtained from workers in the catalysis laboratory[135].

Chapter 3. RESULTS

3.1. Partial oxidation of methane to formaldehyde in the presence of hydrogen peroxide

Partial oxidation of methane by oxygen in the presence of hydrogen peroxide to form formaldehyde, methanol, carbon oxides, and C_2 products (ethane and ethene) has been studied over the series of silica supported catalysts with 3d, 4d, 4f, 5p and 6p - metal oxides in the 500-600°C temperature range under ambient pressure. The catalytic performance of 0.1 mmol of Cr/g of SiO_2 was compared for a wide range of experimental conditions, including the influence of the additive in the feed (H_2O_2 or H_2O). The reactor contained 0.50 or 0.25 g of the catalyst. The catalytic behaviour of this sample at 500, 550 and 600°C in the main reaction zone (T_{cat}), and at 250, 300°C in the post catalytic zone (T_{post}) is presented in Table 3.1 in terms of methane conversion, and product selectivities. The conversion of methane in the presence of hydrogen peroxide increased with increasing contact time, while the selectivity to formaldehyde gradually decreased. It is surprising that the selectivity to CO_2 remained almost constant, while a compensating relationship in selectivity was observed between formaldehyde and carbon monoxide. The formation of ethane became noticeable at higher reaction temperatures, indicating the initiation of the oxidative coupling of me-

Table 3.1. Effect of the reaction temperature, contact time (τ) and the presence of H_2O_2 or H_2O on the CH_4 conversion and product selectivities over 0.1 mmol Cr/g SiO_2.

T_{cat}/T_{post}	Flow rates (ml/min)			τ	X_{CH4}	Selectivity (%)			
(°C)	CH_4	O_2	Additive	(s)	(%)	HCHO	CH_3OH	C_2	CO_x
600/300	75	34	70-H_2O_2	0.50	4.9	–	–	20.7	79.3
500/300	154	65	140-H_2O_2	0.25	0.7	22.9	–	–	77.1
500/250	180	45	140-H_2O_2	0.25	0.8	19.2	–	28.8	52.0
500/250	180	45	140-H_2O	0.12	0.002	100	–	–	–
500/250	180	45	140-H_2O_2	0.12	0.3	77.9	2.1	1.6	18.4

Table 3.2. Methane partial oxidation on silica and silica-supported catalysts, including 3d, 4d, 4f, 5p and 6p metals at loadings of 0.1 mmol of M/g of SiO_2 for all samples. Reaction conditions: T_{cat} = 500°C, T_{post} = 250°C, flow rates of CH_4 = 180, O_2 = 45 and H_2O_2 (21 wt.%) = 140 ml/min, W = 0.25 g, τ = 0.12 s.

Catalyst	BET surf. area (m^2/g)	CH_4 conversion (%)	Selectivity (%)			
			HCHO	CH_3OH	C_2	CO_x
Ti	394	0.2	80.3	17.7	–	–
V	398	0.1	100	–	–	–
Cr	343	0.3	77.9	2.1	1.6	18.4
Fe	347	0.4	69.0	–	2.8	28.2
Mo	378	0.2	58.3	8.3	20.8	12.6
Sn	332	3.5	32.3	5.4	29.4	32.9
Sb	330	1.9	54.5	5.0	0.8	39.0
Pb	399	0.04	100	–	–	–
Bi	340	0.8	54.0	6.3	25.0	12.9
La	362	0.3	68.0	12.5	–	19.5
SiO_2	400	0.7	80.3	15.2	1.5	3.0

thane. The addition of pure water instead of 21 wt.% hydrogen peroxide solution to the reaction mixture caused a drastic decrease in methane conversion and carbon oxides formation. The selectivity to formaldehyde, however, was improved during H_2O addition, and this indicated that the retardation of the formaldehyde formation by water vapor was weaker than CO_X formation.

The use of the experimental conditions (T_{cat} = 500°C in the main reaction zone and T_{post} = 250°C in the post catalytic zone, contact time = 0.12 s, flow rates of CH_4 = 180, O_2 = 45 and H_2O_2 = 140 ml/min), determined after preliminary blank tests, revealed that the contribution of the homogeneous gas phase reaction or blank effect of the "walls" of the reactor could be completely neglected. The results of a comparative study of the catalytic properties of different metal oxides supported on silica in the presence of hydrogen peroxide are presented in Table 3.2. One can see that the pure silica exhibits remarkable activity toward formaldehyde formation. All transition metals

Table 3.3. Product distribution of the methane oxidation over silica catalysts impregnated with varying quantities of Sn^{4+} in the presence of H_2O_2 or H_2O (*). Reaction conditions: $T_{cat} = 500°C$, $T_{post} = 250°C$, $W = 0.25$ g.

Catalyst	Flow rates (ml/min)			τ	X_{CH4}	Selectivity (%)			
	CH_4	O_2	Addit.	(s)	(%)	HCHO	CH_3OH	C_2	CO_X
0.1 mmol/ g of SiO_2	180	45	140	0.12	3.5	32.3	5.4	29.4	32.9
	180	45	140*	0.12	0.01	100	–	–	–
	60	0	65	0.80	0.6	94.6	5.4	–	–
	100	40	100	0.20	0.7	85.1	13.5	–	1.4
	215	94	140	0.10	0.4	88.0	12.0	–	–
1 mmol/ g of SiO_2	180	45	140	0.12	2.1	30.4	4.8	0.5	64.3
0.4 mmol/ g of SiO_2	180	45	140	0.12	2.0	31.0	5.0	4.8	59.2
0.03mmol /g of SiO_2	180	45	140	0.12	1.3	51.1	4.5	36.8	7.6

as well as La lower the activity of the bare silica, including V which has been shown to be the best promoter of silica in the reaction used for conventional methane oxidation with oxygen[115] in the absence of H_2O_2. A similar lowering effect was found for 6p elements (Pb and Bi). The only elements which enhanced bare silica activity were the 5p metals, Sn and Sb. A maximum combined formaldehyde and methanol yield of 1.32% at a methane conversion of 3.5% was observed at a tin loading of 0.1 mmol/g SiO_2. Apparently, the support contributes significantly to the overall methane conversion. However, the product distributions obtained from the 0.1 mmol Sn/g SiO_2 catalyst and that from the bare silica are quite different. The main selectivity difference lies in the considerable amounts of C_2 hydrocarbons and CO_X formed over the Sn/SiO_2 catalyst. By contrast, it was observed that over the unpromoted SiO_2 the major products are formaldehyde and methanol with negligible amounts of C_2 hydrocarbons and CO_X. It is noteworthy that the methane conversion and the yield to formaldehyde of the catalysts with the lower surface area (~ 330 m^2/g) achieved maximum values, approximately 8-10 times as large as those with the higher suface area (~ 400 m^2/g).

In addition, the effect of the tin loading on the catalyst performance under typical reaction conditions (reaction temperature T_{cat}/T_{post} = 500/250°C, contact time = 0.1-0.8 s and total flow rate = 125-480 ml/min), was investigated in the presence of H_2O_2 or pure water (Figure 3.3). To attain a better understanding of the tin-silica system for methane oxidation, experiments without hydrogen peroxide or oxygen were performed. Only traces of oxy-products have been found after the reaction with addition of H_2O instead of H_2O_2. Thus, the presence of hydrogen peroxide is crucial for oxy-product formation. In the reaction without oxygen but with hydrogen peroxide in the reaction mixture, formaldehyde production dropped only about two fold, though methanol completely disappeared from the reaction products.

Studying the title reaction on a series of differently loaded Sn/SiO_2 catalysts, it was observed that the selectivities to formaldehyde and C_2 hydrocarbons decreased and the selectivity to carbon oxides increased with the amount of tin on the catalyst surface. The methane conversion and the yield of formaldehyde increased with tin loading on the catalyst. The yield passed through a maximum at intermediate loadings and then decreased at higher loadings (Table 3.3). It was found that Sn loading of 0.1 mmol per g of SiO_2 gave the best performance.

In the present research, it was noticed that the product distribution for methane partial oxidation over silica supported catalysts depended on the reaction temperature. Low temperatures clearly favored the formation of formaldehyde over the C_2 hydrocarbons, and vice versa at high temperatures. The results definitively confirm that Sn and Sb promoted catalysts were more active than bare precipitated SiO_2 and the addition of Ti, V, Cr, Fe, Mo, Pb, Bi, and La produced a considerable decrease in the activity of the bare precipitated SiO_2 surface toward oxy-product formation.

3.2. Partial oxidation of methane to methanol

3.2.1. Gas phase partial oxidation of methane to methanol. The influence of the reaction parameters (pressure, temperature, residence time, oxygen feed concentration) on the methane conversion and the product selectivities has been systematically studied using specially designed high-pressure flow microreactors, described in Chapter 2. Table 3.4 shows how the methanol, ethane and ethene yields vary with the residence time at various temperatures in the hot zone of the reactor. A reactant mixture of methane and oxygen ($CH_4 : O_2 = 4.5:1$) was used under atmospheric pressure with 5,

Table 3.4. The temperature dependency of the product yields for different residence times. Reactant mixture: 82% CH_4 and 18% O_2. Pressure = 1 bar.

T	$t = 216$ s			$t = 120$ s			$t = 95$ s		
(°C)	Y_{CH3OH}	Y_{C2H6}	Y_{C2H4}	Y_{CH3OH}	Y_{C2H6}	Y_{C2H4}	Y_{CH3OH}	Y_{C2H6}	Y_{C2H4}
460	–	0.02	–	–	–	–	–	–	–
470	–	0.03	–	–	0.01	–	–	–	–
480	–	0.04	–	–	0.02	–	–	0.01	–
490	–	0.06	0.01	–	0.03	–	–	0.02	–
500	0.02	0.11	0.02	–	0.04	–	–	0.04	–
510	0.03	0.21	0.06	–	0.04	–	–	0.04	–
520	0.04	0.35	0.13	–	0.09	0.01	–	0.07	–
530	0.07	0.46	0.23	0.02	0.16	0.03	–	0.10	0.01
540	0.07	0.65	0.40	0.05	0.20	0.05	0.02	0.13	0.02
550	0.09	0.84	0.61	0.05	0.33	0.11	0.04	0.25	0.07
560	0.09	0.94	0.86	0.06	0.48	0.22	0.06	0.32	0.14
570	0.09	1.12	1.03	0.09	0.65	0.37	0.09	0.53	0.25
580	0.09	1.24	1.28	0.10	0.83	0.57	0.10	0.70	0.41
590	0.10	1.36	1.54	0.11	1.00	0.81	0.09	0.71	0.50
600	0.09	1.48	1.83	0.12	1.17	1.07	0.08	0.76	0.52
610	0.09	1.57	2.09	0.15	1.37	1.48	0.08	0.83	0.67
620	0.08	1.68	2.39	0.13	1.48	1.75	0.07	0.99	0.96

9 and 11.4 ml/min flow rates, which gave residence times of 216, 120 and 95 s respectively.

For the following observations the pressure and the O_2 feed concentration were kept constant for the different residence times. As expected, the methane conversion as well the ethane and ethene yields increased gradually with increasing temperature. The methanol yield also went up with increasing temperature, until the oxygen conversion reached 100% at 600°C, and then it started decreasing slightly even at higher residence times. Obviously a higher residence time increased the conversion of methane. Depending on the residence time, selectivities to methanol of up to 30% could be reached with methane conversions of 0.3-0.4% at 590-600°C. At higher CH_4 conversions levels of 1.2% observed at 620°C (t = 216 s) the selectivity to methanol dropped to 7%. At low CH_4 conversion the methanol yield was very small, almost zero, but it increased with increasing residence time. The highest methanol yield was observed at 610°C with a residence time of the reactant gases in the reactor of 120 s. Small amounts of formaldehyde were detected at low reaction temperatures (below 560°C) and its selectivity decreased with increasing residence time, but it never surpassed 1%. When the oxygen conversion reached 100%, formaldehyde could no longer be detected as a product. The effect of the temperature on the selectivity in the experiments performed at atmospheric pressure was not as clear as that of the residence time. However, the results showed that as the residence time was increased the temperature at which methanol was first detected was lowered, from 540°C with t = 95 s to 500°C with t = 216 s.

Table 3.5. Methane conversion, product selectivities and methanol yield obtained in the gas phase reaction at 3 bar pressure and different reaction temperature. t = 102 s.

T	X_{CH4}	Selectivity (%)				Y_{CH3OH}
(°C)	(%)	CH_3OH	C_2	CO	CO_2	(%)
470	11.7	13.9	0.6	68.3	17.1	1.6
475	12.2	13.8	0.6	68.4	17.2	1.7
480	12.7	12.8	1.0	68.8	17.4	1.6
485	12.9	10.7	1.3	70.5	17.4	1.4
490	13.8	8.6	1.5	72.0	18.0	1.2

Table 3.6. Methane conversion, product selectivities and methanol yield obtained in the gas phase reaction at 50 bar pressure and different reaction temperature.

t	T	X_{CH4}	Selectivity (%)				Y_{CH3OH}
(s)	(°C)	(%)	CH_3OH	C_2	CO	CO_2	(%)
	450	2.4	50.0	0.3	45.5	4.2	1.2
	455	2.7	48.1	0.4	47.1	4.4	1.3
6.6	460	2.8	43.8	0.4	50.6	5.3	1.2
	465	3.1	35.7	0.5	51.5	12.4	1.1
	470	3.2	30.3	0.5	54.9	14.3	1.0
	450	2.2	54.7	0.5	44.7	–	1.2
	455	2.3	53.3	0.5	45.0	1.2	1.2
6.2	460	2.6	50.6	0.5	45.2	2.8	1.3
	465	2.7	44.2	0.6	45.2	10.0	1.2
	470	2.7	39.0	0.7	46.8	13.5	1.1
	450	2.1	57.2	0.6	42.3	–	1.2
	455	2.1	56.9	0.6	42.5	–	1.2
5.8	460	2.3	56.5	0.7	42.8	–	1.3
	465	2.3	55.2	0.8	43.0	1.1	1.3
	470	2.5	46.1	0.9	43.7	9.4	1.2

Data shown in Table 3.5 were obtained at a pressure of 3 bar using a methane : oxygen : nitrogen mixture (80 : 17 : 3) with 21 ml/min flow rate, which gave 102 s residence time. The temperature dependency of the methane conversion and product selectivities was determined by altering the temperature from 470°C to 490°C and keeping the other reaction parameters constant.

The results of the experiments performed in the 450-470°C temperature range at 50 bar pressure are shown in Table 3.6. The pressure and the oxygen feed concentration were kept constant and only the residence time was varied from 6.6 to 5.8 s by changing the total flow rate of the reactant mixture (95.8% CH_4 and 4.2% O_2) from 29 to 33 ml/min.

At higher pressures as well as at atmospheric pressure the selectivity to methanol increased at low methane conversion levels and decreased at higher conversion levels,

when the temperature was increased. Selectivities to methanol of up to 57% could be reached at pressure of 50 bar with methane conversions of 2.0-2.5%. At higher conversions levels of 12-13% at 3 bar pressure (Table 3.5) the selectivity to methanol dropped to 10-13%. The highest methanol yield (1.7%) was obtained at 3 bar pressure and a methane conversion of 12.2%. At the lower temperatures (450°C) the selectivity to methanol usually decreased as the residence time increased. The results also show that as the pressure or residence time were increased the temperature at which methanol was first detected was lowered considerably.

The selectivity to carbon dioxide was almost zero at low residence times and low methane conversion, but as the residence time increased, the selectivity to carbon dioxide also went up. It was found that the selectivity both to CO_2 and to CO decreased moderately with increasing pressure. At constant pressure the selectivity to carbon monoxide changed slightly over the range of temperaures investigated and it always increased monotonically with increasing contact time and methane conversion.

Considerable amounts of C_2 products (mostly ethane at 3 and 50 bar pressure) were observed at high methane conversion. However, with decreasing conversion the selectivity toward C_2 products dropped to insignificant levels.

The selectivity to formaldehyde was always below 1% and it practically disappeared from the detectable products with rising pressure. The experimental results showed that high pressure favours methanol production and low pressure (1 bar) favours that of formaldehyde. In both cases the selectivity to methanol and formaldehyde was over 50% at low conversions (less than 3%), but the selectivity decreased significantly at high methane conversions.

3.2.2. Catalytic oxidation of methane to methanol. If the influence of the pressure and the temperature on the selectivity toward methanol is considered, the lowering the temperature without significant lowering of the methane conversion is possible. This was done by increasing the pressure and the residence time of the gas in the reactor. It may be worthwhile to increase the pressure still further, to see if this trend is continued. Another possible way to increase the CH_4 conversion at lower temperatures is the use of a catalyst. Efforts toward the development of suitable catalysts for this

Table 3.7. Effect of reaction temperature on methanol, ethane and ethene yields for the partial oxidation of methane over various catalysts. Pressure = 1 bar, t = 95 s.

T	0.1 mmol Sn/SiO_2			0.6% Pt/CaO			30% H_3BO_3/Al_2O_3		
(°C)	Y_{CH3OH}	Y_{C2H6}	Y_{C2H4}	Y_{CH3OH}	Y_{C2H6}	Y_{C2H4}	Y_{CH3OH}	Y_{C2H6}	Y_{C2H4}
460	–	–	–	–	–	–	–	–	–
470	–	0.01	–	–	–	–	–	–	–
480	–	0.02	–	–	–	–	–	–	–
490	0.01	0.03	–	–	–	–	0.01	0.02	–
500	0.02	0.03	–	–	0.01	–	0.03	0.02	–
510	0.03	0.06	–	–	0.02	–	0.04	0.05	–
520	0.04	0.11	0.02	–	0.03	–	0.09	0.08	0.01
530	0.05	0.19	0.04	–	0.[illegible]	–	0.15	0.15	0.02
540	0.07	0.30	0.08	–	0.06	–	0.17	0.28	0.07
550	0.07	0.46	0.16	0.01	0.10	–	0.18	0.42	0.13
560	0.06	0.49	0.21	0.03	0.18	0.03	0.18	0.57	0.20
570	0.05	0.55	0.26	0.05	0.30	0.07	0.16	0.72	0.42
580	0.05	0.61	0.30	0.07	0.42	0.12	0.16	0.84	0.54
590	0.04	0.68	0.33	0.08	0.55	0.20	0.16	0.97	0.60
600	0.04	0.79	0.39	0.07	0.69	0.29	0.15	1.13	0.67
610	0.03	0.93	0.45	0.07	0.86	0.42	0.15	1.21	0.75
620	0.03	1.12	0.52	0.06	1.03	0.60	0.14	1.38	0.82

reaction were undertaken and the results of the non-catalytic gas phase oxidation presented above were used as a reference for the comparison of the non-catalytic and the catalytic partial oxidation of methane on various catalysts.

To allow comparison with the homogeneous reaction performed at atmospheric pressure experiments using 0.25 g of catalysts were carried out under identical conditions. The results obtained while keeping the residence time of the reaction mixture (82% CH_4 and 18% O_2) constant at 95 s and varying the temperature are presented in Table 3.7 in terms of CH_3OH and C_2 product yields.

When 0.1 mmol Sn/SiO_2 and 30% H_3BO_3/Al_2O_3 catalysts were in the reactor, the reaction temperature at which methanol was first observed was lower than that for the

homogeneous reaction (Table 3.4). Consequently, the methanol yield was significantly higher in the presence of either of these catalysts than for the empty reactor at low methane conversions of 0.2-0.5% (at temperatures below 560°C). The temperature difference can be explained by the accelerating effect of the catalysts. In the presence of 30% H_3BO_3/Al_2O_3 catalyst the methanol yield was increased up to 0.18% at 550°C. The 0.6% Pt/CaO catalyst was less active toward the methanol production due to subsequent oxidation of CH_3OH, HCHO and C_2 hydrocarbons to carbon oxides. However, 30% H_3BO_3/SiO_2, 10% V_2O_5/SiO_2, 2.5% SO_4^{2-}/ZrO_2 and 0.34% Pt/ 2.5% SO_4^{2-}/ZrO_2 have not shown any catalytic activity for the partial oxidation of methane. The selectivity to methanol in all experiments was much lower than that obtained from the purely homogeneous reaction.

The adsorption on MoO_3, K_2O, SiO_2 and MgO surfaces of more complex molecules associated with methanol synthesis, such as formic acid, methanol, and formaldehyde, has been characterised previously using FT-IR spectroscopy[76,136,137]. It was of subsequent interest to examine the effect which H_3BO_3 addition to Al_2O_3 has on the adsorption of methyl alcohol molecules. The absence of reported studies of this system has, therefore, led to the FT-IR study of methanol adsorption on 30% H_3BO_3/Al_2O_3 catalyst.

At the start of each series of runs, the IR spectrum of the Al_2O_3 or 30% H_3BO_3/Al_2O_3 discs was recorded and digitized for use as the standard background adsorption. The build-up of alcohol species on the surface was studied by adding known aliquots of alcohol vapour to the cell at 120°C and recording the spectrum; 15 min was allowed for each methanol addition to equilibrate with the surface. The desorption of species from the surface at higher temperatures was studied by heating the sample in the presence of H_2O vapour to 400°C.

Figure 3.1 (a) displays spectra of the untreated Al_2O_3 sample with a surface area of 144 m^2/g. Figure 3.1 (b) shows spectra resulting from the addition of 2µl of methanol at 120°C. Infrared bands appeared at 2940 and 2820 cm^{-1} which can be associated with the presence of methoxy groups on the Al_2O_3 surface. These bands all grew with further addition of alcohol and showed a steady decrease in intensity with increasing temperature. The results obtained from CD_3OH adsorption on MgO[136] confirm that these bands arise from CH vibrations (H/D shift ratio 1.37). Introduction of water va-

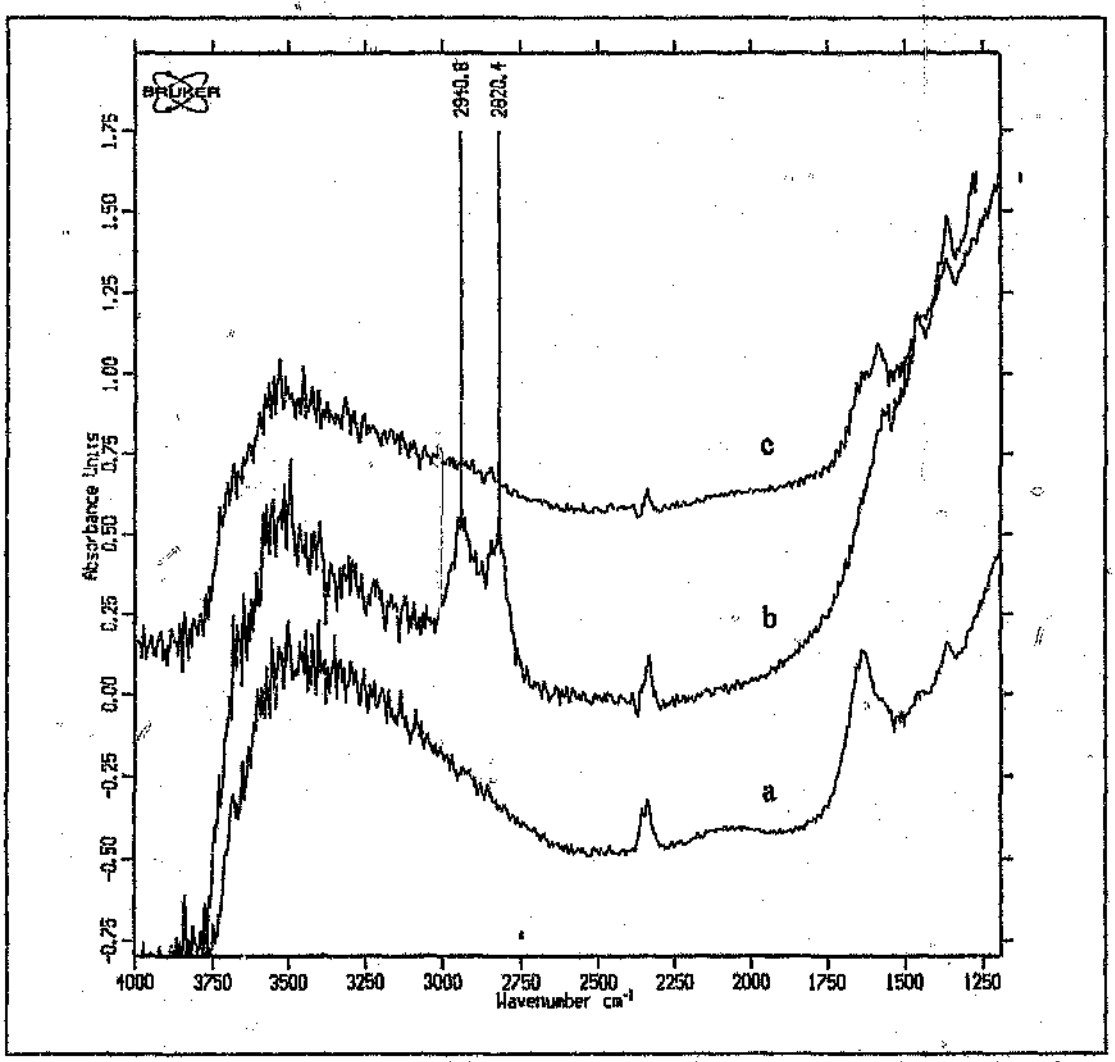


Figure 3.1. Infra-red spectra of the (a) untreated Al_2O_3, (b) exposed to methanol at 120°C and (c) followed by thermal desorption at 400°C in the presence of H_2O vapour.

pour at 400°C removed all these bands from the surface (Figure 3.1 (c)) indicating a very weak bond with respect to high temperatures and the presence of H_2O.

The BET surface area of Al_2O_3 after impregnation of boric acid was decreased from 144 m^2/g to 102 m^2/g. The spectra of the untreated 30% H_3BO_3/Al_2O_3 are shown in Figure 3.2 (a). The adsorption of methyl alcohol on the surface of 30% H_3BO_3/Al_2O_3 gave two peaks at 2952 and 2873 cm^{-1} which were characteristic of methoxy groups on Al_2O_3. In addition, peaks at 3016 and 3002 cm^{-1} were detected. These peaks were ascribed to vibrations of methoxy groups on H_3BO_3. It was also discovered that adsorption of methyl alcohol on an Al_2O_3 sample containing H_3BO_3 resulted in a slight

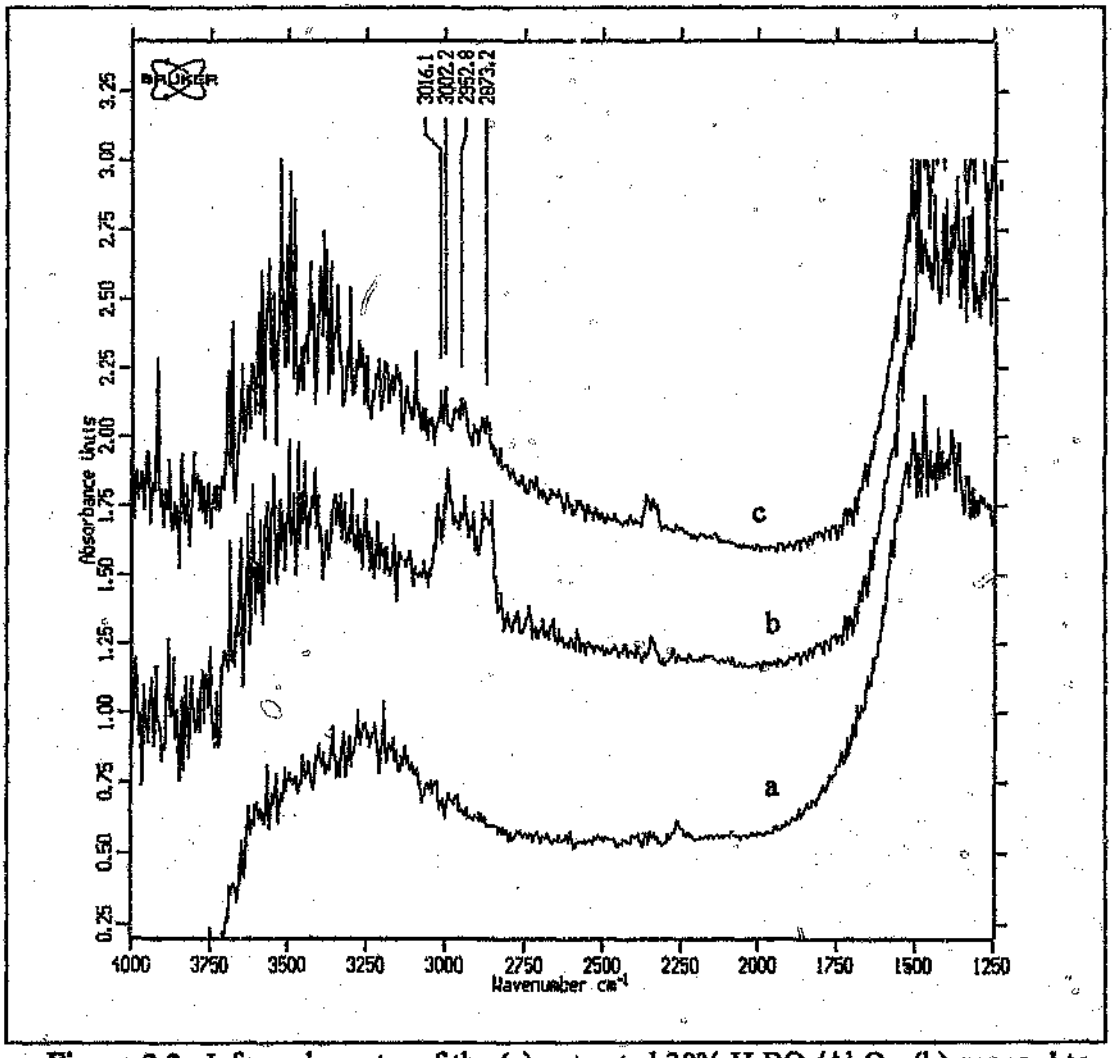


Figure 3.2. Infra-red spectra of the (a) untreated 30% H_3BO_3/Al_2O_3, (b) exposed to methanol at 120°C and (c) followed by thermal desorption at 400°C in the presence of H_2O vapour.

shift of the vibrational frequencies to higher wavenumbers. However, the intensities of these peaks for bare Al_2O_3 were slightly greater than those noted for methyl alcohol on 30% H_3BO_3/Al_2O_3. After heating the sample in the presence of H_2O vapour the bands attributed to the vibrations of alumina and boron methoxy species remained, and new strong bands appeared at 3370-3625 cm^{-1} (Figure 3.2 (c)). The region about 3500 cm^{-1} has been suggested by many authors[136,138,139,140] to be characteristic of the stretching vibrations of the hydroxyl group in various environments.

In summary, a comparison of the influence of residence time, pressure, and temperature on the selectivity to the methane partial oxidation products cannot be viewed independently of the changing conversion levels. Our results show a strong pressure dependence for the product selectivity. Thus, increasing pressure leads to an increase in conversion, which in turn leads to a change in product selectivity. Increasing the pressure favours both selectivity to methanol as well as methane conversion. A higher oxygen concentration in the feed lowers the methanol selectivity, but increases the conversion to such an extent that the yield is increased. High temperatures are detrimental to the methanol selectivity. It appears that the low selectivity to methanol is due to the fact that a larger fraction of the methane was converted directly into carbon monoxide.

By using glass-lined reactors it is possible to ensure that the reaction is essentially purely homogeneous.The experimental results in our work also confirm that the reaction temperature for homogeneous reaction was significantly decreased by increasing the residence time or by using 0.1 mmol Sn/SiO_2 and 30% H_3BO_3/Al_2O_3 catalysts. FT-IR study showed that the adsorption of methanol on Al_2O_3 resulted in the formation of methoxy species on aluminum. On 30% H_3BO_3/Al_2O_3 the adsorption of methanol leads to the formation of methoxy groups ligated to aluminum and also of methoxy groups ligated to boron. An important aspect of this study is that 30% H_3BO_3/Al_2O_3 reveals the presence of relatively strong CH stretching vibrations which were more stable during thermal treatment than those noted for Al_2O_3 alone. The vibration frequencies for aluminum methoxy species were shifted to higher wavenumber.

3.3 Methane oxidative coupling

3.3.1. Catalytic oxidative coupling of methane in the absence of hydrogen peroxide. The methane oxidative coupling reaction was carried out over a wide number of catalysts in the temperature range of 600-1100°C. The influence of temperature, residence time, linear flow rate of the feed gas on the properties of the catalysts was explored. The reaction was performed in three different reactors which were designed to investigate the effect of the volumes of the main catalytic and post catalytic zones on the reaction products. Table 3.8 shows the effect of high residence time of the reaction mixture in the post catalytic zone (~26.5 cm^3, Figure 2.3 (c)) on the methane conversion and the product selectivity over 0.6% Pt/ CaO, 3% PbO/CaO and 5% La_2O_3/CaO catalysts. In contrast, the smaller volume of the post catalytic reaction zone (~1.9 cm^3, Figure 2.3 (b)) allowed the products to pass rapidly out of the heated zone without secondary transformations (Table 3.9). For the following observations the contact time (τ = 0.5 s) and the oxygen feed concentration were kept

Table 3.8. Conversion and selectivity data for the methane oxidative coupling reaction performed in a fixed-bed continuous-flow quartz reactor with small catalytic (1.9 cm^3) and large post catalytic (26.5 cm^3) reaction zones. Reaction conditions: total flow rate of the feed gases (CH_4 : O_2 = 2.5 : 1) = 100 ml/min, W = 0.7 g.

Catalyst	$T_{cat} = T_{post}$ (°C)	CH_4 conv. (%)	Selectivity (%)		
			C_2	C_3 - C_4	CO_X
0.6% Pt/CaO	700	8.9	35.6	–	64.4
	800	21.8	5.4	–	94.6
	900	41.4	0.2	–	99.7
3% PbO/CaO	700	3.8	23.9	0.8	75.3
	800	17.0	24.8	1.6	73.6
	900	30.7	17.1	1.9	80.7
5% La_2O_3/CaO	700	19.4	15.6	0.3	84.1
	800	24.0	20.5	0.9	78.2
	900	28.3	21.5	1.1	76.9

3.3 Methane oxidative coupling

3.3.1. Catalytic oxidative coupling of methane in the absence of hydrogen peroxide. The methane oxidative coupling reaction was carried out over a wide number of catalysts in the temperature range of 600-1100°C. The influence of temperature, residence time, linear flow rate of the feed gas on the properties of the catalysts was explored. The reaction was performed in three different reactors which were designed to investigate the effect of the volumes of the main catalytic and post catalytic zones on the reaction products. Table 3.8 shows the effect of high residence time of the reaction mixture in the post catalytic zone (~26.5 cm^3, Figure 2.3 (c)) on the methane conversion and the product selectivity over 0.6% Pt/ CaO, 3% PbO/CaO and 5% La_2O_3/CaO catalysts. In contrast, the smaller volume of the post catalytic reaction zone (~1.9 cm^3, Figure 2.3 (b)) allowed the products to pass rapidly out of the heated zone without secondary transformations (Table 3.9). For the following observations the contact time ($\tau = 0.5$ s) and the oxygen feed concentration were kept

Table 3.8. Conversion and selectivity data for the methane oxidative coupling reaction performed in a fixed-bed continuous-flow quartz reactor with small catalytic (1.9 cm^3) and large post catalytic (26.5 cm^3) reaction zones. Reaction conditions: total flow rate of the feed gases (CH_4 : O_2 = 2.5 : 1) = 100 ml/min, W = 0.7 g.

Catalyst	$T_{cat} = T_{post}$ (°C)	CH_4 conv. (%)	Selectivity (%)		
			C_2	C_3 - C_4	CO_x
0.6% Pt/CaO	700	8.9	35.6	–	64.4
	800	21.8	5.4	–	94.6
	900	41.4	0.2	–	99.7
3% PbO/CaO	700	3.8	23.9	0.8	75.3
	800	17.0	24.8	1.6	73.6
	900	30.7	17.1	1.9	80.7
5% La_2O_3/CaO	700	19.4	15.6	0.3	84.1
	800	24.0	20.5	0.9	78.2
	900	28.3	21.5	1.1	76.9

Table 3.9. Conversion and selectivity data for the methane oxidative coupling reaction performed in a fixed-bed continuous-flow quartz reactor with large catalytic (26.5 cm^3) and small post catalytic (1.9 cm^3) reaction zones. Reaction conditions: total flow rate of the feed gases ($CH_4 : O_2 = 2.5 : 1$) = 100 ml/min, W = 0.7 g.

Catalyst	$T_{cat} = T_{post}$ (°C)	CH_4 conv. (%)	Selectivity (%)		
			C_2	$C_3 - C_4$	CO_x
0.6% Pt/CaO	700	8.6	36.0	–	64.0
	800	21.5	11.1	–	88.9
	900	41.0	1.7	–	98.2
3% PbO/CaO	700	3.4	23.0	0.3	76.7
	800	16.9	27.1	1.4	71.5
	900	29.4	18.6	1.6	79.8
5% La_2O_3/CaO	700	19.3	16.2	0.3	83.5
	800	23.8	25.7	0.7	73.6
	900	27.9	25.6	0.8	73.1

constant and only the temperature was varied. In the bl[illegible] experiment performed on 5% La_2O_3/CaO catalyst (Table 3.10) the effect of temperature in the range 200°C to 1100°C in the post catalytic zone (T_{post}) was investigated. The lower temperature (200°C) ensured that the reaction was mostly heterogeneous; while the higher temperature (1000-1100°C) allowed us to observe thermal coupling of methane and reaction products.

The catalytic results presented show that promoting the CaO with La_2O_3 leads to a system which was more productive in C_2 hydrocarbons than the other two. The rate of methane conversion was very high on 0,6% Pt/CaO and 3% PbO/CaO above 800°C, however the selectivity to C_{2+} products was poor due to subsequent oxidation of these products to carbon oxides. The Pt promoted catalyst was found to be overactive for the methane oxidative coupling reaction, i.e., at higher conversion levels of 41.4% (Table 3.8) the selectivity to C_2 hydrocarbons dropped to 0.2%. For 5% La_2O_3/CaO the conversion of methane was not as strong a function of temperature as

Table 3.10. Conversion and selectivity data for the methane oxidative coupling over 5% La_2O_3/CaO catalyst performed in a quartz tube with 4 mm i.d. and the volume of the catalytic reaction zone 1.9 cm^3. Reaction conditions: total flow rate of the feed gases (CH_4 : O_2 = 2.5 : 1) = 100 ml/min, W = 0.7 g.

T_{cat} / T_{post} (°C)	CH_4 conv. (%)	Selectivity (%)			
		C_2	C_3 - C_4	C_6H_6	CO_X
700 / 200	18.9	16.1	0.2	–	83.7
800 / 200	22.8	24.1	0.4	–	75.3
900 / 200	23.2	24.4	0.5	–	74.9
900 / 1000	28.9	27.5	3.6	9.4	59.9
900 / 1100	35.7	30.2	4.2	13.1	53.1

the other two systems, so that below 800°C the conversion of methane was much higher but at high temperatures it was comparable or lower. This catalyst was also far more selective at high temperatures, that is the highest yield to C_2 hydrocarbons (7.1%) was obtained at a methane conversion of 27.9% at 900°C.

Comparison of the results of the experiments performed in the three different types of reactors reveals that decreasing the residence time of the reaction mixture in the empty volume of the post catalytic zone leads to a significant improvement in the C_2 hydrocarbon selectivity. It is also evident that the methane conversion did not vary considerably with the residence time in the post catalytic reaction zone for all the catalysts tested.

As stated in Chapter 1, catalysts used for the oxidative coupling of methane generated some intermediate complexes which prolonged the coupling reaction or interacted with products in the post catalytic zone via homogeneous gas phase reactions. An decrease the temperature of the post catalytic reaction zone (T_{post}) to 200°C (Table 3.10) resulted in lowering of the C_2 hydrocarbon yield from 7.1 to 5.8%. The reason for this is that these intermediates most likely serve as initiators for consecutive gas phase oxidation coupling reactions. However, at 200°C, these intermediates are captured on the "cold" reactor walls and hence a decrease in the CH_4 conversion and selectivity to C_{2+} products can be seen. The additional gas phase initiation of methane can be achieved at far higher post catalytic zone temperatures. A

review of the literature[141] suggests a temperature of 1000°C and above should be used to observe the effect. Hence a study of a two reactor system in which the reaction mixture passing out of a main catalytic zone at T_{cat} = 900°C was then directed into a post catalytic zone held at T_{post} = 1000°C or above was performed. The results are given in Table 3.10. The major products in the gaseous samples were ethylene, acetylene and carbon oxides, and the minor products were ethane, propene, propane and butenes. In the liquid samples (quenched) the products were benzene and naphthalene. Likewise, at the investigated temperatures, naphthalene only appeared in a trace amount (selectivity < 1%). The maximum methane conversion achieved in these experiments was 35.7% at 1100°C in the post catalytic reaction zone. It appears that the C_2H_4/C_2H_6 and the C_2H_2/C_2H_4 ratios increased with temperature.

A comparison of the experimental data let one assume that the homogeneous gas phase processes are responsible for producing additional amounts of C_2, C_3 and C_4 hydrocarbons. Hence when the post catalytic zone was held at low temperature (200°C), the intermediates generated on the catalytic bed did not have their life times prolonged as they would in a heated post catalytic zone. Rather the gases were quenched by the cool post catalytic zone reactor walls and so resulted in a lower C_{2+} hydrocarbon yield. However when the post catalytic zone was heated to the same temperature as in the main catalytic reaction zone or above (1000-1100°C), the C_{2+} hydrocarbon yield was significantly increased. A possible reason for this effect is probably as follows. The intermediates generated on the catalytic bed produced C_{2+} hydrocarbons by coupling homogeneously in the gas phase. These coupled hydrocarbon products then entered the heated post catalytic zone and decomposed into radicals, which in the presence of methane acted as initiators for further homogeneous coupling processes. This ultimately resulted in a chain propagation radical reaction which consecutively lead to an increase the C_2 hydrocarbon yield and to the formation of aromatics.

3.3.2. Gas phase oxidative coupling of methane in the presence of hydrogen peroxide. The gas phase reaction without any catalyst was performed in a quartz reactor (Figure 2.3 (a)) in the temperature range 400-800°C using the reaction mixtures CH_4-N_2 and CH_4-air, with a total flow rate of 40-100 ml/min. A hydrogen peroxide solution of either 7.6 or 23 wt.% at a flow rate of 0.03-0.09 ml/min was added into the reaction stream. In the blank experiments pure water was used instead

Table 3.11. Influence of hydrogen peroxide on the reaction of methane oxidative coupling.

Feed (10^{-3} mol · min^{-1})	T (°C)	CH_4 conversion (%)	C_2 selectivity (%)	O_2 outlet (10^{-3} mol · min^{-1})
	550	0.5	100	0
CH_4 (1.56)	600	1.0	100	0
N_2 (2.90)	650	1.5	100	0.006
H_2O_2 (0.22)	700	3.2	60.0	0.006
H_2O (1.41)	750	4.3	52.7	0.031
	800	5.6	41.2	0.026
	600	4.3	30.1	0.504
CH_4 (1.56)	650	9.0	33.4	0.464
air (2.90)	700	10.5	39.9	0.482
H_2O_2 (0.22)	750	13.0	36.4	0.420
H_2O (1.41)	800	19.4	37.1	0.362
	600	0.02	100	0.607
CH_4 (1.56)	650	0.03	100	0.607
air (2.90)	700	0.1	100	0.607
H_2O (1.67)	750	0.8	51.4	0.589
	800	2.8	56.7	0.558
CH_4 (0.89)	400	2.3	14.5	0.232
air (0.89)	500	10.5	26.7	0.210
H_2O_2 (0.21)	600	15.0	18.8	0.188
H_2O (4.60)	800	18.6	18.6	0.152

of hydrogen peroxide solution. The major products found at the lower temperatures (below 650°C) were carbon monoxide, ethane and water with smaller amounts of ethylene and carbon dioxide. As the temperature increased, the selectivity to ethylene and carbon dioxide also went up. The results of the experiments are presented in Table 3.11.

It can be seen that addition of the hydrogen peroxide solution into the mixture of methane and air resulted in product formation which started at temperatures as low as 400°C. A higher rate of the reaction was observed when the hydrogen peroxide solution was added into a reaction mixture consisting of methane and air. However, using a mixture, containing methane and air, with an addition of pure water gave no reaction under the mentioned conditions. The analysis of the oxygen concentration in the outlet reactor effluent (last column in Table 3.11) showed that the observed effect cannot be related to the increase of oxygen concentration in the reaction mixture due to hydrogen peroxide partial decomposition. This is evident from the comparison of the results of experiments using a methane-air mixture and pure water, and a methane-nitrogen mixture with addition of hydrogen peroxide solution.

The Arrhenius plots, shown in Figure 3.3, reveal that the rate of C_2 hydrocarbon production increases with addition of hydrogen peroxide into the reaction mixture. For the methane oxidative coupling in the presence of hydrogen peroxide the apparent activation energy was in the range of 55.7 to 64.8 kJ mol^{-1} (E_{a2}, E_{a3} and E_{a4}, Figure 3.3). When H_2O_2 was substituted for pure H_2O there was a dramatic decrease in the methane conversion and the C_2 hydrocarbon yield; the apparent activation energy increased by about 225.8 kJ mol^{-1} (E_{a1}, Figure 3.3). It is important to note that these E_a values were obtained under pure homogeneous gas phase reaction conditions, at very low CH_4, O_2 and N_2 partial pressures.

These results indicate that hydrogen peroxide, which is stable enough under the reaction conditions of the methane oxidative coupling performance, can selectively oxidize methane into C_2 products as well as serve as an accelerator of the reaction of methane with oxygen.

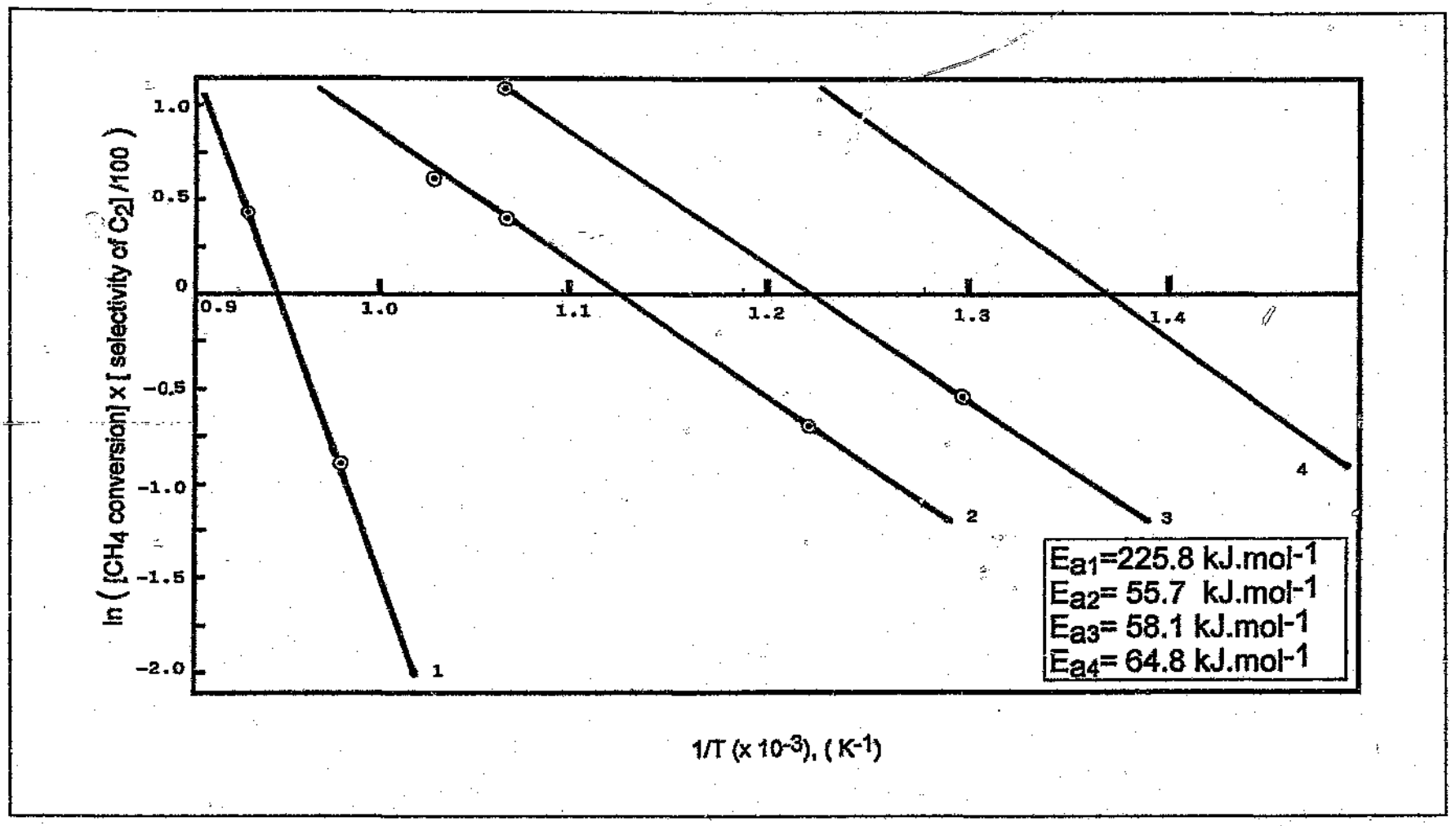


Figure 3.3. Arrhenius plots for C_2 hydrocarbon formation in the homogeneous gas phase methane oxidative coupling in the presence of (1) H_2O (CH_4/air), (2) H_2O_2 solution of 23 wt.% (CH_4/air); (3) H_2O_2 solution of 23 wt.% (CH_4/N_2), (4) H_2O_2 solution of 7.6 wt.% (CH_4/air).

3.3.3. Catalytic oxidative coupling of methane in the presence of hydrogen peroxide. As was mentioned above, hydrogen peroxide can serve as an oxidant as well as an initiator for the pure gas phase homogeneous methane oxidative coupling reaction. On the other hand, hydrogen peroxide can be formed *in situ* under the conditions of catalytic methane oxidative coupling. Indeed, H_2O_2 formation in the process of methane oxidative coupling could explain the effect of reaction mixture quenching which is observed to take place in the region after the catalytic bed[142].

Taking into account the two above mentioned possibilities of acceleration of the methane oxidative coupling, using a catalyst and a gas phase initiator together in the reaction appears attractive.

Table 3.12. Conversion and selectivity data for the methane oxidative coupling reaction over various catalysts in the presence of 2.6 wt.% solution of hydrogen peroxide.

Catalyst	τ (s)	T (°C)	X_{CH4} (%)	Selectivity (%)			Y_{C2+} (%)
				C_2	C_3-C_4	CO_X	
4% PbO/MgO W = 0.7 g	0.21	650	23.3	35.7	0.7	63.6	8.5
		700	25.6	42.2	1.4	56.4	11.2
		750	27.4	41.3	1.4	57.3	11.7
		800	28.5	37.7	1.5	60.8	11.2
0.25% Fe/CaO W = 0.2 g	0.06	600	23.6	20.9	0.1	79.0	4.9
		650	23.8	30.6	0.4	69.0	7.4
		700	24.5	31.6	0.5	67.9	7.9
		750	25.2	30.5	0.5	69.0	7.8
21% La_2O_3/ 5.5% MoO_3/CaO W = 0.7 g	0.19	600	26.6	37.2	0.2	62.6	9.9
		650	27.7	38.7	0.3	61.0	10.8
		700	28.5	43.5	0.5	56.0	12.5
		800	29.3	41.9	0.6	57.5	12.4
21% La_2O_3/ 5.5% MoO_3/MgO W = 0.7 g	0.18	600	22.0	17.4	0.1	82.5	3.8
		650	23.0	20.5	0.1	79.4	4.7
		700	24.1	17.3	0.2	82.5	4.2
		800	25.1	16.7	0.2	83.1	4.2

Four samples containing lead, iron, molybdenum and lanthanum were used in catalytic testing of the methane oxidative coupling reaction in the presence of hydrogen peroxide. This was done since it can be predicted that these metals could activate H_2O_2 to form radicals in the gas phase. Gold and strontium supported on the lanthanum-calcium system were chosen for a comprehensive study of the effect of the addition of hydrogen peroxide to the reaction mixture on the methane conversion and product selectivity in the title process.

3.3.3.1. Pb, Fe, Mo and La promoted catalysts. The results obtained during methane oxidative coupling on 4% PbO/MgO, 0.25% Fe/CaO, 21% La_2O_3/ 5.5% MoO_3/CaO and 21% La_2O_3/ 5.5% MoO_3/MgO catalysts in the presence of hydrogen peroxide are presented in Table 3.12. The reaction was studied in the temperature range 600-800°C (in both the catalytic and post catalytic reaction zones) under normal pressure with the reaction mixture: methane - 100, oxygen - 45 and nitrogen - 15 ml/min. An aqueous solution of hydrogen peroxide with concentration of 2.6 wt.% was added to the reaction mixture via an evaporator at a rate of 0.03 ml/min. The experiments were performed in a quartz reactor with an internal diameter of 4 mm (Figure 2.3 (d)) which had been found previously, using the optimum reaction conditions, to give the highest methane conversion and C_2 hydrocarbon yield.

A maximum C_{2+} hydrocarbon yield of 12.5% was obtained at a relatively short contact time (0.19 s) at 700°C over 21% La_2O_3/ 5.5% MoO_3/CaO catalyst in the presence of hydrogen peroxide. However, using MgO as a support for the same system drasticly lowered the selectivity to C_2 products from 43.5% for 21% La_2O_3/ 5.5% MoO_3/CaO to only 17.3% for 21% La_2O_3/ 5.5% MoO_3/MgO at 700°C. In addition, when 21% La_2O_3 and 5.5% MoO_3 are supported on CaO, an increase in both the methane conversion (~ 4%) and ethene-to-ethane ratio were observed. Apparently, the support contributes significantly to the overall methane conversion and at the same time plays an important role in the product distribution.

When 4% PbO was introduced into MgO, the methane conversion increased up to 28.5% and the selectivity to C_2 hydrocarbons up to 37.7% at 800°C in the presence of hydrogen peroxide.

The selectivity to C_3 and C_4 hydrocarbons as well as the methane conversion for all tested catalysts increased monotonically with rising temperature. When the temperature was increased, the combined selectivity to ethane and ethene seems to increase at low methane conversion levels and decline at higher conversion levels.

3.3.3.2. Catalytic testing of 5% La_2O_3/CaO, 1% Au/ 5% La_2O_3/CaO and 28% La_2O_3/ 7% SrO/CaO. The reaction was performed in the presence of hydrogen peroxide which was added as an aqueous solution (2.6, 7.6 and 21 wt.%); thus it was necessary to investigate the effect of the dilution of the reactant gases with water vapour.

The comparison of the activity of 5% La_2O_3/CaO catalyst under the different experimental conditions is reported in Table 3.13. The oxidative coupling of methane was studied in the temperature range 650-850°C using the reaction mixture, consisting of methane, oxygen, nitrogen and H_2O or H_2O_2 ($CH_4/O_2/N_2$/additive = 100/45/15/40). An aqueous solution of hydrogen peroxide of 21 wt.% or pure water was introduced to the reaction mixture at a rate of 0.03 ml/min.

It can be seen that without the addition of any liquid the maximum yield of C_{2+} hydrocarbons was 8.9% at a CH_4 conversion of 28.6%. The addition of pure water increased the C_{2+} hydrocarbons yield up to 14.4%. This increase was due to a rise in the total selectivity of the C_2, C_3 and C_4 products as well as in the methane conversion (31.9 %). The considerable rise in conversion could be related to dilution of the reaction mixture by water vapour. The formation of a small quantity of benzene was observed, which started at temperatures as low as 800°C. However, dilution of the reactant gases with water vapour substantially decreased the ethene-to-ethane ratio (last column in Table 3.13). The addition of hydrogen peroxide solution caused an increase in the methane conversion at 800°C and above, as well as the selectivity to C_2 - C_6 hydrocarbons, which resulted in an enhanced yield (16.3%).

A comparison of the results obtained under aforementioned reaction conditions reveals that the 5% La_2O_3/CaO catalyst becomes more selective toward ethene production in the presence of hydrogen peroxide. The C_2H_4/C_2H_6 ratio increased from 2.7 (in the experiment without any liquid addition) to 4.4 at 850°C. It can be also seen

Table 3.13. Influence of hydrogen peroxide on activity of 5% La_2O_3/CaO catalyst BET surf. area = 40 m^2/g) in the methane oxidative coupling. W = 0.7 g, τ = 0.12 s.

T (°C)	Addit.	X_{CH4} (%)	Selectivity (%)					Total Y_{C2+} (%)	C_2H_4/C_2H_6
			C_2H_4	C_2H_6	C_{3+}	C_6H_6	CO_X		
650	–	16.2	4.1	10.4	–	–	85.5	2.3	0.4
	H_2O	29.4	16.7	21.3	0.1	–	61.9	11.2	0.8
	H_2O_2	25.8	12.8	16.2	0.1	–	71.0	7.5	0.8
700	–	25.8	11.6	6.4	0.2	–	81.7	4.7	1.8
	H_2O	31.0	20.5	19.4	1.3	–	60.1	12.8	1.0
	H_2O_2	27.3	18.4	16.8	1.4	–	64.4	10.0	1.1
750	–	25.8	13.0	6.9	0.3	–	79.8	5.2	1.9
	H_2O	31.4	22.7	19.0	1.5	–	56.7	13.6	1.2
	H_2O_2	30.5	24.9	14.9	1.7	–	58.5	12.7	1.7
800	–	27.5	19.1	8.2	0.6	–	72.0	7.7	2.3
	H_2O	31.9	23.8	18.2	1.6	1.6	54.8	14.4	1.3
	H_2O_2	34.8	29.5	13.5	2.1	1.8	53.0	16.3	2.2
850	–	28.6	22.4	8.4	0.6	–	68.6	8.9	2.7
	H_2O	33.1	18.5	14.8	1.7	2.4	62.7	12.4	1.3
	H_2O_2	35.6	28.3	6.4	2.3	4.1	58.9	14.6	4.4

from Table 3.13 that low reaction temperatures clearly favoured the formation of carbon oxides over the C_{2+} hydrocarbons, and vice versa at high temperatures.

A review of the literature shows that doping oxidative-coupling catalysts with noble metals tends to produce systems that give elevated yields for the carbon oxides and concomitant low yields for hydrocarbon products. An attempt was made in this work to dope 5% La_2O_3/ CaO catalyst with the noble metal gold rather than palladium or platinum. The logic behind this was that most of the noble metals except for gold exhibit over active catalytic tendencies which lead to complete oxidation of hydrocarbon products to CO_X.

Table 3.14. Influence of hydrogen peroxide on methane oxidative coupling reaction over a 1% Au/ 5% La_2O_3/CaO catalyst (BET surface area = 29 m^2/g). Total flow rate of the reactant mixture = 200 ml/min, W = 0.7 g, τ = 0.11 s.

T (°C)	Additive	X_{CH4} (%)	Selectivity (%)					Total Y_{C2+} (%)
			C_2H_4	C_2H_6	C_3-C_4	C_6H_6	CO_x	
600	none	0.5	1.4	4.4	–	–	94.2	0.03
700		31.6	19.1	14.7	1.1	–	65.1	11.0
800		32.3	24.5	11.3	1.2	–	63.0	11.9
600	H_2O	0.2	8.6	20.0	–	–	71.4	0.06
700		32.5	24.6	20.3	1.4	5.5	48.2	16.8
800		32.9	28.3	16.3	1.7	6.6	47.1	17.4
600	H_2O_2	0.1	12.2	16.9	–	–	70.9	0.03
700	(2.6wt.%)	35.4	25.1	20.1	1.8	9.8	43.0	20.1
800		35.9	29.5	15.6	2.1	12.0	40.0	21.3
600	H_2O_2	0.1	13.1	17.8	–	–	68.9	0.03
700	(7.6wt.%)	35.8	27.7	20.5	1.9	10.3	39.4	21.6
800		36.0	31.8	15.9	2.4	12.9	37.0	22.7
600	H_2O_2	0.1	16.5	16.6	–	–	66.8	0.03
700	(21 wt.%)	35.9	29.0	19.4	2.3	16.2	32.6	24.0
800		38.3	32.7	15.5	3.4	19.2	28.4	27.1

The influence of hydrogen peroxide and its concentration in the reaction mixture on CH_4 conversion and C_{2+} hydrocarbon selectivity was examined over a 1% Au/5% La_2O_3/ CaO catalyst in the temperature range 600-800°C with a reactant mixture of $CH_4/O_2/N_2$ = 100/45/15. An aqueous solution of hydrogen peroxide with concentrations varying from 2.6 to 21 wt.%, or pure water, was added to the reactant mixture via an evaporator at a rate of 0.03 ml/min. The results of the experiments with water, hydrogen peroxide as well as without any liquid addition to the feed are presented in Table 3.14.

It can be seen that the maximum yield of C_{2+} hydrocarbons in the absence of liquid additive was about 12% at a methane conversion of 32%. The addition of pure water

increased the maximum yield to 17.4%. This increase in yield was due to a rise in the total selectivity of C_{2+} products as well as an increase in the methane conversion. The formation of a small quantity of benzene was observed. The rise in conversion could be related to dilution of the reaction mixture by water vapour[143]. Surprisingly, the addition of even 2.6 wt.% hydrogen peroxide solution to the reaction mixture had a strong positive effect on the methane conversion as well as the selectivity to the C_{2+} products, which resulted in a yield enhancement. The higher the concentration of added hydrogen peroxide, the higher the methane conversion and the higher the yield of C_{2+} products obtained (Table 3.14). The selectivity to carbon monoxide decreased with increasing temperature and was never greater than 10%. When the oxygen conversion reached 100% at 800°C in the presence of hydrogen peroxide, carbon monoxide could no longer be detected as a product.

The peculiarity of the performed reaction was the formation of a noticeable quantity of benzene. This could be related to an acceleration of the process of olefin aromatization by hydrogen peroxide as well as by the metal component (gold) on the catalyst surface. The maximum yield of C_{2+} products obtained was 27% with a corresponding 7.3% yield of benzene.

The increase of hydrogen peroxide concentration also resulted in an increase in the ethylene/ethane ratio when compared with that of pure water. The higher ethylene/ethane ratio in the experiment without any liquid addition could be due to the lack of benzene formation under the aforementioned reaction conditions, as ethylene is likely to be the precursor of the aromatic products[144].

A comparison of the results given in Table 3.13 and 3.14 clearly shows that the 1%Au/ 5% La_2O_3/CaO catalyst was markedly more active and selective towards desirable products than unpromoted 5% La_2O_3/CaO. Loading of only 1% Au on the lanthanum-calcium system caused a significant increase of C_{2+} hydrocarbon selectivity and a rather small increase in the CH_4 conversion. It also gave a decrease in BET surface area from 40 m^2/g of the 5% La_2O_3/CaO to 29 m^2/g of the 1%Au/ 5% La_2O_3/CaO sample. One can predict, that gold plays an important role in the hydrogen peroxide dissociation reaction and radical formation under conditions of heterogeneous-homogeneous methane oxidative coupling.

The selected results of the methane oxidative coupling obtained for 28% La_2O_3/ 7%SrO/CaO catalyst after optimization of the reaction conditions (CH_4/O_2 ratio, contact time and temperature) are shown in Table 3.15. The catalyst was tested in a 4 mm i.d. quartz tube (Figure 2.3 (d)) in the temperature range 650-950°C. At the optimum reaction condition, i.e., total flow rate of the reactant mixture ($CH_4/O_2/N_2$/additive = 68/17/5/90) equal 180 ml/min, which corresponded to contact time of 0.11 s, the best catalytic performance was observed in the presence of water vapour. The data reported shows maximum selectivity to all coupled hydrocarbons of 70% at a methane conversion of about 30%. Substantial amounts of hydrogen were produced during the reaction. However, the heavy fractions (benzene and naphthalene) completely disappeared from the detectable products under these reaction conditions.

Previous studies have shown that the alkali and alkaline earth promoted La_2O_3 samples show the highest C_2 selectivity at the lowest reaction temperature[37,49,73,145,146]. The alkaline earth oxides, on the other hand, exhibit lower overall activity and a maximum C_2 selectivity at much higher temperatures than the rare earth oxides. Strontium oxide exhibits very low activity, converting only 36% of the O_2 feed at 850°C [95,147]. It was shown that many of the effective catalysts are chemically similar: they are solid bases, possessing one stable oxidation state, and strongly adsorb CO_2 and H_2O from the atmosphere. Conversely, multiple oxidation states of the d and f block metals promote complete oxidation of the methane through a redox reaction mechanism. Among the many possible combinations of oxides that catalyze the oxidative coupling of methane, La_2O_3 promoted with SrO gave the best performance.

During experiments the catalyst rapidly attained a steady-state activity which remained constant over 72 hours. The catalytic results presented in Table 3.15 show that promotion of the CaO supported La_2O_3 with SrO was a more selective system towards C_2 hydrocarbons than the 5% La_2O_3/CaO and 1% Au/ 5% La_2O_3/CaO catalysts. It appears that not only an appreciable amount of lanthanum on the surface of the specimen but also strontium is necessary for the system to be selective. The combined selectivity to ethylene and ethane was much higher than that to CO_x under optimum reaction conditions, but the molar C_2H_4/C_2H_6 ratio was less than that obtained at 850°C on 5% La_2O_3/CaO catalyst (2.2 and 4.4, respectively). This seems to indicate that the presence of SrO enhanced the selectivity to C_2 products and decre-

Table 3.15. Influence of hydrogen peroxide on methane oxidative coupling reaction over a 28% La_2O_3/ 7% SrO/CaO catalyst (BET surface area = 4 m^2/g). Total flow rate of the reactant mixture ($CH_4/O_2/N_2$/additive = 68/17/5/90) = 180 ml/min, W = 0.7 g, $\tau = 0.11$ s.

T (°C)	Addit.	X_{CH4} (%)	Selectivity (%)					Total Y_{C2+} (%)
			C_2H_4	C_2H_6	C_3-C_4	CO_2	CO	
650	–	5.3	15.4	27.5	–	39.6	17.5	2.3
	H_2O	4.8	9.0	29.6	–	47.0	14.4	1.8
	H_2O_2	8.1	4.9	26.1	–	49.8	19.2	2.5
700	–	8.8	17.4	31.7	0.8	34.2	15.9	4.4
	H_2O	12.6	23.6	31.0	1.3	35.5	8.6	7.0
	H_2O_2	15.1	12.1	25.6	0.3	48.9	13.1	5.7
750	–	18.1	27.3	30.0	2.3	31.2	9.2	10.8
	H_2O	21.2	35.0	29.0	1.8	33.0	1.2	13.9
	H_2O_2	25.6	27.9	25.2	1.7	38.2	7.0	14.0
800	–	23.4	37.5	27.0	2.5	29.4	3.6	15.7
	H_2O	26.6	39.1	26.5	2.1	32.3	–	18.0
	H_2O_2	29.8	37.8	22.6	2.0	35.3	2.3	18.6
850	–	25.2	41.1	18.0	3.0	32.9	5.0	15.6
	H_2O	28.3	44.0	24.2	2.4	28.9	0.5	20.0
	H_2O_2	30.7	45.3	20.7	2.2	31.8	–	20.9
900	–	26.7	41.0	8.6	3.5	38.3	8.6	14.2
	H_2O	31.4	46.4	15.9	3.5	32.4	1.8	21.0
	H_2O_2	32.2	43.8	10.9	3.2	40.5	1.6	18.6
950	–	26.9	36.3	3.2	4.2	44.3	12.0	11.8
	H_2O	31.6	42.0	8.2	4.0	37.0	8.8	17.1
	H_2O_2	32.8	38.5	7.8	4.4	40.1	9.2	16.6

ased the ethylene-to-ethane ratio, though the best absolute yield of C_2H_4 + C_2H_6 remained ~ 20%. The results also show that at low CH_4 and O_2 conversions substantial amounts of CO_2, CO and C_2H_6 were produced. As the temperature and CH_4 (O_2)

conversions increased, a large increase in the selectivity to C_2H_4 relative to CO_2 and CO was observed. The selectivity to carbon monoxide droped to practically zero at 800°C in the presence of water vapour, but as the temperature increased, the selectivity to carbon monoxide also went up. The results suggests that CO_2 may be formed by the oxidation of CO. However, this must be viewed as a tentative conclusion, because of the high concentration of CO_2 relative to CO, and the competing influence of the water gas shift equilibrium.

A comparison of the results given in Tables 3.13, 3.14 and 3.15 shows that a catalyst with a lower surface area exhibites a higher C_2 product selectivity and reduces the formation of carbon oxides. It seems that the CO_X formation takes place mainly on the catalyst surface, which is in agreement with the published results of Deboy and [illegible]s[145,146]. The data obtained by these authors for the apparent activation energies for ethane and CO_X formation can give an understanding of the mechanism by which the carbon oxides are formed. As discussed above, ethane is formed by the recombination of methyl radicals in the gas phase, while CO_X is formed by the reaction of methyl radicals with O_2 either in the gas phase or on the catalyst surface. Since the activation energy for methyl radical recombination is near zero[148], the overall activation energy for ethane formation must equal the overall activation energy for forming gas-phase methyl radicals, E_{CH3}. Thus, $E_{CH3} = E_{C2H6} = 36.8$ kcal/mol. If CO_X is formed by the gas phase reaction of methyl radicals and O_2, then the overall activation energy for CO_X formation from methane must at a minimum equal the energy for generating the methyl radicals. However, the apparent activation energy for CO_X formation was found to be only 23.9 kcal/mol, substantially less than E_{CH3}. It was concluded, therefore, that over 1% SrO/La_2O_3 the CO_X is not formed in the gas phase but on the catalyst surface.

When the highly exothermic methane oxidative coupling reaction was performed adiabatically using a specifically designed quartz reactor (Figure 2.4 (e)), a temperature excursion from 685°C to 950°C was noted over the 28% La_2O_3/ 7% SrO/CaO catalyst and one from 720°C to 880°C over the 5% La_2O_3/CaO catalyst. After the initial evolution of heat the oxygen conversion was always 100%. The high activity of the 28% La_2O_3/ 7% SrO/CaO catalyst, which caused the ignition temperature of the methane oxidative coupling reaction to be lower and the range of the temperature

excursion to be greater, can be attributed to the presence of strontium oxide and the higher loading of lanthanum oxide.

The results shown in Tables 3.13, 3.14 and 3.15 may be summarized as follows:

1. Comparable methane conversions were achieved at a much lower temperatures in the presence or absence of hydrogen peroxide in the reaction mixture.

2. The addition of hydrogen peroxide as well as pure water to the reaction mixture caused an increase in the methane conversion and the selectivity to C_{2+} hydrocarbons.

3. A peculiarity of the reaction on 1% Au/ 5%La_2O_3/CaO catalyst was the formation of a noticeable quantity of benzene in the presence of hydrogen peroxide. The C_{2+} hydrocarbon selectivity increased remarkably by increasing the concentration of added hydrogen peroxide. The highest C_{2+} product yield obtained at 800°C was 27% with a corresponding 7% yield of benzene.

4. The product distribution obtained from the 5% La_2O_3/CaO, 1% Au/ 5% La_2O_3/ CaO and 28% La_2O_3/ 7% SrO/CaO catalysts are quite different. The main selectivity difference lay in the considerable amounts of C_2 hydrocarbon formed during the introduction of hydrogen peroxide to the reaction mixture.

5. The total C_2 hydrocarbon selectivity increased from 49.6 to 62.3% at corresponding CH_4 conversions of 26.7% and 31.4% as the reactant gas was diluted by water vapour in the reaction performed on 28% La_2O_3/ 7% SrO/CaO catalyst. An absolute yield of 20% of both C_2H_4 and C_2H_6 was obtained at a CH_4/O_2 ratio of 4.0 and a residence time of 0.11 s.

6. It appeared that the ethylene-to-ethane ratio increased with a rise in the reaction temperature. The highest C_2H_4/C_2H_6 ratio was observed in the experiment using 5% La_2O_3/CaO catalyst in the presence of 21 wt.% solution of hydrogen peroxide.

3.3.4. Catalyst characterisation. The surface areas of the 5% La_2O_3/CaO, 1% Au/ 5% La_2O_3/CaO and 28% La_2O_3/ 7% SrO/CaO catalysts were determined by the BET method. X-Ray Diffraction analysis (XRD) and Scanning Electron Microscopy (SEM) coupled with Energy Dispersive X-Ray analysis were used to determine the crystalline structure, morphology and distribution of elements on the surface of these catalysts.

3.3.4.1. Surface area determination. The BET surface area decreased after impregnation the lanthanum-calcium system with 1% Au from 40 m^2/g of the 5% La_2O_3/CaO sample to 29 m^2/g of the 1% Au/ 5% La_2O_3/CaO sample. Increasing the La_2O_3 loading from 5% to 28% and replacing 1% Au with 7% SrO resulted in a further decrease in surface area of the catalyst to 4 m^2/g. The colour of the 1% Au/ 5% La_2O_3/CaO sample was dark purple, whereas the 5% La_2O_3/CaO and 28% La_2O_3/ 7% SrO/CaO samples remained white even after the high temperature experimental investigations.

3.3.4.2. XRD analysis. The bulk structure of the 5% La_2O_3/CaO, 1% Au/ 5% La_2O_3/CaO and 28% La_2O_3/ 7% SrO/CaO samples were examined by the XRD method before and after catalytic testing. The X-ray patterns of the 5% La_2O_3/CaO catalyst before the methane oxidative coupling reaction (a) and after ~24 hours on stream (b) at the temperature range 650-850°C are shown in Figure 3.4. These XRD results clearly indicate that well-crystallized sharp peaks which correspond to cubic CaO and hexagonal La_2O_3 phases have disappeared during the high temperature catalytic testing, and new poorly crystallized structure of hexagonal $Ca(OH)_2$ and $La(OH)_3$ have been detected.

An X-ray diffraction investigation of 1% Au/ 5% La_2O_3/CaO was also carried out on both fresh (calcined) and high temperature treated samples (Figure 3.5 (a) and (b)). The crystalline structure of CaO and La_2O_3 phases appeared in the XRD pattern for fresh 1% Au/ 5% La_2O_3/CaO. The position and shape of the diffraction peaks are identical to those of unpromoted 5% La_2O_3/CaO. In addition four peaks of cubic Au at 2θ values of 38.19°, 44.39°, 77.55° and 115.26° were detected (Figure 3.5 (a)). This structure was transformed during the methane oxidative coupling to a mixture of

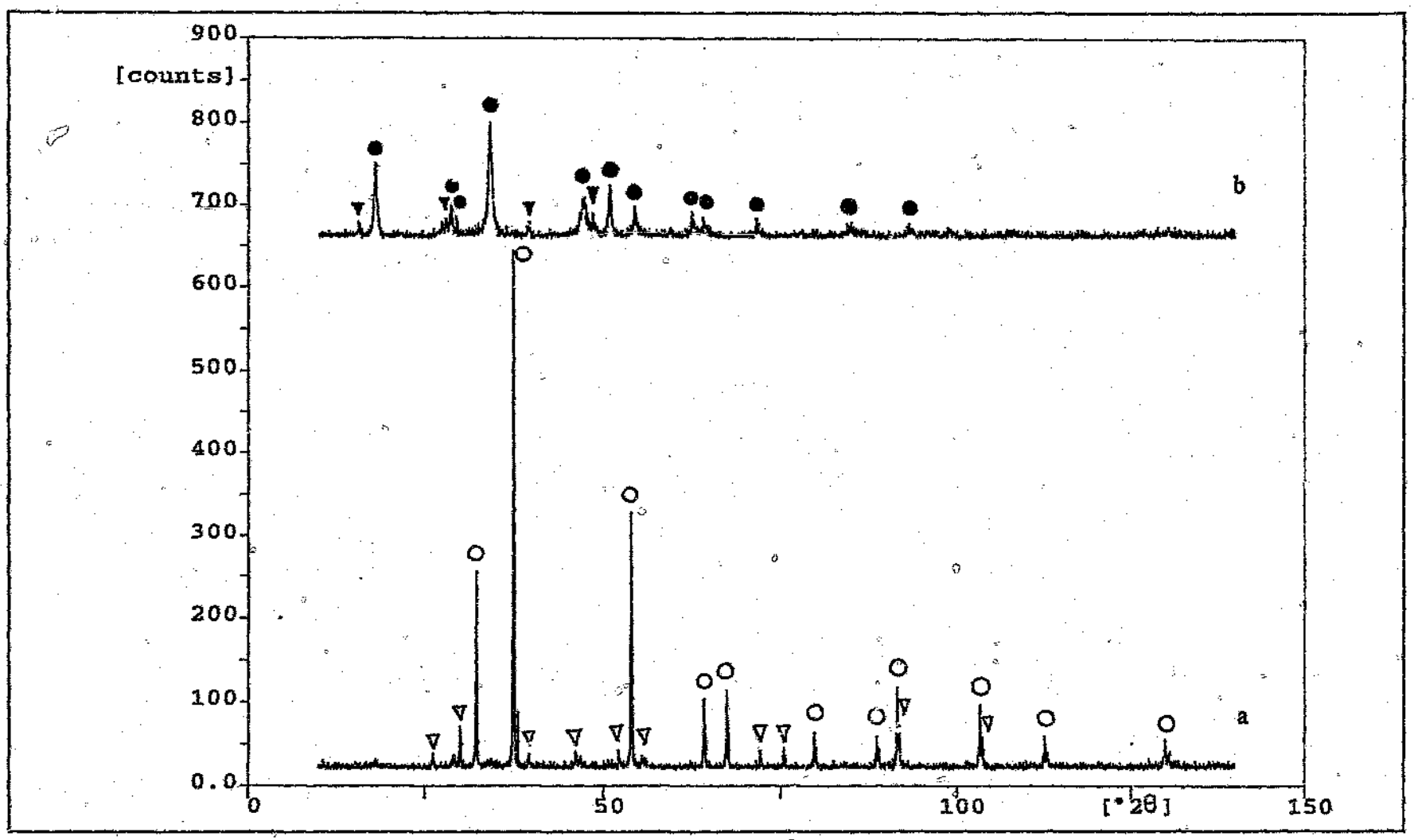


Figure 3.4. X-ray diffraction pattern of 5% La_2O_3/CaO (a) before and (b) after catalytic reaction. (O) CaO, (V) La_2O_3, (●) $Ca(OH)_2$, (▼) $La(OH)_3$.

hexagonal $Ca(OH)_2$, $La(OH)_3$ and cubic Au phases (Figure 3.5 (b)). There is no evidence to suggest that elemental Au undergoes to any structural modifications or interacts with the neighboring phases.

The X-ray diffraction pattern of the 28% La_2O_3/ 7% SrO/CaO sample freshly prepared and subsequently calcined (Figure 3.6 (a)) displayed well-crystallized sharp peaks which correspond to cubic CaO, SrO and hexagonal La_2O_3 phases. It can be seen in Figure 3.6 (b) that the XRD pattern of the same sample after exposure to the reaction mixture (CH_4, O_2, N_2 and H_2O vapour) in the temperature range 650-950°C revealed the coexistence of $Ca(OH)_2$ (hexagonal structure) and $CaCO_3$ (rhombohedral structure), $La(OH)_3$ (hexagonal structure) and $La_2O_2CO_3$ (hexagonal structure), and $SrCO_3$ (orthorhombic structure). The XRD analysis did not detect a Sr-La phase after the thermal treatment of the sample during the methane oxidative coupling reaction, but it should be noted that the low intensities and broadened peaks observed for $SrCO_3$ and $La_2O_2CO_3$ were due to the poorly crystalline structure of these phases.

The tendency of La_2O_3 to react with CO_2 is well documented. When La_2O_3 is exposed to dry CO_2 or to atmospheric air at room temperature, surface carbonates or hydroxycarbonates are formed respectively, whereas when CO_2 is chemisorbed at temperatures higher than 450°C, dioxymonocarbonates $La_2O_2CO_3$ are obtained[149,150]. It is also known[151,152], that the carbonation of La_2O_3 in air is much less strong than its hydration, the intensity of the former process depending on the surface area of the sample. Exposure of rare-earth oxides to the air for up to three years causes an increase of X-ray diffraction lines attributable to the hydroxides for La_2O_3 and Sm_2O_3[149]. In the present study the samples with comparetively high surface areas (40 and 29 m^2/g) showed the presence of only $La(OH)_3$ in post-reaction characterization, whereas the sample with low surface area (4 m^2/g) showed diffraction peaks, typical of hexagonal $La_2O_2CO_3$.

The influence of carbonates and oxycarbonates on the catalytic performance has already been suggested for the oxidative coupling of methane[153,154]. The incorporation of stable carbonates into rare earth oxides as well as the transformation of La_2O_3 into $La_2O_2CO_3$ have been found to improve the C_{2+} hydrocarbon selectivity.

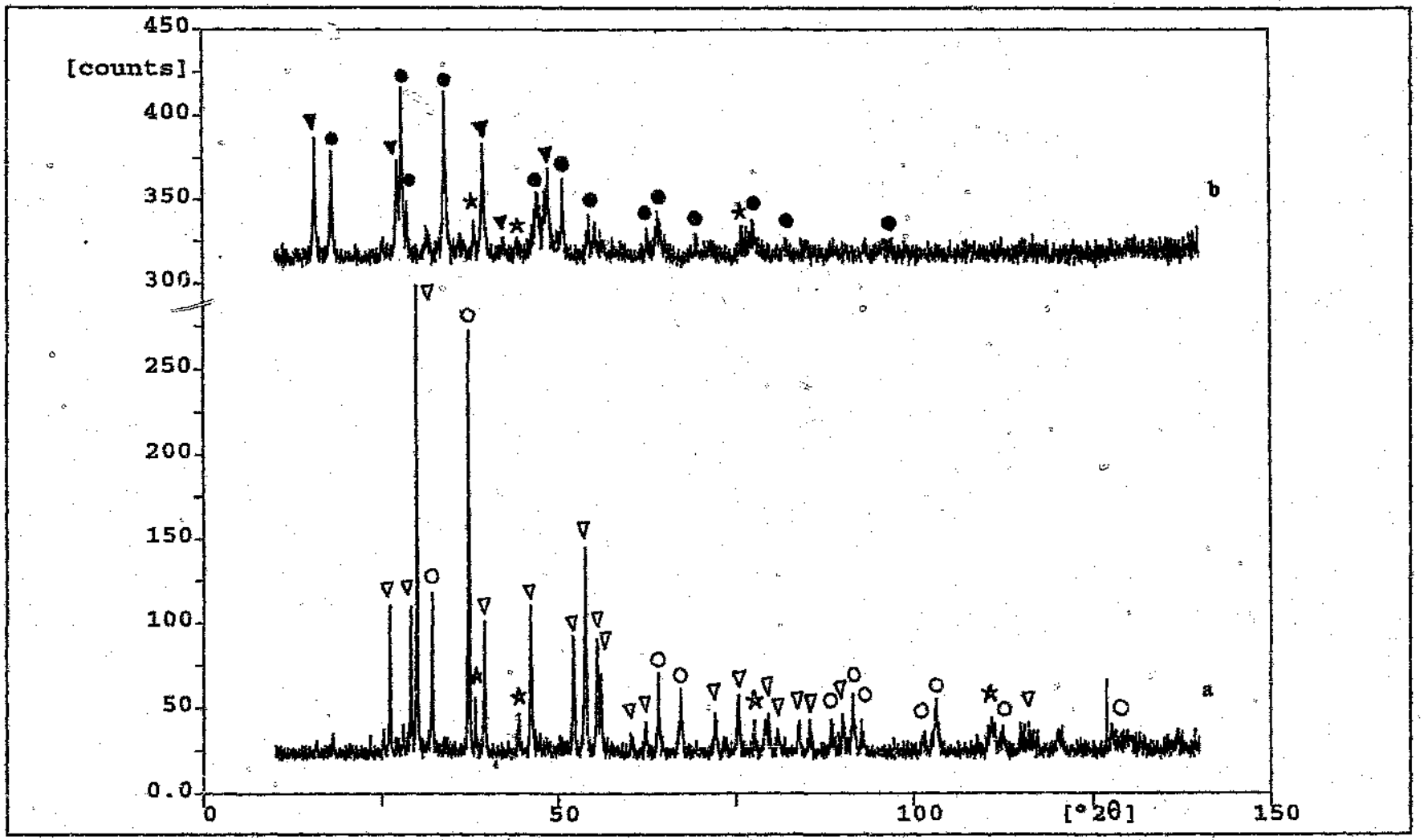


Figure 3.5. X-ray diffraction pattern of 1% Au/ 5% La_2O_3/CaO (a) before and (b) after catalytic reaction. (O) CaO, (▽) La_2O_3, (●) $Ca(OH)_2$, (▼) $La(OH)_3$, (★) Au.

The high reactivity of La_2O_3 towards CO_2 was suggested to give rise to the reversible formation of $La_2O_2CO_3$, at temperatures above 450°C, according to the equilibrium:

$$La_2O_3 + CO_2 \leftrightarrow La_2O_2CO_3$$

The oxycarbonate is formed via the insertion of CO_2 molecules between the $(LaO)_2$ layers of La_2O_3, a process which requires a thermal activation. When the CO_2 partial pressure over La_2O_3 is higher than the equilibrium pressure, La_2O_3 may completely transform into $La_2O_2CO_3$. The higher the CO_2 partial pressure in comparison with the equilibrium pressure, the faster the rate of the transformation. However, the catalytic results obtained by Le Van et al.[153] showed that the formation of $La_2O_2CO_3$ does not proceed from gas-phase CO_2 adsorption, but arises more likely from the surface oxidation of CH_4. According to this proposal, even at 650°C a large amount of $La_2O_2CO_3$ (~15%) can be produced. Moreover, the amount of $La_2O_2CO_3$ produced during the catalytic test at 650°C was constant in the 2-45 hours of reaction. It was suggested that the formation and decomposition of $La_2O_2CO_3$ occurs according to the following scheme:

$$La_2O_3 + CH_4 + O_2 \xrightarrow{k_1} La_2O_2CO_3 \xrightarrow{k_2} La_2O_3 + CO_2$$

In this scheme, the amount of $La_2O_2CO_3$ appears to depend on the k_1/k_2 ratio of the rate constants of formation and decomposition, and $La_2O_2CO_3$ is assumed to be an intermediate for the production of CO_2.

The results presented here show that the occurrence of *in situ* deep carbonation phenomena can play an important role in determining the catalytic behaviour of the La_2O_3 promoted systems for reactions like the methane oxidative coupling, where significant amounts of CO_2 are produced.

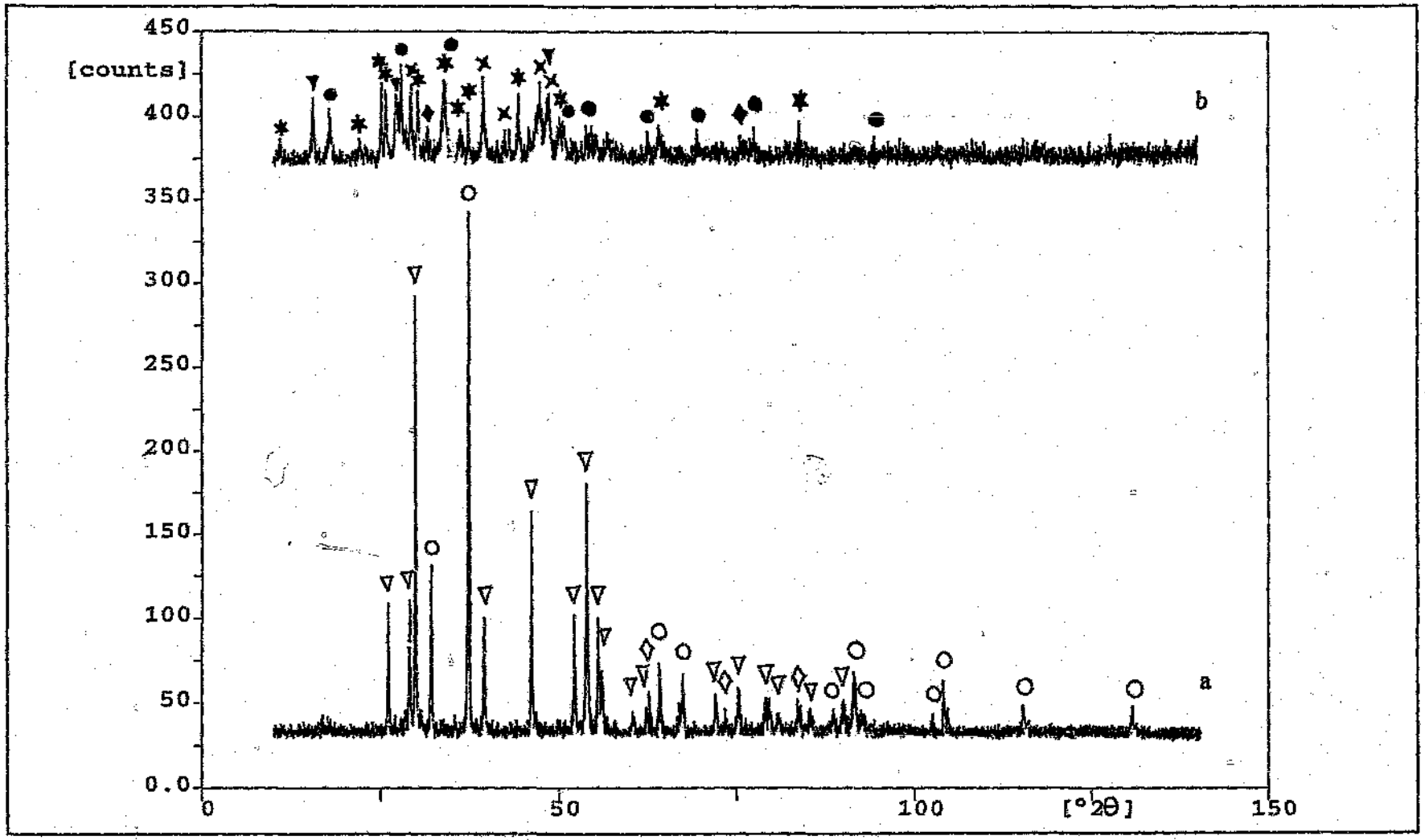
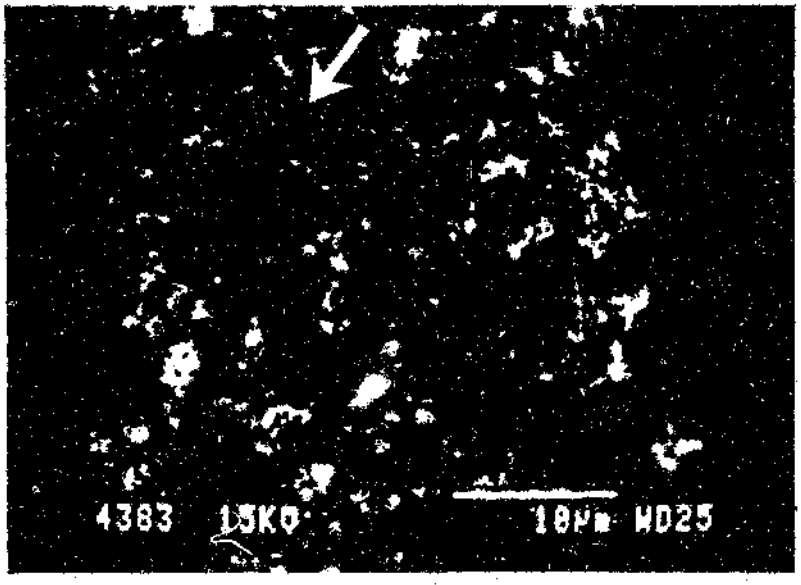


Figure 3.6. X-ray diffraction pattern of 28% La_2O_3/ 7% SrO/CaO (a) before and (b) after catalytic reaction. (O) CaO, (∇) La_2O_3, (◊) SrO, (●) $Ca(OH)_2$, (▼) $La(OH)_3$, (×) $CaCO_3$, (✱) $La_2O_2CO_3$, (◆) $SrCO_3$.

3.3.4.3. SEM and EDX analysis. The influence of the hydration and carbonation phenomena on the morphologies of the 5% La_2O_3/CaO, 1% Au/ 5% La_2O_3/CaO and 28% La_2O_3/ 7% SrO/CaO samples during the methane oxidative coupling reaction was examined by scanning electron microscopy (SEM). Compositional data on individual crystals as well as aggregates of particles were obtained using energy dispersive X-ray analysis (EDX) facilities coupled to the electron microscope.

SEM micrographs of the 5% La_2O_3/CaO sample after catalytic reaction are shown in Figure 3.7 (a) and 3.8 (a). The dark aggregated phase of the support formed a thick layer of about 30 100 μm with a smooth surface. The supported lanthanum hydroxide showed a structure of irregular particles (white inclusions) from 0.1 to 0.5 μm, often coalesced into aggregates of about 3-5 μm. When the electron beam was focussed onto the dark thicker area of the specimen where no white particles could be seen, the EDX spectrum revealed strong Ca and weak La signals (Figure 3.7 (b)). Quantitative EDX analysis showed that the proportion of oxygen with respect to calcium O/Ca was close to 2, which corresponds to $Ca(OH)_2$. The EDX spectrum of the white particle (Figure 3.8 (b)) revealed that most of the surface was covered by lanthanum and oxygen atoms. The surface composition obtained from quantitative EDX was 18 at.% La, 8 at.% Ca and 74 at.% O, which corresponds to the stoichiometry of $Ca(OH)_2$ and $La(OH)_3$. The Si signal, probably, came from the SEM grid.

Figure 3.9 and 3.10 show SEM micrographs and X-ray spectra of 1% Au/ 5% La_2O_3/ CaO after catalytic reaction performed in the temperature range 600-800°C. The morphology is, in general, similar to that of the pure lanthanum-calcium specimen. However, the surface consisted of larger irregularly shaped particles in the size range 10-15 μm (Figure 3.9 (a)). The high content of elemental gold on the surface of the bright white particle (Figure 3.10 (b)) is indicative of the inhomogeneous dispersion of this promoter. The gold distribution was investigated further by varying the size of the electron beam used in the EDX experiment. Initially, a beam about the same size (~0.1 μm) as the particle was used to generate an EDX spectrum, and the beam was then defocussed (underfocussed or overfocussed) to the larger size of 1 μm to obtain another spectrum. The collection time was generally around 100 s. The dead time and counts per second were kept the same for every spectrum. When the beam was spread, the total current of the beam remained constant, so its intensity decreased with the



a

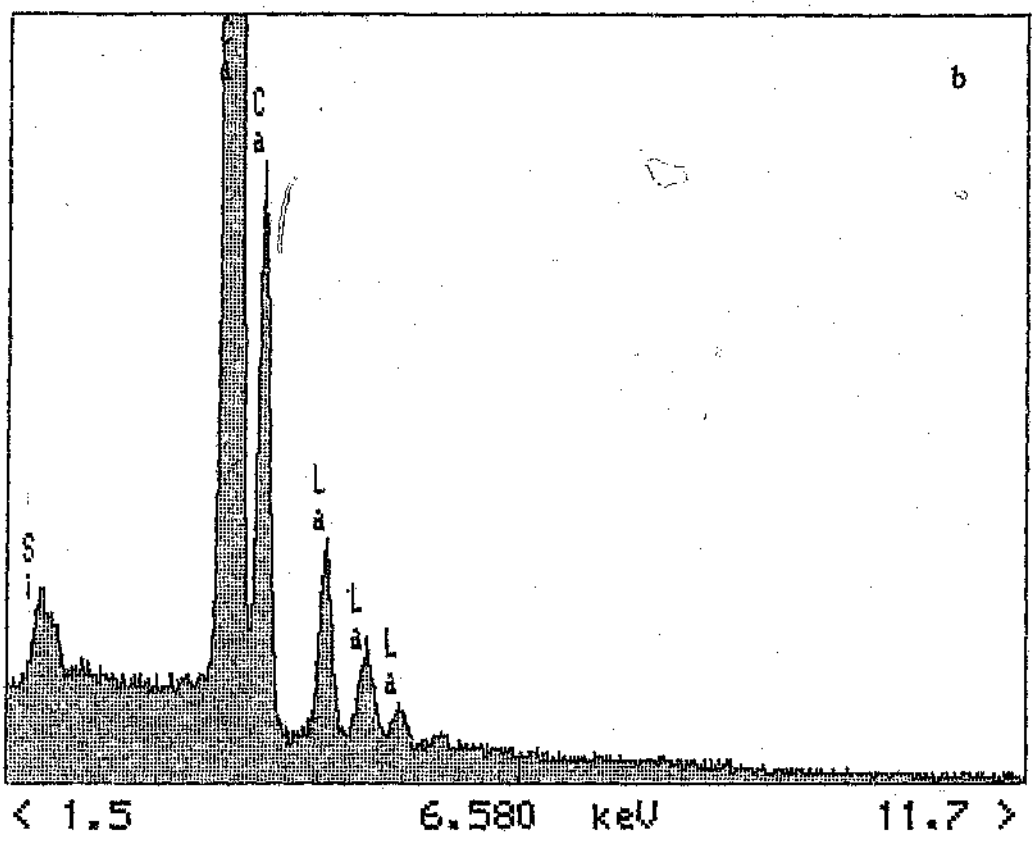
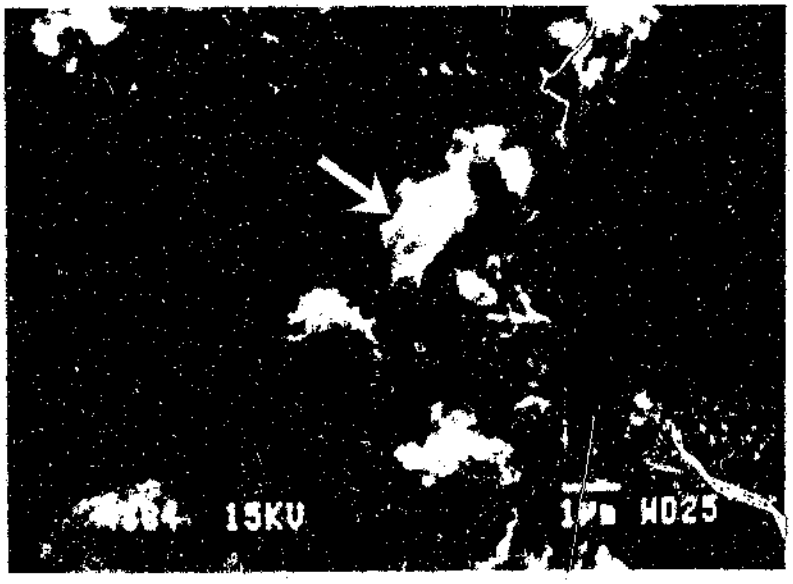


Figure 3.7. 5% La_2O_3/CaO after catalytic reaction: 24 hours at 650-850°C. (a) SEM micrograph. (b) EDX spectra of the dark area on the catalyst surface.



a

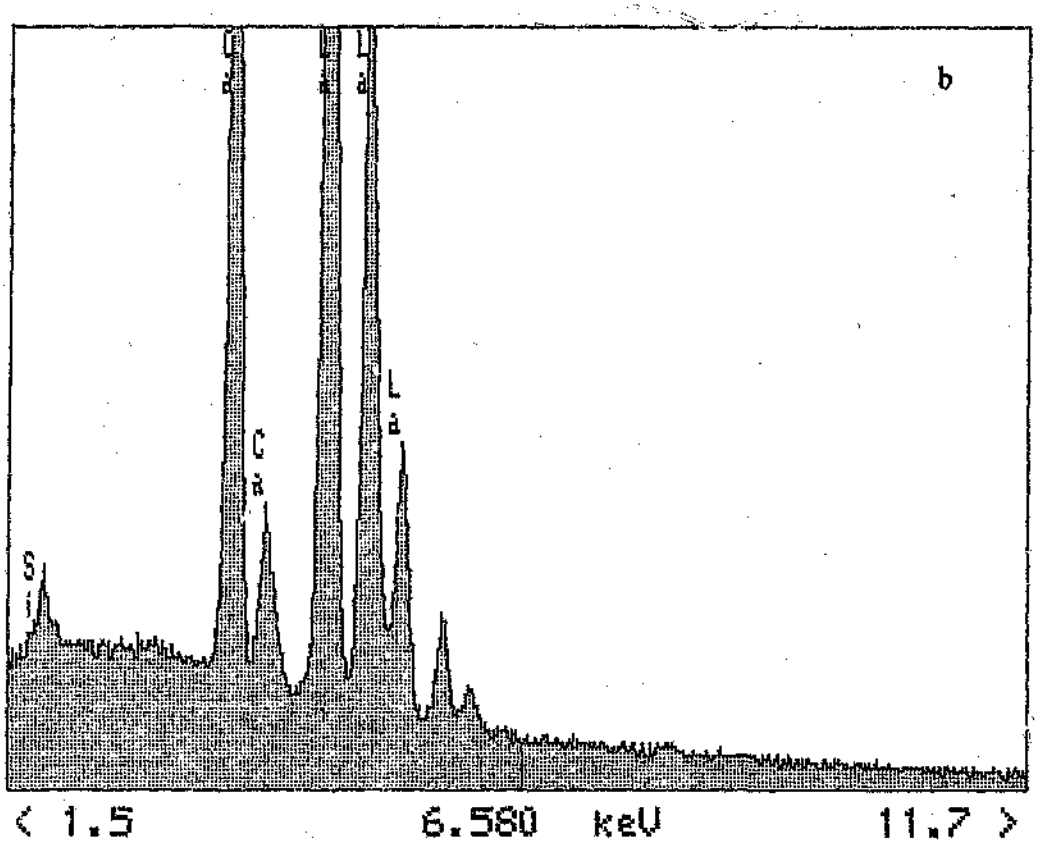


Figure 3.8. 5% La_2O_3/CaO after catalytic reaction: 24 hours at 650-850°C. (a) SEM micrograph. (b) EDX spectra of the white particle on the catalyst surface.

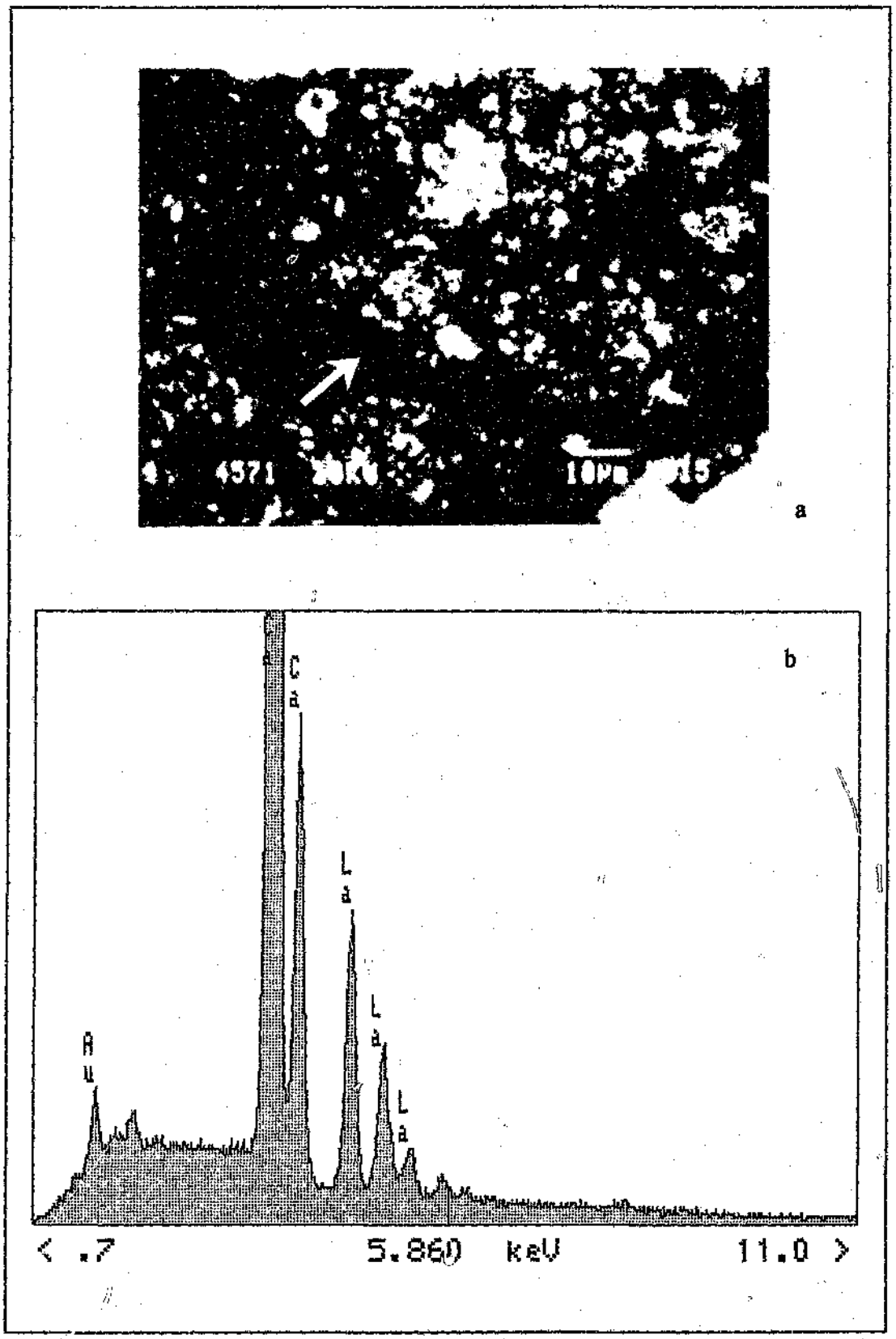


Figure 3.9. 1% Au/ 5% La_2O_3/CaO after catalytic reaction: 24 hours at 600-800°C. (a) SEM micrograph. (b) EDX spectra of the dark area on the catalyst surface.

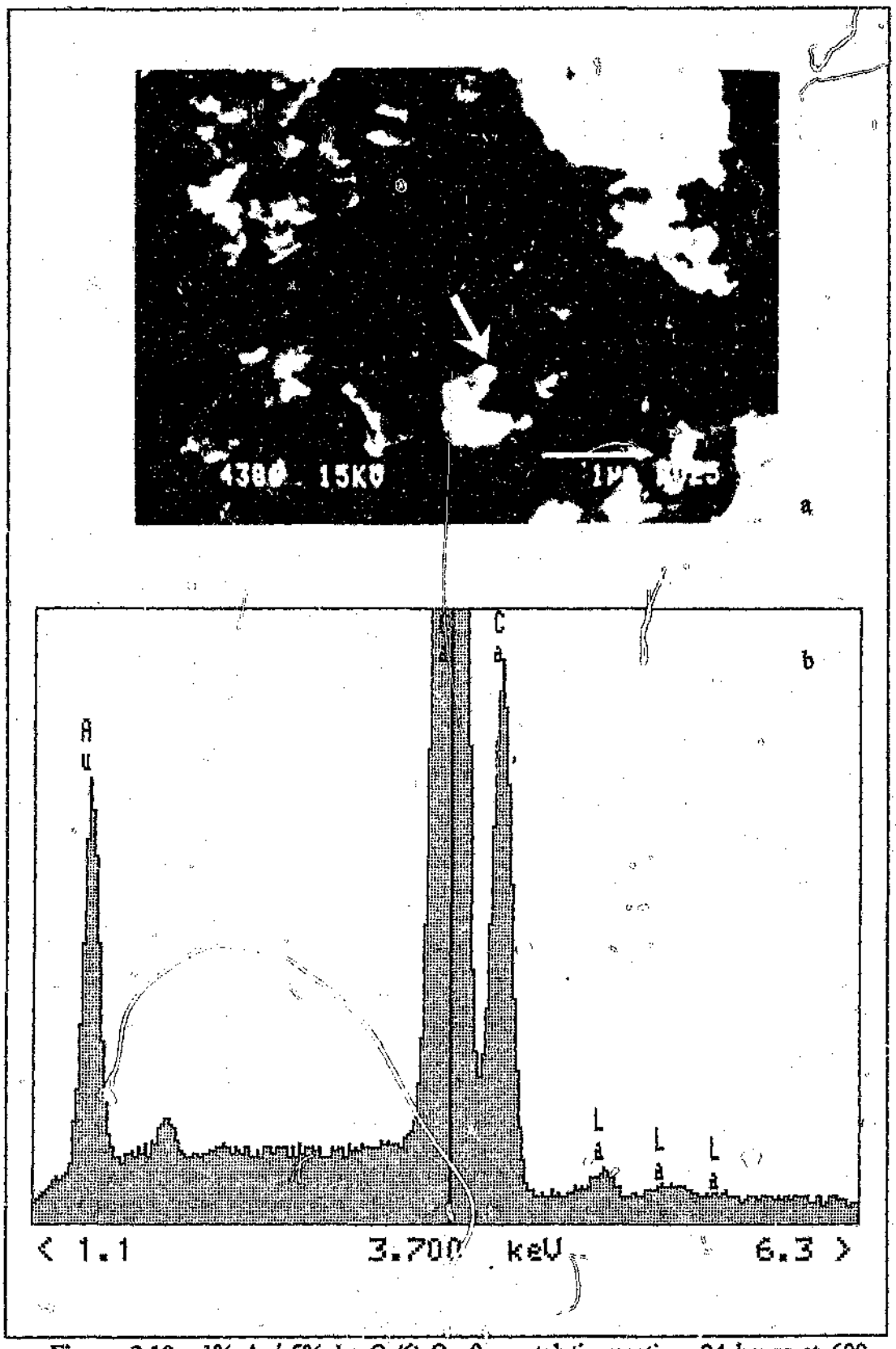
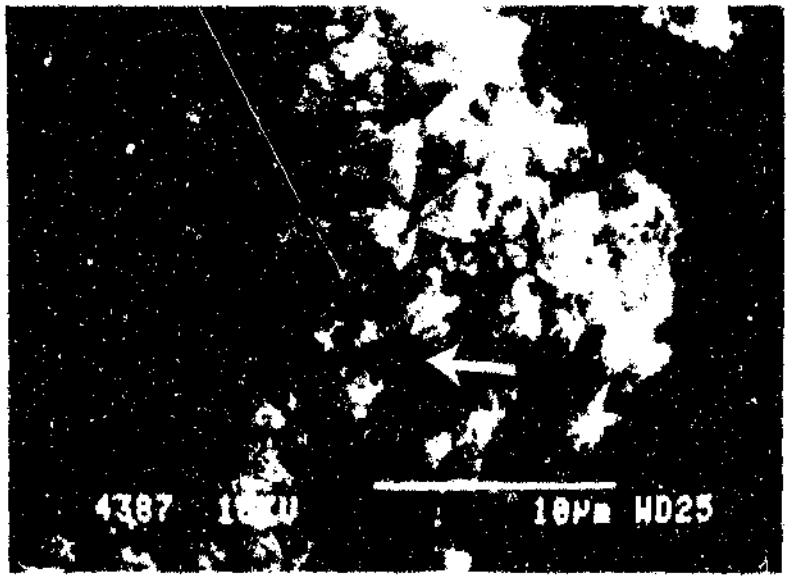


Figure 3.10. 1% Au/ 5% La_2O_3/CaO after catalytic reaction: 24 hours at 600-800°C. (a) SEM micrograph. (b) EDX spectra of the bright white particle in (a).



a

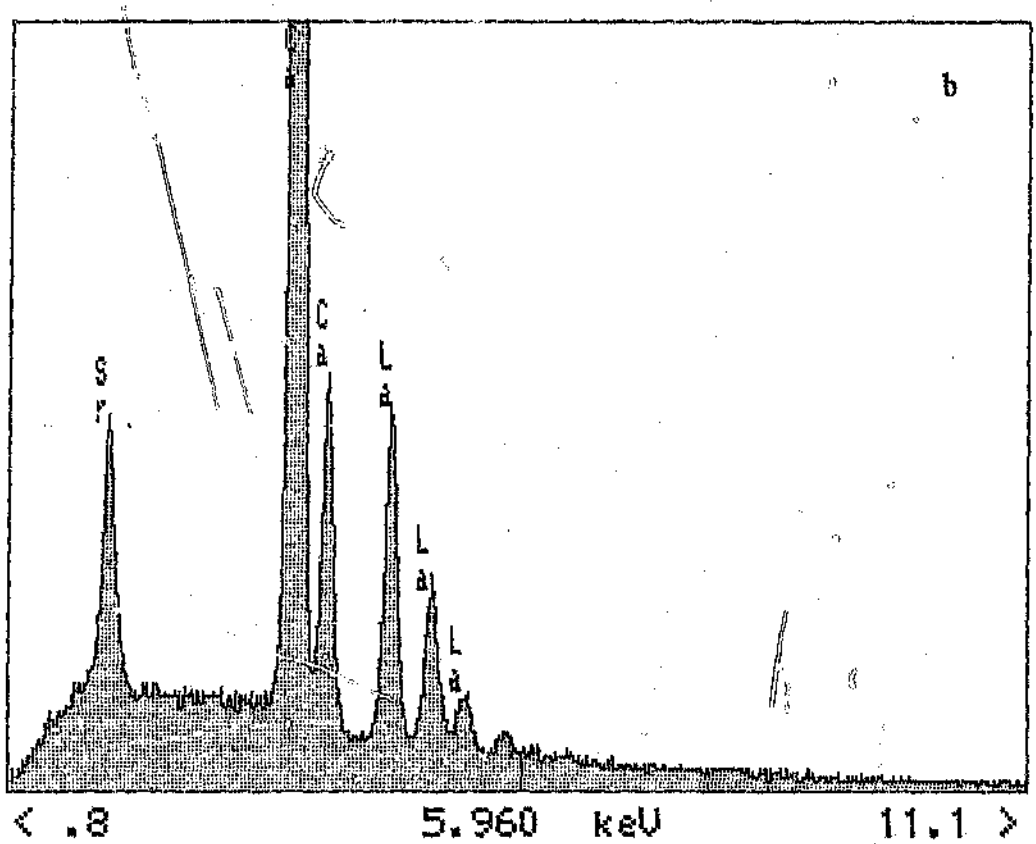


Figure 3.11. 28% La_2O_3/7% SrO/CaO after catalytic reaction: 72 hours at 650-950°C. (a) SEM micrograph. (b) EDX spectra of the dark area on the catalyst surface.

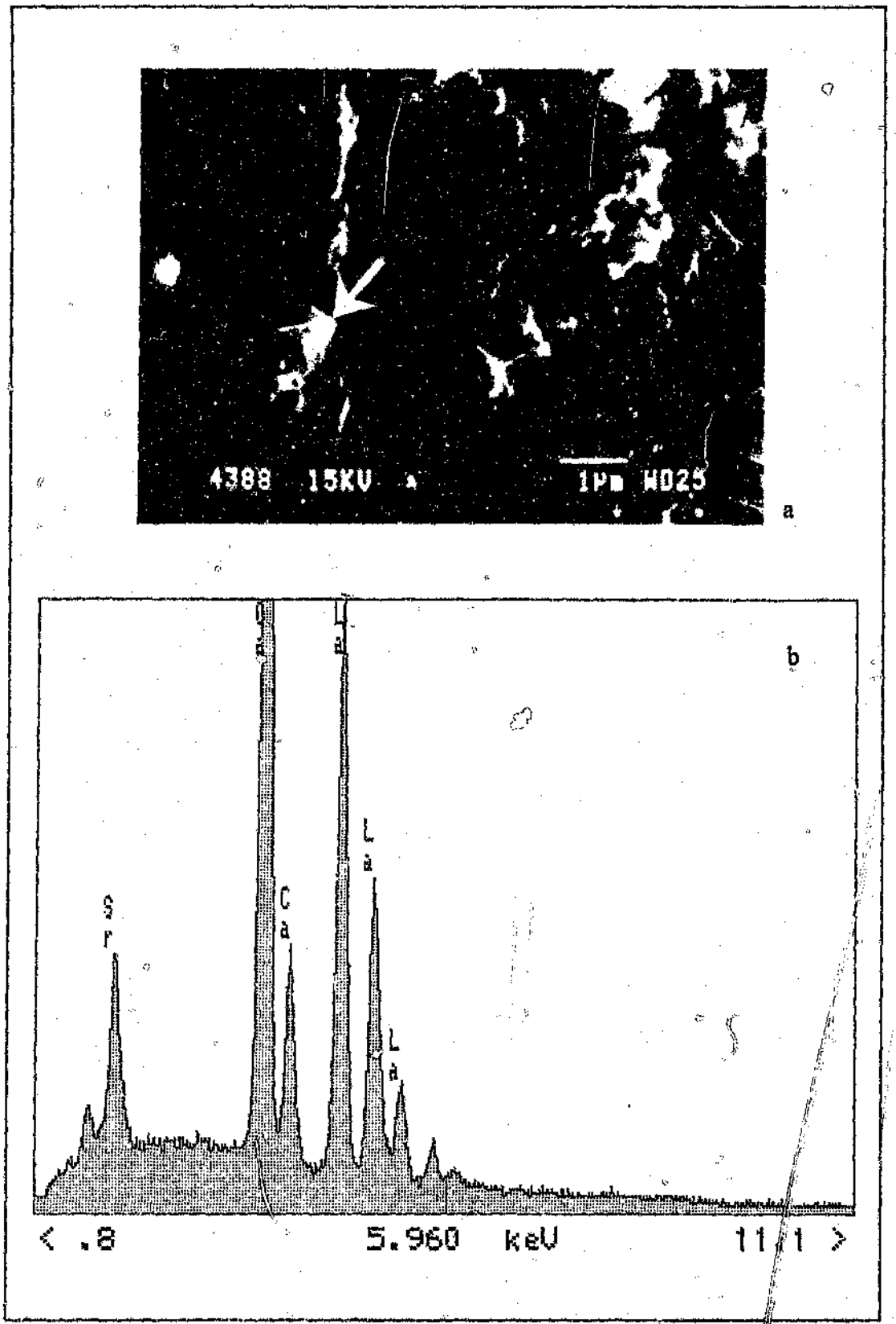


Figure 3.12. 28% La_2O_3/7% SrO/CaO after catalytic reaction: 72 hours at 850-950°C. (a) SEM micrograph. (b) EDX spectra of the bright area on the catalyst surface.

square of the beam size. At the same time, the specimen material included within the beam increased as the square of the beam diameter. This means that the EDX intensity should be a constant if the element is uniformly distributed. Studies of the 1% Au/ 5% La_2O_3/CaO sample concluded that gold was not significantly associated with calcium or lanthanum and was irregularly dispersed as single large Au crystals. The surface composition of such a crystal was estimated by EDX using the defocussed X-ray beam techniques as 2 at.% La, 11 at.% Au, 27 at.% Ca and 60 at.% O. The proportions of O/La and O/Ca revealed the presence of $Ca(OH)_2$ and $La(OH)_3$.

Electron microscopic examination of the 28% La_2O_3/ 7% SrO/CaO sample showed the coral-like structure which should be related both to the support and the supported carbonates (Figure 3.11 (a) and 3.12 (a)). Irregular heaps of aggregated phase (1-2 μm), in which carbon and considerable amounts of lanthanum and strontium were detected by EDX (Figure 3.11 (b) and 3.12 (b)), were observed on the sample surface after extended catalytic use (about 72 hours at 650-950°C). EDX spectrum obtained from the darker area (Figure 3.11 (b)) showed that mostly oxygen, carbon and calcium with small quantities of strontium and lanthanum were present (4 at.% La, 2 wt.% Sr, 14 at.% Ca, 61 at.% O and 19 at.% C). Whereas, oxygen, carbon and lanthanum were detected in large quantities on the surface of the brighter area (12 at.% La, 2 wt.% Sr, 8 at.% Ca, 60 at.% O and 18 at.% C) as shown in Figure 3.12 (b). As can be seen Sr is distributed quite uniformly on the catalyst surface. Quantitative EDX analysis showed that both the dark and bright particles consist of $La_2O_2CO_3$, $CaCO_3$ and $SrCO_3$ phases and there is no formation of compounds between lanthanum and strontium.

In conclusion, the structure sensitivity of the methane oxidative coupling observed on 5% La_2O_3/CaO, 1% Au/ 5% La_2O_3/CaO and 28% La_2O_3/ 7% SrO/CaO catalysts strongly suggests that CO_2 is at least, produced on the surface, providing evidence of the heterogeneous catalytic character of the reaction and points out the very important role of carbonate formation on the methane deep oxidation on the catalyst surface. The rate of CO_2 formation seems to be determined by the decomposition rate of the carbonate species and is likely to affect the final C_2 product selectivity.

The characterization data obtained by means of XRD, SEM and EDX shows that, under the conditions existing during the methane oxidative coupling reaction, strong chemical and structural modifications of the starting catalytic phase occured. The

reaction performed on the 28% La_2O_3/ 7% SrO/CaO catalyst leads to the *in situ* formation of a dioxymonocarbonate ($La_2O_2CO_3$) phase.

The inhomogeneity of gold distribution on the catalyst surface was observed for 1% Au/ 5% La_2O_3/CaO after the catalytic testing. Increasing the La_2O_3 concentration from 5% to 28% and introducing SrO on the surface of a lanthanum-calcium system resulted in marked changes in the structural and morphological properties of the catalyst.

Chapter 4. DISCUSSION

4.1. Partial oxidation of methane to oxy-products

The purpose of the thesis work was to examine the relative importance of homogeneous gas phase and surface-catalysed processes in the synthesis of methanol and formaldehyde from methane in the presence or absence of hydrogen peroxide. Experiments were performed at pressures of 1-50 bar, temperatures of 450-620°C, residence times of 5.8-216 s, and oxygen concentrations in the feed of 4.2, 11.8, 17 and 18 mol %. To investigate a possible promotion effect of hydrogen peroxide on the combined formaldehyde and methanol yield pure water was used in place of H_2O_2 aqueous solution (21 wt.%). Reaction products observed included methanol, formaldehyde, carbon monoxide, water, small amounts of carbon dioxide, and C_2 hydrocarbons (ethane and ethylene).

A specially designed reactor has been used that is suitable for comparative studies of the noncatalytic and the catalytic oxidation.

4.1.1. Partial oxidation of methane to methanol. Figure 4.1 shows the CH_3OH, C_2H_6 and C_2H_4 yields as well as O_2 conversion obtained in the homogeneous partial oxidation of methane at 1 bar pressure as a function of the reaction temperature. The temperature dependency of the product yields was determined by altering the temperature and keeping the other reaction parameters (i.e., pressure and oxygen concentration in the feed) constant. This was done for three different residence times. The results show that as the residence time is increased the temperature at which methanol was first detected is lowered, from 540°C at t = 95 s to 500°C at t = 216 s. At low residence time (Figure 4.1 (a)), the maximum Y_{CH3OH} is shifted toward lower temperatures due to incomplete oxygen conversion and this excess of O_2 leads to methanol oxidation which in turn results in a further decline in methanol yield. At higher residence times (Figure 4.1 (b) and (c)) oxygen is totally converted at the point where the Y_{CH3OH} starts to level off. Therefore, a decrease in methanol yield can be explained only by thermal decomposition of the CH_3OH molecules.

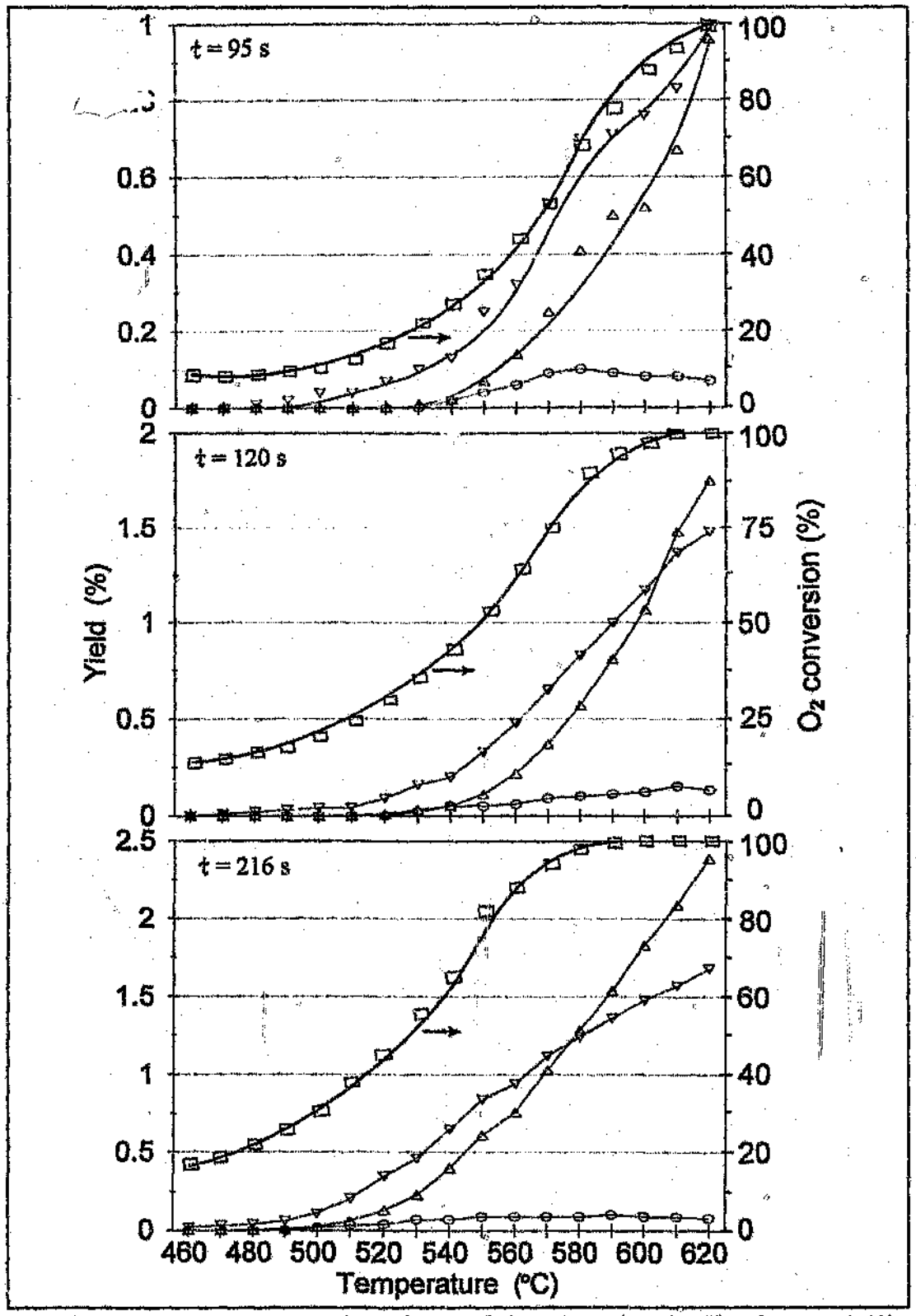


Figure 4.1. Temperature dependency of the (o) methanol, (V) ethane and (Δ) ethylene yields as well as (□) oxygen conversion for three different residence times. Reaction conditions: pressure =1 bar, 82 mol % of CH_4 and 18 mol % of O_2.

The C_2H_6 and C_2H_4 yields increase monotonically with increasing temperature indicating the initiation of the methane oxidative coupling reaction. In fact, when the concentration of CH_3 radicals builds up in the reaction mixture, the chances of two methyl radicals colliding and reacting increases correspondingly[155].

Figure 4.2 shows how the selectivity and the yield of the major products vary with the temperature at 3 bar pressure. The homogeneous oxidation of methane was conducted at residence time of 102 seconds. The behavior of the methanol yield with respect to temperature is similar to that observed at 1 bar pressure, that is it declines slightly with increasing temperature, however it is about one order of magnitude higher at 3 bar pressure. The selectivity to methanol also goes up with increasing temperature, until complete oxygen consumption, and then it starts decreasing slightly at higher temperatures.

It appears that the low selectivity to methanol is due to the fact that a large fraction of methane is converted directly into carbon oxides in the temperature range studied. The methanol yield declines after reaching a maximum; this is due to the increase in methanol selectivity and corresponds to a simultaneous increase in selectivity to carbon monoxide. The selectivity to carbon dioxide , however, is almost unaffected by an increase in the temperature. These results allow us to propose that methanol can either be oxidised to carbon monoxide at high reaction temperatures:

$$CH_3OH + O_2 \rightarrow CO + 2H_2O$$

or thermally decomposed to carbon monoxide and hydrogen:

$$CH_3OH \rightarrow CO + 2H_2$$

It should be noted that these two routes do not contribute at all to the production of carbon dioxide which is formed by a parallel pathway directly from methane in agreement with the experimental data (Figure 4.2 (a)).

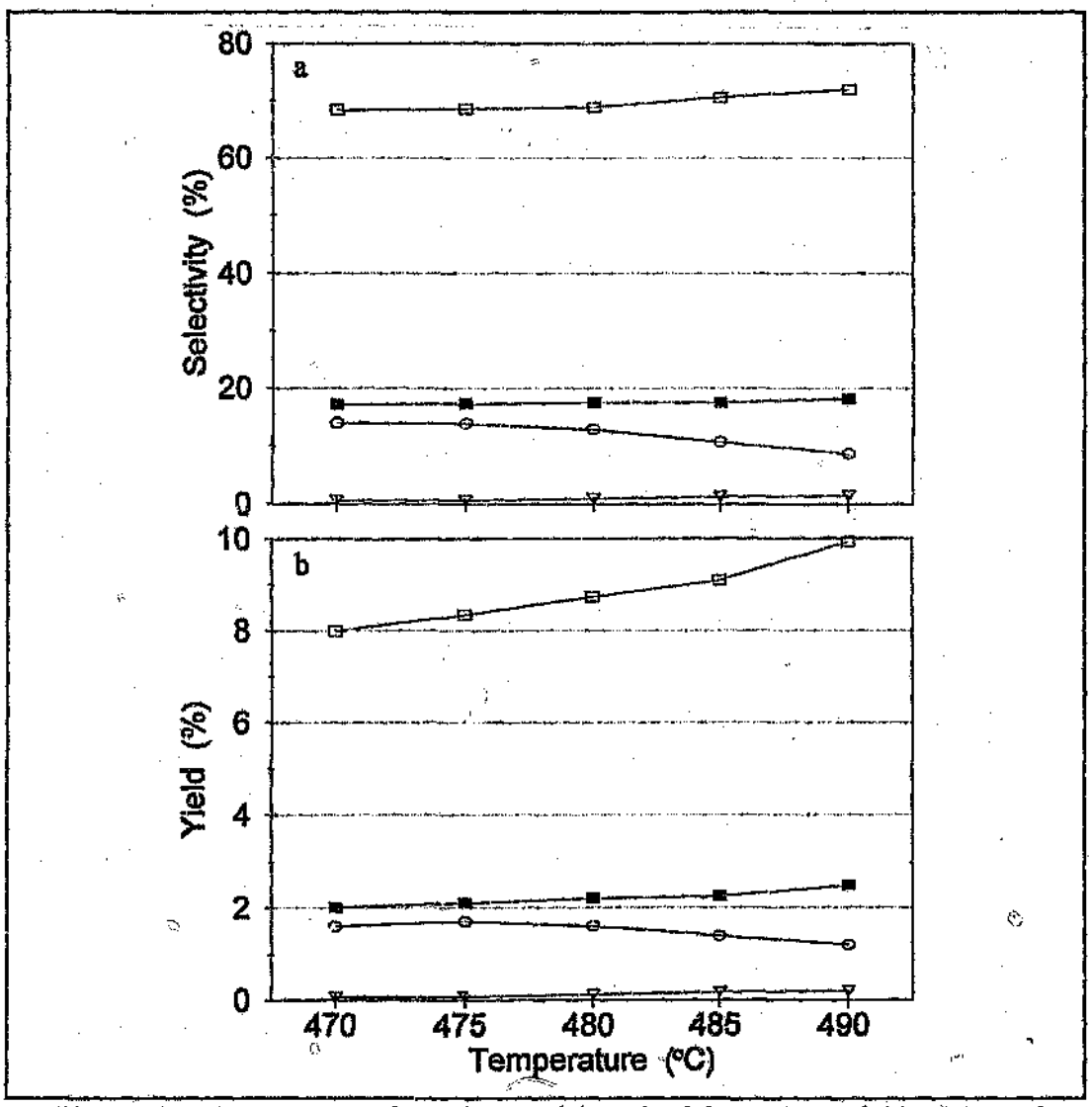


Figure 4.2. Temperature dependency of (a) selectivity and (b) yield of the major products: (o) methanol, (V) C_1 hydrocarbons, (□) carbon monoxide and (■) carbon dioxide. Reaction conditions: pressure = 3 bar, 80 mol % of CH_4, 17 mol % of O_2 and 3 mol % of N_2, residence time = 102 s.

The temperature dependency of the selectivities to the major reaction products obtained in the homogeneous partial oxidation of methane at 50 bar pressure are shown in Figure 4.3 and the yields in Figure 4.4 for three different residence times.

The effect of temperature on the product distribution at 50 bar pressure seems quite different to that observed at 3 bar pressure. The initial selectivity to methanol is comparatively high (57% at low residence time) and it falls monotonically and fairly linearly with increasing temperature or residence time. The selectivity to carbon mono-

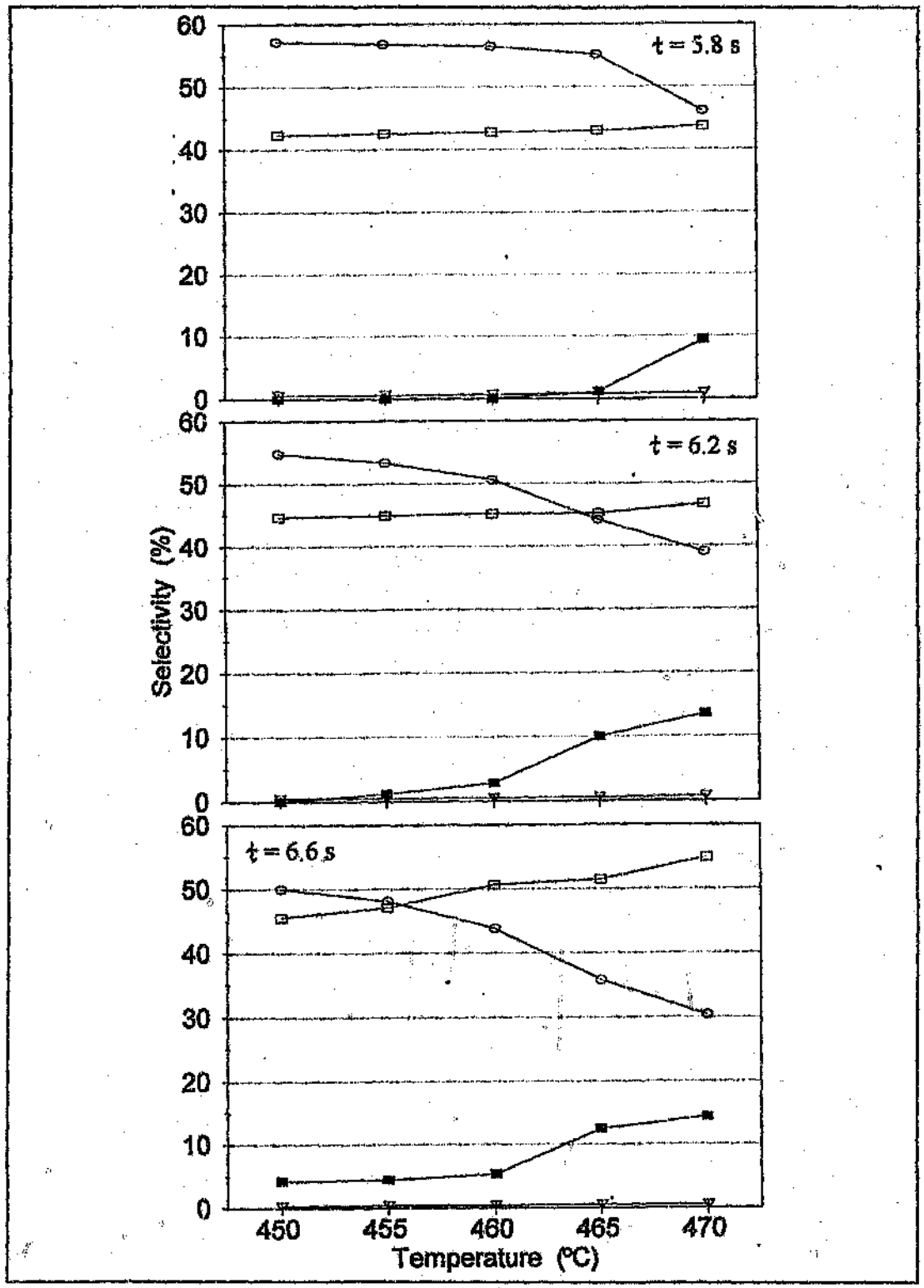


Figure 4.3. Temperature dependency of selectivity to the major reaction products: (o) methanol, (V) C_2 hydrocarbons, (□) carbon monoxide and (■) carbon dioxide, shown for three different residence times. Reaction conditions: pressure = 50 bar, 95.8 mol % CH_4 and 4.2 mol % O_2.

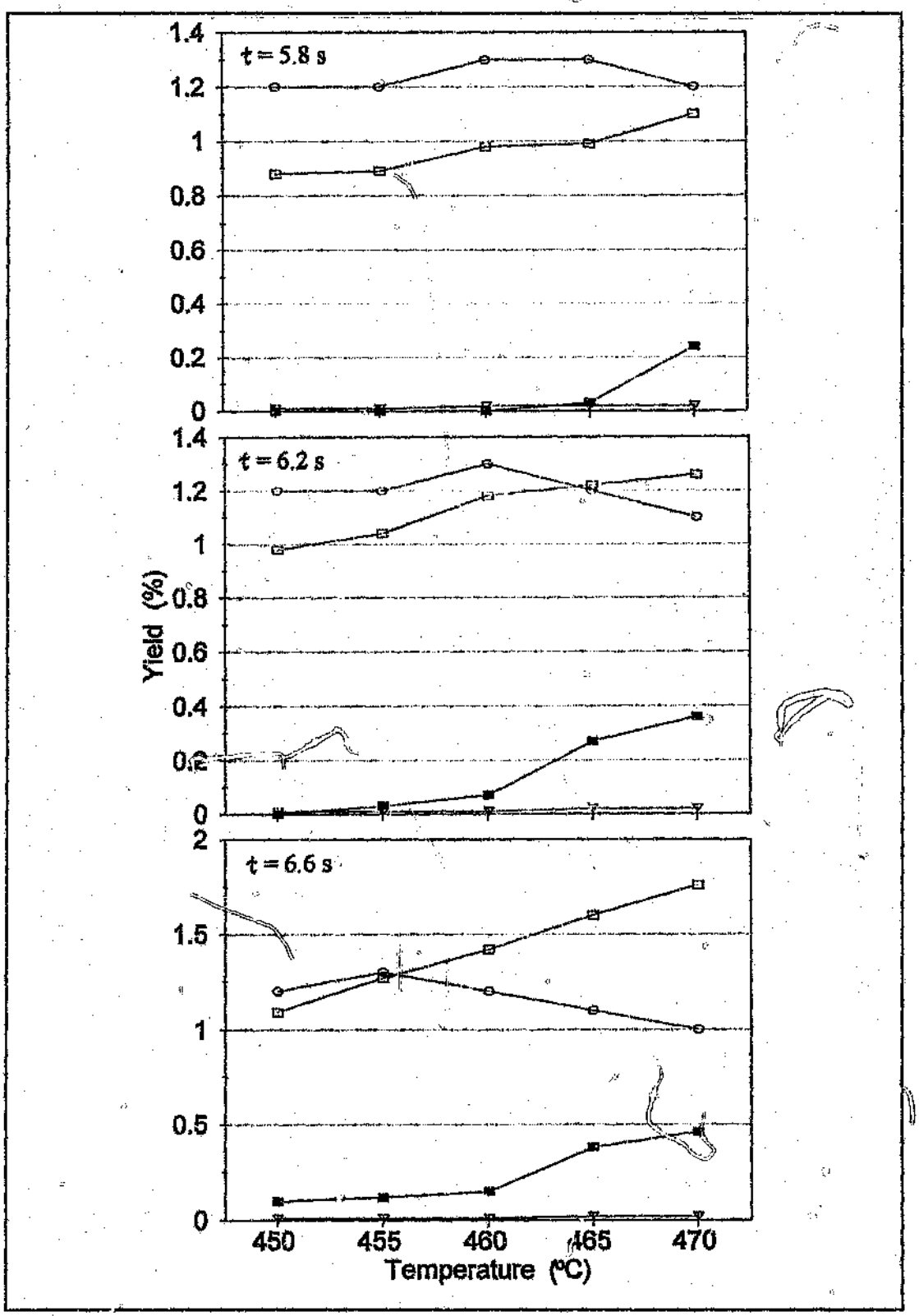


Figure 4.4. Temperature dependency of the (o) methanol, (▽) C_2 hydrocarbons, (□) carbon monoxide and (■) carbon dioxide yields shown for three different residence times. Reaction conditions: pressure = 50 bar, 95.8 mol % CH_4 and 4.2 mol % O_2.

xide, however, is almost unaffected by increasing temperature. This is also true for the C_2 hydrocarbons, the selectivity of which stays at approximately the same level (< 1%) for all the reaction conditions that were used in the experiment. In contrast, the selectivity to carbon dioxide increases substantially as a function of temperature (Figure 4.3). Therefore, we can infer that the increase in selectivity to products of deep oxidation at 50 bar occurs because of the increase in selectivity to carbon dioxide rather than to carbon monoxide as observed at lower pressures (3 bar). This is especially true at high residence times. The balanced equation for the proposed reaction is shown below:

$$CH_3OH + 3/2O_2 \rightarrow CO_2 + 2H_2O$$

The reaction temperature for the homogeneous partial oxidation of methane to methanol can be significantly lowered by increasing the residence time or by using a catalyst. The results of the non-catalytic oxidation presented above can be used as a reference for comparison with the catalytic partial oxidation of methane over various catalysts. The results of the catalytic tests of the 0.1 mmol Sn/g SiO_2, 0.6% Pt/CaO and 30% H_3BO_3/Al_2O_3 samples are shown in Figure 4.5. The methanol yield was improved considerably by using a 30% H_3BO_3/Al_2O_3 catalyst at 1 bar pressure. The presence of 0.1 mmol Sn/g SiO_2 and 30% H_3BO_3/Al_2O_3 in the reactor also had the catalytic effect of lowering the temperature at which methanol was first detected by about 50°C. This is in contradiction with what has been reported by many researchers. It was claimed in recent publications that the reaction tempertures for heterogeneous reactions were not less than those required for homogeneous reactions and the presence of a catalyst significantly reduced the methanol yield[108,111,112,136,157].

Burch et al.[106] reported that Cu catalysed the complete oxidation of methane and/or methanol. Numerous other metallic and non-metallic catalysts were tested, but in all cases the selectivity to methanol was much lower than that obtained from the purely homogeneous reaction. Chun and Anthony[112] have also published results which came to the same depressing conclusion. They obtained better methanol yields for the homogeneous gas phase reaction than for the reactions carried out in the presence of numerous catalysts in a temperature range of 370-480°C. Pyrex beads as well as

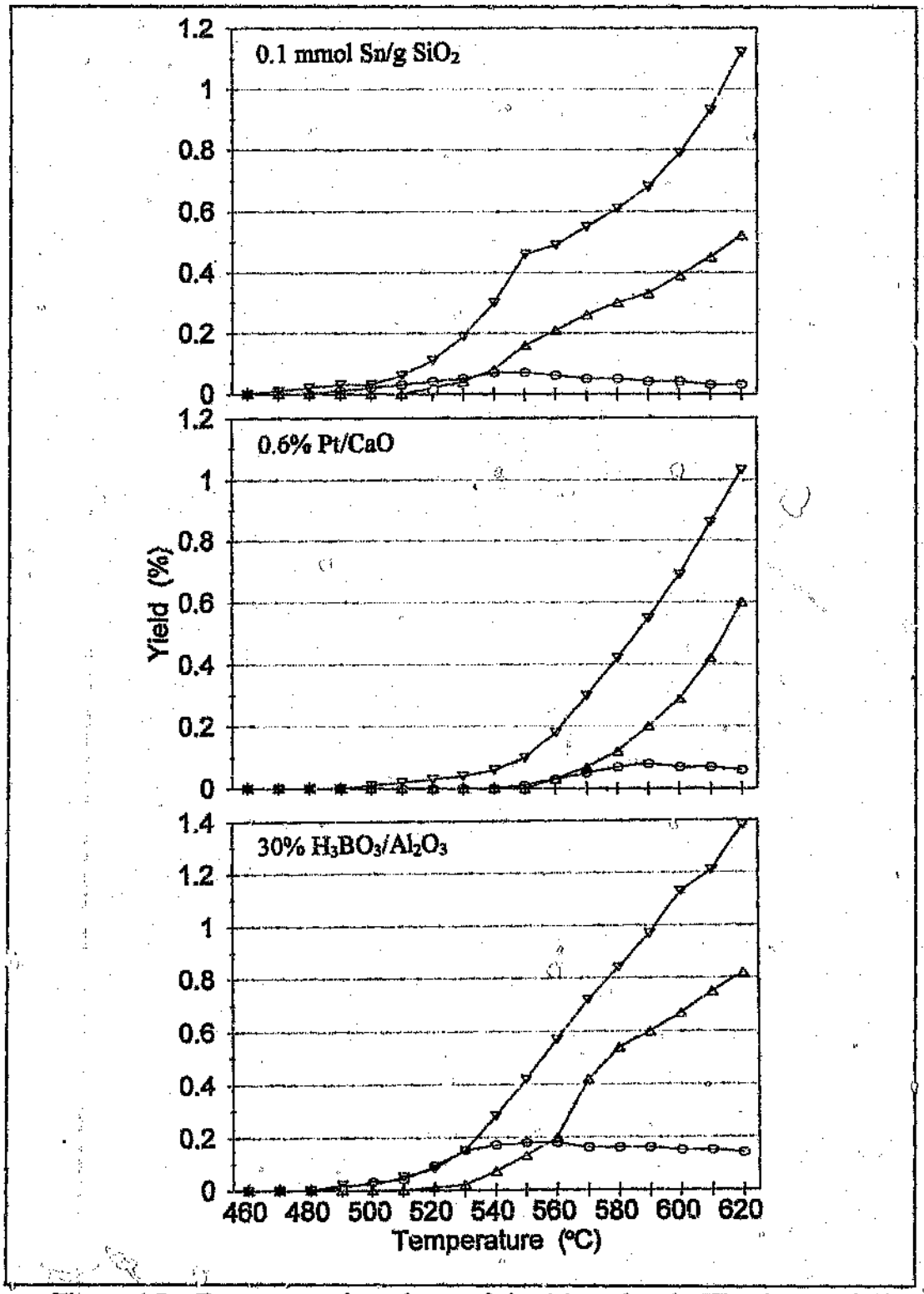


Figure 4.5. Temperature dependency of the (o) methanol, (∇) ethane and (Δ) ethylene yields in the catalytic partial oxidation of methane. Reaction conditions: pressure = 1 bar, 82 mol % CH_4 and 18 mol % O_2, residence time = 95 s.

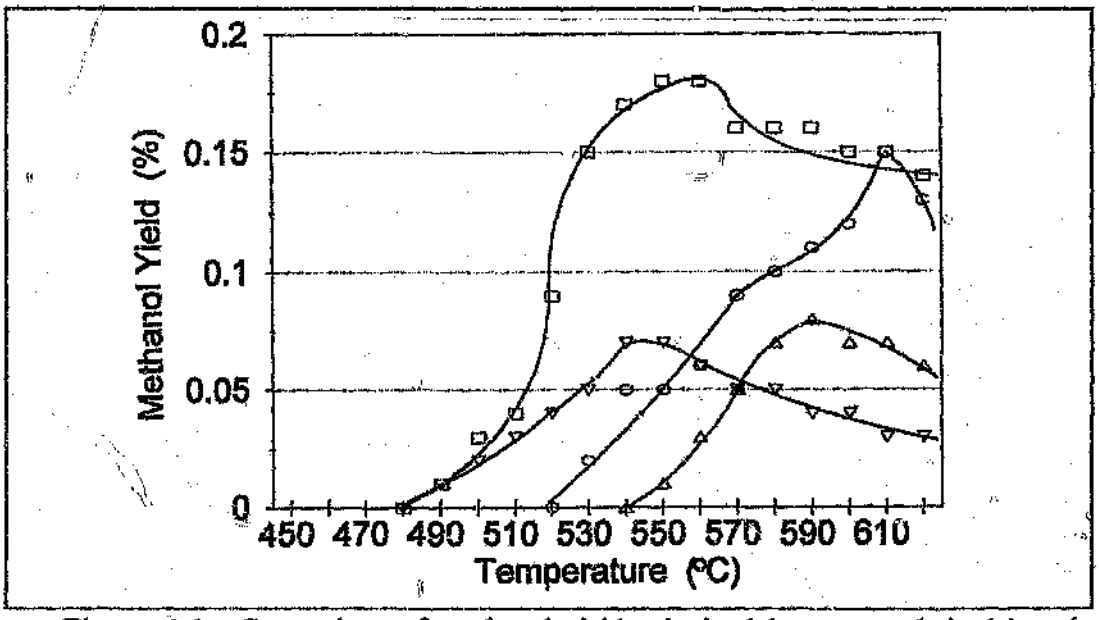


Figure 4.6. Comparison of methanol yields obtained by non-catalytic (o) and catalytic partial oxidation of methane over (□) 30% H_3BO_3/Al_2O_3, (Δ) 0.6% Pt/CaO, (▽) 0.1 mmol Sn/g SiO_2 at 1 bar pressure.

Fe/Mo/S, Fe/Mo/Ti, V/Ti, Cu/Mo, Ti supported on silica gel, Ag/α-Al_2O_3 inhibited the radical reactions. It was, therefore, suggested that homogeneous oxidation in the void volume of the catalyst bed occurred to a significant extent relative to the heterogeneous reactions, and that the catalyst surface inhibited the free-radical homogeneous reactions.

The experimental data, in agreement with recent publications, illustrate the lack of catalytic activity of the 0.6% Pt/CaO sample toward methanol production due to the rapid over-oxidation of methanol, and possibly methane. In contrast, the rather more encouraging results are based on the activating effect of the 0.1 mmol Sn/g SiO_2 and 30% H_3BO_3/Al_2O_3 catalyst. It should be noted that 30% H_3BO_3/Al_2O_3 has never been used before as a methane partial oxidation catalyst.

It is of particular interest to compare the experimental data obtained during the non-catalytic and catalytic partial oxidation of methane at 1 bar pressure. The comparison of the temperature dependency of methanol yield for homogeneous and heterogeneous reactions is presented in Figure 4.6.

The adsorption of methanol on alumina and alumina-supported boric acid has been characterised using FT-IR spectroscopy. A comparison of the spectra resulting from

the introduction of methyl alcohol on the sample surface with the spectra of the untreated sample both before and after heating the sample in the presence of water vapour to 400°C suggests that the catalytic partial oxidation of methane occurs through the formation of methoxy groups on the catalyst surface. The bands corresponded to the CH stretching vibrations for 30% H_3BO_3/Al_2O_3 were found to be very stable during the thermal treatment.

4.1.2. Partial oxidation of methane to formaldehyde over a series of silica supported catalysts. The reaction was studied at atmospheric pressure over a series of silica supported catalysts with 3d, 4d, 4f, 5p and 6p - metal oxides in the presence of hydrogen peroxide. From a comparison of the results obtained for the 0.1 mmol Cr/g SiO_2 and the 0.1 mmol Sn/g SiO_2 catalysts, shown in Table 3.1 and 3.3, under a variety of reaction conditions it emerges that the selectivity to formaldehyde depends solely on methane conversion, which is independent of the temperature - contact time combination that was used to achieve that conversion. Evidently, the methane conversion always depends on the reaction conditions: increasing the reaction temperature or contact time leads to an increase in methane conversion, which in turn leads to a change in product selectivity. As can be seen in Table 3.1 increasing the temperature from 500 to 550°C results in a drastic increase in selectivity to C_2 hydrocarbons and CO_X at the expense of formaldehyde. At 600°C and a comparatively high contact time (0.5 s) the methane conversion reached a maximum of 4.9%. Simultaneously formaldehyde disappeared from the detectable products and most of the methane was converted directly to carbon oxides. In addition, a higher oxygen concentration in the feed lowered the selectivity to formaldehyde, but increased the methane conversion. The product distributions are thus largely affected such that increasing levels of methane conversion correspond to decreasing selectivity to HCHO and a concurrent increase in the selectivity to CO, while that to CO_2 is unchanged. It is surprising that the selectivity to CO_2 remains almost constant, while a compensatory relationship in selectivity is observed between HCHO and CO. This indicates that HCHO is a primary product that decompses to CO. CO_2 may not only be produced directly from CH_4 but could also be produced by the oxidation of CO or by the water -

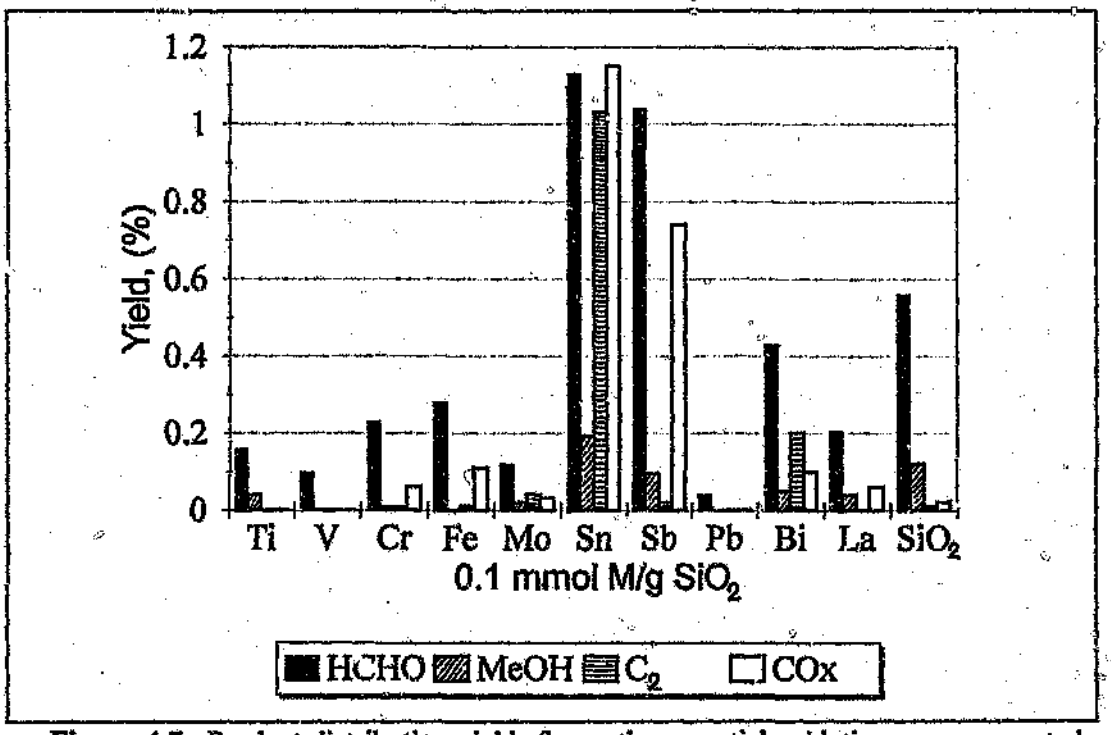


Figure 4.7. Product distribution yields for methane partial oxidation over supported silica catalysts. Conditions: T_{cat} = 500°C, T_{post} = 250°C, $CH_4 : O_2$ = 4:1, τ = 0.12 s.

gas shift reaction. The close link between CO and HCHO suggests that the latter is the main source of CO.

The addition of water vapour instead of hydrogen peroxide to the reaction mixture causes a drastic decrease in the methane conversion and in the formation of carbon oxides. The selectivity to formaldehyde, however, is improved during H_2O addition, and this indicates that the retardation of the formaldehyde formation by water was less than the formation of carbon oxides. It appears that water vapour can affect the CO_x selectivity which is hardly influenced by the reaction temperature.

The major product distribution yields obtained in the title reaction in the presence of hydrogen peroxide at 500°C over various metals supported on silica, compared to bare silica, can be seen in Figure 4.7. Obviously silica itself has some catalytic activity for the formation of oxy-products under the reaction conditions investigated, in agreement with what has been reported in the literature[113,115,158,159,160]. The effect of adding tin or antimony was to increase the selectivity of formaldehyde as well as that of carbon oxides. The presence of titanium, vanadium, chromium, iron, molybdenum, lead, bismith and lanthanum metal oxides appears to suppress the activity of bare silica, as

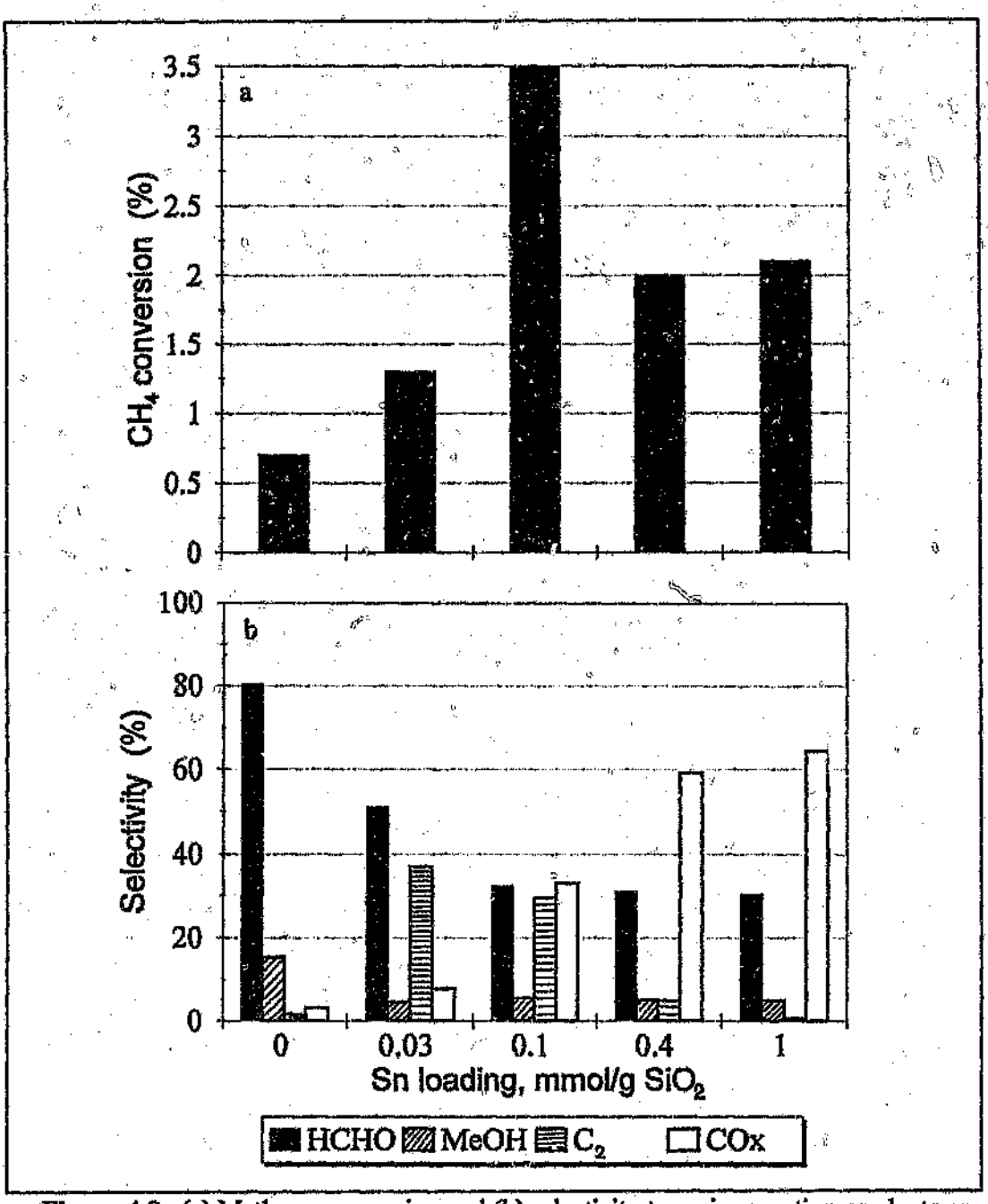


Figure 4.8. (a) Methane conversion and (b) selectivity to major reaction products as a function of tin loading. Reaction conditions: T_{cat} = 500°C, T_{post} = 250°C, W = 0.25g

well as reduce methane conversion and, therefore, formaldehyde yield, under a given set of experimental conditions. The relative activity of these promoters is as follows: Sn > Sb > Bi > Fe > Cr > La > Ti > Mo > V > Pb. The positive effect of doping silica with Sn and Sb can be explained by the possible activation of hydrogen peroxide, on

these elements, and the formation of active radicals, presumably hydroxy radicals. These two, being 5p elements, are not as active for donating and/or accepting electrons as the transition elements. The latter can easily change their valencies and catalyse the decomposition of hydrogen peroxide to water and oxygen and this could explain the inhibition of the M/SiO_2 system relative to the catalytic properties of silica alone. A similar explanation can be proposed for 4f and 6p elements.

Figure 4.8 shows the distribution of the major products obtained at 500°C over silica catalysts impregnated with different amounts of tin. A significant enhancement of the original activity of the SiO_2 is observed for Sn loading in the range of 0.03 - 0.1 mmol/ g of SiO_2, while a further increase in Sn loading results in a drop in methane conversion. It is noted in Figure 4.8 (b) that the selectivity to formaldehyde decreased inversely with increasing tin loading and with a concurrent increase in the selectivity to carbon oxides. At 0.1 mmol loading the selectivity to formaldehyde droped from 80% for unpromoted SiO_2 to only 32% for the Sn/SiO_2 system. Simultaneously, the methane conversion increased to such an extent that the formaldehyde yield increased to 1.13%. It is reasonable to assume that at loadings of 0.03-0.1 mmol, all the sites where Sn can bond strongly to the SiO_2 have been saturated so that tin is highly dispersed on the catalyst surface. Higher loadings lead to the formation of tin dioxide clusters (SnO_2) on the silica surface, which may block active sites, lowering the overall activity and selectivity of the catalyst.

Another interesting finding of the present work is that the addition of tin to the pure silica enhanced the selectivity to C_2 hydrocarbons at the expense of formaldehyde. However, formaldehyde and C_2 hydrocarbons exhibited parallel behavior with respect to the increasing tin loading on the silica support. Both the HCHO and C_2 hydrocarbon selectivities droped with increasing tin loading in the range 0.03 to 1 mmol/g of SiO_2 (Table 3.3). This suggests that the formaldehyde does not originate from methyl radicals, but rather from methoxy complexes formed when methane chemisorbs directly onto the catalyst surface at high reaction temperatures.

In summary. The investigation of methane partial oxidation to oxy-products is suggested to follow a range of pathways for the formation of methanol and formaldehyde in the presence and absence of hydrogen peroxide. The approach used is

based on the generally accepted heterogeneous-homgeneous mechanism[91,161]. Even if the oxygenates (HCHO and CH_3OH) are assumed to be formed on the catalyst surface, this essentially entails the generation of radicals on the surface and the formation of the products in the gas phase.

It is widely accepted that the initial intermediate is a methyl radical (CH_3) which, in the presence of oxygen, will form a methyl peroxy radical (CH_3O_2). The equilibrium:

$$CH_3 + O_2 \leftrightarrow CH_3O_2 \qquad (1\,j)$$

plays a key role in the way products vary with temperature. As is well known, at temperatures below 650°C, this equilibrium favours the formation of methyl peroxy radicals. Decomposition of methyl peroxy radicals or the reaction of these radicals with methyl radicals produces methoxy radicals (CH_3O) which, in turn, react with methane to give methanol:

$$CH_3O_2 \rightarrow CH_3O + O \qquad (2\,j)$$

$$CH_3O_2 + CH_3 \rightarrow 2CH_3O \qquad (3\,j)$$

$$CH_3O + CH_4 \rightarrow CH_3OH + CH_3 \qquad (4\,j)$$

Reaction (4 j) takes place when an excess of methane is present in the reaction mixture. The formation of formaldehyde occurs when a methoxy radical reacts with oxygen:

$$CH_3O + O_2 \rightarrow CH_2O + HO_2 \qquad (5\,j)$$

or by the decomposition of a methyl peroxy radical:

$$CH_3O_2 \rightarrow CH_2O + HO \qquad (6\,j)$$

Although the last reaction has a relatively high activation energy since it is a unimolecular reaction, this self-decomposition of CH_3O_2 may result in the formation of HCHO when the concentration of the radical species is low. This assumption explains the fact that in the methane partial oxidation to methanol at low temperatures some

formaldehyde is always present in the reactor effluent. The results presented in this thesis can also be explained by the above scheme, since it is expected that high pressures and concentrations of methane will make reactions (3 j) and (4 j) more favourable so that methanol is produced, while having little effect on reaction (5 j). By contrast, low pressures and high concentrations of oxygen can explain the prevailing formation of formaldehyde.

The results allow one to propose that the formation of methyl radicals increases dramatically in the presence of hydrogen peroxide. The hydrogen peroxide dissociates to form surface or gas phase active species (presumably, peroxide or superoxide surface species or hydroperoxy and hydroxyl radicals). These species can attack molecules of methane and produce some intermediates (like methyl radicals in the gas phase or methoxy groups on the catalyst surface), which in turn can be transformed into the final oxy-products. According to this reaction pathway one can predict that at low pressure and high oxygen concentration, the major product of the partial oxidation of methane will be formaldehyde, in agreement with the experimental data.

Hydroxyl radicals formed during the dissociation of hydrogen peroxide on the catalyst surface can interact with methane either in the gas phase or with CH_4 molecules adsorbed on the catalyst surface. According to the mechanism for the partial oxidation of methane, by gas phase oxygen or surface active O_2 species, proposed by Parmaliana et al.[115], adsorbed methane can participate in the reaction on silica-supported oxide catalysts at temperatures between 550 and 650°C. The adsorption of methane molecules occurs on the acidic sites of the oxide surface[162,163]. Considering that our experiments were performed at much lower temperatures it can be taken for granted that methane adsorbs on the catalyst surface.

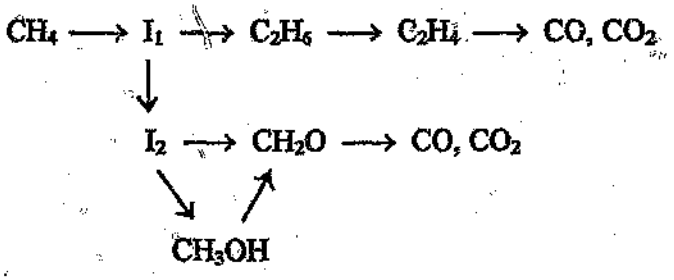
Therefore methane participates in the formation of CH_3 radicals which originate either from the gas phase or from the catalyst surface:

$$\begin{matrix} CH_{4(g)} & \xrightarrow{OH} & \\ & & CH_3 \\ CH_{4(S)} & \xrightarrow{OH} & \end{matrix} \qquad (7\,j)$$

where $CH_{4(g)}$ refers to gas phase methane and $CH_{4(S)}$ to the adsorbed form.

Taking into account the high reactivity of OH radicals it can be proposed that these two channels determine the rate of formation of CH_3 radicals. It has also been shown[115] that, the oxidation of methane to formaldehyde is governed by the formation of active oxygen species on the catalyst surface, which interact with methane. In our case active oxygen species can be produced from hydrogen peroxide, which already contains active partially reduced oxygen. Hence, active species can be formed more readily than from molecular oxygen and the reaction proceeds under "milder" conditions in comparison with oxidation by molecular oxygen.

The results obtained enable us to propose the following general scheme for the partial oxidation of methane to oxy-products:



where I_1 and I_2 represent the intermediate complexes. CH_3 and CH_3O, respectively.

A methyl radical can likely couple with another methyl radical to produce ethane which can be dehydrogenated to ethylene. This scheme suggests that the methyl radicals are not readsorbed on the catalyst surface but oxygenates and C_2 hydrocarbons are parallel products when methane is activated on the catalyst surface at elevated temperatures, consistent with the observations presented in this thesis.

4.1.3. Methane oxidative coupling in the presence and absence of hydrogen peroxide. To better understand the overall effect of hydrogen peroxide addition, we have represented our results in terms of product yield (or selectivities to C_{2+} hydrocarbons and carbon oxides) versus reaction temperature for the 5% La_2O_3/CaO, 1% Au/ 5% La_2O_3/CaO and 28% La_2O_3/ 7% SrO/CaO catalysts in Figures 4.9, 4.11 and 4.12. Since this effect is sufficiently remarkable over the temperature range studied, the plot of the major product selectivities against methane conversion provides

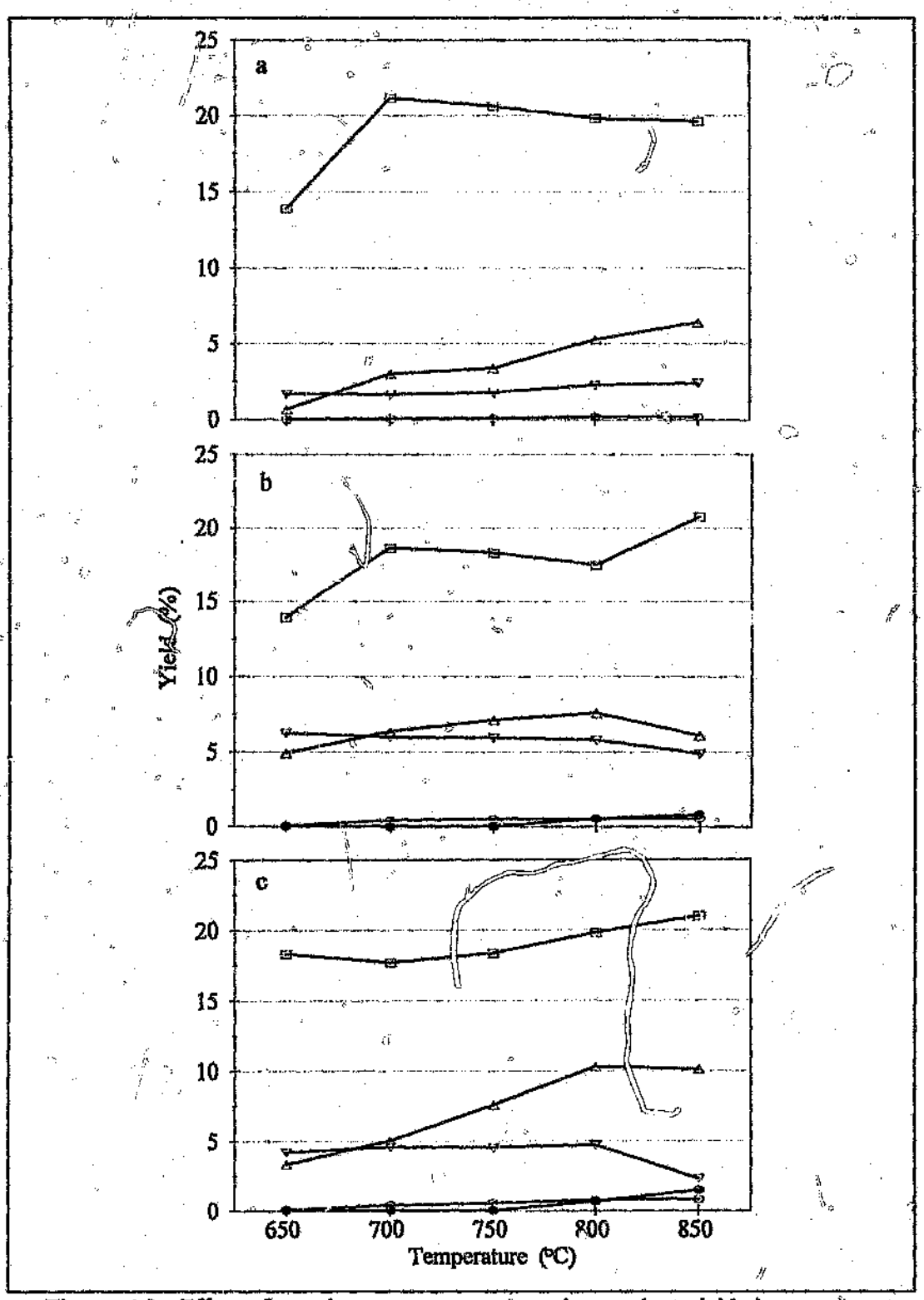


Figure 4.9. Effect of reaction temperature on major product yields in experiments (a) without any liquid addition to the feed, (b) in the presence of pure H_2O and (c) in the presence of H_2O_2 (21 wt.%) over the 5% La_2O_3/CaO catalyst. (▽) C_2H_6, (△) C_2H_4, (○) C_{3+}, (●) C_6H_6, (□) CO_X.

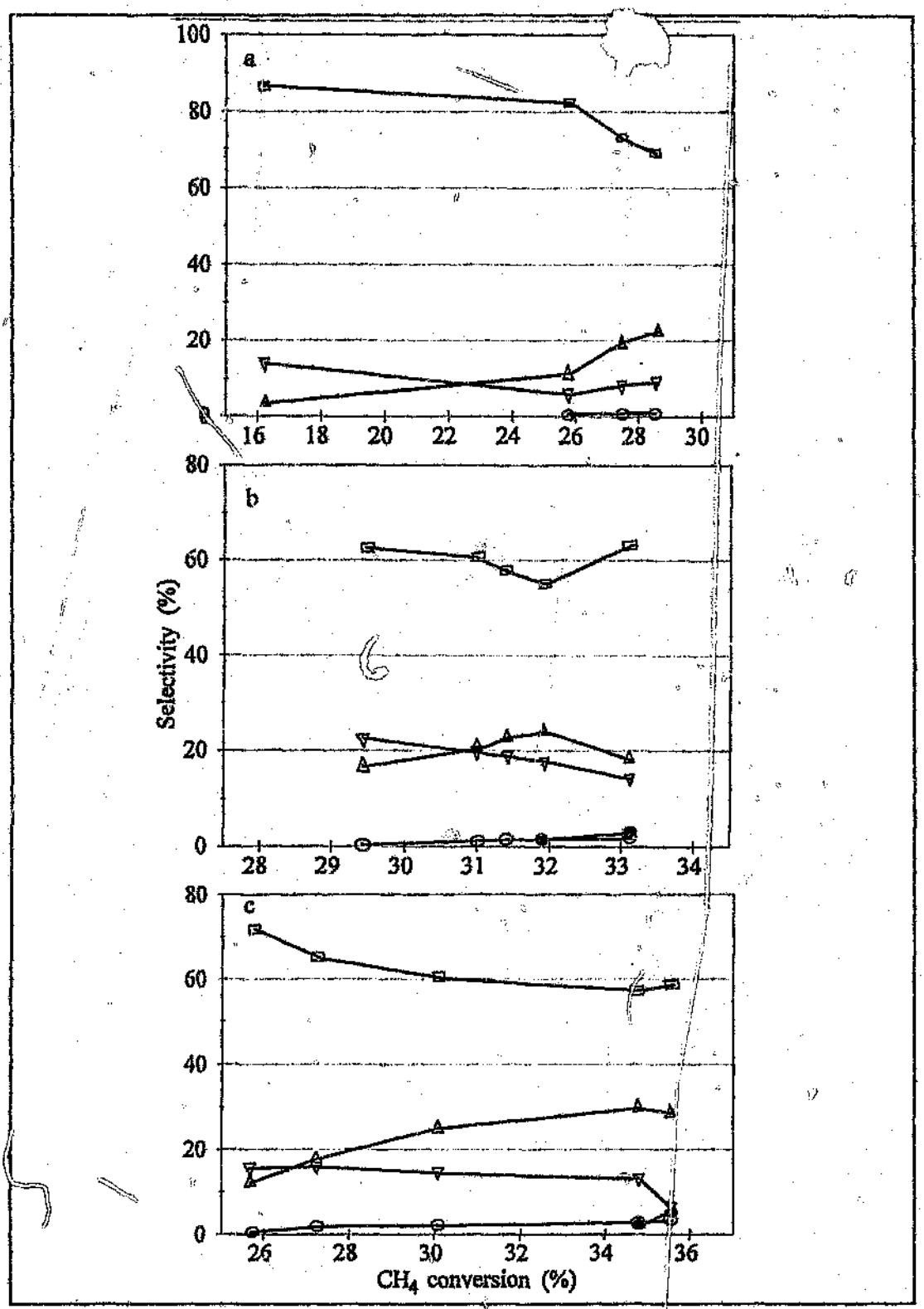


Figure 4.10. Selectivity to (▽) C_2H_6, (△) C_2H_4, (○) C_{3+}, (■) C_6H_6, (□) CO_X as a function of CH_4 conversion in experiments (a) without any liquid addition to the feed, (b) in the presence of pure H_2O and (c) in the presence of H_2O_2 (21 wt.%) over the 5% La_2O_3/CaO catalyst.

an useful method of catalyst performance monitoring. The selectivities to ethane, ethylene, C_{3+} hydrocarbons, benzene and carbon oxides are displayed as a function of methane conversion in Figures 4.10 and 4.13.

As can be seen from a comparison of Figure 4.9 (a) and (b) the addition of water vapour to the reaction mixture enhances the formation of C_2 hydrocarbons but also results in a decrease in carbon oxides formation. The addition of hydrogen peroxide (Figure 4.9 (c)) further increases the ethylene yield to about 10%, and has almost no effect on that of ethane production such that the ethylene-to-ethane ratio increases markedly. In addition the C_{3+} hydrocarbon yield is enhanced slightly. It should be noted that the addition of water vapour (Figure 4.10 (b)) shifts the selectivity-conversion curves to a higher range of methane conversions compared to experiments done without the addition of any liquid. Similarly, in the case of hydrogen peroxide, the maximum methane conversion obtained is 35% instead of 33% for experiments with pure water. An interesting feature of the data presented in Figure 4.10 is the way in which the shapes of the curves for the selectivity to CO_X are mirrored by those for C_2H_4 in all three cases. This leads us to conclude that carbon oxides appear as a result of the deep oxidation of ethylene.

The influence of hydrogen peroxide and its concentration in the reaction mixture on C_{2+} hydrocarbon yield, C_{2+} hydrocarbon and CO_X selectivities in the temperature range 600-800°C over 1% Au/ 5% La_2O_3/CaO is shown in Figure 4.11. We observe that the maximum yield of C_{2+} hydrocarbons is increased from 12% to 17% with the addition of pure water due to a rise in total selectivity to these products as well as an increase in methane conversion. The addition of hydrogen peroxide solution to the reaction mixture further increases the C_{2+} hydrocarbon selectivity and methane conversion. Interestingly, the higher the concentration of added hydrogen peroxide, the higher the yield of C_{2+} products obtained (Figure 4.11 (a) and (b)). The peculiarity of the performed reaction is the formation of a noticeable quantity of benzene. The maximum yield of C_{2+} products (27%) can be seen to occur at 800°C in the presence of 21 wt. % hydrogen peroxide; this is one of the best results obtained to date for the title reaction. It can be also seen from Figure 4.11 (c) that low reaction temperatures clearly favoured the formation of carbon oxides over the C_{2+} hydrocarbons, and vice versa at high temperatures.

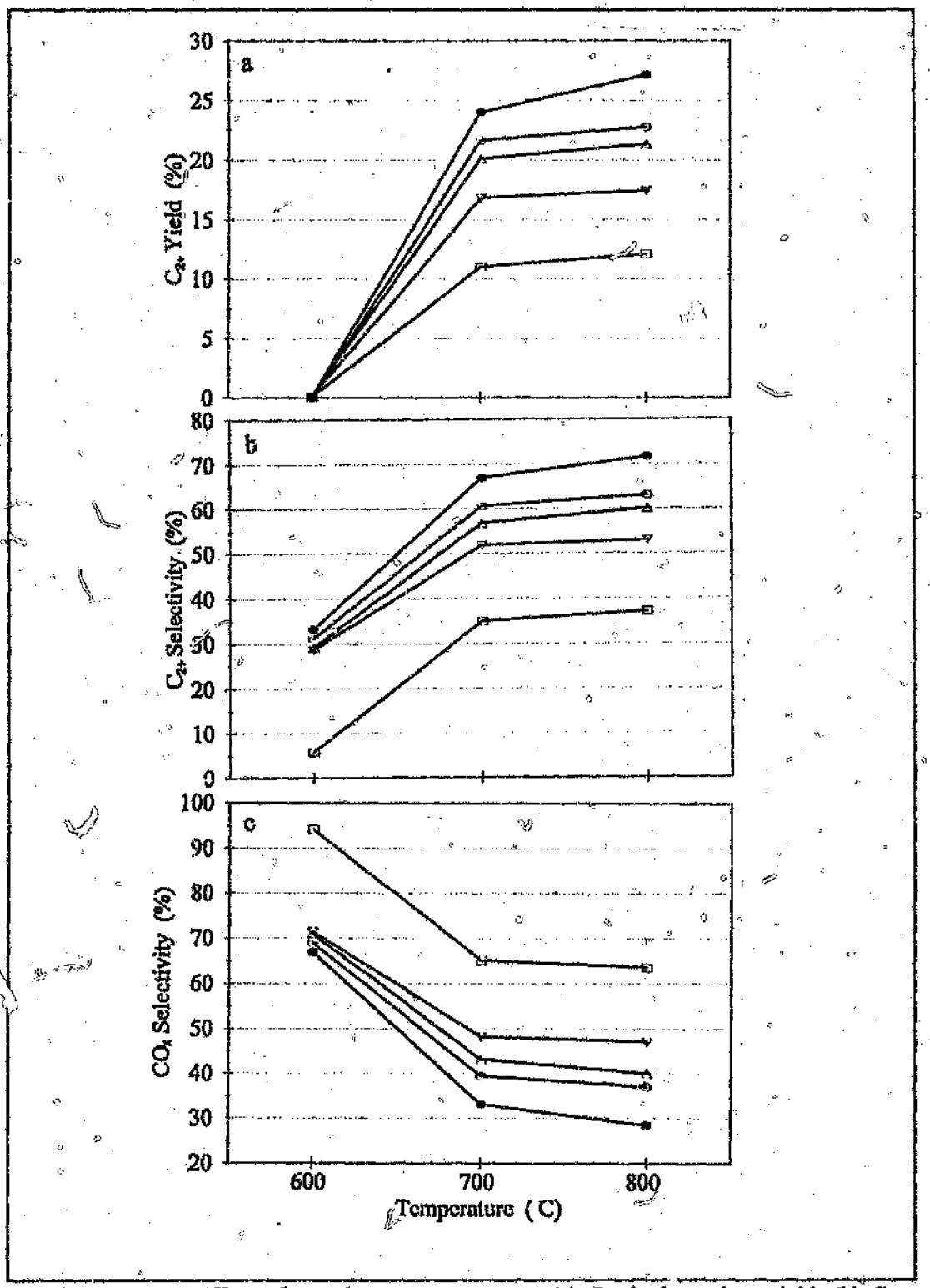


Figure 4.11. Effect of reaction temperature on (a) C_{2+} hydrocarbon yield, (b) C_{2+} selectivity and (c) CO_X selectivity over 1% Au/ 5% La_2O_3/CaO in the presence of (▽) pure water, (△) H_2O_2 - 2.6 wt.%, (○) H_2O_2 - 7.6 wt.%, (●) H_2O_2 - 21 wt.% and (□) without the addition of any liquid.

Figure 4.12 shows the temperature dependence of the major product yields for the 28% La_2O_3/ 7% SrO/CaO catalyst. A comparison of Figure 4.12 (a) and (b) indicates that water vapour significantly improves the ethylene yield at the expense of carbon oxides but has almost no effect on that of ethane, although the combined selctivity to ethane and ethylene is appreciable at 19,6%. When hydrogen peroxide was introduced into the reactants the overall yield of carbon oxides was higher than in the experiment with pure water, while at a temperature of 850°C the yield dropped to a local minimum, allowing us to obtain a very high yield of C_2 products, that is 20,3%.

A comparison of the product selectivity - methane conversion "curves" in Figure 4.13 shows that the addition of water vapour and hydrogen peroxide shifts the curves to significantly higher conversion. The selectivities to CO_x and C_2H_4 have inverse trends enabling us to confirm our previous suggestion that carbon oxides originate from ethylene.

A comparison of the results presented in Figures 4.9 - 4.13 shows that the addition of strontium oxide to the lanthanum-calcium system considerably improves the activity and selectivity of the catalyst under similar reaction conditions, as well as increasing the catalyst stability. According to the data obtained by EDX analysis of 28% La_2O_3/ 7% SrO/CaO after the catalytic testing strontium is distributed quite uniformly on the catalyst surface and occurs as the $SrCO_3$ phase. The XRD results also reveal the coexistence of $SrCO_3$, $La_2O_2CO_3$ and $CaCO_3$ phases on the surface of this sample. It is well known that in the presence of CO_2 strongly basic oxides easily form carbonates of high thermal stability. The higher the carbonate decomposition temperature the higher the basicity of the corresponding oxide[19,20,23,36,51]. Evidently, the introduction of strontium significantly increases the basicity of the lanthanum-calcium system, since these carbonates are present at the high reaction temperatures.

The data in Figures 4.9 - 4.13 indicates that 28% La_2O_3/ 7% SrO/CaO requires higher reaction temperatures (850°C and above) for maximum performance than the 5% La_2O_3/CaO or the 1% Au/ 5% La_2O_3/CaO catalysts. This can be understood in the light of the high decomposition temperatures of $SrCO_3$ and $La_2O_2CO_3$ shown in Figures 1.2 and 1.3. Thus the differences in the catalytic performance of 28 % La_2O_3/7% SrO/CaO and 5% La_2O_3/CaO may be attributed to differences in the basicity of these systems. As can be seen in Figures 4.9, 4.10, 4.12 and 4.13, the maximum

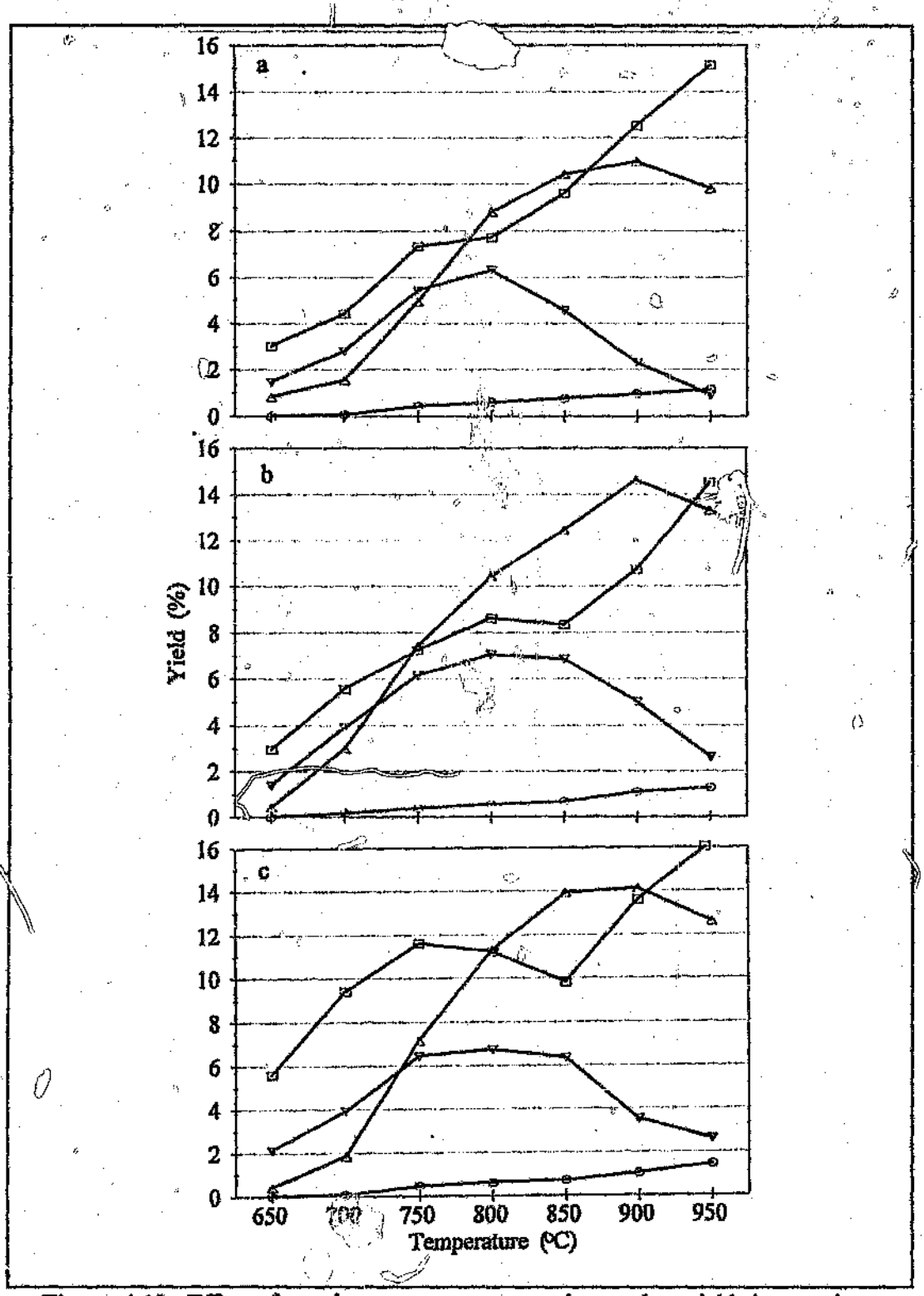


Figure 4.12. Effect of reaction temperature on major product yields in experiments (a) without any liquid addition to the feed, (b) in the presence of pure H_2O and (c) in the presence of H_2O_2 (21 wt.%) over the 28% La_2O_3/ 7% SrO/CaO catalyst. (V) C_2H_6, (Δ) C_2H_4, (o) C_{3+}, (□) CO_X.

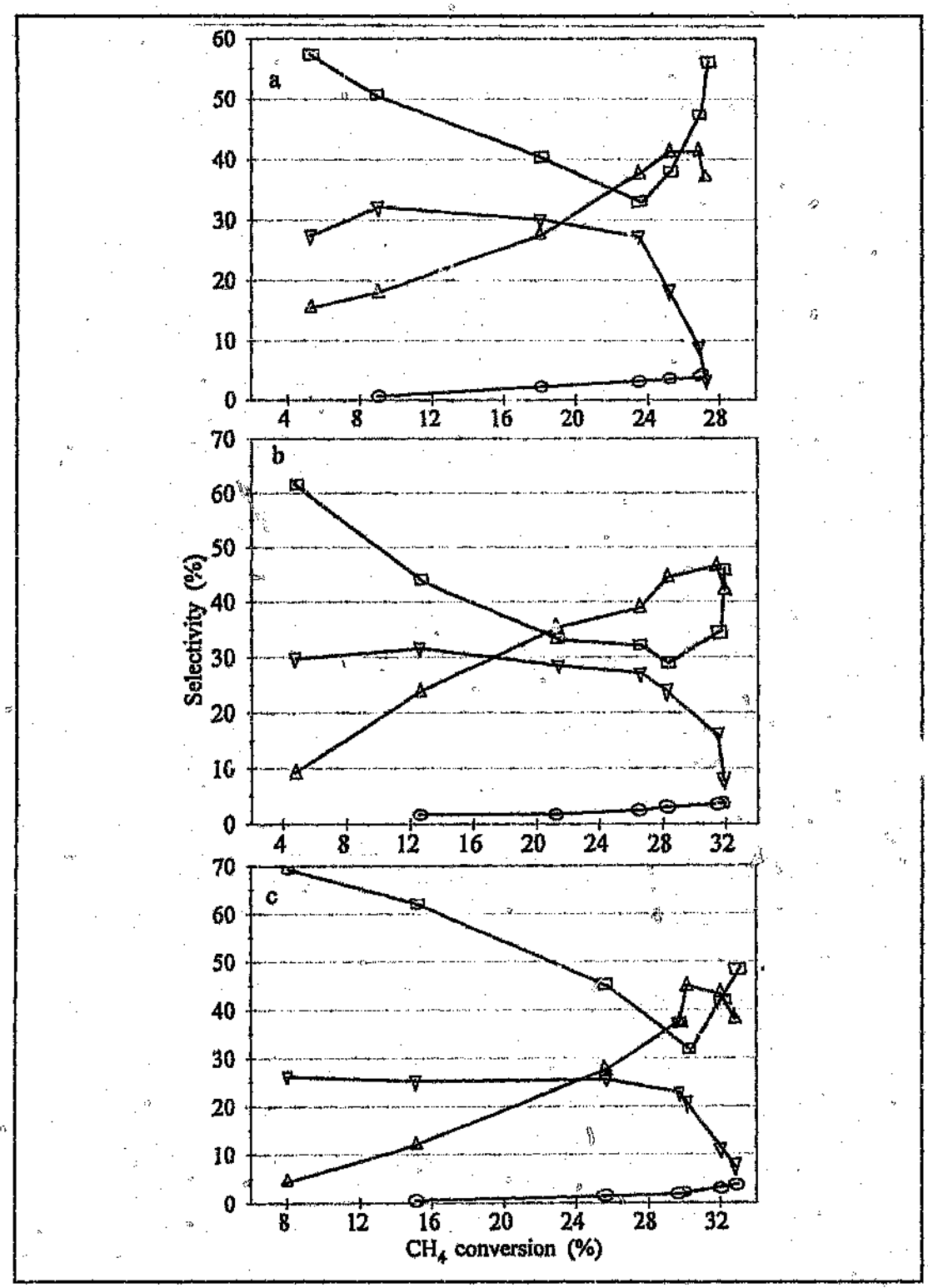


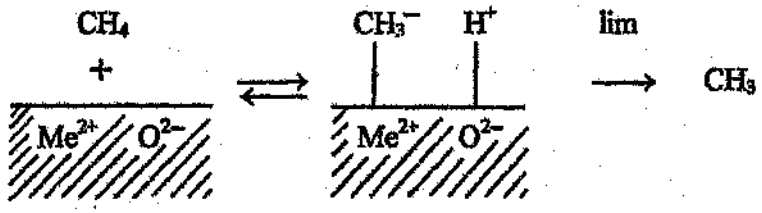
Figure 4.13. Selectivity to (▽) C_2H_6, (△) C_2H_4, (○) C_{3+}, and (□) CO_X. as a function of CH_4 conversion in experiments (a) without any liquid addition to the feed, (b) in the presence of pure H_2O and (c) in the presence of H_2O_2 (21 wt.%) over the 28% La_2O_3/ 7% SrO/CaO catalyst.

selectivity to C_{2+} products is 46.9% at 800°C for the lanthanum-calcium system which increased to 68.2% at 850°C when doped with strontium oxide. The C_{2+} product yield increased from 16% to 21% in the presence of hydrogen peroxide.

These results appear to suggest that the role of strontium lies in increasing the overall basicity of the lanthanum-calcium system which in turn leads to a drastic improvement in the selectivity of the catalyst. One may consider that carbon dioxide and water vapour suppress the deep oxidation of both methane and the reaction products, and block the active surface centers by producing surface carbonates and hydroxides. Obviously, increasing the basicity leads to the same effect. However, more strongly basic centers which occur as a result of the equilibruim dissociation of the surface carbonates seems to activate methane much more effectively, thereby compensating for the large number of blocked catalytically important oxide sites.

A similar relationship between basicity and performance can be seen for 21% La_2O_3/ 5.5% MoO_3/ CaO and 21% La_2O_3/ 5.5% MoO_3/ MgO. The acidic dopant, MoO_3, in the lanthanum-calcium system does not provide any noticeable effect on its catalytic properties. A decrease in the yield of C_{2+} products is observed. Furthermore, supporting MoO_3 on the lanthanum-magnesium system provides a low actitivty and selectivity towards desirable products (Table 3.12).

The above results provide valuable insight into the mechanism of methane oxidative coupling and explain the links between the basicity of the catalyst surface, activation of the reactants and the selectivity towards C_{2+} products. As has already been mentioned in Chapter 1, the oxygen states, namely O^- and O^{2-}, can be proposed as active sites for methane oxidative coupling on basic catalysts. These states can easily remove a hydrogen atom from the CH_4 molecule, thus producing the methyl radical. Primary activation of methane can occur via heterolytic splitting of the C-H bond into a proton and a carbanionic fragment. The latter fragment donates an electron to acceptor sites on the catalyst and this leads eventually to the formation of gas phase methyl radicals:



The implication of this scheme is that the effectiveness of a catalyst depends on its strength as a base. Basicity of an oxide is strongly influenced by the cation. This suggests that either adsorption or dissociation (or both) of weakly acidic methane on the surface are an important step in the sequence leading to radical formation.

The presence of hydrogen peroxide reveals a new reaction pathway for methyl radical formation and therefore of coupled products. It can be seen from Figure 3.3 that the apparent activation energies obtained during homogeneous gas phase methane oxidative coupling in the absence and presence of hydrogen peroxide are: E_a = 225.8 kJ mol^{-1} and 55.7-64.8 kJ mol^{-1}, respectively, which allowed us to suggest that methane activation occurs via the interaction of radicals formed during the dissociation of H_2O_2. Whereas, for homogeneous-heterogeneous methane oxidative coupling in the absence of hydrogen peroxide the activation of methane and the formation of CH_3 radicals proceeds mainly on the catalyst surface with the participation of active basic centers. However, in the presence of hydrogen peroxide an additional channel for the formation of methyl radicals becomes evident. As was suggested previously, the influence of hydrogen peroxide can be related to the formation of hydroxyl radicals:

$$H_2O_2 + M \rightarrow 2OH \qquad (1\,k)$$

which could interact with methane to form methyl radicals

$$CH_4 + OH \rightarrow CH_3 + H_2O \qquad (2\,k)$$

Taking into account the presence of hydrogen in the reaction mixture (particularly due to ethane dehydrogenation) the following chain-branching process can be initiated:

$$OH + H_2 \rightarrow H_2O + H \qquad (3\,k)$$

$$H + O_2 \rightarrow OH + O \qquad (4\,k)$$

$$O + H_2 \rightarrow OH + H \qquad (5\,k)$$

This process increases the amount of radicals, which could participate in methane activation.

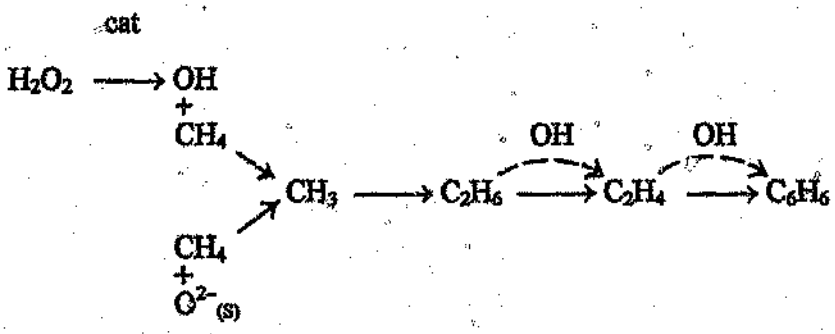
The above reaction pathway for methyl radical formation could also be important for the conventional catalytic methane oxidative coupling reaction, where the formation of hydrogen peroxide occurs *in situ* according to the reaction:

$$CH_4 + HO_2 \rightarrow CH_3 + H_2O_2 \qquad (6\,k)$$

The hydroperoxy radical creation proceeds mainly via the oxidative dehydrogenation of formyl and ethyl radicals[127].

A comparison of the performance of the catalysts in the presence of hydrogen peroxide shows that gold plays a key role in the activation of H_2O_2 as well as in the acceleration of the olefin aromatization process. Since gold is a noble metal, it remains in its unoxidized elemental form under the reaction conditions, therefore we suggest that Au can effectively participate in an electron exchange with hydrogen peroxide and activate the dissociation of the O-O bond. Due to the high activation energy, the rate of hydrogen peroxide dissociation slows down sharply with a decrease in temperature, resulting in a blockage of the additional channel for methyl radical formation. Obviously other noble metals such as platinum or palladium would have the same effect. However, these metals are known as catalysts for deep the oxidation of methane and higher hydrocarbons, and therefore, cannot be used in the title reaction.

In summary, all the data obtained, taken together, make it possible to suggest a general scheme for methane oxidative coupling over the catalytic systems investigated:



where (s) refers to surface species with a low coordination number.

As can be seen in the proposed scheme there are two channels for methyl radical formation, one homogeneous and the other heterogeneous. Recombination of methyl radicals yields ethane:

$$CH_3 + CH_3 \rightarrow C_2H_6 \qquad (7\,k)$$

Ethane undergoes a series of dehydrogenation steps resulting in the formation of ethyl radicals:

$$C_2H_6 + CH_3 \rightarrow C_2H_5 + CH_4 \qquad (8\,k)$$

$$C_2H_6 + H \rightarrow C_2H_5 + H_2 \qquad (9\,k)$$

Attack by hydroxyl radicals is another significant route for ethyl radical formation:

$$C_2H_6 + OH \rightarrow C_2H_5 + H_2O \qquad (10\,k)$$

Ethylene originates from ethyl radicals via thermal or catalytic decomposition as well as from the direct oxidation of the ethyl radicals by molecular oxygen:

$$C_2H_5 \rightarrow C_2H_4 + H \qquad (11\,k)$$

$$C_2H_5 + O_2 \rightarrow C_2H_4 + HO_2 \qquad (12\,k)$$

Ethylene can then be transformed into aromatic hydrocarbons. This process takes place more effectively in the presence of hydrogen peroxide over the 1% Au/ 5% La_2O_3/CaO catalyst, which can be related to the accelerating effect of the metal component (gold).

Thus, the above results show that the methane conversion and the C_{2+} product yield are remarkably enhanced by hydrogen peroxide, which can serve as a gas phase initiator for methyl radical formation, presumably by generation of hydroxyl radicals. This channel to methyl radical formation can also be important for the conventional catalytic methane oxidative coupling reaction. In this reaction hydrogen peroxide is formed *in situ*, and leads to a degenerate chain-branching reaction in the post catalytic zone, resulting in an additional amount of C_2 hydrocarbons being formed.

Chapter 5. CONCLUSION

A number of conclusions can be drawn from the study of the relationship between the ability of catalysts to activate methane and oxygen, and their performance in the partial oxidation and oxidative coupling reactions.

The use of 30% H_3BO_3/Al_2O_3 had a visible catalytic effect on the partial oxidation of methane performed at low pressure. Not only was it possible to detect methanol at temperatures lower than that used for the pure gas-phase homogeneous process, but an increase in the maximum methanol yield was also observed with this catalyst. Although the methanol yield obtained in our work is still far to low to be of economic interest, nevertheless the catalytic oxidation of methane has proven to be an exciting subject for investigation.

The adsorption of methanol on alumina and alumina-supported boric acid has been characterised using FT-IR spectroscopy. A comparison of the IR spectra resulting from the introduction of methyl alcohol on the sample surface, with the spectra of the untreated sample both before and after heating the sample in the presence of water vapour to 400°C, suggested that the catalytic partial oxidation of methane occurs through the formation of methoxy groups on the catalyst surface. The bands corresponding to the CH stretching vibrations for 30% H_3BO_3/Al_2O_3 were found to be very stable during the thermal treatment.

Partial oxidation of methane by oxygen in the presence of hydrogen peroxide to form formaldehyde and methanol was studied over a series of silica supported catalysts with 3d, 4d, 4f, 5p and 6p - metal oxides in the 500-600°C temperature range under ambient pressure.

It was shown that the pure precipitated SiO_2 exhibited remarkable activity toward formaldehyde formation. The presence of titanium, vanadium, chromium, iron, molybdenum, lead, bismith and lanthanum metal oxides appeared to suppress the activity of bare silica as well as reduce methane conversion, and therefore formaldehyde yield, under a given set of experimental conditions. The only elements which enhanced bare silica activity were the 5p metals, tin and antimony. A maximum combined formaldehyde and methanol yield of 1.32% at a methane conversion of 3.5%

was observed at a tin loading of 0.1 mmol/g SiC_2. The positive effect of doping silica with Sn and Sb can be explained by the possible activation of hydrogen peroxide on these elements, and the formation of active radicals, presumably hydroxyl radicals.

To attain a better understanding of the tin-silica system for methane oxidation, experiments with absence of hydrogen peroxide or oxygen were performed. Only traces of oxy-products were observed after the reaction using H_2O instead of H_2O_2. Thus, the presence of hydrogen peroxide is crucial for oxy-product formation. In the reaction without oxygen, but with hydrogen peroxide in the reaction mixture, formaldehyde production dropped by about two fold, while methanol completely disappeared from the reaction products.

On the basis of the experimental results a reaction scheme was proposed for the methane activation in the presence of hydrogen peroxide. By this mechanism the hydrogen peroxide dissociates to form surface or gas phase active species (presumably, peroxide or superoxide surface species or hydroperoxy and hydroxyl radicals). These species can attack molecules of methane and produce intermediates (such as methyl radicals in the gas phase or methoxy groups on the catalyst surface), which in turn can be transformed into the final oxy-products. According to this reaction pathway, it can be predicted that, the major product of the partial oxidation of methane at low pressure and high oxygen concentration will be formaldehyde, in agreement with the experimental data.

The possibility of methane oxidative coupling occurring via a heterogeneous-homogeneous mechanism, i.e., a reaction initiated on the catalyst surface and the oxidation continuing in the gas phase, suggests a route to increasing the C_2 product yield by improving the gas phase reaction. This approach was tested by the introduction of a gas phase initiator into the reaction mixture.

Hydrogen peroxide was used as an initiator as well as oxidant for both the homogeneous non-catalytic methane oxidative coupling and the oxidative conversion of methane in the presence of a catalyst. The possibility of the formation of *in situ* hydrogen peroxide in the process of oxidative coupling on solid catalysts suggests that it may also be used for the subsequent activation of methane in the gas phase, which would result in the formation of additional amounts of C_2 products. Thus, hydrogen peroxide could also serve as a source of active species, e.g., peroxide or superoxide

surface species or HO_2 and OH radicals. These species could interact with methane to form reactive surface intermediates or gas-phase methyl radicals, which could recombine to form ethane, an ethyl radical, or ethylene.

A comparison of the apparent activation energies, obtained from the gas phase oxidative coupling of methane performed in the temperature range of 400 to 800°C with the reaction mixtures CH_4-N_2 or CH_4-air, in the presence and absence of hydrogen peroxide (E_a = 55.7-64.8 kJ mol^{-1} and 225.8 kJ mol^{-1}, respectively), indicate that CH_4 activation occurs via the interaction of radicals formed during the dissociation of H_2O_2.

The results obtained from the catalytic methane oxidative coupling in the presence of hydrogen peroxide showed that the 1%Au/ 5% La_2O_3/CaO catalyst was markedly more active and selective towards desirable products than unpromoted 5% La_2O_3/CaO. A loading of only 1% Au on the lanthanum-calcium system caused a significant increase in the C_{2+} hydrocarbon selectivity and a rather small increase in the CH_4 conversion. Obviously, gold plays an important role in the hydrogen peroxide dissociation reaction and radical formation under conditions of heterogeneous-homogeneous methane oxidative coupling. A peculiarity of the performed reaction was the formation of a noticeable quantity of benzene. This could be related to an acceleration of the process of olefin aromatization by hydrogen peroxide as well as by the metal component (gold) on the catalyst surface. The maximum yield of C_{2+} products, obtained in the presence of 21 wt. % hydrogen peroxide, was 27% with a corresponding 7.3% yield of benzene; this is one of the best results obtained to date for the title reaction.

Among the many possible combinations of oxides that catalyze the oxidative coupling of methane, La_2O_3 promoted with SrO gave the best performance. The catalytic results showed that promotion of the CaO supported La_2O_3 with SrO was a more selective system towards C_2 hydrocarbons than the 5% La_2O_3/CaO and 1% Au/ 5% La_2O_3/CaO catalysts. It appears that not only is an appreciable amount of lanthanum on the surface of the system necessary for the catalyst to be selective, but that strontium is also a prerequisite for selectivity. The total C_2 hydrocarbon selectivity increased from 49.6 to 62.3% at corresponding CH_4 conversions of 26.7% and 31.4% as the reactant gas was diluted by water vapour in the reaction performed on 28%

La_2O_3/ 7% SrO/CaO catalyst. An absolute yield of 20% of both C_2H_4 and C_2H_6 was obtained at a CH_4/O_2 ratio of 4.0 and a residence time of 0.11 s.

The XRD analysis revealed the coexistence of $SrCO_3$, $La_2O_2CO_3$ and $CaCO_3$ phases in the bulk of this sample. It is well known that in the presence of CO_2 strongly basic oxides easily form carbonates of high thermal stability. The higher the carbonate decomposition temperature, the higher the basicity of the corresponding oxide. Evidently, the introduction of strontium significantly increased the basicity of the lanthanum-calcium system, since these carbonates were present at high reaction temperatures.

A similar relationship between basicity and performance was observed for 21% La_2O_3/ 5.5% MoO_3/ CaO and 21% La_2O_3/ 5.5% MoO_3/ MgO. The acidic dopant, MoO_3, in the lanthanum-calcium system had a negative effect on its catalytic properties. A decrease in the yield of C_{2+} products was observed. Furthermore, addition of MoO_3 to the lanthanum-magnesium system yielded a catalyst with low activity and selectivity towards the desired products.

The characterization data obtained by means of XRD, SEM and EDX showed that, under the conditions existing during the methane oxidative coupling reaction, strong chemical and structural modifications of the starting catalytic phase occured. The reaction performed on the 28% La_2O_3/ 7% SrO/CaO catalyst led to the *in situ* formation of a dioxymonocarbonate ($La_2O_2CO_3$) phase.

An inhomogeneity of the gold distribution on the catalyst surface was observed for 1% Au/ 5% La_2O_3/CaO after catalytic testing. Increasing the La_2O_3 concentration from 5% to 28% and introducing SrO onto the surface of a lanthanum-calcium system resulted in marked changes in the structural and morphological properties of the catalyst.

Comparison of the results of the experiments performed in the three different types of reactors used in this study revealed that a decrease in the residence time of the reaction mixture in the empty volume of the post catalytic zone led to a significant improvement in the C_2 hydrocarbon selectivity. It was also evident that the methane conversion did not vary considerably with the residence time in the post catalytic reaction zone for all the catalysts tested. Hence, it was assumed that the homogeneous gas phase processes are responsible for the production of the additional amounts of C_2,

C_3 and C_4 hydrocarbons. When the post catalytic zone was held at low temperature (200°C), the intermediates generated on the catalytic bed did not have prolonged life times as was found in a heated post catalytic zone. Rather the gases were quenched by the "cool" post catalytic zone reactor walls and so a lower C_{2+} hydrocarbon yield resulted. However, when the post catalytic zone was heated to the same temperature as the main catalytic reaction zone or above (1000-1100°C), the C_{2+} hydrocarbon yield was significantly increased. It was suggested that the intermediates generated on the catalytic bed produced C_{2+} hydrocarbons by coupling homogeneously in the gas phase. These coupled hydrocarbon products then entered the heated post catalytic zone and decomposed into radicals which, in the presence of methane, acted as initiators for further homogeneous coupling processes. This ultimately resulted in a chain propagation radical reaction which consecutively led to an increase in the C_2 hydrocarbon yield and to the formation of aromatics.

All the data obtained, taken together, made it possible to propose a reaction scheme for methane oxidative coupling over the catalytic systems investigated which consisted of both homogeneous and heterogeneous channels for methyl radical formation.

Thus, the above results showed that the methane conversion and the C_{2+} product yield were remarkably enhanced by hydrogen peroxide, which served as a gas phase initiator for methyl radical formation (presumably by generation of hydroxyl radicals). This channel to methyl radical formation was also important for the conventional catalytic methane oxidative coupling reaction. The presence of hydrogen peroxide in this reaction led to a degenerate chain-branching reaction in the post catalytic zone, resulting in the formation of an additional amount of C_2 hydrocarbons.

REFERENCES

[1] J. Saint-Just, J.M. Basset and G.A. Martin, Natural Gas: a feedstock for tomorrow, Recherche, 21, 733 (1990).

[2] N.D. Parkyns, C.I. Warburton and J.D. Wilson, *Catal. Today*, 18, 385-442 (1993).

[3] H.D. Gesser and N.R. Hunter, The direct conversion of methane to methanol (DMTM), Direct Methane Conversion by Oxidative Processes - Fundamental and Engineering Aspects, Rheinhold, (1990).

[4] J.M. Fox, *Catal. Rev.-Sci. Eng.*, 35(2), 169-212 (1993).

[5] G.E. Keller and M.M. Bhasin, *J. Catal.*, 73, 9 (1982).

[6] J. Lunsford, *Catal. Today*, 6, 235 (1990).

[7] D. Gray and G. Tomlinson, Direct methane conversion - An assessment, DOE Contract, 56-9937 (1987-88).

[8] F.M. Dautzenberg, J.C. Schlatter, J.M. Fox, J.R. Rostrup-Nielsen and L.J. Christiansen, *Catal. Today*, 13, 503 (1992).

[9] U. Preub and M. Baerns, *Chem. Eng. Techn.*, 10, 297 (1987).

[10] W. Hinsen, W. Bytyn and M. Bearns, *Verlag Chemie*, 3, 581 (1985).

[11] J.A. Labinger and K.C. Ott, *J. Phys. Chem.*, 91, 2682 (1987).

[12] V.D. Sokolovskii, S. M.Aliev, O.V. Buyevskaya and A.A. Davydov, *Catal. Today*, 4, 293 (1989).

[13] V.D. Sokolovskii, S. M.Aliev, O.V. Buyevskaya and A.A. Davydov, *Stud. Surf. Sci. Catal.*, 55, 437 (1990).

[14] I. Matsuura, Y. Utsumi, T. Doi and Y. Yoshida, *Appl. Catal.*, 47, 299 (1989).

[15] T. Ito, T. Watanabe, T. Tashiro and K. Toi, *J. Chem. Soc., Faraday Trans. 1*, 85, 2381 (1989).

[16] K. Tanabe, in J.R. Anderson and M. Boudart (Editors), *Catalysis Science and Technology*, Vol. 2, Springer-Verlag, 5 (1981).

[17] G.Zhang, H. Hattori and K. Tanabe, *Appl. Catal.*, 36, 189 (1988).

[18] V.R. Choudhary and V.H. Rane, *Catal. Lett.*,4, 101 (1990).

[19] A.M. Maitra, I. Campbell and R.J. Tyler, *Appl. Catal.*, 85, 27 (1992).

[20] A.M. Maitra, *J. Therm. Anal.*, 36, 657 (1990).

[21] H. Vinek, H. Noller, M. Ebel and K. Schwartz, *J. Chem. Soc., Faraday Trans. 1*, 73, 734 (1977).

[22] P.A. Hathway and M.E. Davis, *J. Catal.*, 116, 263 (1989).

[23] L. Lehmann and M. Baerns, *J. Catal.*, 135, 467 (1992).

[24] A.M. Maitra, *Appl. Catal. A: General*, 104, 11 (1993).

[25] M.Y. Sinev, V.Y. Bychkov and V.N. Korchak, *Kinet. Catal.*, 30, 1137 (1989).

[26] M.Y. Sinev, V.Y. Bychkov and V.N. Korchak, *Kinet. Catal.*, 30, 1421 (1989).

[27] C.H. Lin, J.X. Wang and J.H. Lunsford, *J. Catal.*,111, 302 (1988).

[28] F.P. Larkins and M.R. Nordin, *Stud. Surf. Sci. Catal.*, 36, 409 (1988).

[29] E.J. Erekson, A.L. Lee, S.P. Baron and I.J. Solomon, US Patent 4945078 (1990).

[30] Y. Bi, K. Zhen, Y. Jiang, C. Teng and X. Yang, *Appl. Catal.*, 39, 185 (1988).

[31] K. Aika, T. Moriyama, N. Takasaki and E. Iwamatsu, *J. Chem. Soc., Chem. Commun.*, 1210 (1986).

[32] J.A.S.P. Carreiro and M. Baerns, *J. Catal.*, 117, 258 (1989).

[33] S.J. Korf, J.A. Roos, J.W.H.C. Derksen, J.A. Vreeman, J.G. van Ommen and J.R.H. Ross, *Appl. Catal.*, 59, 291 (1990).

[34] O.V. Buyevskaya, A.I. Suleimanov, S.M. Aliev and V.D. Sokolovskii, *React. Kinet. Catal. Lett.*, 33, 223 (1987).

[35] N. Matsuda, K. Ohyachi and I. Matsuura, *Chem. Express*, 5, 533 (1990).

[36] B. Fubini and F.S. Stone, Proc.10th Int. Symp.on the Reactivity of Solids, 85 (1984).

[37] T. Ito and J.H. Lunsford, *Nature*, 314, 721 (1985).

[38] F.P. Larkins and M.R. Nordin, Symp. on the Produc. of Fuels and Chem., Auckland, 409 (1987).

[39] E.L. Head and C.E. Holley, Rare Earth Research III, Gordon and Breach, New York, 707 (1965).

[40] M.Y. Sinev, V.N. Korchak and O.V. Krylov, *Kinet. Catal.*, 28, 1376 (1987).

[41] M. Matsukata, E. Okanari, K. Komori, T. Matsuda, E. Kikuchi and Y. Morita, Symp. on Methane Activation, Conversion and Utilization, Hawaii, 85 (1989).

[42] A.I. Suleimanov, S.M. Aliev and V.D. Sokolovskii, *React. Kinet. Catal. Lett.*, 31, 291 (1986).

[43] K. Otsuka, K. Jinno and A. Morikawa, *Chem. Lett.*, 4, 499 (1985).

[44] K. Otsuka, K. Jinno and A. Morikawa, *J. Catal.*, 100, 353 (1986).

[45] R. Burch and S.C. Tsang, *Appl. Catal.*, 65, 259 (1990).

[46] V.R. Choudhary and V.H. Rane, *J. Catal.*, 130, 411 (1991).

[47] M.Y. Sinev, V.N. Korchak and O.V. Krylov, *Kinet. Catal.*, 28, 1376 (1987).

[48] H. Yamashita, Y. Machida and A. Tomita, *Appl. Catal.*, 79, 203 (1991).

[49] C.H. Lin, K.D. Campbell, J.X. Wang and J.H. Lunsford, *J. Phys. Chem.*, 90, 534 (1986).

[50] C. Louis, T.L. Chang, M. Kermares, T. Le Van, J.M. Tatibouet and M. Che, *Catal. Today*, 13, 283 (1992).

[51] T. Le Van, M. Che, M. Kermarec, C. Louis and J.M. Tatibouet, *Catal. Lett.*, 6, 395 (1991).

[52] S.J. Korf, J.A. Roos, L.J. Veltman, J.G. van Ommen and J.R.H. Ross, *Appl. Catal.*, 56, 119 (1989).

[53] J.M. De Boy and R.F. Hicks, *J. Chem. Soc., Chem. Commum.*, 982 (1988).

[54] K.D. Campbell, H. Zhang and J.H. Lunsford, *J. Phys. Chem.*, 92, 750 (1988).

[55] S. Bartsch, J. Falkowski and H. Hoffman, *Catal. Today*, 4, 421 (1989).

[56] S.J. Korf, J.A. Roos, J.M. Diphoorn, R.H.J. Veehof, V.G. van Ommen and J.R.H. Ross, Proc.1st Workshop.Catalytic Methane Conversion, *Catal. Today*, 4, 279 (1989).

[57] V.D. Sokolovskii, O.V. Byevskaya, L.M. Plyasova, G.S. Lytvak and N.F. Uvarov, *Catal. Today*, 6, 489 (1990).

[58] I.A. Guliev, S.A. Dzhamalova and I.A. Timakov, VI Conf.on Oxidation Catal., USSR, 13 (1988).

[59] A.K. Mamedov, P.A. Shiryaev and D.P. Shashkin, VI Conf.on Oxidation Catal., USSR, 15, (1988).

[60] J.M. Thomas, X. Kian and J. Stachurski, J. Chem. *Soc. Chem. Commun.*, 162 (1988).

[61] W. Hinsen, W. Bytyn and M. Baerns, 8th Intern. Congr. Catal., V3, Weinheim, 581 (1984).

[62] I.I.A. Emesh and Y. Amenomiya, *J. Phys. Chem.*, 90, 4785 (1986).

[63] J.A.S.P. Carreiro and M. Baerns, *React. Kinet. Catal. Lett.*, 35, 349 (1987).

[64] J.L. Jezl, G.O. Michaels, M.J. Spangler and M.L. Winzenburg, US Patent 4 814 539 (1989).

[65] V.P. Vislovskii, I.V. Baidikova, E.A. Mamedov and R.G. Rizayev, *React. Kinet. Catal. Lett*, 47, 193 (1992).

[66] J.A. Labinger, *Catal. Lett.*, 1, 371 (1988).

[67] M. Utajama, H. Hattori and K. Tanabe, *J. Catal.*, 53, 237 (1978).

[68] K.P. Peil, J.G. Goodwin and G.J. Marcelin, *J. Catal.*, 132, 556 (1991).

[69] A. Ekstrom and J.A. Lapszewicz, *J. Phys. Chem.*, 93, 5230 (1989).

[70] I. Matsuura and M. Kirishiki, *Chem. Lett.*, 1441 (1986).

[71] J. Rasko, G Somorjai and H. Heinemann, *Appl. Catal.*, 84, 57 (1992).

[72] V.D. Sokolovskii, *React. Kinet. Catal. Lett.*, 32, 159 (1986).

[73] T. Ito, J.X. Wang, C.H. Lin and J.H .Lunsford, *J. Am. Chem. Soc.*, 107, 5062 (1985).

[74] D.J. Driscoll, W. Marth, J.X. Wang and J.H. Lunsford, *J. Am. Chem. Soc.*, 107, 58 (1985).

[75] K. Otsuka, M. Hatano and T. Komatsu, *Catal. Today*, 4, 409 (1989).

[76] V.D. Sokolovskii, O.V. Buyevskaya, S.M. Aliev and A.A. Davydov, New Developments in Selective Oxidation. Ed. by G. Centi and F. Trifiro., Amsterdam, Elsevier, 437 (1990).

[77] M. Utiyama, H. Hattori and K. Tanabe, *J. Catal.*, 53, 237 (1978).

[78] C.T. Mortimer, Reactions Heats and Bond Strengths, *Pergamon Press*, NY (1962).

[79] S.A. Driscoll, D.K. Gardner and U.S. Ozkan, *Cat. Lett.*, 25, 191 (1994).

[80] P.F. Nelson, C.A. Lukey and N.W. Cant, *J. Catal.*, 120, 216 (1989).

[81] J.B. Kimble and J.H. Kolts, *CHEMTECH*, 501 (1987).

[82] H. Zanthoff and M. Baerns, *Ind. Eng. Chem. Res.*, 29, 2 (1990).

[83] Q. Chen, J.H.B.J. Hoebink and G.B. Marin, *Ind. Eng. Chem. Res.*, 30, 2088 (1991).

[84] I.A. Vardanyan and A.B. Nalbandyan, *Int. J. Chem. Kinet.*, 17, 901 (1985).

[85] G.J. Tjatjopoulos and I.A. Vasalos, *Appl. Catal.*, A88, 213 (1992).

[86] L.M. Aparicio, S.A. Rossini, D.G. Sanfilippo, J.E. Rekoske, A.A. Trevino and J.A. Dumesic, *Ind. Eng. Chem. Res.*, 30, 211 (1991).

[87] O.V. Krylov, *Kinet. Catal.*, 34, 11 (1993).

[88] K. Otsuka and K. Jinno, *Inorg. Chim. Acta*, 121, 237 (1986).

[89] K. Otsuka and T. Nakajima, *J. Chem. Soc. Faraday Trans.1*, 83, 1315 (1987).

[90] M.Y. Sinev, V.N. Korchak and O.V. Krylov, *Kinet. Catal.*, 30, 860 (1989).

[91] V.D. Sokolovskii and E.A. Mamedov, *Catal. Today*, 14, 331 (1992).

[92] A.B. Anderson and J. Yu, *J. Catal.*, 119, 135 (1989).

[93] J.M. Aigler and J.H. Lunsford, *Appl. Catal.*, 70, 29 (1991).

[94] J.H. Lunsford, *Stud. Surf. Sci. Catal.*, 61, 3 (1991).

[95] T. Moriyama, N. Takasaki, E. Iwamatsu and K. Aika, *Chem. Lett.*, 1168 (1986).

[96] M.Y. Kogn, V.A. Shvets, K.I. Slovetskaya and V.B. Kazanskii, *Kinet. Catal.*, 15, 469 (1974).

[97] K.N. Spiridonov and O.V. Krylov, *Kinet. Catal.*, 16, 7 (1975).

[98] T. Ito, T. Tashiro, T. Watanabe, K. Toi and I. Ikemoto, *Chem. Lett.*, 1723 (1987).

[99] T. Ito, T. Tashiro, M. Kawasaki, T. Watanabe, K. Toi and H. Kobayashi, *J. Phys. Chem.*, 95, 4476 (1991).

[100] Z.L. Zhang and M. Baerns, *J. Catal.*, 135, 317 (1992).

[101] M.Y. Sinev, V.N. Korchak and O.V. Krylov, *Kinet. Catal.*, 27, 1164 (1986).

[102] A.I. Suleimanov, E.G. Ismailov, S.M. Aliev and V.D. Sokolovskii, *React. Kinet. Catal. Lett.*, 34, 51 (1987).

[103] V.D. Sokolovskii, *React. Kinet. Catal. Lett.*, 35, 337 (1987).

[104] A.A. Davydov, A.A. Budneva, S.M. Aliev and V.D. Sokolovskii, *React. Kinet. Catal.Lett.*, 36, 491 (1988).

[105] E. Garrone and F.S. Stone, *Verlag Chemie*, 3, 441 (1984).

[106] R. Burch, G.D. Squire and S.C. Tsang, *J. Chem. Soc., Faraday Trans.1*, 85, 3561 (1989).

[107] L.A. Morton, H.D. Gesser and N.R. Hunter, *Fuel Science and Technology International*, 9, 913 (1991).

[108] D.W. Rytz and A. Baiker, *Ind. Eng. Chem. Res.*, 30, 2287 (1991).

[109] L.B. Han, S. Tsubota, T. Kobayashi and M. Haruta, *J. Chem. Soc., Chem. Commun.*, 93 (1995).

[110] K. Omata, N. Fukuoka and K. Fujimoto, *Catal. Letters*, 12, 227 (1992).

[111] R. Burch, G.D. Squire and S.C. Tsang, *J. Chem. Soc., Faraday Trans.1*, 85, 3561 (1989).

[112] J.W. Chun and R.G. Anthony, *Ind. Eng. Chem. Res.*, 32, 259 (1993).

[113] S. Kasztelan and J.B. Moffat, *J. Chem. Soc. Chem. Commun.*, 1663 (1987).

[114] M. Kennedy, A. Sexton, B. Karthouser, E. MacGiolla, J.B. McMonagle and B.K. Hodness, *Catal. Today*, 13, 447 (1992).

[115] A. Parmaliana, V.D. Sokolovskii, D. Miceli, F. Arena and N. Giordano, *J. Catal.*, 148, 514 (1994).

[116] K. Otsuka and T. Nakajima, *J. Chem. Soc. Faraday Trans.*, 83, 1315 (1987).

[117] G.J. Hutchings, M.S. Scurrell and J.R. Woodhouse, *J. Chem. Soc. Chem. Commun.*, 1388 (1987).

[118] G.J. Hutchings, M.S. Scurrell and J.R. Woodhouse, *J. Chem. Soc. Faraday Trans.*, 85, 2507 (1989).

[119] H. Yamamoto, H.Y. Chu, M. Xu, C. Shi and J.H. Lunsford, *J. Catal.*, 142, 325 (1993).

[120] K. Otsuka and Y. Wang, *Catal. Letters*, 24, 85 (1994).

[121] S.S. Shepelev and K.G. Ione, *J. Catal.*, 117, 362 (1989).

[122] K. Asami, T. Shikada and K. Fujimoto, *Bull. Chem. Soc. Jpn.*, 64, 266 (1991).

[123] H.D. Gesser, N.R. Hunter and P.A. Das, *Catal. Letters*, 15, 217 (1992).

[124] Z.G. Osipova, L.M. Plyasova and V.D. Sokolovskii, Sov. Jpn. Seminar on Catalysis, 41 (1990).

[125] Z.G. Osipova, S.B. Ushkov, V.D. Sokolovskii and A.V. Kalinkin, New Developments in Selective Oxidation, Elsevier Science Publishers B.V., 527 (1990).

[126] A. Labinger and K.C. Ott, *J. Phys. Chem.*, 91, 2682 (1987).

[127] G.J. Tjatjopoulos and I.A. Vasalos, *Appl. Catal. A*, 88, 213 (1992).

[128] F.T. Weiss, Determination of Organic Compounds, Wiley-Intersci., NY, 94-104 (1970).

[129] J.F. Walker, Formaldehyde, Reinhold, NY, 489 (1964).

[130] G.M. Cooper and P.J. Weizevich, Effects of Temperature and Pressure on the Upper Explosive Limit of Methane-Oxygen Mixture, *Ind. Eng. Chem.*, 21, 1210 (1929).

[131] A. Melvin, Spontaneous Ignition of Methane-Air Mixtures at High Pressure, *Combust. Flame*, 10, 120 (1966).

[132] T.R. Baldwin, R. Burch, E.M. Crabb, G.D. Squire and S.C. Tsang, *Appl. Catal.*, 56, 219 (1989).

[133] J.M. Thomas, W. Ueda, J. Williams and D.M. Harris, *Faraday Discuss., Chem. Soc.*, 87, 33 (1989).

[134] J.R. Mellor, Ph.D Thesis, The Water Gas Shift Reaction: A Deactivation Study, University of the Witwatersrand, (1993).

[135] J. Wollbrandt, Ph.D Thesis, An In Situ DRIFTS and Reactor Study of Catalyzed Ethanol Transformation Reactions, University of the Witwatersrand, (1993).

[136] A.J. Tench, D. Giles and J.F.J. Kibblewhite, *J. Chem. Soc. Trans. Faraday Soc.*, 67, 854 (1971).

[137] G.J. Millar, C.H. Rochester and K.C. Waugh, *J. Catal.*, 142, 263 (1993).

[138] M. Falk and E. Whalley, *J. Chem. Phys.*, 34, 1554 (1961).

[139] S.S. Mitra, *Solid State Phys.*, 13, 1 (1962).

[140] J.B. Peri, *J. Phys. Chem.*, 69, 220 (1965).

[141] F.G. Billaud and F. Baronnet, *Ind. Eng. Chem. Res.*, 32, 1549 (1993).

[142] V.D. Sokolovskii, C.D. Pearcey and N.J. Coville, *React. Kinet. Catal. Lett.*, 52, 341 (1994).

[143] O.V. Buyevskaya, M.P. Vanina, N. Saputina and V.D. Sokolovskii, *Catal. Today*, 13, 589 (1992).

[144] J.B. Claridge, M.L.H. Green, S.C. Tsang and A.P.E. York, *Appl. Catal.*, A89, 103 (1992).

[145] J.M. Deboy and R.F. Hicks, *J. Catal.*, 113, 517 (1988).

[146] J.M. Deboy and R.F. Hicks, *Ind. Eng. Chem. Res.*, 27, 1577 (1988).

[147] T. Moriyama, N. Takasaki, E. Iwamatsu and K. Aika, *J.Chem.Soc., Chem.Commun.*, 1210 (1986).

[148] C.H. Lin, K.D. Cambell, J.X. Wang and J.H. Lunsford, *J. Phys. Chem.*, 91, 2682 (1987).

[149] M.P. Rosynek and D.T. Magnuson, *J. Catal.*, 48, 417 (1977).

[150] R. Alvero, J.A. Odriozola and J.M. Trillo, *J. Chem. Soc. Dalton Trans.*, 87 (1984).

[151] S. Bernal, F.J. Botana, R. Garcia and J.M. Rodriguez-Izquierdo, *Reactiv. Solids*, 4, 23 (1987).

[152] S. Bernal, G.A. Martin, P. Moral and V. Perrichon, *Catal. Letters*, 6, 231 (1990).

[153] T. Le Van, M. Che, M. Kermarec, C. Louis and J.M. Tatibouet, *Catal. Letters*, 6, 395 (1990).

[154] T. Le Van, M. Che, J.M. Tatibouet and M. Kermarec, *J. Catal.*, 142, 18 (1993).

[155] A. Chauvel, G. Lefebvre and L. Castex, Procedes de Petrochimie Caracteristiques techniques et economiques, Ed. Technip: Paris, 1, 343, (1985).

[156] N.R. Foster, *Appl. Catal.*, 19, 1 (1985).

[157] H.D. Gesser, N.R. Hunter and C.B. Prakash, *Chem. Rev.*, 85, 235 (1985).

[158] N.D.Spencer, *J. Catal.*, 109, 187 (1988).

[159] N.D. Spencer and C.J. Pereira, *J. Catal.*, 116, 399 (1989).

[160] A. Parmaliana, F. Frusteri, D. Miceli, A. Mezzapica, M.S. Scurrell and N. Giordano, *Appl. Catal.*, 78 (1991).

[161] T.A. Garibyan and I.Y. Margolis, *Catal. Rev.-Sci. Eng.*, 31, 355 (1989).

[162] R. Pitchai and K. Klier, *Catal. Rev.-Sci. Eng.*, 28, 13 (1986).

[163] K. Otsuka and M. Hatano, *J. Catal.*, 108, 252 (1987).

Author: Eskendirov Igor.
Name of thesis: Direct methane transformation into higher hydrocarbons and oxy-products.

PUBLISHER:
University of the Witwatersrand, Johannesburg
©2015

LEGALNOTICES:

Copyright Notice: All materials on the University of the Witwatersrand, Johannesburg Library website are protected by South African copyright law and may not be distributed, transmitted, displayed or otherwise published in any format, without the prior written permission of the copyright owner.

Disclaimer and Terms of Use: Provided that you maintain all copyright and other notices contained therein, you may download material (one machine readable copy and one print copy per page)for your personal and/or educational non-commercial use only.

The University of the Witwatersrand, Johannesburg, is not responsible for any errors or omissions and excludes any and all liability for any errors in or omissions from the information on the Library website.